

**Elucidation of the Transport and Fate of Per- and Polyfluoroalkyl
Substances in the High Arctic of Canada**

by

© John J. MacInnis

A dissertation submitted to the School of Graduate Studies in partial fulfillment of the
requirements for the degree of

Doctor of Philosophy

Department of Chemistry

Memorial University of Newfoundland

March 2020

St. John's, Newfoundland and Labrador

Abstract

Per- and polyfluoroalkyl substances (PFAS) are anthropogenic chemicals that were manufactured since the 1950s. Perfluoroalkyl acids (PFAA) are an important class of PFAS and are used for a number of industrial and commercial applications related to fluoropolymer manufacturing and surface treatments imparting stain, oil, and water repellency. The detection of PFAS in remote environments, such as the Arctic, where they are neither produced nor used, suggests they undergo long-range transport. It is suggested the long-range transport of PFAS to the Arctic occurs through the ocean, atmosphere, or some combination of the two. This thesis demonstrates that remote sample collection is an effective strategy for understanding the long-range transport of PFAS to the Arctic of Canada. The analysis of snow, ice, and sediment demonstrates PFAA are continuously transported to the Arctic of Canada. PFAA deposition is increasing over time in many Arctic regions in Canada, and their occurrence in these environments is primarily attributed to the long-range atmospheric transport and oxidation of volatile precursor chemicals. The results in this thesis support the hypothesis that long-range atmospheric transport is an important pathway for PFAA to the Arctic, however, they also provide unique insights into the post-depositional transport and fate of PFAS in the Arctic, especially in environments that are responding to climate warming. These results demonstrate for the first time that climate warming is an important vector for PFAS deposition through the action of enhancing glacier and permafrost ice melting, which remobilizes historically archived PFAS in glacier and permafrost ice into recipient freshwater ecosystems in the High Arctic of Canada.

Acknowledgements

Firstly, I would like to thank my co-supervisors and committee members Drs. Amila De Silva, Travis Fridgen, and Christina Bottaro. Amila, it has been a true pleasure working with you. I have learned so much from you both professionally and personally. You have been there for me every step of the way and I will be forever grateful for all of your unwavering support.

Secondly, I would also like to thank several collaborators for their contributions. Drs. Alison Criscitiello and Torsten Meyer, thank you for your assistance dating our ice core. Drs. Igor Lehnherr, Roberto Quinlan, Vincent St. Louis, Kyra St. Pierre, and Derek Muir thank you all for your efforts collecting samples and providing editorial comments on manuscripts. I would also like to thank Charles Talbot, Raymond Biastoch, Christopher Luszczek, and Andrew Medeiros for assistance in sediment core collection, Fan Yang and Johan Wiklund for sediment core dating, and Christine Spencer for guidance and assistance in the laboratory.

Thirdly, I would like to thank the Natural Science and Engineering Research Council (NSERC) of Canada for a post-graduate scholarship. I would also like to thank the Northern Contaminants Program, Environment Canada Chemical Management Plan, Environment Canada Grants and Contributions, Polar Continental Shelf Program, NSERC, and Garfield Weston Foundation for funding.

Lastly, I would also like to thank all family and friends that provided unwavering support during my pursuit of this degree.

Table of Contents

Abstract	i
Acknowledgements.....	ii
List of Tables	ix
List of Figures	xix
List of Abbreviations, Acronyms, and Symbols.....	xxvi
List of Appendices	xxx
Preface.....	xxxii
1 Introduction.....	1
1.1 Overview of Per- and Polyfluoroalkyl Substances	2
1.2 PFAS Manufacturing	4
1.2.1 Electrochemical Fluorination.....	4
1.2.2 Telomerization	5
1.2.3 Utility of PFAS in Industrial and Commercial Applications.....	5
1.2.4 Environmental Emissions of PFAS during Manufacturing, Usage, and Waste Disposal.....	7
1.2.5. Rationale for Industry Phase-out and Domestic/International Regulations on PFAS	10
1.3 Long-range Transport of PFAS to the High Arctic	12
1.4 Atmospheric Chemistry	15
1.5 PFAS in the Arctic Abiotic Environment	19

1.5.1 Arctic Atmosphere	19
1.5.2 Arctic Landscape and Freshwater Environment	27
1.5.2.1 Water	27
1.5.2.2 Lake Sediments	30
1.5.2.3 Soil	32
1.5.2.4 Non-marine Snow and Ice	33
1.5.3 Arctic Marine Environment	36
1.5.3.1 Seawater	36
1.5.3.2 Marine Snow and Ice	41
1.6 Climate Warming in the High Arctic	42
1.6.1 Climate Implications for PFAS in the Arctic	45
1.7 Objectives and Goals	46
1.8 Literature Cited	49
2 Emerging Investigator Series: A 14-year Depositional Ice Record of Perfluoroalkyl Substances in the High Arctic	60
2.1 Abstract	61
2.2 Introduction	62
2.3 Methods	63
2.3.1 Sample Collection	63
2.3.2 Sample Analysis	64
2.4 Results and Discussion	66
2.4.1 PFCA on the Devon Ice Cap	66

2.4.2 PFSA and FOSA on the Devon Ice Cap	73
2.4.3 Temporal Trends	74
2.4.4 Direct Transport of PFAS to the Arctic	78
2.5 Conclusions	83
2.6 Literature Cited	85
3 Characterization of Perfluoroalkyl Substances in Sediment Cores from High and Low Arctic Lakes in Canada	96
3.1 Abstract	97
3.2 Introduction	99
3.3 Methods	102
3.3.1 Study Area	102
3.3.2 Sampling	105
3.3.3 Sample Extraction	106
3.3.4 Instrumental Analysis	107
3.3.5 Sediment Dating	107
3.3.6 Data Treatment	108
3.4 Results and Discussion	109
3.4.1 Composition of PFAS in Sediments	109
3.4.2 Temporal Trends	113
3.4.3 Implications for PFAS Deposition in the Arctic of Canada	122
3.5 Conclusions	125
3.6 Literature Cited	126

4 Fate and Transport of Perfluoroalkyl Substances from Snowpacks into a Lake in the High Arctic of Canada	134
4.1 Abstract	135
4.2 Introduction	136
4.3 Methods	139
4.3.1 Study Area	139
4.3.2 Sampling	141
4.3.3 Sample Extraction	142
4.3.4 Instrumental Analysis	143
4.3.5 Data Treatment	143
4.4 Results and Discussion	144
4.4.1 Concentrations and Loads of PFAS in Snowpacks	144
4.4.2 Indirect Sources of PFAS in Snowpacks	148
4.4.3 Direct Sources of PFAS in Snowpacks	153
4.4.4 Seasonal Melting Inputs of PFAS into the Lake Hazen Water Column	156
4.5 Conclusions	161
4.6 Literature Cited	162
5 Permafrost and Glacier Melt as Sources of Perfluoroalkyl Substances to Freshwater Ecosystems of the High Arctic of Canada	170
5.1 Abstract	171
5.2 Introduction	173
5.3 Methods	175

5.3.1 Study Area	175
5.3.2 Sampling	177
5.3.3 Sample Extraction	179
5.3.4 Instrument and Data Analysis	179
5.4 Results and Discussion	180
5.4.1 Composition of PFAS along the Skeleton Continuum	180
5.4.2 Transport and Partitioning of PFAS along the Skeleton Continuum.....	186
5.4.3 PFAS in Rivers from the Lake Hazen Watershed	189
5.4.4 Glacial Riverine Discharge of PFAS into Lake Hazen.....	192
5.5 Conclusions	195
5.6 Literature Cited	197
6 Conclusions.....	202
6.1 Summary	203
6.2 Future Outlook	204
6.2.1 Atmospheric Transport and Fate of PFAS in the Arctic.....	204
6.2.2 Implications of Climate Warming on PFAS in the Arctic.....	205
6.3 Literature Cited	208
Appendix A Supporting Information for Chapter 2.....	210
Section A1 Chemicals and QA/QC.....	211
Appendix B Supporting Information for Chapter 3	221
Section B1 Study Area.....	222
Section B2 Chemicals.....	222

Section B3 Sediment Extraction	223
Section B4 QA/QC	225
Section B5 Determining Sedimentation Rates in the High Arctic.....	226
Section B6 Temporal Trends in Lake Hazen and Lake B35 Sediments, and Wildlife Bank Tissue Archives	227
Literature Cited	240
Appendix C Supporting Information for Chapter 3	243
Section C1 Chemicals	244
Section C2 QA/QC	245
Literature Cited	263
Appendix D Supporting Information for Chapter 4.....	264
Section D1 Chemicals.....	265
Section D2 QA/QC	266
Literature Cited	276

List of Tables

Table 1.1 Overview of PFAS acronyms and formulae.	3
Table 1.2 Summary of PFCA and PFSA precursors (i.e., neutral PFAS) concentrations (pg m ⁻³) during active air monitoring campaigns in the High Arctic. Detection frequencies are shown in parenthesis.	21
Table 1.3 Summary of PFAA concentrations (pg m ⁻³) during active and passive air monitoring campaigns in the High Arctic. Mean concentrations are presented in brackets. Data from Rauert et al. ³⁴ corresponds to April-September sampling periods. The annotation “High Volume” refers to active air sampling and SIP-PAS designates passive air sampling using polyurethane foam and XAD-resin combined in a sorbent-impregnated passive sampling device.	26
Table 1.4 PFAA concentrations (ng L ⁻¹) in lake waters from the High Arctic of Canada and Norway. Mean concentrations are presented in parenthesis where available.....	28
Table 1.5 PFAA concentrations (pg L ⁻¹) in surface snow from the High Arctic of Canada and Norway, and the Central Arctic. Mean concentrations are presented in parentheses where available.	34
Table 3.1 An overview of the Lake Hazen and Lake B35 study areas. Annual precipitation data for Lake Hazen and Lake B35 is reported by Thompson et al. ³⁰ and Environment and Climate Change Canada. ³¹ *Corresponds to the mid-basin depth due to unknown bathymetry in this lake.....	104

Table 3.2 Comparison of doubling times (and 95% confidence interval) of PFAS fluxes in Lake Hazen and Lake B35 sediments with reported sediment and wildlife bank tissue archives. Doubling times for all sites are calculated using only detected concentrations.	115
Table 3.3 Comparison of mean PFAS sedimentation fluxes ($\text{ng m}^{-2} \text{ year}^{-1}$) in Lake Hazen and Lake B35 sediments to Lake Ontario sediment sediments. ³⁵ Sedimentation rates are expressed in $\text{g cm}^{-2} \text{ year}^{-1}$. Range of fluxes are presented in parentheses.	116
Table 4.1 Concentrations of PFAS (ng L^{-1}) in light and dark snowpacks collected from the Lake Hazen region during 2013 and 2014 (this study) and literature survey of other locations. Compounds not measured are designated as N.M.	145
Table 5.1 Concentration ranges (ng L^{-1}) and detection frequencies (%) of PFAS along the Skeleton Continuum and in glacial rivers during July-August 2015. Detection frequencies are calculated as the percent number of samples out of the sampling dates (<i>n</i>) with concentrations equal to or greater than the LOD and are presented in bold text in parentheses. PFDoDA, PFHxDA, and PFDS are <LOD in all samples.	181
Table 5.2 Glacial inputs (kg) and the net change (Δ_{PFAS} , kg) of total PFAS, PFCA, and PFSA in the Lake Hazen watershed during 2015. Glacial inputs are calculated as the sum of daily glacial riverine fluxes during the 2015 glacier melting season from 1 June to 19 August. Fluxes are estimated using a LOADEST log-linear model. Uncertainty is represented by standard error.	193

Table A1 PFAS concentrations (ng L ⁻¹) in field, stay, and method blanks, as well as the limits of detection (LOD) and quantitation (LOQ). Stay and field blanks consist of 500 mL of HPLC grade water.	212
Table A2 Recovery of internal and instrument performance standards in sample extracts. Internal standards are added before extraction to monitor recovery and instrument performance standards are added after extraction prior to analysis to monitor matrix effects. Recovery is based on a comparison of internal standard peak area in sample extracts to the peak area in a solvent standard at equivalent concentrations. Mean (standard error) recovery reported for n=18 samples from the Devon Ice Cap.	213
Table A3 Overview of native, internal, and instrument performance PFAS standards...	214
Table A4 Overview of precursor/product ion mass-to-charge ratios (m/z), cone voltages (V), and collision energies (eV) for PFAS analysis on the Devon Ice Cap. Product ion scans for PFCA target perfluoroalkyl moieties (i.e., F(CF ₂) _x CO ₂ ⁻ to F(CF ₂) _x), while product ion scans for PFSA target sulfonic acid moieties (i.e., F(CF ₂) _x SO ₃ ⁻ to FSO ₃ ⁻ or SO ₃ ⁻). The product ion scan for FOSA targets a SO ₂ N moiety (i.e., CF ₃ (CF ₂) ₇ SO ₂ NH ₂ to SO ₂ N).	215
Table A5 Overview of precursor/product ion mass-to-charge ratios, cone voltages (V), and collision energies (eV) for internal and instrument performance PFAS standard analysis.	216
Table A6 Summary of chromatographic, mass spectrometric, and inlet conditions.	217

Table A7 Overview of PFAS concentrations (pg L^{-1}) in the snowpit from the Devon Ice Cap. Detection frequency (%) is calculated as the number samples equal to or greater than the LOD, divide by the sample size, and multiply by 100.218

Table A8 Spearman rank correlation analysis of natural log-transformed PFAS concentrations (ng L^{-1}) in snow collected from the Devon Ice Cap ($n=28$) from 1993 to 2007. Spearman rank correlation coefficients (r_s) is used to evaluate correlation strength on PFAS concentrations equal to or greater than the LOQ for congeners with detection frequencies equal to or greater than 50%.....219

Table A9 First-order kinetics of natural log-transformed PFAS fluxes on the Devon Ice Cap during 1993-2007. Temporal trends are determined using natural log-transformed PFAS mass flux ($\text{ng m}^{-2} \text{ year}^{-1}$) for congeners with detection frequencies $\geq 50\%$. Doubling times (t_2) and half-life ($t_{1/2}$) are calculated using the first-order rate (k) obtained from the slope of a linear regression of natural log-transformed mass flux versus year of deposition. Standard error is used to represent the uncertainty of k , while a 95% confidence interval (CI) represents the uncertainty for t_2 and $t_{1/2}$. The temporal trend for PFBS spans a period of 1996-2007 due to concentrations $< \text{LOD}$ in samples. Statistically significant ($p < 0.05$) temporal trends are not observed for PFBA, PFHxA, PFTrDA, PFOS, PFECHS, and FOSA.....220

Table B1 Overview of native, internal, and instrument performance PFAS standards...229

Table B2 Summary of PFAS concentrations (pg g^{-1} dw) in method blanks, with corresponding LOD and LOQ. FOSA is not measured (N.M) in Lake B35 samples.230

Table B3 Recoveries of internal, instrument performance standards, and native spike and recovery experiments in Lake Hazen and Lake B35 sediments. Internal standards are added before extraction to monitor recovery and instrument performance standards are added after extraction prior to analysis to monitor matrix effects. Recovery is based on a comparison of internal standard peak area in sample extracts to the peak area in a solvent standard at equivalent concentrations. The uncertainty is represented by standard deviation. FOSA is not measured (N.M) in Lake B35 samples.....231

Table B4 Overview of precursor/product ion mass-to-charge ratios (m/z), cone voltages (V), and collision energies (eV) for PFAS analysis in Arctic sediments. Product ion scans for PFCA target perfluoroalkyl moieties (i.e., $\text{F}(\text{CF}_2)_x\text{CO}_2^-$ to $\text{F}(\text{CF}_2)_x$), while product ion scans for PFSA target sulfonic acid moieties (i.e., $\text{F}(\text{CF}_2)_x\text{SO}_3^-$ to FSO_3^- or SO_3^-). The product ion scan for FOSA targets a SO_2N moiety (i.e., $\text{CF}_3(\text{CF}_2)_7\text{SO}_2\text{NH}_2$ to SO_2N) and product ion scans for ADONA and Cl-PFESA target perhalogenated alkoxy moieties (i.e., $\text{CF}_3\text{O}(\text{CF}_2)_3\text{OCHFCF}_2\text{CO}_2^-$ to CF_3O or $\text{CF}_3\text{O}(\text{CF}_2)_3\text{O}$ for ADONA and $\text{ClCF}_2(\text{CF}_2)_5\text{O}(\text{CF}_2)_2\text{SO}_3^-$ to $\text{ClCF}_2(\text{CF}_2)_5\text{O}$ for 6:2 Cl-PFESA).232

Table B5 Overview of precursor/product ion mass-to-charge ratios, cone voltages (V), and collision energies (eV) for internal and instrument performance PFAS standard analysis.	233
Table B6 Overview of liquid chromatograph, mass spectrometric, and inlet parameters used for PFAS sediment analysis.	234
Table B7 Overview of blank-, extraction-, and matrix-corrected PFAS concentrations ($\mu\text{g g}^{-1}$ dw) in Lake B35 and Lake Hazen sediments. Detection frequency (%) is calculated as the number samples equal to or greater than the LOD, divide by the sample size, and multiply by 100.	235
Table B8 First-order kinetics of natural log-transformed PFAS fluxes in Lake Hazen sediments from a 0-16 cm depth and Lake B35 from a 0.0-4.5 cm depth, corresponding to depositional periods of 1963-2011 and 1952-2009, respectively. Temporal trends are determined using natural log-transformed PFAS mass flux ($\text{ng m}^{-2} \text{ year}^{-1}$) for congeners with detection frequencies $\geq 50\%$. Doubling times (t_2) are calculated using the first-order rate (k) obtained from the slope of a linear regression of natural log-transformed mass flux versus year of deposition. Standard error is used to represent the uncertainty of k , while a 95% confidence interval (CI) represents the uncertainty for t_2 . Statistical significance is set to 5%. Temporal trends for PFOA, PFDA, PFBS, and PFOS span a temporal period of 1963-2011, 1975-2009, 1975-2011, and 1975-2011, respectively due to concentrations $< \text{LOD}$ in samples. For Lake B35, temporal trends for PFHpA, PFOA, PFNA, and PFUnDA span a temporal	

period from 1986-2009, 1952- 2009, 1963-2009, and 1963-2009, respectively, due to concentrations <LOD in samples.	236
Table B9 Spearman rank correlation analysis (r_s) of paired (n) natural log-transformed PFAA fluxes in Lake Hazen and Lake B35 sediments with natural-log transformed fluorotelomer-based (FT) and perfluorooctane sulfonyl fluoride (POSF) production volumes (ton year ⁻¹). ^{16,17} Correlation analysis is applied to natural log-transformed PFAA fluxes and production volumes during 1963-2005 and 1963-2009 in Lake Hazen and Lake B35, respectively.	237
Table C1 Hydrological cycle in the Lake Hazen watershed, adapted from St. Pierre et al. 2019. ¹	246
Table C2 Snow and water column sampling in the Lake Hazen watershed.	247
Table C3 Overview of native, internal, and instrument performance PFAS standards. ...	248
Table C4 Summary of native PFAS concentrations (ng L ⁻¹) in HPLC-grade water transported to the field site (field blank), HPLC grade water kept in the lab (stay blank), and method blanks. Method blanks correspond to Oasis® WAX SPE cartridge blanks.....	249
Table C5 Summary of mean ± standard error recovery of internal, instrument performance standards, and native spike and recovery experiments in Lake Hazen water samples. The recovery of internal and instrument performance standards in Lake Hazen water samples is calculated by comparing analyte peak area in water	

extracts to analyte peak area in a solvent standard at equivalent concentration. N/A refers analytes without an available corresponding isotopically labeled standard...250

Table C6 Overview of precursor/product ion mass-to-charge ratios (m/z), cone voltages (V), and collision energies (eV) for native PFAS analysis. Product ion scans for PFCA target perfluoroalkyl moieties (i.e., $F(CF_2)_xCO_2^-$ to $F(CF_2)_x$), while product ion scans for PFSA target sulfonic acid moieties (i.e., $F(CF_2)_xSO_3^-$ to FSO_3^- or SO_3^-). The transition for FOSA targets a SO_2N moiety (i.e., $CF_3(CF_2)_7SO_2NH_2$ to SO_2N).
.....251

Table C7 Overview of precursor/product ion mass-to-charge ratios, cone voltages (V), and collision energies (eV) for internal and instrument performance PFAS standard analysis.252

Table C8 Overview of liquid chromatograph, mass spectrometric, and inlet parameters used for PFAS quantitation in Lake Hazen snow and water samples.253

Table C9 Detection frequencies for PFAS in snow and water. Detection frequency (%) is calculated as the number samples equal to or greater than the LOQ, divide by the sample size, and multiply by 100.254

Table C10 Spearman rank correlation (r_s) analysis of natural log-transformed PFAS concentrations ($ng\ L^{-1}$) in light snowpacks collected from the Lake Hazen watershed during May 2013. PFAS concentrations equal to or greater than the LOQ for congeners with detection frequencies equal to or greater than 50% are included in correlation analysis.255

Table C11 Spearman rank correlation (r_s) analysis of natural log-transformed PFAS concentrations (ng L^{-1}) in light snowpacks collected from Lake Hazen ice during June 2014. PFAS concentrations equal to or greater than the LOQ for congeners with detection frequencies equal to or greater than 50% are included in correlation analysis.	256
Table C12 Spearman rank correlation (r_s) analysis of natural log-transformed PFAS concentrations (ng L^{-1}) in dark snowpacks collected from Lake Hazen ice during June 2014. PFAS concentrations equal to or greater than the LOQ for congeners with detection frequencies equal to or greater than 50% are included in correlation analysis.	257
Table C13 Spearman rank correlation (r_s) analysis of natural log-transformed PFAS (ng L^{-1}) and major ion ($\mu\text{g L}^{-1}$ or mg L^{-1}) concentrations in light snowpacks collected from Lake Hazen ice during June 2014. Correlation analysis is limited to PFAS concentrations equal to or greater than the LOQ for congeners with detection frequencies equal to or greater than 50%.	258
Table C14 Spearman rank correlation (r_s) analysis of natural log-transformed PFAS (ng L^{-1}) and major ion ($\mu\text{g L}^{-1}$ or mg L^{-1}) concentrations in dark snowpacks collected from Lake Hazen ice during June 2014. Correlation analysis is limited to PFAS concentrations equal to or greater than the LOQ for congeners with detection frequencies equal to or greater than 50%.	259
Table D1 Location of sampling sites along the Skeleton Continuum.	258

Table D2 Hydrological overview of glacier-fed tributaries in the Lake Hazen watershed. ¹ Uncertainty is denoted by the standard error estimated daily from July 1 to August 15 2015.	258
Table D3 Overview of native, internal, and instrument performance PFAS standards. Internal standards are added before extraction to monitor recovery and instrument performance standards are added after extraction prior to analysis to monitor matrix effects.....	268
Table D4 Limits of detection and quantification, and PFAS concentrations (ng L ⁻¹) in field and stay blanks.	269
Table D5 Overview of precursor/product ion mass-to-charge ratios (m/z), cone voltages (V), and collision energies (eV) for native PFAS analysis. Product ion scans for PFCA target perfluoroalkyl moieties (i.e., F(CF ₂) _x CO ₂ ⁻ to F(CF ₂) _x), while product ion scans for PFSA target sulfonic acid moieties (i.e., F(CF ₂) _x SO ₃ ⁻ to FSO ₃ ⁻ or SO ₃ ⁻). The transition for FOSA targets a SO ₂ N moiety (i.e., CF ₃ (CF ₂) ₇ SO ₂ NH ₂ to SO ₂ N).	270
Table D6 Overview of precursor/product ion mass-to-charge ratios, cone voltages (V), and collision energies (eV) for internal and instrument performance PFAS standard analysis.	271
Table D7 Overview of liquid chromatograph gradient elution, mass spectrometric, and inlet parameters used for PFAS quantitation along the Skeleton Continuum and in glacial rivers.	272

List of Figures

- Figure 1.1 Structures of Industrially Produced PFAS including the perfluoroalkyl acids (PFAA) such as perfluoroalkyl sulfonic acids (PFSA) and perfluoroalkyl carboxylic acids (PFCA) and precursors which can undergo environmental transformation to produce PFCA and PFSA.7
- Figure 1.2 Direct and Indirect Sources of PFAA.....8
- Figure 1.3 Atmospheric oxidation mechanism for a $x:2$ fluorotelomer alcohol (FTOH) producing perfluoroalkyl carboxylic acids (PFCA) with x and $x+1$ carbons in a 1:1 ratio. Atmospheric reagents include hydroxyl radicals ($\cdot\text{OH}$), oxygen (O_2), nitric oxide ($\text{NO}\cdot$), hydroperoxyl radicals ($\text{HO}_2\cdot$), and alkyl peroxy radicals ($\text{ROO}\cdot$). Perfluoroalkyl radical unzipping produces shorter chain PFCA. Other products formed are fluorotelomer aldehyde (FTAL), perfluoroalkyl aldehyde (PFAL), water (H_2O), nitrogen dioxide (NO_2), carbon dioxide (CO_2), and HF (hydrofluoric acid). The mechanism is adapted from Wallington et al.⁴16
- Figure 1.4 Atmospheric oxidation mechanism for N-methyl polyfluoroalkyl sulfonamido ethanol (N-MeFASE) producing perfluoroalkyl sulfonic acid (PFSA) and perfluoroalkyl radicals. Perfluoroalkyl radical can react with peroxy radicals and water to produce PFCA. PFSAm oxidation yields PFSA and PFCA in a 1: 10 ratio. The mechanism is adapted from D'eon et al.⁴⁶18
- Figure 1.5 Map of air monitoring stations in the High Arctic. Stations are designated by colored circles: yellow (Andøya, Norway), red (Zeppelin, Norway), orange (Station

Nord, Greenland), blue (Alert, Nunavut), and green (Cornwallis Island). Map source: Ocean Data View (Schlitzer, R., Ocean Data View, <https://odv.awi.de>, 2019.).20

Figure 1.6 Overview of global seawater Σ PF_{AA} concentrations (pg L^{-1}).^{26,38,44,53,57,59} The magnitude of Σ PF_{AA} concentration is proportional to the size of green circles and is indicated numerically at select sites. Map source: Global Topography Relief Raster in Igor Pro (v 6.37).37

Figure 1.7 Long-term records of mean temperature ($^{\circ}\text{C}$, y-axes) and number of ice days at High (Eureka, 80°N) and Low (Baker Lake, 64°N) Arctic regions in Canada as a function of time (year, x-axis). Ice days refers to the number of days where the maximum daily temperature is equal to or less than 0°C . Empirical measurements are denoted by red lines and modelled measurements are denoted by blue lines. Modelled measurements are estimated according to greenhouse gas concentration estimates from Representative Concentration Pathway 8.5. Historical and modelled data are obtained from www.climatedata.ca.43

Figure 2.1 Comparison of PF_{AA} concentrations from sampling campaigns at the Devon Ice Cap in 2006⁶ and 2008.67

Figure 2.2 Flux ratios of even-odd PF_{CA} as a function of year on the Devon Ice Cap. ...69

Figure 2.3 PF_{AS} fluxes on the Devon Ice Cap (a) PF_{OS} from Young et al.;⁶ (b) PF_{OS}; (c) PF_{BS}; (d) F_{OSA}. Lines represent three-year moving averages.75

Figure 2.4 Comparison of chloride: sodium molar ratios on the Devon Ice Cap to expected ocean ratios. The dashed orange line corresponds to the average chloride: sodium ratio on the Devon Ice Cap, and the dashed black line corresponds to the expected ocean ratio. ⁶¹	79
Figure 2.5 Ratios of observed concentrations in the Devon Ice Cap in 2004-2006 compared to levels in the Canadian Archipelago and Arctic Oceans collected in 2005 and to the Atlantic Ocean. ⁶³	80
Figure 3.1 Concentration profiles (ng g ⁻¹ dw) of PFAS in sediment cores versus midpoint depth (left y-axes, cm) and year (right y-axes) in Lake Hazen (top panel) and Lake B35 (bottom panel). The legend applies to both panels.	112
Figure 3.2 Natural log-transformed PFAS fluxes (ng m ⁻² year ⁻¹) into Lake Hazen (solid black circles, 1923-2011), and Lake B35 (solid red squares, 1940-2009) sediments. Fluxes are estimated at Lake Hazen (unfilled circles) and Lake B35 (unfilled squares) using substituted sediment concentrations equal to LOD.	114
Figure 3.3 Comparison of glacier meltwater discharge (Gt year ⁻¹ , left y-axis, grey bars) in the Lake Hazen watershed and PFOA fluxes (ng m ⁻² year ⁻¹ , right y-axis, red line) in the Lake Hazen sediment core versus time (bottom x-axis, 1963-2011). PFOA fluxes are estimated for Lake Hazen data <LOD by using LOD-substituted concentrations for flux calculations.	119

Figure 3.4 Comparison of PFOA and PFOS flux deposition ($\text{ng m}^{-2} \text{ year}^{-1}$, y-axis) in Lake Hazen and Lake B35 sediment to an ice core from the summit of the Devon Ice Cap¹⁸ over a 1982-2011 temporal period. PFAS fluxes are estimated for Lake Hazen data <LOD by using LOD-substituted concentrations for flux calculations. 123

Figure 4.1 Map of Lake Hazen and surrounding area in Quttinirpaaq National Park, Ellesmere Island, Canada. Triangles indicate peaks and corresponding elevations, labels in grey italics correspond to glaciers and in blue are major rivers. Map adapted from Toporama (<https://atlas.gc.ca/toporama/en/index.html>). Toporama is a public on-line mapping service developed by Natural Resources Canada and is licensed under the Open Government Licence of Canada..... 140

Figure 4.2 PFAS loads in snowpacks collected in 2013 (n=6 sites) and in paired light and dark snowpacks in 2014 (n=8 sites) from the ice surface of Lake Hazen. Box is 25-75% range, line is the median and whiskers are the 95% confidence interval..... 146

Figure 4.3 Even-odd PFCA concentration ratios in light and dark snowpacks from the Lake Hazen region during 2013-2014. Ratios in light snowpacks collected during 2013 are represented by black triangles, while light and dark snowpacks collected during 2014 are represented by red circles and blue diamonds, respectively. Solid black lines correspond to even-odd ratios within a factor of 1, while the dashed red lines correspond to even-odd ratios within a factor of 6, which represents the range of ratios expected from the oxidation of FTOH in the presence of heterogeneous particles.³² 150

Figure 4.4 PFAS depth profiles in the Lake Hazen water column during ice-covered periods on 15-18 May 2013 and 19-22 May 2014; during snowmelt on 2-4 June 2012 (0.5, 20, 80, 200, 258 m depths) and 29-30 May 2014; as well as during an ice-free period on 27-29 July 2015. Concentrations (left panels, ng L^{-1}) and composition (right panels, % of ΣPFAS) profiles correspond to depths between 0 to 258 m.157

Figure 5.1 Overview of sites along the Skeleton Continuum. Sampling sites S1 through S5 are represented by coloured circles and legend. Location of the Lake Hazen base camp and the glacier-fed river, Blister Creek are also shown. Map source: ESRI World Imagery base map. Inset map presents location of Lake Hazen on Ellesmere Island and the two closest human settlements: Grise Fiord (population 129) on Ellesmere Island and Resolute (population 198) on Cornwallis Island. Inset map source: Toporama (atlas.gc.ca), a topographic reference product produced by Natural Resources Canada using CanVec data.....178

Figure 5.2 Concentrations (ng L^{-1}) of PFBA and other PFAS along the Skeleton Continuum (A) from July 9 to August 1 2015. * indicates no sampling was conducted because Skeleton Creek began flowing on July 18. Lake Hazen snow from May 2013 and June 2014 are shown in (B).182

Figure 5.3 PFAS composition (%) along the Skeleton Continuum (A) from July 9 to August 1 2015 and Lake Hazen snow (B) sampled during May 2013 and June 2013. * indicates no sampling was conducted because Skeleton Creek began flowing on July 18.183

Figure 5.4 Map (top), concentration (ng L^{-1}) and composition (% , bottom) of PFAS in rivers from the Lake Hazen watershed in July 2015. Map source: ESRI.....	190
Figure B1 Activity profiles (x-axes, disintegrations per minute per gram, dpm g^{-1}) of unsupported ^{210}Pb (black circles) and ^{137}Cs (red squares) in Lake Hazen and Lake B35 sediments. Depth (midpoint, cm) and corresponding yearly interval are plotted on the left and right y axes, respectively. Error bars correspond to the uncertainty of ^{210}Pb and ^{137}Cs analysis.	238
Figure B2 Natural-log transformed PFAA fluxes ($\text{ng m}^{-2} \text{ year}^{-1}$, red circles) and concentrations ($\text{ng g}^{-1} \text{ dw}$, black squares) in Lake Hazen sediments as a function of year and depth (cm), respectively.....	239
Figure C1 Lake Hazen study area: a) 2014 sampling sites for paired light and dark snowpacks and b) photograph of ice surface of Lake Hazen during 2014. Frequent windstorms in the Lake Hazen region created distinct snow drifts with different enrichments of particles.	260
Figure C2 Comparison of molar ratios (left and right y axes) of major ions in paired light (blue circles) and dark (orange triangles) snowpacks collected from Lake Hazen ice during 2014. Expected molar ratios of major ions in ocean water are represented by a dashed line. ^{2,3}	261
Figure C3 PFAS depth profiles in the Lake Hazen water column before (red circles) and during (black squares) snowmelt in May 2014. Concentration (ng L^{-1}) profiles	

correspond to depths between 0 to 250 m. Concentrations less than the LOD are substituted with LOD concentrations before (unfilled circles) and during snowmelt (unfilled squares).262

Figure D1 Photo of water flowing from a seep in the uplands of the Skeleton Continuum in the Lake Hazen watershed.273

Figure D2 Meteorological conditions at Lake Hazen: a) mean \pm standard deviation daily temperature and maximum daily temperature and b) mean \pm standard deviation daily wind speed, based on hourly recording from July 5 to August 2 using a CR10X Weather logger (Campbell Scientific).274

Figure D3 Glacial riverine fluxes of total PFAS in the Lake Hazen watershed from 1 June to 19 August 2015. Glacial riverine fluxes are estimated using a LOADEST log-linear model.275

List of Abbreviations, Acronyms, and Symbols

pK _a	acid dissociation constant
ADONA	ammonium 4,8-dioxa-3H-perfluorononanoate
APFO	ammonium perfluorooctanoate
AFFF	aqueous film-forming foams
AWV	areal water volume
bar	barometric pressure
BASL	Biogeochemical Analytical Service Laboratory
BC	black carbon
CCIW	Canada Centre for Inland Waters
cm	centimeter
r ²	coefficient of determination
CI	confidence interval
CRS	constant rate of supply
cm ³	cubic centimeter
km ³	cubic kilometer
m ³	cubic meter
CE	current era
°	degrees
°C	degrees Celsius
°N	degrees north
°W	degrees west
dpm	disintegrations per minute
K _d	distribution coefficient
t ₂	doubling time
dw	dry weight
ECF	electrochemical fluorination
EtFOSA	ethyl perfluorooctane sulfonamide
EtFOSE	ethyl perfluorooctane sulfonamido ethanol
BEH	ethylene bridged hybrid
EU	European Union
k	first-order rate constant
FT	fluorotelomer
FTOH	fluorotelomer alcohols
FTAL	fluorotelomer aldehydes
FTCA	fluorotelomer carboxylic acids
FTI	fluorotelomer iodides
FTSA	fluorotelomer sulfonic acids
FTUCA	fluorotelomer unsaturated carboxylic acid
FF	focusing factor
Gt	gigaton
GAPS	Global Atmospheric Passive Sampling

g	gram
g_f	gravitational force
$t_{1/2}$	half-life
HPLC	high-performance liquid chromatography
hr	hour
HFC	hydrofluorocarbons
HFE	hydrofluoroethers
I.D.	internal diameter
kg	kilogram
km	kilometer
kt	kiloton
kV	kilovolt
LAP	light-absorbing particles
LOD	limit of detection
LOQ	limit of quantitation
L	liter
m/z	mass-to-charge ratio
m	meter
MeOH	methanol
MeHg	methyl mercury
MeFBSA	methyl perfluorobutane sulfonamide
MeFBSE	methyl perfluorobutane sulfonamido ethanol
MeFOSA	methyl perfluorooctane sulfonamide
MeFOSE	methyl perfluorooctane sulfonamido ethanol
μg	microgram
μL	microliter
μm	micrometer
mg	milligram
mL	millilitre
mm	millimeter
mM	millimolar
min	minute
ng	nanogram
NO_x	nitrogen oxides
N.M	not measured
K_{oc}	organic carbon partitioning coefficient
OCP	organochlorine pesticides
PC	particulate carbon
PN	particulate nitrogen
r	Pearson correlation coefficient
PFAS	per- and polyfluoroalkyl substances
PFSAm	perfluoroalkane sulfonamido substances
PFAA	perfluoroalkyl acids
PFOH	perfluoroalkyl alcohol
PFAL	perfluoroalkyl aldehydes

PFCA	perfluoroalkyl carboxylic acids
PFAI	perfluoroalkyl iodides
FASA	perfluoroalkyl sulfonamides
FASE	perfluoroalkyl sulfonamido ethanols
PFBS	perfluorobutane sulfonic acid
PBSF	perfluorobutane sulfonyl fluoride
PFBA	perfluorobutanoic acid
PFDS	perfluorodecane sulfonic acid
PDSF	perfluorodecane sulfonyl fluoride
PFDA	perfluorodecanoic acid
PFDoDA	perfluorododecanoic acid
PFECHS	perfluoro-4-ethylcyclohexane sulfonic acid
PFHpS	perfluoroheptane sulfonic acid
PFHpA	perfluoroheptanoic acid
PFHxDA	perfluorohexadecanoic acid
PFHxS	perfluorohexane sulfonic acid
PHxSF	perfluorohexane sulfonyl fluoride
PFHxA	perfluorohexanoic acid
PFNA	perfluorononanoic acid
PFOcDA	perfluorooctadecanoic acid
POCF	perfluorooctane carbonyl fluoride
FOSA	perfluorooctane sulfonamide
PFOS	perfluorooctane sulfonic acid
POSF	perfluorooctane sulfonyl fluoride
PFOA	perfluorooctanoic acid
PFPeA	perfluoropentanoic acid
PFTeDA	perfluorotetradecanoic acid
PFTrDA	perfluorotridecanoic acid
PFUnDA	perfluoroundecanoic acid
pg	picogram
PCTFE	polychlorotrifluoroethylene
PFECA	polyfluoroalkyl ether carboxylic acids
PFESA	polyfluoroalkyl ether sulfonic acids
diPAP	polyfluoroalkyl phosphate diester
PP	polypropylene
PTFE	polytetrafluoroethylene
PUF	polyurethane foam
PVDF	polyvinylidene fluoride
p-value	probability value
QA/QC	quality assurance/quality control
QEI	Queen Elizabeth Islands
REACH	Registration, Evaluation, Authorization and Restriction of Chemicals
RH	relative humidity
s	second
C _{sed}	sediment concentration

F_{sed}	sedimentation flux
R_{sed}	sedimentation rate
S/N	signal-to-noise ratio
SPE	solid phase extraction
SIP-PAS	sorbent impregnated-passive air sampler
r_s	Spearman correlation coefficient
cm^2	square centimeter
km^2	square kilometer
m^2	square meter
SE	standard error
SD	standard deviation
SML	surface microlayer
MS/MS	tandem mass spectrometry
TFE	tetrafluoroethylene
THg	total mercury
UPLC	ultra-performance liquid chromatography
US EPA	United States Environmental Protection Agency
USA	United States of America
V	volts
v/v	volume/volume ratio
WAX	weak anion exchange

List of Appendices

Appendix A – Supporting Information for Chapter 2

Appendix B – Supporting Information for Chapter 3

Appendix C – Supporting Information for Chapter 4

Appendix D – Supporting Information for Chapter 5

Preface

This thesis is composed of a series of manuscripts published in or to be submitted to peer-reviewed journals. As such, repetition of introductory and experimental material is unavoidable. All manuscripts are written by John J. MacInnis, with critical comments provided by Amila De Silva and co-authors, as outlined below.

Chapter One – Introduction

Author List – John J. MacInnis

Contributions – This chapter was prepared by John J. MacInnis with editorial comments provided by Amila De Silva.

Chapter Two – Emerging investigator series: a 14-year depositional ice record of perfluoroalkyl substances in the High Arctic

Chapter Two is published as a full article and has been reproduced and adapted from reference *Sci.: Processes Impacts*, 2017, 19, 22-30, with permission from the Royal Society of Chemistry.

Author List – John J. MacInnis, Katherine French, Derek C.G. Muir, Christine Spencer, Alison Criscitiello, Amila O. De Silva, and Cora J. Young

Contributions – This manuscript was prepared by John J. MacInnis with editorial comments provided by Alison Criscitiello, Amila O. De Silva, Derek C.G. Muir and Cora J. Young. Sample collection and planning was led by Derek Muir and Torsten Meyer. Ice core dating was completed by Torsten Meyer. Sample extraction and analysis was

completed by Christine Spencer. Data analysis and responding to Reviewer comments was led by John J. MacInnis, Amila O. De Silva, and Cora Young.

Chapter Three – Characterization of Perfluoroalkyl Substances in Sediment Cores from High and Low Arctic Lakes in Canada

© 2019. Chapter Three is published as a full article from reference *Sci. Total Environ.* 2019, 666, 414-422, with permission from the Publisher Elsevier and made available under the creative commons license CC-BY-NC-ND 4.0

license <http://creativecommons.org/licenses/by-nc-nd/4.0/>

Author List – John J. MacInnis, Igor Lehnerr, Derek C.G. Muir, Roberto Quinlan, and Amila O. De Silva

Contributions – This manuscript was prepared by John J. MacInnis with editorial comments provided by Igor Lehnerr, Derek C.G. Muir and Amila O. De Silva. Sample collection and planning was led by Derek C.G. Muir and Roberto Quinlan. Sediment core dating was completed by Fan Yang and Johan A. Wiklund. Sediment extractions and instrumental analysis was completed by John J. MacInnis. Data analysis and interpretation was completed by John J. MacInnis and Amila O. De Silva. Responding to Reviewer comments was led by John J. MacInnis and Amila O. De Silva.

Chapter Four – Fate and transport of perfluoroalkyl substances from snowpacks into a lake in the High Arctic of Canada

Chapter Four is published as a full article and has been reprinted (adapted) with permission from (*Environ. Sci. Technol.* 2019, 53, (18), 10753-10762). Copyright (2019) American Chemical Society.

Author List – John J. MacInnis, Igor Lehnerr, Derek C.G. Muir, Kyra St. Pierre, Vincent St. Louis, Christine Spencer, and Amila O. De Silva

Contributions – This manuscript was prepared by John J. MacInnis with editorial comments provided by Igor Lehnerr, Derek C.G. Muir, Kyra St. Pierre, Vincent St. Louis, and Amila O. De Silva. Sample collection and planning was led by Igor Lehnerr, Derek C.G. Muir, Kyra St. Pierre, and Vincent St. Louis. Sample extraction and analysis was completed by Christine Spencer and Amila De Silva. Data analysis and interpretation was completed by John J. MacInnis and Amila De Silva. Responding to Reviewer comments was led by John J. MacInnis and Amila O. De Silva.

Chapter Five – Permafrost and glacier melt as sources of perfluoroalkyl substances to freshwater ecosystems of the High Arctic of Canada

Author List – John J. MacInnis, Igor Lehnerr, Derek C.G. Muir, Kyra St. Pierre, Vincent St. Louis, Christine Spencer, and Amila O. De Silva

Contributions – This chapter was prepared by John J. MacInnis with editorial comments provided by Igor Lehnerr, Derek C.G. Muir, Kyra St. Pierre, Vincent St. Louis, and Amila O. De Silva. Sample collection and planning was led by Igor Lehnerr, Derek C.G. Muir, Kyra St. Pierre, and Vincent St. Louis. Sample extraction and analysis was completed by Christine Spencer and Amila De Silva. Data analysis and interpretation was completed by John J. MacInnis, Amila O. De Silva, and Kyra St. Pierre.

Chapter Six – Conclusions

Author List – John J. MacInnis

Contributions – Prepared by John J. MacInnis with editorial comments provided by
Amila De Silva.

1 Introduction

1.1 Overview of Per- and Polyfluoroalkyl Substances

Per- and polyfluoroalkyl substances (PFAS) are anthropogenic chemicals that were manufactured since the 1950s for industrial and commercial applications. PFAS contain a $F(CF_2)_x$ moiety, where x corresponds to the number of perfluorinated carbon atoms. Important classes of PFAS are fluorotelomer alcohols (FTOH) and per- and polyfluoroalkyl sulfonamido substances (PFSAm), which are precursors of perfluoroalkyl acids (PFAA).¹⁻⁴ FTOH contain a $F(CF_2)_x(CH_2)_yOH$ moiety and are named in a $x:y$ format, where x and y correspond to the number of perfluorinated and hydrogenated carbon atoms, respectively. PFSAm contain a $F(CF_2)_xSO_2N-R'R''$ moiety, where x corresponds to the number of perfluorinated carbon atoms, and R is an alkane, ethanol (i.e., CH_3CH_2OH), and/or hydrogen. PFAA are categorized into perfluoroalkyl carboxylic acids (PFCA, $F(CF_2)_xCO_2H$) and perfluoroalkyl sulfonic acids (PFSA, $F(CF_2)_xSO_3H$). PFCA and PFSA are classified on the basis of perfluoroalkyl chain length, whereby a long-chain PFCA has at least seven perfluorinated carbon atoms (i.e., $C_7F_{15}CO_2H$), and a long-chain PFSA has at least six perfluorinated carbon atoms (i.e., $C_6F_{13}SO_3H$). Polyfluoroalkyl ether carboxylic acids (PFECA) and polyfluoroalkyl ether sulfonic acids (PFESA) are replacement compounds for perfluorooctanoic acid (PFOA) and perfluorooctane sulfonic acid (PFOS), respectively (Section 1.2.4). PFESA are named according to the number of per- and polyfluoroalkyl carbon atoms bonded to the oxygen moiety. PFAS, including formulae and acronyms, is presented in Table 1.1. A comprehensive overview of legacy and emerging PFAS can be found in Pan et al.⁵

Table 1.1 Overview of PFAS acronyms and formulae.

Perfluoroalkyl carboxylic acid, PFCA		Perfluoroalkyl sulfonic acid, PFSA	
PFBA	$\text{CF}_3(\text{CF}_2)_2\text{CO}_2\text{H}$	PFBS	$\text{CF}_3(\text{CF}_2)_3\text{SO}_3\text{H}$
PFPeA	$\text{CF}_3(\text{CF}_2)_3\text{CO}_2\text{H}$	PFHxS	$\text{CF}_3(\text{CF}_2)_5\text{SO}_3\text{H}$
PFHxA	$\text{CF}_3(\text{CF}_2)_4\text{CO}_2\text{H}$	PFHpS	$\text{CF}_3(\text{CF}_2)_6\text{SO}_3\text{H}$
PFHpA	$\text{CF}_3(\text{CF}_2)_5\text{CO}_2\text{H}$	PFOS	$\text{CF}_3(\text{CF}_2)_7\text{SO}_3\text{H}$
PFOA	$\text{CF}_3(\text{CF}_2)_6\text{CO}_2\text{H}$	PFECHS	$\text{C}_6\text{F}_{10}(\text{CF}_2\text{CF}_3)\text{SO}_3\text{H}$
PFNA	$\text{CF}_3(\text{CF}_2)_7\text{CO}_2\text{H}$	PFDS	$\text{CF}_3(\text{CF}_2)_9\text{SO}_3\text{H}$
PFDA	$\text{CF}_3(\text{CF}_2)_8\text{CO}_2\text{H}$		
PFUnDA	$\text{CF}_3(\text{CF}_2)_9\text{CO}_2\text{H}$		
PFDoDA	$\text{CF}_3(\text{CF}_2)_{10}\text{CO}_2\text{H}$		
PFTTrDA	$\text{CF}_3(\text{CF}_2)_{11}\text{CO}_2\text{H}$		
PFTeDA	$\text{CF}_3(\text{CF}_2)_{12}\text{CO}_2\text{H}$		
PFHxDA	$\text{CF}_3(\text{CF}_2)_{14}\text{CO}_2\text{H}$		
PFOcDA	$\text{CF}_3(\text{CF}_2)_{16}\text{CO}_2\text{H}$		
Perfluoroalkyl ether carboxylic acid, PFECA		Chloro-perfluoroalkyl sulfonic acid, Cl-PFSA	
ADONA	$\text{CF}_3\text{O}(\text{CF}_2)_3\text{OCHFCF}_2\text{CO}_2^- \text{NH}_4^+$	8-Cl PFOS	$\text{ClCF}_2(\text{CF}_2)_7\text{SO}_3\text{H}$
Fluorotelomer alcohol, FTOH		Chloro-perfluoroalkyl ether sulfonate, Cl-PFESA	
4:2 FTOH	$\text{CF}_3(\text{CF}_2)_3(\text{CH}_2)_2\text{OH}$	6:2 Cl-PFESA	$\text{ClCF}_2(\text{CF}_2)_5\text{O}(\text{CF}_2)_2\text{SO}_3\text{H}$
6:2 FTOH	$\text{CF}_3(\text{CF}_2)_5(\text{CH}_2)_2\text{OH}$	8:2 Cl-PFESA	$\text{ClCF}_2(\text{CF}_2)_7\text{O}(\text{CF}_2)_2\text{SO}_3\text{H}$
8:2 FTOH	$\text{CF}_3(\text{CF}_2)_7(\text{CH}_2)_2\text{OH}$		
10:2 FTOH	$\text{CF}_3(\text{CF}_2)_9(\text{CH}_2)_2\text{OH}$		
12:2 FTOH	$\text{CF}_3(\text{CF}_2)_{11}(\text{CH}_2)_2\text{OH}$		
Fluoropolymers		Perfluoroalkyl sulfonamide	
PTFE	$\text{F}(\text{CF}_2\text{CF}_2)_n\text{F}$	FBSA	$\text{CF}_3(\text{CF}_2)_3\text{SO}_2\text{NH}_2$
PVDF	$\text{H}(\text{CH}_2\text{CF}_2)_n\text{F}$	FOSA	$\text{CF}_3(\text{CF}_2)_7\text{SO}_2\text{NH}_2$
PCTFE	$\text{F}(\text{CF}_2\text{CFCl})_n\text{F}$		
		N-alkyl polyfluoroalkyl sulfonamide, FASA	
		N-MeFBSA	$\text{CF}_3(\text{CF}_2)_3\text{SO}_2\text{N}(\text{CH}_3)(\text{CH}_3)\text{H}$
		N-EtFBSA	$\text{CF}_3(\text{CF}_2)_3\text{SO}_2\text{N}(\text{CH}_3)(\text{CH}_2\text{CH}_3)\text{H}$
		N-MeFOSA	$\text{CF}_3(\text{CF}_2)_7\text{SO}_2\text{N}(\text{CH}_3)(\text{CH}_3)\text{H}$
		N-EtFOSA	$\text{CF}_3(\text{CF}_2)_7\text{SO}_2\text{N}(\text{CH}_3)(\text{CH}_2\text{CH}_3)\text{H}$
		N-alkyl polyfluoroalkyl sulfonamidoethanol, FASE	
		N-MeFBSE	$\text{CF}_3(\text{CF}_2)_3\text{SO}_2\text{N}(\text{CH}_3)(\text{CH}_2\text{CH}_2\text{OH})$
		N-EtFBSE	$\text{CF}_3(\text{CF}_2)_3\text{SO}_2\text{N}(\text{CH}_2\text{CH}_3)(\text{CH}_2\text{CH}_2\text{OH})$
		N-MeFOSE	$\text{CF}_3(\text{CF}_2)_7\text{SO}_2\text{N}(\text{CH}_3)(\text{CH}_2\text{CH}_2\text{OH})$
		N-EtFOSE	$\text{CF}_3(\text{CF}_2)_7\text{SO}_2\text{N}(\text{CH}_2\text{CH}_3)(\text{CH}_2\text{CH}_2\text{OH})$

1.2 PFAS Manufacturing

1.2.1 Electrochemical Fluorination

One method of industrial PFAS synthesis is by electrochemical fluorination (ECF). During ECF, an electric current (5-7 V) is applied to a mixture of an organic compound dissolved in anhydrous hydrogen fluoride (HF) in a metal cell.⁶ ECF results in the substitution of all hydrogen atoms with fluorine atoms in the aliphatic chain of the organic compound.⁶ Historically, for instance, PFOS and PFOA were manufactured by ECF of octane sulfonyl fluoride ($C_8H_{17}SO_2F$) and octane carbonyl fluoride ($C_8H_{17}COF$), respectively, to yield perfluorooctane sulfonyl fluoride (POSF, $C_8F_{17}SO_2F$) and perfluorooctane carbonyl fluoride (POCF, $C_8F_{17}COF$).¹ POSF is used in the synthesis of perfluorooctane sulfonamido substances.¹ ECF is also used for the manufacturing of perfluorobutane sulfonamido substances and perfluorobutane sulfonic acid (PFBS), particularly in recent years due to market changes in PFAS manufacturing (Section 1.2.4). ECF products contain chain length impurities with linear and branched molecular geometries.¹ For example, ECF PFOS contains PFBS, perfluorohexane sulfonic acid (PFHxS), perfluoroheptane sulfonic acid (PFHpS), and perfluorodecane sulfonic acid (PFDS) impurities.⁷ In North America, PFSA impurities, such as PFHxS and PFDS, are removed from POSF-based products and used for industrial and commercial applications; however, this practice is not implemented in China.⁸

1.2.2 Telomerization

A second method of industrial PFAS synthesis is by telomerization. During telomerization, a perfluoroalkyl iodide (PFAI), commonly pentafluoroiodoethane ($\text{CF}_3\text{CF}_2\text{I}$) is irradiated with ultraviolet radiation forming a perfluoroalkyl radical ($\text{CF}_3\text{CF}_2^\bullet$), which undergoes free radical addition (i.e., telomerization) with tetrafluoroethylene (TFE, $\text{CF}_2=\text{CF}_2$).⁶ The free radical polymerization successively increases the chain length of the perfluoroalkyl radical. The perfluoroalkyl radical can also be reacted with ethene (i.e., $\text{CH}_2=\text{CH}_2$), leading to the production of a fluorotelomer iodide (FTI, $\text{F}(\text{CF}_2)_x\text{CH}_2\text{CH}_2\text{I}$).⁶ The oxidation and carboxylation of perfluorooctyl iodide yields PFOA and perfluorononanoic acid (PFNA), while the hydrolysis of FTI yields FTOH.^{1,6} Similar to ECF, PFAS products manufactured via telomerization contain chain length impurities,⁹ particularly even-numbered homologues due to the successive addition of TFE to growing polymer chains.⁶ Unlike ECF, however, telomerization products retain the molecular geometry of the starting material (i.e., $\text{CF}_3\text{CF}_2\text{I}$), which is typically linear.¹

1.2.3 Utility of PFAS in Industrial and Commercial Applications

The unique properties of PFAS are exploited for industrial and commercial applications. The C-F bond is highly polarized due to the high electronegativity of fluorine, rendering it one of the strongest bonds in organic chemistry.¹⁰ The high electronegativity of fluorine imparts low polarizability and poor electron donating ability, thereby limiting intermolecular interactions with nonpolar and polar substances, such as oil and water. Taken together, these factors render a perfluoroalkyl chain resistant to

degradation (e.g., from heat, acids, and bases) and insoluble in water. It is for these reasons that PFAS are used as surfactants for industrial processing and commercial applications relevant to oil and water repellency.¹ Figure 1.1 presents examples of the multitude of PFAS structures that are industrially produced for a variety of applications. The ammonium salt of PFOA is primarily used as a polymerization aid during the manufacturing of fluoropolymers, such as polytetrafluoroethylene (PTFE).⁹ The ammonium salt of PFNA is used as an aid during the polymerization of polyvinylidene fluoride (PVDF).¹ PTFE is incorporated into non-stick kitchenware and weatherproofed garments (e.g., Gore-Tex®). Certain PFAS derived from POSF, such as methyl/ethyl perfluorooctane sulfonamido ethanol (N-MeFOSE and N-EtFOSE), are used as building blocks for phosphate esters and other fluoropolymers found in water- and grease-proof food paper packaging, and for stain repellency in textiles and carpets. Similarly, FTOH are used as building blocks for surfactants and polymers for treatment of paper, carpets, and textiles to impart oil, stain, and water repellency.¹ The thermal stability of the perfluoroalkyl chain has been exploited in high-performance applications such as PFOS in aqueous film forming foams (AFFF) for fighting fuel-based fire and perfluoro-4-ethylcyclohexane sulfonate (PFECHS) is used in aircraft hydraulic fluids. N-ethyl perfluorooctane sulfonamide (N-EtFOSA) is marketed as an insecticide under the trade name Sulfluramid.¹

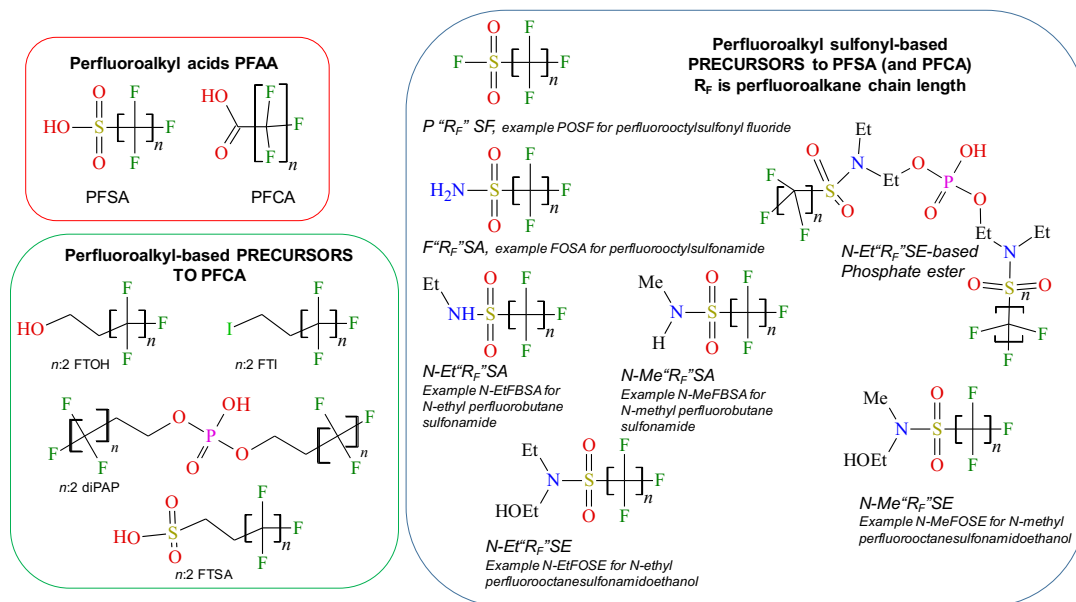


Figure 1.1 Structures of Industrially Produced PFAS including the perfluoroalkyl acids (PFAA) such as perfluoroalkyl sulfonic acids (PFSA) and perfluoroalkyl carboxylic acids (PFCA) and precursors which can undergo environmental transformation to produce PFCA and PFSA.

1.2.4 Environmental Emissions of PFAS during Manufacturing, Usage, and Waste Disposal

The durable properties that lend enhanced performance characteristics to PFAA in industrial and commercial applications also render their persistence in the environment. PFAA can be emitted into the environment during the manufacturing, usage, and disposal of products that contain PFAA from direct and indirect emission sources.^{8,11,12} A direct emission source corresponds to the direct emission of PFAA into the environment, such as the release of PFOS into groundwater from AFFF discharge during fire-fighting

training activities on military bases and the discharge of PFCA in the effluent from a fluorochemical plant. An indirect source corresponds to the emission of a PFAA precursor compound into the environment, such as the emission of FTOH during fluoropolymer manufacturing, which consequently undergoes environmental reactions to produce PFAA.⁹ Figure 1.2 compares indirect versus direct sources of PFAA.

Environmental transformation pathways of precursors are detailed in Section 1.4.

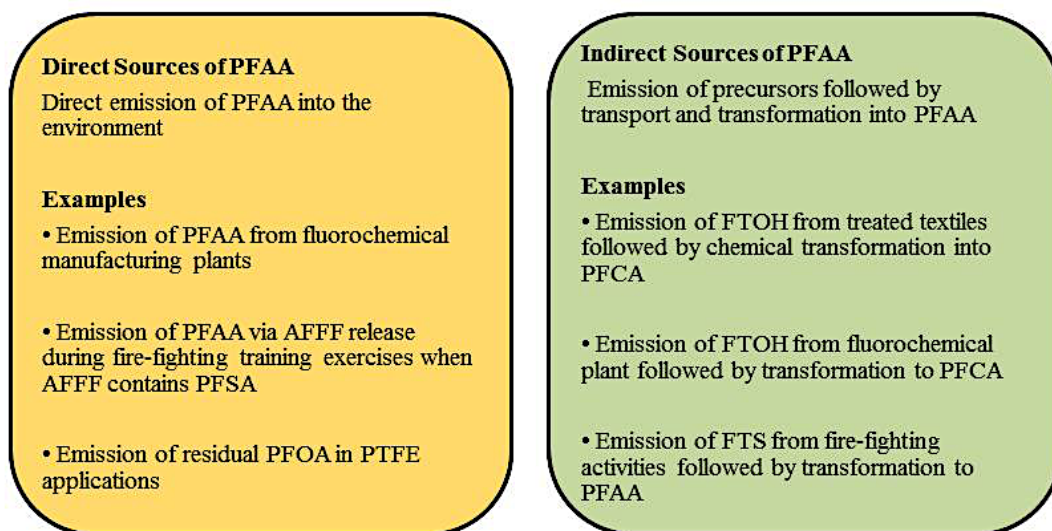


Figure 1.2 Direct and Indirect Sources of PFAA.

In recent years, several studies provide emission inventory estimates of PFAA throughout the life cycle of PFAS products. Wang et al. report total global emission inventories of C₄-C₁₄ PFCA of 2610-21400 tonnes during 1951-2015.⁹ In the latter study, Wang et al. note the majority of global C₄-C₁₄ PFCA emissions occur during fluoropolymer manufacturing using PFOA and PFNA (i.e., direct sources), however, PFCA emissions from the life-cycle of fluorotelomer-based products are dominant post-

2002 (i.e., indirect sources).⁹ Global emission inventories are also estimated for PFSA and their precursors during the product life cycle of perfluorohexane sulfonyl fluoride-(PHxSF), POSF-, and perfluorodecane sulfonyl fluoride-(PDSF) based products. Boucher et al. report total global emission inventories of 120-1022 and 38-378 tonnes for PFHxS and PFDS, respectively, and 80 and 4 tonnes for their volatile precursors PHxSF and PDSF, respectively during 1958-2015.⁸ Wang et al. report total global emission inventories of 1228-4930, 1230-8738, and 670 tonnes for PFOS, FOSA/FOSEs, and POSF, respectively, during 1958-2015.¹¹ The majority of PFSA emissions in these studies occur primarily during the usage and disposal of perfluoroalkane sulfonyl fluoride-based products (i.e., products containing fluorochemicals that originate from PHxSF, POSF and PDSF).^{8,11}

Temporal trends in global emissions of PFAA are estimated in these studies.^{8,11} For example, Wang et al. estimate PFSA in ocean waters from 1958 to 2030 in six latitudinal zones as well as analogous temporal and spatial estimates of PFSA precursors in air, whereby the greatest precursor emissions occur during 1980-2002. PFCA modeled global emissions are similar, whereby the majority of PFCA emissions occur during 1980-2002; however, followed by a reduction in 2002.⁹ The decline in PFAA emissions post-2002 estimated in these models can be attributed to well-documented production phase-out initiatives led by industry and government policies on restricting production and usage.

1.2.5. Rationale for Industry Phase-out and Domestic/International Regulations on PFAS

Actions by industry and government were due to concerns of environmental persistence and bioaccumulation of long-chain PFAS,^{13,14} and reports of reproductive, liver, immune, and metabolic toxicities.¹⁵ In 2001, the 3M Company, which is the largest global manufacturer of PFAS, voluntarily phased out its production of perfluorooctane-based substances, including PFOA, PFOS, their precursors, and longer-chain PFAS.¹⁶ This phase-out was followed by the PFOA Stewardship Program led by the US EPA in 2006. The US EPA invited several major fluorochemical manufacturers to voluntarily participate in the PFOA Stewardship Program. The goal of this program was to reduce and eventually phase-out perfluorooctane-based substances and longer-chain PFAS from products and facility emissions with full elimination by 2015.¹⁷ In Canada, which was the first country to regulate long-chain PFAA and their precursors, an environmental performance agreement was implemented by the government with Environment and Climate Change Canada, Health Canada, and four PFAS manufacturers to meet the same commitments as the PFOA Stewardship Program in 2006.¹⁸ All manufacturers participating in the PFOA Stewardship Program and environmental performance agreement report they were successful in meeting the goals of these initiatives.

In 2009, PFOS and its salts, as well as POSF were added to Annex B of the international treaty, Stockholm Convention on Persistent Organic Pollutants.¹⁹ Several countries, including the United States and Italy, are not signatories to the Stockholm Convention. More recently, PFOA-based substances were added to the EU REACH Annex XVII in 2017,²⁰ and Annex A of the Stockholm Convention in 2019. As of 2020,

PFHxS-based substances are currently under review for listing in the Stockholm Convention. Despite these phase-out initiatives, several countries continue to or have initiated new manufacturing of perfluorooctane-based chemistry. For example, the manufacturing of PTFE, using PFOA as a polymerization aid, increased from 6.6 kilotons (kt) in 1999 to 64 kt in 2012 in China.⁹ Similarly, POSF production in China increased from 3 tons (t) in 1999 to 250 t in 2006, although production decreased thereafter, reaching 170 tonnes in 2015.¹¹

The phase-out of perfluorooctane-based substances promoted a shift towards PFAS derived from perfluorobutyl containing substances,¹⁶ which are suggested to be less bioaccumulative.¹³ Similarly, PFAS manufacturing shifted towards the development of alternative organofluorine chemistries such as polyfluorinated substances with ether groups intercepting shorter perfluoroalkyl units. Another alternative organofluorine combines fluorine and chlorine in the perhalogenated alkyl moiety, in recognition of the relatively diminished recalcitrance of carbon-chlorine bonds. For instance, ammonium 4,8-dioxa-3H-perfluorononanoate ($\text{CF}_3\text{C}_3\text{F}_6\text{OCHF}_2\text{CO}_2\text{NH}_4$, ADONA) is marketed a replacement compound for APFO,²¹ while chloro-perfluoroalkyl ether sulfonates (Cl-PFESA) such as 6:2 Cl-PFESA ($\text{Cl}(\text{CF}_2)_6\text{OC}_2\text{F}_4\text{SO}_3^-$) and 8:2 Cl-PFESA ($\text{Cl}(\text{CF}_2)_8\text{OC}_2\text{F}_4\text{SO}_3^-$) are components of a technical mixture marketed as a replacement for PFOS as a mist suppressant for electroplating in China.²² It is suggested that PFAS alternatives have similar environmental partitioning properties as PFOA and PFOS.²³ Furthermore, the widespread detection of PFAS alternatives in the environment demonstrates their long-range transport ability.²⁴

1.3 Long-range Transport of PFAS to the High Arctic

PFAS are detected ubiquitously in remote environments, such as the High Arctic, where local pollution is limited, suggesting these chemicals can undergo long-range transport.

Long-range oceanic transport is a relevant pathway for PFAS to the Arctic. Ocean currents transport contaminants in the bulk dissolved phase as well as in the sea-surface microlayer to the Arctic²⁵⁻²⁷ on the scale of decades. The water solubility of PFAS is attributed to their acidic properties (i.e., pK_a) promoted by the strong electron withdrawing effect of fluorine atoms in the perfluoroalkyl chain, which stabilizes the conjugate bases of PFAS in their deprotonated, anionic form. The electron withdrawing effect is only prominent across four perfluoroalkyl carbons, thus, the pK_a of a homologous series of PFAS (e.g., C₄-C₁₈ PFCA) is independent of perfluoroalkyl chain length.²⁸ While it is accepted that PFSA are strong acids ($pK_a < 1$), the pK_a of PFCA is a subject of debate in the literature, with values ranging from < 1 to 3.8,^{28,29} however, despite this discrepancy, PFAS should be present primarily in their anionic form under most environmental conditions. In their anionic form, PFAS are water-soluble and have low vapour pressure.³⁰ These properties, combined with the stability of the perfluoroalkyl chain to environmental degradation, renders PFAS suitable tracers for global oceanic circulation.²⁵

The occurrence of PFAS in the High Arctic is also attributed to long-range atmospheric transport. Relative to oceanic transport, gas-phase atmospheric transport of volatile precursors to the High Arctic is fast, occurring on the scale of weeks.^{3,31} For perspective, given an atmospheric lifetime of 20 days and an average global wind speed

of 13.8 km hr^{-1} ,³⁰ an FTOH emitted from St. John's, Newfoundland and Labrador can travel to Alert, Nunavut in approximately 12 days (3897 km). Smog chamber experiments have demonstrated that atmospheric lifetimes of PFAA volatile precursors are sufficient to reach the High Arctic due to their high vapour pressure.^{3,31} Volatile precursors can undergo atmospheric oxidation to produce PFAA in the High Arctic (Section 1.4), which are subsequently removed by wet and dry deposition in the form of precipitation and atmospheric particles, respectively. Some of the most compelling evidence of volatile precursors as sources of PFAA in the High Arctic is demonstrated by atmospheric monitoring studies detecting FTOH and PFSAm in the Arctic atmosphere,³²⁻³⁵ and ice cores from high altitude glaciers³⁶⁻³⁸ (Section 1.5.4).

Since the ocean and atmosphere are modes of long-range transport, it is possible there is an interaction between them. A third proposed mechanism of long-range transport is through the production of marine aerosols. Marine aerosols are suspensions of ocean-derived particles in air (i.e., sea spray). Marine aerosols are produced when wind action at the ocean surface promotes breaking waves, which entrain air pockets below the ocean surface. These air pockets rise to the surface and entrain material in the sea surface microlayer (SML) before they burst into the atmosphere. The SML is the interface between the ocean and atmosphere and is rich in organic compounds.³⁹ It is suggested that PFAA partition into the SML because they are organic compounds with strong surface-active properties, making them amenable to ocean-atmosphere exchange. Two studies examined the water-air transport of PFAA using bubble-bursting simulators. McMurdo et al. note bubble-bursting results in an enrichment of PFOA in air relative to the bulk aqueous phase from which it is derived.⁴⁰ Reth et al. demonstrate that the water-

air transport behaviour of PFAA is contingent on chain-length, whereby long-chain PFAA are more readily transported into air from the aqueous phase during bubble-bursting events.⁴¹ While these laboratory studies support the hypothesis that PFAA are amenable to ocean-atmosphere exchange, environmental monitoring studies suggest this mode of transport is limited, particularly in the High Arctic.^{36,37}

It is clear that the long-range oceanic and atmospheric transport are important pathways for PFAA to the High Arctic, however, there is a debate in the literature regarding the predominance of these transport mechanisms on the occurrence of PFAA in the High Arctic. In 2007, Wania estimated the transport of PFOA to the Arctic from direct sources such as AFFF and fluoropolymers compared to indirect sources of PFOA from FTOH oxidation. These results suggest that oceanic transport of directly emitted PFOA could account for its occurrence in the Arctic Ocean, however this model did not consider other fluorotelomer or phosphate ester surfactant precursors, particle-mediated atmospheric transport, or fluoropolymer degradation.⁴² Armitage et al. report similar observations in their modelling study, whereby the oceanic transport of PFOA from direct sources is the primary pathway for the occurrence of PFOA in the Arctic Ocean, however, this study had similar limitations to the work of Wania et al.⁴³ In contrast to these earlier studies, Yeung et al. more recently used a more thorough set of PFAS measurements in the Arctic Ocean and a 3-compartment box model based on ocean stratification and differential transport. In this work, it was suggested that the oxidation of fluorotelomer precursors accounts for 34-59% of PFOA in ocean waters from the polar mixed layer of the Arctic Ocean, while direct emission sources were dominant for PFOS.⁴⁴ Overall, these studies indicate that oceanic transport is an important pathway for PFAA to the High

Arctic, particularly those that were historically produced in large quantities, such as PFOA and PFOS. The contributions from PFAA with limited historical production, as well as ongoing manufacturing of long-chain precursors, will contribute to the occurrence of long-chain PFAA in the High Arctic environment.

1.4 Atmospheric Chemistry

An overview of the atmospheric oxidation of $x:2$ FTOH ($F(CF_2)_xCH_2CH_2OH$) is presented in Figure 1.3. In this mechanism, hydroxyl radical ($\cdot OH$) initiates the oxidation of FTOH via hydrogen abstraction on the carbon bearing the alcohol moiety.⁴ The resulting hydroxy alkyl radical reacts with oxygen (O_2) to yield a fluorotelomer aldehyde (FTAL). Further reaction with $\cdot OH$ yields an acyl peroxy radical, which can undergo reactions to form fluorotelomer carboxylic acid (FTCA) and perfluoroalkyl aldehyde (PFAL). PFAL reacts with $\cdot OH$ and O_2 to yield a perfluoroacyl peroxy radical, which subsequently reacts with hydroperoxyl radical ($HO_2\cdot$) to produce a PFCA with $x+1$ carbons. The perfluoroacyl peroxy radical can also undergo reaction with nitric oxide ($NO\cdot$) and O_2 to produce a perfluoroalkyl peroxy radical, which has several reaction pathways ultimately leading to PFCA production. One pathway involves reactions with alkyl peroxy radicals containing a α -hydrogen, such as CH_3O_2 (i.e., $ROO\cdot$), producing a perfluoroalkyl alcohol (PFOH). The PFOH heterogeneously decomposes to produce a perfluoroalkyl carbonyl fluoride, which hydrolyses to PFCA with x carbons.

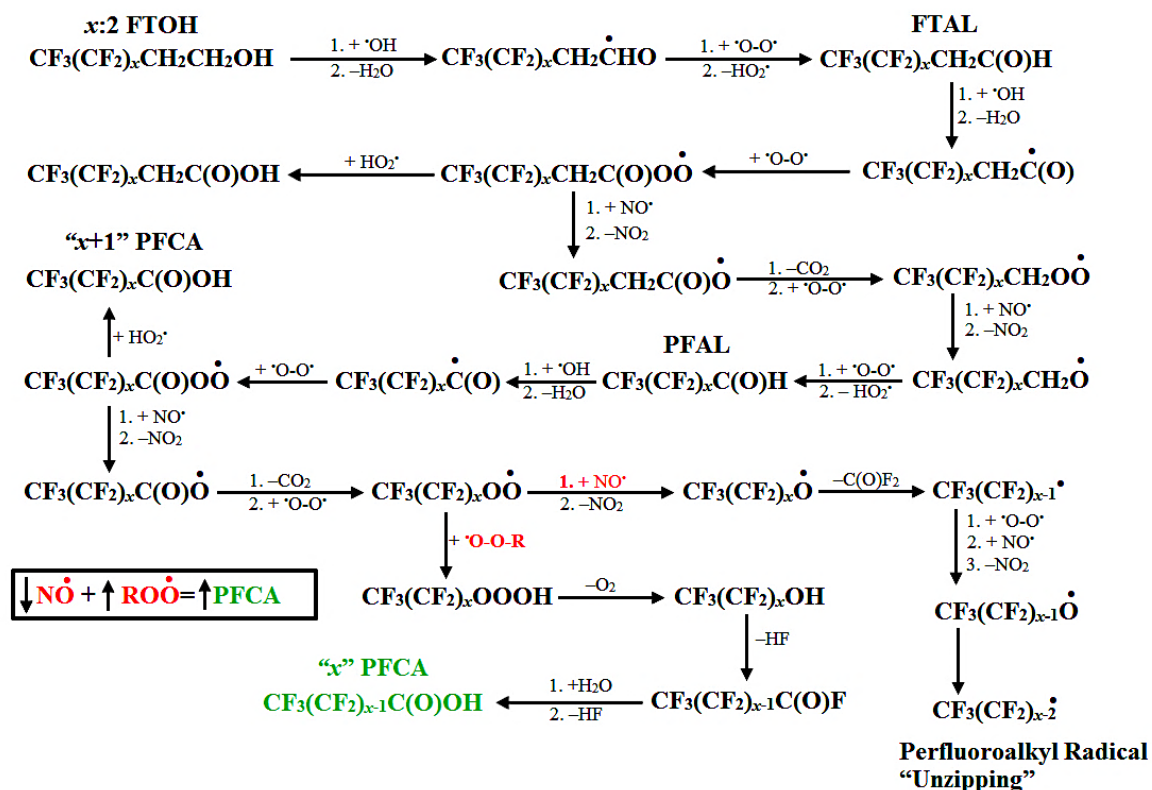


Figure 1.3 Atmospheric oxidation mechanism for a $x:2$ fluorotelomer alcohol (FTOH) producing perfluoroalkyl carboxylic acids (PFCA) with x and $x+1$ carbons in a 1:1 ratio. Atmospheric reagents include hydroxyl radicals ($\cdot\text{OH}$), oxygen (O_2), nitric oxide ($\text{NO}\cdot$), hydroperoxyl radicals ($\text{HO}_2\cdot$), and alkyl peroxy radicals ($\text{ROO}\cdot$). Perfluoroalkyl radical unzipping produces shorter chain PFCA. Other products formed are fluorotelomer aldehyde (FTAL), perfluoroalkyl aldehyde (PFAL), water (H_2O), nitrogen dioxide (NO_2), carbon dioxide (CO_2), and HF (hydrofluoric acid). The mechanism is adapted from Wallington et al.⁴

An alternative pathway involves reaction with NO^\bullet to produce a perfluoroalkoxy radical, which can degrade into a perfluoroalkyl radical. Perfluoroalkyl radicals can undergo reaction with O_2 and generate a perfluoroalkoxy radical with $x-1$ carbons. An important aspect of this $x:2$ FTOH oxidation mechanism is the formation of a full suite of PFCA including $x + 1$ PFCA, x PFCA, and all of the shorter chain PFCA including trifluoroacetic acid (TFA). This occurs via reaction of $\text{F}(\text{CF}_2)_x\text{CO}^\bullet$ with CO_2 and loss of COF_2 to produce a perfluoroalkyl radical. Successive truncation in chain length of the perfluoroalkyl radical leads to the a homologous series of PFCA through this “unzipping”.^{4,7} Other volatile PFAS may also undergo this oxidation such as hydrofluoroethers (HFE), fluorotelomer olefins, FTI, fluorotelomer acrylates, etc. to form a series of PFCA.

The formation of PFCA from the oxidation of FTOH is favourable under representative conditions of the Arctic atmosphere (i.e., low NO_x conditions).⁴⁵ NO_x refers to nitrogen oxides in the atmosphere (i.e., $\text{NO} + \text{NO}_2$), which are sourced from the incomplete combustion of fossil fuels. The atmospheric concentrations of these pollutants are higher in regions of high population density, thus, in urban environments, the production of PFCA from the atmospheric oxidation of FTOH will be limited by competing NO_x chemistry (Figure 1.3).

The atmospheric oxidation of PFSAm is also a source of PFAA under low NO_x conditions (Figure 1.4). Atmospheric oxidation of N-methyl polyfluoroalkyl sulfonamido ethanol (N-MeFASE) proceeds by the addition of $^\bullet\text{OH}$ to the sulfonyl bond to form $\text{CF}_3(\text{CF}_2)_x\text{S}(\text{O})(\text{OH})(\text{O}^\bullet)\text{NMeEtOH}$.⁴⁶

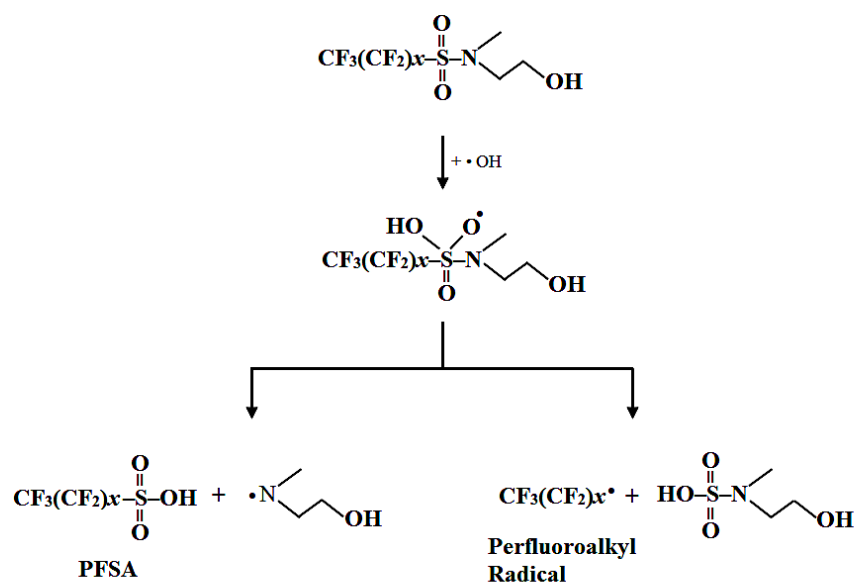


Figure 1.4 Atmospheric oxidation mechanism for N-methyl polyfluoroalkyl sulfonamido ethanol (N-MeFASE) producing perfluoroalkyl sulfonic acid (PFSA) and perfluoroalkyl radicals. Perfluoroalkyl radical can react with peroxy radicals and water to produce PFCA. PFSAm oxidation yields PFSA and PFCA in a 1: 10 ratio. The mechanism is adapted from D’eon et al.⁴⁶

Two primary reaction pathways are reported, whereby the homolytic cleavage of the C-S bond results in the formation of a perfluoroalkyl radical and an amidosulfamic acid. The perfluoroalkyl radical then further reacts to form a series of PFCA. Alternatively, the OH-addition intermediate can undergo S-N bond cleavage to form a PFSA (C₄F₉SO₃H, PFBS) and a nitrogen-centered radical. The ratio of PFCA to PFSA yield is approximately 10:1, suggesting a higher likelihood of C-S bond cleavage.⁴⁶ As this mechanism is independent of chain length, oxidation of larger polyfluoroalkyl sulfonamides such as N-MeFBSE would produce PFOS, PFNA, PFOA, and shorter PFCA.⁷

1.5 PFAS in the Arctic Abiotic Environment

1.5.1 Arctic Atmosphere

PFAS are measured in the Arctic atmosphere by active and passive air sampling. Active air sampling refers to a sampling technique that employs a vacuum pump to draw a large volume of air from the atmosphere through a filter-sorbent combination to collect gases and particles. In passive air sampling, a sorbent is mounted typically using polyurethane foam (PUF), XAD-resin, or a PUF and XAD combined in the sorbent-impregnated passive sampling (SIP) device. A map of air monitoring stations in the High Arctic of Canada and Norway is presented in Figure 1.5. A temporal series of PFAS is reported from a study using a continuous, long-term, active air monitoring campaign in the High Arctic of Canada and Norway during 2006-2014. The highest concentrations of neutral PFAS in the High Arctic of Canada at Alert (82° N) were 8:2 FTOH, 10:2 FTOH, and 6:2 FTOH (Table 1.2).³² Other neutral PFAS are detected at Alert, albeit with lower concentrations of FTOH. The polyfluoroalkyl sulfonamidoethanol (N-EtFOSE and N-MeFOSE) concentrations are higher than the corresponding sulfonamides, N-EtFOSA and N-MeFOSA, at Alert.³² FTOH were not monitored in the Norwegian Arctic archipelago, however, higher concentrations and detection frequencies are reported for FOSA at Zeppelin, located in Svalbard, than those at Andøya, an island in the northern coast of Norway.³² Similar observations are reported in other Arctic regions.

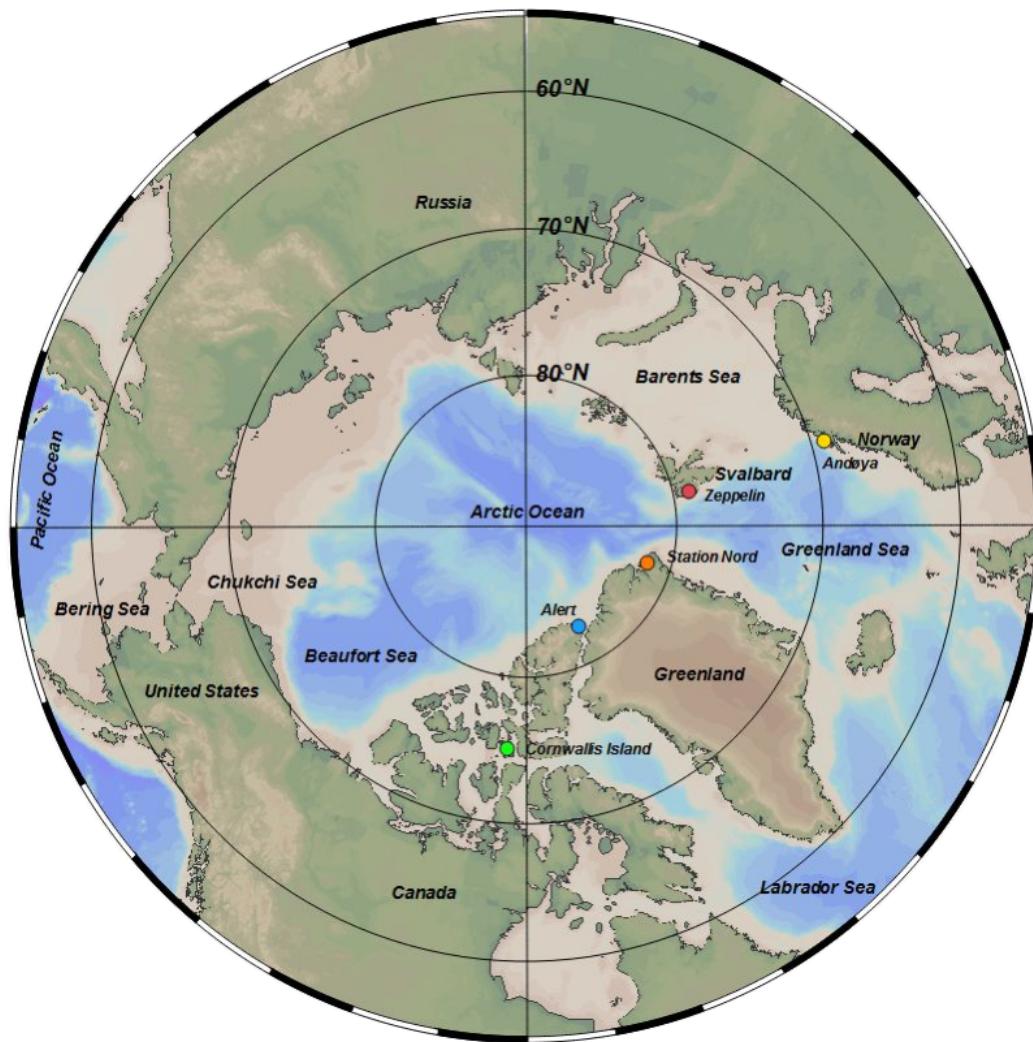


Figure 1.5 Map of air monitoring stations in the High Arctic. Stations are designated by colored circles: yellow (Andøya, Norway), red (Zeppelin, Norway), orange (Station Nord, Greenland), blue (Alert, Nunavut), and green (Cornwallis Island). Map source: Ocean Data View (Schlitzer, R., Ocean Data View, <https://odv.awi.de>, 2019.).

Table 1.2 Summary of PFCA and PFSA precursors (i.e., neutral PFAS) concentrations (pg m⁻³) during active air monitoring campaigns in the High Arctic. Detection frequencies are shown in parenthesis.

Active Air Sampling (High Volume)	Sample	6:2 FTOH	8:2 FTOH	10:2 FTOH	N-MeFOSA	N-EtFOSA	N-MeFOSE	N-EtFOSE	N-MeFBSA	N-MeFBSE
Alert (82° N) 2006-2014 ³²	Gas and Particle	<0.086-3.9 (38)	<0.065-21 (95)	<0.015-8.7 (96)	<0.008-0.64 (93)	<0.006-0.25 (81)	<0.044-2.7 (89)	<0.056-3.9 (60)		
Cornwallis Island (73-75° N) 2004 ⁴⁷	Gas	<13.6-19.7 (30)	<2.3-18.6 (50)	<1.5-3.5 (10)		<9.3-18.6 (50)	<29.4-39.2 (40)	<26.6 (0)		<17.7-34.0 (20)
	Particle	<11.3 (0)	<5.2 (0)	<3.0-4.1 (10)		<5.6-5.3 (20)	<9.7-26.9 (30)	<13.2-27.9 (20)		<0.7-5.4 (40)
Oden cruise (58-74° N) 2005 ³⁴	Gas	<1.1-5.98 (55)	4.16-22.7 (100)	1.45-16.4 (100)			<1.9-23.6 (95)	<1.0-5.17 (95)		
	Particle	<0.001 (0)	1.07-8.37 (100)	0.29-1.57 (100)			<1.7-15.0 (95)	<0.001-5.5 (25)		
Amundsen cruise (56-74° N) 2007-2008 ³³	Gas	<1.1-29 (88)	15-83 (100)	3.5-31 (100)	<0.08-3.6 (89)	<0.04-1.7 (92)	<0.06-22 (80)	<0.06-1.4 (87)		
	Particle	<LOD (0)	<LOD-1.0 (80)	<LOD-0.6 (75)	<LOD-0.3 (25)	<LOD-0.2 (20)	<0.4-7.4 (75)	<0.03-3.2 (90)		
R/V Snow Dragon cruise (72-81° N) 2010 ⁴⁸	Gas	0.9-4.9 (100)	82-155 (100)	6.1-29 (100)	0.1-0.2 (100)	0.2-0.9 (100)	0.1-0.3 (100)	0.1 (100)	0.2-0.9 (100)	1.7-3.7 (100)
	Particle	0.1-0.2 (100)	0.2-2.3 (100)	0.1-0.4 (100)	<0.1-0.1 (60)	0.1 (100)	0.11-0.3 (100)	0.1-0.4 (100)	<0.01-0.02 (80)	0.1-1.8 (100)
Station Nord (81° N) 2008-2013 ⁴⁹	Gas and Particle	<0.45-16.5 (92)	<0.45-22.4 (93)	<0.20-9.68 (93)	<0.20-3.41 (71)	<0.22-1.93 (63)	<0.15-7.46 (64)	<0.11-5.96 (60)		
Ny-Ålesund (79° N) 2011-2012 ⁵⁰	Gas and Particle	0.6-5.1	3.7-25	0.4-9.3	0.1-0.5	0.1-0.5	<0.1-0.8	<0.1-0.4	0.1-1.8	

8:2 FTOH is the most abundant neutral PFAS in air samples from Cornwallis Island in 2004,⁴⁷ Ny Ålesund during 2011-2012,⁵⁰ Station Nord (North Greenland, 81°N) during 2008-2013,⁴⁹ and in Arctic air monitoring cruises aboard research vessels *Oden*,³⁴ *Amundsen*,³³ and *Snow Dragon*.⁴⁸ FOSA is detected in most air samples from Cornwallis Island, with higher concentrations than those at Zeppelin and Andøya (<8.0-61.3 pg/m³).⁴⁷ Interestingly, the highest FTOH concentrations are reported during summer months at Alert,³² which is also noted in air samples from Northern Greenland.⁴⁹ Higher summer concentrations of FTOH is attributed to greater volatilization due to warmer temperatures, which is consistent with reports in snowpacks from Ny-Ålesund.⁵⁰ Maximum concentrations are reported for FOSA during the summer at Zeppelin, although this is not observed at Andøya.³²

In addition to neutral volatile PFAA precursors, Wong et al. also reported a homologous series of PFAA in air at Alert, including C₄-C₁₄, C₁₆, C₁₈ PFCA and C₄, C₆, C₈, C₁₀ PFSA (Table 1.3). PFBA, PFOA, PFOS and PFBS are most abundant at Alert.³² In the latter study, PFBA is detected in the gas phase, which was in contrast to other detected PFAA that were predominately associated with the particle phase. It was suggested that differences in physicochemical properties or the oxidation of HFC and/or HFE corroborated evidence of gas phase PFBA in the High Arctic.³² Concentrations of C₁₀-C₁₄ PFCA at Alert during 2006-2014 are on the same order of magnitude as those detected in air samples sampled collected during the *Amundsen* cruise in 2007 and 2008.³³ In the latter study, Ahrens et al. report high concentrations of PFCA and FTOH in particles over the Labrador Sea,³³ suggesting FTOH partition to atmospheric particles and undergo oxidation. Stock et al. report similar findings, whereby the detection of long-

chain PFCA in particles from Cornwallis Island is attributed to the atmospheric degradation of volatile precursor compounds.⁴⁷ C₆-C₁₁ PFCA and C₈, C₁₀ PFSA are detected in air samples from Zeppelin and Andøya during 2006-2014. In general, PFBS and PFOS concentrations at Zeppelin are similar to those reported at Alert.³² PFBS and PFHxS were not detected at Andøya, although PFOS concentrations were similar to those at Zeppelin. Wong et al. note that PFOA concentrations are significantly lower at Alert than those at Zeppelin and Andøya, which is attributed to enhanced marine aerosol deposition in the High Arctic of Norway due to the close proximity of these sites to the ocean.³² While PFOA concentrations are lower at Alert compared to Zeppelin and Andøya, maximum concentrations were reported during the summer, suggesting marine aerosol and/or atmospheric precursor degradation are likely sources of PFOA at Alert.³² Stock et al. also note that marine aerosol deposition is a possible source of PFAA in air samples from Cornwallis Island during 2004.⁴⁷ The concentrations of PFOA, PFNA, and PFDA in the latter study are comparable to those from Zeppelin and Andøya during 2006-2014.³²

PFAS are also measured in the Arctic atmosphere by passive air sampling. During passive air sampling, samplers containing a semipermeable membrane, such as polyurethane foam (PUF), which can be impregnated with a sorbent such as XAD resin, consisting of spheres made out of cross-linked polystyrene polymer. These samplers are deployed to sample gases and particles from the atmosphere. Passive air sampling is useful for sample collection in remote, off-grid sites because they do not require electricity for operation and can be deployed by non-technical volunteers, unlike active air monitoring instrumentation. For this reason, passive samplers have been used as part

of a global atmospheric passive sampling program (GAPS). Recently, Rauert et al. report global concentrations of PFAS from Arctic locations within the GAPS Network in 2009, 2013, and 2015 using SIP-PAS.³⁵ At Alert, the most abundant PFAS are 6:2 FTOH (<0.4-59 pg m⁻³) and 8:2 FTOH (5.4-11 pg m⁻³) during April-September. Similar profiles are reported at Ny-Ålesund, whereby 6:2 FTOH (<0.4-16 pg m⁻³) and 8:2 FTOH (1.1-10 pg m⁻³) are most abundant from 2009 to 2015.³⁵ N-EtFOSA is detected at Alert (0.083-0.086 pg m⁻³) and Ny-Ålesund (0.085-0.12 pg m⁻³), whereas FOSEs are below the detection limit.³⁵ The concentrations of FTOH and N-EtFOSA in the latter study are generally on the same order of magnitude as those reported during an active air sampling at Alert and Ny-Ålesund during 2006-2014.³²

PFAA are detected across the GAPS Network in 2009, 2013, and 2015 (Table 1.3). PFBA is most abundant at Alert and Ny-Ålesund.³⁵ ΣPFAA concentrations (excluding PFBA and PFPeA) at Alert in 2013 (March-July, 8.0 pg m⁻³) are similar to those reported by Wong et al. at Alert during 2006-2014 (<0.006-9.1 pg m⁻³), although higher concentrations are reported in 2015 (March-July, 20 pg m⁻³).³⁵ Likewise, ΣPFAA concentrations increased at Ny-Ålesund from 2013 to 2015 (March-July periods, 11 to 38 pg m⁻³).³⁵ These observations suggest PFAA emissions are increasing in the High Arctic.

Several active and passive air monitoring campaigns have reported temporal trends for PFAS in the Arctic atmosphere. Wong et al. report increasing temporal trends for 8:2 FTOH (doubling time, $t_2 = 5$ y) and 10:2 FTOH ($t_2 = 7$ y) at Alert during 2006-2014,³² however, this trend is not observed during an active air monitoring campaign in Northern Greenland, in which FTOH are constant during 2008-2013.⁴⁹ Similar observations are reported in a passive air monitoring campaign from sites across the

GAPS Network, whereby concentrations of FTOH are constant from 2009 to 2015.³⁵ Increasing temporal trends are reported during active air monitoring for PFBA ($t_2 = 2.5$), PFOA ($t_2 = 3.7$ y), PFBS ($t_2 = 2.6$ y), and PFOS ($t_2 = 2.9$ y) at Alert.³² Rauert et al. also report increasing concentrations of PFSA during passive air monitoring at Alert and Ny-Ålesund from 2009 to 2015 and indicated concentrations of PFCA are typically higher in 2015 than in 2009 and 2013 in the Arctic.³⁵ In contrast, decreasing or constant temporal trends are reported for concentrations of PFOA (half-life, $t_{1/2} = 7.2$ y), PFOS ($t_{1/2} = 67$ y), and FOSA ($t_{1/2} = 63$ y) at Zeppelin during 2006-2014, and concentrations of PFOA ($t_{1/2} = 1.9$ y) and PFOS ($t_{1/2} = 11$ y) at Andøya during 2010-2014³².

Table 1.3 Summary of PFAA concentrations (pg m^{-3}) during active and passive air monitoring campaigns in the High Arctic. Mean concentrations are presented in brackets. Data from Rauert et al.³⁴ corresponds to April-September sampling periods. The annotation “High Volume” refers to active air sampling and SIP-PAS designates passive air sampling using polyurethane foam and XAD-resin combined in a sorbent- impregnated passive sampling device.

Active Air Sampling (High Volume)		Sample	PFBA	PFPeA	PFHxA	PFHpA	PFOA	PFNA	PFDA	PFUnDA	PFDoDA	PFTeDA	PFBS	PFHxS	PFOS	PFDS
Zeppelin (79° N) 2011-2012 ³²	Gas and Particle			<0.089- 3.1 (0.26)	<0.17- 4.9 (0.38)	<0.12- 4.0 (0.50)	<0.079- 3.6 (0.32)	<0.085- 11 (0.54)	<0.14- 4.9 (0.35)				<0.026- 1.2 (0.056)	<0.038- 0.35 (0.036)	<0.037- 2.2 (0.081)	<0.031- 0.21 (0.033)
Andøya (79° N) 2011-2012 ³²	Gas and Particle			<0.12- 5.3 (0.32)	<0.14- 5.1 (0.44)	<0.12- 5.5 (0.54)	<0.072- 11 (0.50)	<0.051- 11 (0.79)	<0.050- 6.8 (0.49)						<0.043- 0.43 (0.09)	<0.031- 0.29 (0.043)
Cornwallis Island (73-75° N) 2004 ⁴⁷	Particle					(1.4)	(0.4)	(0.4)						(0.2)	(5.9)	(0.2)
<i>Amundsen</i> cruise (56-74° N) 2007-2008 ³³	Particle							<0.01- 0.012	<0.02- 0.076	<0.01- 0.081	<0.01- 0.030					
Passive Air Sampling (SIP-PAS)		Sample	PFBA	PFPeA	PFHxA	PFHpA	PFOA	PFNA	PFDA	PFUnDA	PFDoDA	PFTeDA	PFBS	PFHxS	PFOS	PFDS
Alert (82° N) 2009, 2013, 2015 ³⁵	Gas and Particle	88-153 (127)	<9	<1-2.8	<1-1.8	<3	<0.2-1.5	<0.3- 0.52	<0.05- 0.29	<0.07- 0.13	<0.08- 0.09	1.0-3.9 (2.4)	0.26-1.2 (0.6)	1.9-6.2 (3.4)	<0.06	
Ny-Ålesund (79° N) 2009, 2013, 2015 ³⁵	Gas and Particle	53-195 (109)	<1-22	<1-9.5	<1-4.7	<3-3.0	<0.2-8.1	<0.3- 0.86	<0.05- 0.65	<0.07- 0.15	<0.1	0.19-9.8 (4.6)	<0.07- 2.2	0.16-4.2 (2.7)	<0.06	

1.5.2 Arctic Landscape and Freshwater Environment

In this section, a summary of PFAS measurements in freshwater lakes and sediment and soil from the Arctic landscape is presented. All of these concentrations are limited to PFAA (i.e., PFCA and PFSA) as neutral PFAS precursors have not been targeted in these environmental samples and are also not likely to be present based on physical properties.

1.5.2.1 Water

Several studies investigate the distribution of PFAS in freshwater from the High Arctic. Stock et al. detect C₇-C₁₂ PFCA and C₆, C₈, C₁₀ PFSA in lake water on Cornwallis Island (Nunavut, Canada, 73-75° N) in 2003 and 2005 (Table 1.4).⁴⁷ PFOA and PFUnDA are the most abundant PFAS in Amituk and Char Lakes, respectively, in 2003, although higher concentrations of PFDA are reported in Char Lake in 2005. PFOS is the only PFSA detected in both lakes in 2003 and 2005. In contrast, higher concentrations of PFHpA, PFOA, PFHxS, and PFOS are reported in Resolute Lake in 2003 and 2005. Similar concentration profiles are reported in Meretta Lake in 2005 for PFHpA, PFOA, PFHxS, and PFOS. It is noteworthy that concentrations of C₁₀-C₁₂ PFCAs are similar in all lakes. These results by Stock et al. highlight the influence of regional PFAS contamination as well as long-range diffuse PFAS sources. For example, the lower PFAA concentrations in Amituk and Char Lakes are attributed to long-range atmospheric transport and deposition, whereas higher concentrations in Resolute and Meretta Lakes are linked to contamination from a local airport.⁴⁷

Table 1.4 PFAA concentrations (ng L⁻¹) in lake waters from the High Arctic of Canada and Norway. Mean concentrations are presented in parenthesis where available.

Canada	Latitude	Year(s)	PFBA	PFPeA	PFHxA	PFHpA	PFOA	PFNA	PFDA	PFUnDA	PFDoDA	PFBS	PFHxS	PFOS
Char Lake	74° N	2003 ⁴⁷				<LOD-0.5 (0.3)	1.8-3.4 (2.6)	<LOD-1.4 (0.5)	<LOD-7.3 (4.2)	4.1-5.9 (4.9)	<LOD		<LOD	1.1-2.3 (1.8)
		2005 ⁴⁷				<LOD-1.6 (0.5)	0.5-1.9 (0.9)	0.3-2.5 (1.5)	7.5-13 (10.1)	2.7-3.9 (3.5)	<LOD		<LOD	0.9-2.5 (1.8)
		2010-2011 ⁵¹					(0.62)		(0.04)					(0.12)
Amituk Lake	73° N	2003 ⁴⁷				<LOD-1.0 (0.6)	1.9-8.4 (4.1)	0.2-0.4 (0.3)	0.5-1.4 (1.1)	1.4-3.4 (2.5)	<LOD-0.6 (0.4)		<LOD	0.9-1.5 (1.2)
Resolute Lake	74° N	2003 ⁴⁷				18-49 (31)	12-16 (14)	<LOD-6.1 (2.0)	<LOD-2.9 (1.8)	1.0-5.0 (2.9)	<LOD-2.3 (0.8)		19-24 (21)	49-90 (69)
		2005 ⁴⁷				3.1-15 (5.7-12)	5.0-12 (5.6-10)	0.9-3.0 (1.7-2.8)	3.3-29 (6.3-17)	3.5-5.8 (4.0-4.9)	<LOD-0.9		1.5-17 (2.9-14)	23-46 (23-46)
		2010-2011 ⁵¹					(9.4)		(0.11)					(19.7)
Meretta Lake	74° N	2005 ⁴⁷				17-29 (20-26)	13-15 (13-14)	3.0-4.4 (3.5-4.1)	7.2-24 (9.9-19)	0.2-0.5 (0.3-0.4)	<LOD-0.5		8.9-18 (11-16)	50-57 (52-56)
		2010-2011 ⁵¹				(17)			(0.13)				(30)	(41)
North Lake	75° N	2010-2011 ⁵¹				(0.66)			(0.08)				(0.01)	(0.02)
Small Lake	75° N	2010-2011 ⁵¹				(0.60)			(0.06)				(0.11)	(0.22)
9 Mile Lake	75° N	2010-2011 ⁵¹				(0.69)			(0.08)				(0.02)	(0.001)
Lake A	83° N	2007-2008 ⁵²				0.059-0.190 (0.104)	0.085-0.245 (0.149)	0.057-0.192 (0.118)	0.003-0.027 (0.015)	0.001-0.016 (0.008)		0.011-0.024 (0.016)	0.003-0.024 (0.009)	0.013-0.071 (0.025)
Norway		Year(s)	PFBA	PFPeA	PFHxA	PFHpA	PFOA	PFNA	PFDA	PFUnDA	PFDoDA	PFBS	PFHxS	PFOS
Longyearbyen	78° N	2006 ³⁸	0.427	1.387	0.073	0.061	0.173	0.131	0.018	0.012	0.006		0.063	0.141
Lake Linnévatnet	78° N	2015 ⁵³	<0.08-1.37 (0.64)	<0.01	<0.02-0.13 (0.024)	<0.03-0.42 (0.11)	<0.06-1.78 (0.20)	<0.03-0.16 (0.087)	<0.02-0.61 (0.053)		<0.02-0.16 (0.017)		<0.005-0.023 (0.005)	0.044-0.23 (0.12)

Stock et al. was one of the first studies in which the ratio of even/odd (i.e., x and $x+1$ PFCA with formula $F(CF_2)_xCO_2-$) was used to distinguish atmospheric indirect sources to the Arctic. Lescord et al. also report lower concentrations in atmospherically supplied Char, Small, North, and 9 Mile Lakes, than those in Meretta and Resolute Lakes during 2010-2011. In the latter study, Lescord et al. note that PFHxA and PFBS are most abundant in all lakes. The cyclic PFSA, PFECHS, is detected in Meretta and Resolute Lakes (0.18 ± 0.12 and 0.05 ± 0.07 ng L⁻¹), which is attributed to local airport pollution.⁴⁷ PFECHS is currently used as a tracer for direct PFAS emissions since it has no known volatile PFAS precursor and a very specific use in aircraft hydraulic fluid. Lower PFAA concentrations are reported at higher latitudes within the High Arctic. Veillette et al. detect C₇-C₁₁ PFCA and C₄, C₆-C₈ PFSA in water of Lake A, a meromictic lake on northern Ellesmere Island in 2007 and 2008.⁵² The highest concentrations in surface waters are reported for PFHpA, PFOA, PFNA, and PFOS. The vertical distribution of PFAA in the water column of Lake A was investigated in 2008. Higher concentrations are reported in the mixed layer of Lake A (i.e., 2-10 m depth, 376-456 pg L⁻¹) than concentrations in the monimolimnion (i.e., 32 m depth, 27-93 pg L⁻¹) due to limited mixing of surface and deep waters.⁵² Kwok et al. detect C₄-C₁₂ PFCA and C₈ PFSA in water from the Longyearbreen glacier and water from a river and lake near Longyearbyen (Svalbard, Norway, 78° N) in 2006.³⁸ The most abundant PFAA in glacial meltwaters are PFBA (287 ± 57 pg L⁻¹), PFPeA (839 ± 60 pg L⁻¹), PFHxA (104 ± 12 pg L⁻¹), PFHpA (110 ± 6 pg L⁻¹), and PFOA (107 ± 10 pg L⁻¹). The mean Σ PFAA concentration is 1600 pg L⁻¹ in glacial meltwaters. Kwok et al. report higher concentrations of PFBA (1158 ± 631 pg L⁻¹), PFPeA (1047 ± 1310 pg L⁻¹), PFHxA (259 ± 82 pg L⁻¹), PFOA (305 ± 193 pg

L⁻¹), and PFOS (290 ± 370 pg L⁻¹) downstream from the Longyearbreen glacier in river water.³⁸ PFHxS is only detected in river (159 ± 202 pg L⁻¹) and lake water (63 pg L⁻¹) downstream from the Longyearbreen glacier. Higher PFAS concentrations in downstream locations are attributed to local pollution sources in the Longyearbyen area.³⁸ These observations are generally consistent with more recent studies in Svalbard, Norway. Skaar et al. indicate local fire-fighting training sites as sources of PFAS in freshwaters from Longyearbyen during 2014 and 2015 and in Ny-Ålesund during 2016.⁵³ Skaar et al. also detect PFAA in water of Lake Linnévatnet (Svalbard, Norway, 78° N) and meltwater (i.e., snow and glacier ice) from its catchment in 2014 and 2015. In Lake Linnévatnet, C₄, C₆-C₁₀, C₁₂ PFCA and C₆, C₈ PFSA are detected.⁵³ The highest concentrations are reported for PFBA and PFOA. Σ PFAA concentrations in Lake Linnévatnet (1400 ± 800 pg L⁻¹) are similar to those reported by Lescord et al. in atmospherically-supplied lakes from Cornwallis Island.⁵¹ The composition of PFAA in meltwater from the Linnévatnet catchment is variable, possibly due to different melting inputs from snowpacks in the catchment.⁵³ The lower range of Σ PFAA concentration in meltwater from the Lake Linnévatnet catchment (1100-4200 pg L⁻¹) are in line with those reported in glacial meltwaters from the Longyearbreen glacier (1600 pg L⁻¹).³⁸

1.5.2.2 Lake Sediments

The detection of PFAS in lake sediments from the High Arctic is limited to sites in Canada. Stock et al. detect C₇-C₁₁ PFCA and C₄, C₆, C₈ PFSA in sediment cores from Arctic lakes on Cornwallis Island in 2003.⁴⁷ PFAS concentrations decrease with depth in

sediment cores from all Arctic lakes. In Char Lake, PFOA ($<1.1-1.7 \text{ ng g}^{-1} \text{ dw}$) and PFOS ($<0.35-1.1 \text{ ng g}^{-1} \text{ dw}$) are most abundant, and maximum concentrations occur at 0-1 cm depth, corresponding to 1996-2003. In Amituk Lake, PFHpA ($<2.9-3.9 \text{ ng g}^{-1} \text{ dw}$), PFOA ($<0.29-0.96 \text{ ng g}^{-1} \text{ dw}$), and PFHxS ($<0.058-1.0 \text{ ng g}^{-1} \text{ dw}$) are most abundant in sediments, particularly at 1.5-2.5 cm and 0-1.5 cm depths, corresponding to 1942-1975 and 1976-2003, respectively. A similar profile is reported in Resolute Lake sediments, although the concentrations are higher. PFOS ($24-85 \text{ ng g}^{-1} \text{ dw}$), PFOA ($<1.8-7.5 \text{ ng g}^{-1} \text{ dw}$), PFHpA ($<0.18-6.8 \text{ ng g}^{-1} \text{ dw}$), PFHxS ($1.2-3.5 \text{ ng g}^{-1} \text{ dw}$), and PFNA ($<2.5-3.2 \text{ ng g}^{-1} \text{ dw}$) are most abundant, and maximum concentrations occur at 0-1 cm depth, corresponding to 1997-2003. Lescord et al. report similar observations in lake sediments from Cornwallis Island in 2010 and 2011.⁵¹ Σ PFCA concentrations are most abundant in sediments from atmospherically supplied (i.e., land-locked) lakes ($0.15-1.9 \text{ ng g}^{-1} \text{ dw}$), whereas Σ PFSA concentrations are most abundant in sediments from Resolute and Meretta Lakes, dominated by PFOS (49 ± 29 and $28 \pm 43 \text{ ng g}^{-1} \text{ dw}$).⁵¹ These reports are consistent with earlier observations that local and diffuse sources are relevant to PFAS deposition on Cornwallis Island.⁴⁷ Veillette et al. detect PFOS in sediments from Lake A in 2008.⁵² PFOS concentrations decrease with depth in sediments from Lake A, and the highest concentration occur at 0-0.5 cm depth, corresponding to 1985-2008 ($66 \text{ pg g}^{-1} \text{ dw}$). Veillette et al. attribute high concentrations of PFOS in surface sediments to increasing emissions from the global manufacturing of PFOS-based substances.⁵² Other PFAA are below the detection limit in Lake A sediments.

1.5.2.3 Soil

The study of PFAS in surface soils is limited in the High Arctic. In a recent study, Cabrerizo et al. detect a suite of PFAA (i.e., C₄-C₁₃ PFCA and C₄, C₆-C₈, C₁₀ PFSA) in surface soil from Cape Bounty on Melville Island and Cornwallis Island in 2015 and 2016.⁵⁴ The most abundant PFAA in soils are PFBA (<LOD-0.25 ng g⁻¹ dw), PFOA (0.01-0.40 ng g⁻¹ dw), and PFNA (0.02-0.87 ng g⁻¹ dw). ΣPFCA concentrations (0.20-2.05 ng g⁻¹ dw) are higher than ΣPFSA concentrations (0.003-0.031 ng g⁻¹ dw).⁵⁴ Similar ΣPFCA (0.27 ng g⁻¹ dw) and ΣPFSA concentrations (0.018 ng g⁻¹ dw) are reported in soils from Inuvik (Northwest Territories, Canada, 68° N).⁵⁵ ΣPFCA concentrations in soil from Cornwallis Island (0.33-1.92 ng g⁻¹ dw) are similar to those in soils from Cape Bounty. ΣPFSA concentrations in soils from Amituk and North Lakes (0.001-0.024 ng g⁻¹ dw) are similar to those at Cape Bounty, although higher ΣPFSA concentrations, dominated by PFOS, are reported in soils from the catchments of Meretta (7.60 ng g⁻¹ g dw), Resolute (0.28 ng g⁻¹ dw), and Small Lakes (0.47 ng g⁻¹ dw) due to emissions from a local airport,⁵⁴ as well as numerous waste landfills which is consistent with earlier reports on Cornwallis Island.^{47,51} Skaar et al., also attribute high soil concentrations of PFOS (0.91-7.06 ng g⁻¹ dw) at specific sites in Ny-Ålesund in 2016 to local airport emissions and greater anthropogenic activity.⁵³ Ny-Ålesund has numerous research facilities, an airport, a wastewater treatment plant and a former coal mining site.

1.5.2.4 Non-marine Snow and Ice

The detection of PFAS in snow from the High Arctic of Canada is limited (Table 1.5). Ice caps in the High Arctic of Canada are valuable for determining atmospheric deposition of contaminants due to their remote proximity from human settlements and high altitude. Surface snow from ice caps indicated trace levels of C₈-C₁₁ PFCA and PFOS from Agassiz, Devon, Melville, and Meighen Ice Caps in 2005 and 2006.³⁷ PFOA and PFNA are most abundant, followed by PFUnDA, PFOS, and PFDA. Similar profiles are observed for PFAA in surface snow from the Lake A catchment in May and August of 2008,⁵² although higher concentrations are reported. Veillette et al. detect C₇-C₁₁ PFCA and C₄, C₆-C₈ PFSA in snow, and the most abundant PFAS are PFHpA, PFOA, and PFNA.⁵² Higher ΣPFAA concentrations are reported in snowpacks that had accumulated atmospheric PFAS pollution over the winter (May 2008, 732-848 pg L⁻¹) compared to freshly deposited snow (August 2008, 134 pg L⁻¹).⁵²

Several studies have investigated PFAS in snow from the High Arctic of Norway. Kwok et al. detect C₄-C₁₂, C₁₄ PFCA and C₆, C₈ PFSA in snow from Svalbard in 2006. PFBA and PFOA are dominant in snow.³⁸ In the latter study, ΣPFAA concentrations are higher in snow near the coastal settlement of Longyearbyen (1471 pg L⁻¹) than those in snow near Longyearbreen glacier (458 pg L⁻¹), suggesting local pollution sources contribute to PFAA in snow from coastal Svalbard.³⁸ Skaar et al. detect C₈-C₁₂ PFCA and C₈ PFSA in snow from the Lake Linnévatnet catchment in 2015.⁵³ The most abundant PFAS in snowpacks are PFOA, PFNA, and PFOS. Meltwaters from the Lake Linnévatnet catchment are dominated by PFBA, whereas PFOA, PFNA, and PFOS are predominate in snow.

Table 1.5 PFAA concentrations (pg L⁻¹) in surface snow from the High Arctic of Canada and Norway, and the Central Arctic.

Mean concentrations are presented in parentheses where available.

High Arctic of Canada	Year	PFBA	PFPeA	PFHxA	PFHpA	PFOA	PFNA	PFDA	PFUnDA	PFDoDA	PFBS	PFHxS	PFOS
Devon Ice Cap (75° N)	2005 ⁵⁶					16.6	9.1	4.2					4.0
Melville Ice Cap (75° N)	2005 ⁵⁶					16.3	9.8	4.5					2.4
	2006 ⁵⁶					38.6	7.6	1.6	2.8				4.6
Meighan Ice Cap (79° N)	2006 ⁵⁶					15.1	12.1	2.2	3.9				1.6
Agassiz Ice Cap (80° N)	2005 ⁵⁶					13.1	10.0	3.9					1.4
	2006 ⁵⁶					53.7	9.4	2.6	5.1				2.3
Lake A (83° N)	2008 ⁵²				37-244 (165)	27-239 (155)	32-273 (167)	0.3-41 (23)	0.2-30 (16)		3-4 (3)	0.7-3 (1.9)	35-70 (40)
High Arctic of Norway	Year	PFBA	PFPeA	PFHxA	PFHpA	PFOA	PFNA	PFDA	PFUnDA	PFDoDA	PFBS	PFHxS	PFOS
Longyearbreen (78° N)	2006 ³⁸	(108)	(30)	(76)	(17)	(112)	(50)	(22)	<LOQ	7		<LOQ	(34)
Longyearbyen (78° N)	2006 ³⁸	(253)	(81)	(89)	(123)	(396)	(245)	(90)	(35)	(16)		(18)	(118)
Central Arctic	Year	PFBA	PFPeA	PFHxA	PFHpA	PFOA	PFNA	PFDA	PFUnDA	PFDoDA	PFBS	PFHxS	PFOS
Sea Ice (82-89° N)	2012 ⁴⁴			26-109 (60)	14-49 (29)	72-294 (152)	33-253 (116)	33-142 (75)	21-92 (53)	<10-88	<5	<5-18	34-343 (140)
Sea Ice (77-87° N)	2010 ⁵⁷	<130-1000	<20-66	<27	23-99 (61)	39-82 (58)	38-110 (80)	<35-50	<21-34	<8.6	<17-170	<66	<21

Skaar et al. suggest these observations are attributed to preferential elution of these compounds during snowmelt, whereby short-chain PFAA are flushed from the snowpack and long-chain PFAA are retained, highlighting the importance of post-depositional snowpack interactions.⁵³ Xie et al. also note the importance of post-depositional interactions of volatile PFAA precursors in snow from Ny-Ålesund in 2012.⁵⁸ In the latter study, air-snow exchange fluxes were calculated to investigate the post-depositional fate and transport of volatile precursors in snowpacks. The net air-snow exchange fluxes indicated that FTOH ultimately evaporate from snowpacks, whereas FOSE remain in snow, although it was suggested that increasing air temperature and snowmelt are expected to enhance FOSE fluxes to the air.⁵⁸

Snow and ice have been used to determine long-term, chronological records of PFAS in the High Arctic. Temporal trends are determined for PFAS using long-term snow and ice records on Devon Ice Cap in 2006.³⁷ The highest concentrations of PFAS occur during the spring and summer, which is attributed to the accumulation of atmospheric PFAS over the winter and enhanced photochemical oxidation of precursors.³⁷ The ice record in the latter study indicates concentrations of PFOA and PFUnDA are constant, while concentrations of PFNA and PFDA increased during 1996-2005.³⁷ Notable temporal variability is reported for PFOS concentrations on Devon Ice Cap. For example, PFOS concentrations increased from 1996 to 1998, decreased from 1998 to 2001, and are constant from 2001 to 2005³⁷. The decreasing temporal trend for PFOS on Devon Ice Cap is attributed to emission reductions from POSF manufacturing, in response to global phase out initiatives.³⁷ Similar observations are reported by Kwok et al. in an ice core from Longyearbreen glacier, whereby concentrations of PFOS reach a

maximum during 1998, decreased in 1999, and are constant from 1999-2002.³⁸ Dynamic temporal trends are also reported in a recent ice core study from Devon Ice Cap. Fluxes of PFOA and PFNA increased on Devon Ice Cap from 1977 to 1995, are constant from 1996 to 2012, and decreased from 2012 to 2015.³⁶ Decreasing trends are noted for other PFCA (i.e., C₅-C₇, C₁₀-C₁₃) post-2012, which is attributed to post-depositional melting effects (i.e., loss of PFCA in snow via percolation), dating errors, and/or reductions in emissions of PFCA and their precursors in North America.³⁶ Increasing trends are reported for FOSA, a volatile precursor to PFOS, from 1977 to 1995, however, it is sporadically detected post-2000, possibly due to its phase out by the 3M Company during 2000-2002.³⁶ PFOS was consistently detected during 1977-2013, with maximum fluxes reported in 2013, suggesting FOSA is not a primary source for PFOS, and ongoing usage of PFOS and its precursors in Asia may corroborate the depositional trends on Devon Ice Cap.³⁶ The fluxes on Devon Ice Cap are higher than those in the High Arctic of Norway, consistent with the enhanced delivery of PFAS to the High Arctic of Canada.³²

1.5.3 Arctic Marine Environment

1.5.3.1 Seawater

Several studies have investigated the occurrence of PFAS in seawater from the central Arctic Ocean and its marginal seas. An overview of global Σ PFCA concentrations is shown in Figure 1.6.

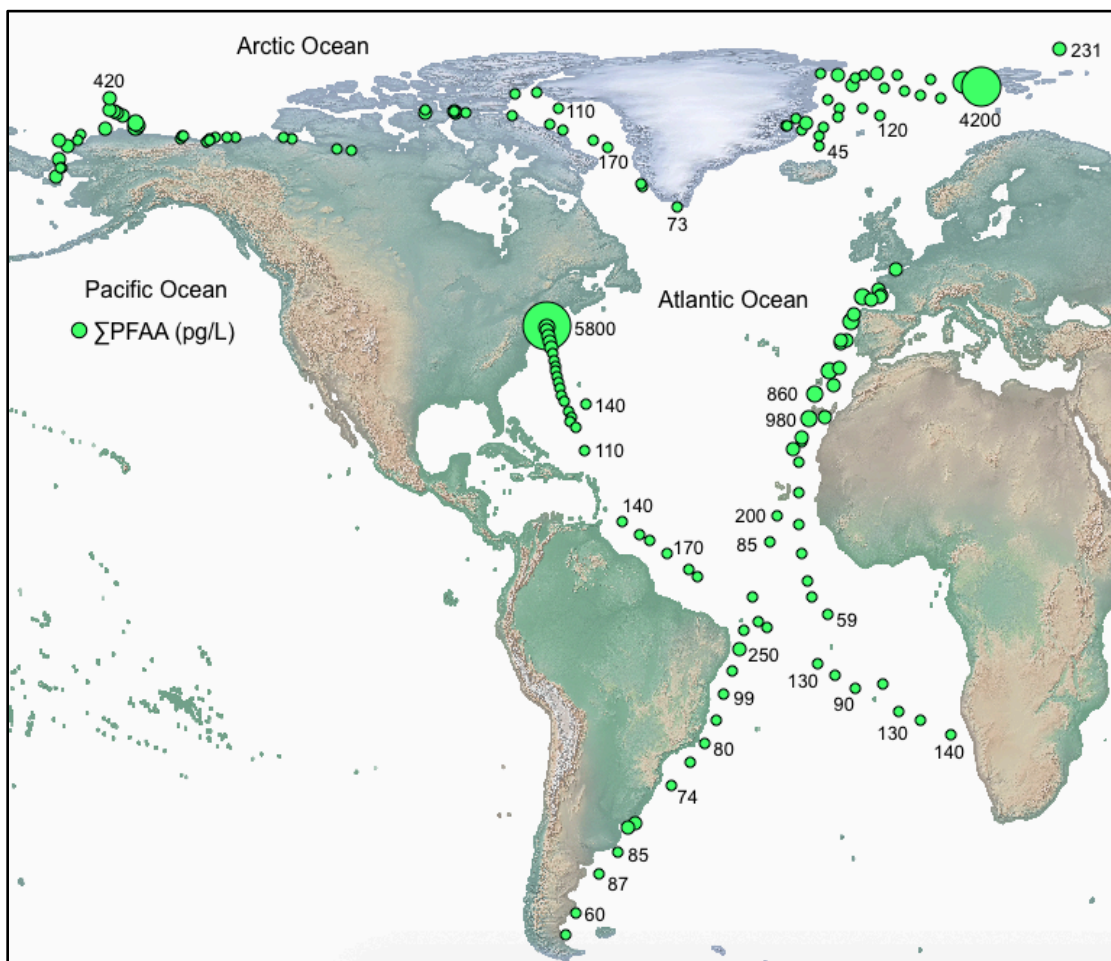


Figure 1.6 Overview of global seawater Σ PFAA concentrations (pg L^{-1}).^{26,38,44,53,57,59} The magnitude of Σ PFAA concentration is proportional to the size of green circles and is indicated numerically at select sites. Map source: Global Topography Relief Raster in Igor Pro (v 6.37).

Cai et al. report C₄-C₁₁ PFCA, C₄, C₈, C₁₀ PFSA, FOSA, N-EtFOSA, N-MeFOSE, and N-EtFOSE in Arctic seawater.⁵⁷ PFBA (<130-360 pg L⁻¹) and PFPeA (21-260 pg L⁻¹) are most abundant in seawater from the Bering, Beaufort, and Chukchi Seas in 2012. ΣPFAA concentrations increased along a transect from the Pacific Ocean to the Bering Sea (230 to 480 pg L⁻¹), possibly due to the transport of terrestrial run-off via Alaska current to the Bering Sea.⁵⁷ ΣPFAA concentrations in the Bering Sea (mean 263, 120-480 pg L⁻¹) are similar to those in the Beaufort and Chukchi Seas (mean 342, 210-650 pg L⁻¹), suggesting inputs from the Pacific Ocean are likely sources of PFAS in these regions.⁵⁷ Cai et al. note the importance of sea ice to PFAS flux into seawater. Higher ΣPFAA concentrations occur in seawater at sites covered by seasonal ice (600-750 pg L⁻¹) than those covered by multiyear ice (260-490 pg L⁻¹), suggesting different magnitudes of sea ice melt can impact PFAS concentrations in seawater.⁵⁷ Li et al. detect a similar suite and magnitude of PFAS (ΣPFAA 347-784 pg L⁻¹) in seawater from the Bering and Chukchi Seas, and Arctic Ocean in 2014.⁶⁰ In both studies, the abundance of PFBA and PFPeA in seawater was attributed to sea ice melting.^{57,60} Yeung et al. investigate the vertical distribution of PFAS in the Arctic Ocean and Chukchi Sea shelf. C₆-C₉, C₁₁ PFCA and C₄, C₆, C₈ PFSA are detected in the polar mixed layer (i.e., 10-30 m below surface) and halocline (i.e., 75-150 m below surface) of the Arctic Ocean, however, PFAS are rarely detected below these depths, possibly due to oceanic dilution and mixing regimes limiting the vertical transport of PFASs to deep waters.⁴⁴ Yeung et al. note that the composition profiles of PFAS varies along the Chukchi Sea shelf, such that higher ratios of PFOA/PFNA were reported in offshore sites than nearshore sites, and PFDA was only detected at nearshore sites. It was suggested that higher contributions of PFNA (i.e., to the PFOA/PFNA ratio)

and exclusive detection of PFDA in nearshore sites was attributed to riverine inputs.⁴⁴ A similar suite of PFAS (i.e., C₆-C₁₁ PFCA, C₈ PFSA, and FOSA) is reported by Yeung et al. in melt-pond water from the Central Arctic (83-84° N) in 2012.⁴⁴ The highest concentrations in surface waters are reported for PFHxA (16-150 pg L⁻¹), PFOA (57-62 pg L⁻¹), PFNA (85-106 pg L⁻¹), and PFOS (34-42 pg L⁻¹), and ΣPFAS concentrations ranged from 231-416 pg L⁻¹.⁴⁴ The concentrations of PFAS in the latter study are lower than those reported in the High Arctic of Norway (Table 1.5).

Several studies have investigated PFAS in seawater from the Greenland Sea. Yamashita et al. detect PFOA, PFBS, and PFOS in water columns from southwest and southeast Greenland in 2004.²⁵ The most abundant PFAS at southwest Greenland is PFOA, whereas PFBS dominates at southeast Greenland. While surface seawater concentrations of PFAS are higher at southeast Greenland, the vertical distribution of PFAS is similar at both sites. The concentrations of PFAS in the southwest and southeast water columns are generally well mixed from the surface to 2000 m, and higher concentrations of PFOA and PFBS are observed below 2000 m at both sites. Higher concentrations of PFOA and PFBS in deep waters is attributed to the delivery of PFAS from a deep water current from the Denmark Strait.²⁵ Surface seawater PFAS profiles in the Greenland Sea are also determined. Busch et al. detect C₆-C₈ PFCA, C₆, C₈ PFSA, and FOSA in surface seawater from the Eastern Greenland Arctic Ocean in 2009 (67-80° N).⁶¹ The most abundant PFAS are PFOA (51 ± 30 pg L⁻¹) and FOSA (61 ± 73 pg L⁻¹). Higher ΣPFAS concentrations (i.e., sum of PFAS and FOSA) are reported in coastal water (193 pg L⁻¹) than those reported in seawater (133 pg L⁻¹). It is suggested surface runoff water from rain and/or melted snow from mainland Greenland is a source of C₆-C₈

PFCA and PFHxS in coastal water.⁶¹ FOSA concentrations are comparable in coastal water and seawater, suggesting oceanic and atmospheric transport are relevant to FOSA deposition in the East Greenland Arctic Ocean.⁶¹ Zhao et al. detect C₆, C₈, C₉ PFCA and C₄, C₆-C₈ PFSA in seawater from the Greenland Sea in 2009.⁵⁹ The highest concentrations are reported for PFOA (45-150 pg L⁻¹), PFBS (<51-65 pg L⁻¹), and PFHxS (<6.5-45 pg L⁻¹), although PFBS is not detected frequently. Higher PFOA concentrations in seawater is linked to the delivery of snow and ice melt from the High Arctic via East Greenland Current.⁵⁹ Zhao et al. note that higher PFOA concentrations are detected in coastal waters, suggesting melting glaciers on mainland Greenland are sources of PFOA in the Greenland Sea.⁵⁹

The detection of PFAS in seawater from the High Arctic of Norway is limited. Kwok et al. detect C₄-C₉ PFCA and C₆, C₈ PFSA in seawater from the coast of Longyearbyen in 2006.³⁸ PFPeA (352 ± 33 pg L⁻¹), PFOS (109 ± 69 pg L⁻¹), and PFOA (74 ± 20 pg L⁻¹) are dominant in seawater. Low PFAS concentrations in seawater near Longyearbyen are attributed to oceanic dilution.³⁸ Ahrens et al. also report low concentrations of PFOA (10 pg L⁻¹) in the Norwegian Sea in 2007, whereas other PFAS were below the detection limit.⁶² More recently, Skaar et al. note high concentrations of PFBA (<0.5-1510 pg L⁻¹) in seawater from Ny-Ålesund in 2016, although other PFAS are typically below the detection limit.⁵³ In contrast, C₅-C₉ PFCA and C₄, C₆, C₈ PFSA are detected in seawater near Longyearbyen in 2014, dominated by PFPeA (1290-1550 pg L⁻¹) and PFHxA (2660-3020 pg L⁻¹). In the latter study, local fire-fighting training sites are identified as a dominant local pollution sources of PFAS in Longyearbyen.⁵³

1.5.3.2 Marine Snow and Ice

Several studies investigate PFAS in snow from the Central Arctic Ocean. Cai et al. report C₄, C₅, C₇-C₁₁, C₁₃ PFCA and PFBS in surface snow from the Central Arctic Ocean in 2010.⁵⁷ The highest concentrations are reported for PFBA, PFBS, PFNA, PFHpA, and PFOA. Spatial variability is reported for PFAA in snow from the Central Arctic, whereby higher Σ PFAA concentrations are reported at 77° N (1400 pg L⁻¹) and 87° N (1200 pg L⁻¹) than at 80° N (220 pg L⁻¹).⁵⁷ Similar observations are noted in surface snow from the Central Arctic in 2012. Yeung et al. detect C₆-C₁₂ PFCA and C₆, C₈, C₁₀ PFSA in surface snow.⁴⁴ PFOA, PFNA, and PFOS are dominant in snow and spatial variability is reported for Σ PFAA concentrations in the Central Arctic at 84° N (262 pg L⁻¹), 82° N (1388 pg L⁻¹), and 89° N (340 pg L⁻¹).⁴⁴

The occurrence of PFAS in sea ice cores from the Central Arctic Ocean is used to infer temporal trends in PFAS deposition in the High Arctic. Cai et al. note that the profile for C₇-C₁₄ PFCA in a sea ice core at 77° N is similar with depth, suggesting this site was impacted by similar sources over time.⁵⁷ It is interesting to note that Σ PFAA concentrations in snow on a sea ice core at 77° N (400 pg L⁻¹) are higher than concentrations in the underlying sea-ice (880-1100 pg L⁻¹) due to elevated concentrations of PFBA (1000 pg L⁻¹). A different profile is reported in a sea ice core at 80° N. Higher concentrations of C₈-C₁₀ PFCA and C₄, C₈ PFSA are reported in the surface sea ice core layer (i.e., 0-15 cm) than overlying snow, particularly for PFBS. PFBS concentrations in the surface ice layer are approximately 38 times higher than in overlying snow. Cai et al. suggest that high concentrations of PFBS in surface ice layer is due to snowpack melting during the summer of 2010, such that PFBS melted from overlying snowpacks and

became enriched in the surface ice layer.⁵⁷ A similar profile is reported in a sea ice core from site at 87° N, indicating that snowpack melting can enhance PFAA concentrations in sea ice. The abundance of PFBA and PFBS in snow and ice from the Central Arctic is linked to increasing direct emissions of these compounds and their precursors due to the phase-out of POSF-based substances.⁵⁷ It is challenging to determine temporal trends using sea ice because its extent is declining in the Arctic due to climate warming.⁶³ Furthermore, as noted by Cai et al.,⁵⁷ warming enhances sea ice melting and remobilizes PFAS within sea ice layers, which can bias the annual assignment of PFAS in sea ice.⁵⁷

1.6 Climate Warming in the High Arctic

The Earth is responding rapidly to climate warming. Natural forcings such as changes in solar radiation from the Sun, volcanic activity, ocean and atmospheric circulation, as well as anthropogenic forcings such as the emission of greenhouse gases from the combustion of fossil fuels promote climate warming. The Arctic is an area that is experiencing the fastest rate of climate change and greatest perturbations such as higher temperatures (Figure 1.7) and anthropogenic pollution (e.g., particles and gases) promoted by increasing ship traffic and land development, which are relevant to the glacier mass balance in the Arctic. For instance, higher air temperatures and light-absorbing particles (LAP) emitted from natural and anthropogenic sources (e.g., mineral dust and combustion particles) enhance snow and glacial ice melting in the Arctic. It is possible enhanced freshwater discharge via snow and glacier melting in the Arctic will alter thermohaline oceanic circulation (i.e., ocean currents).

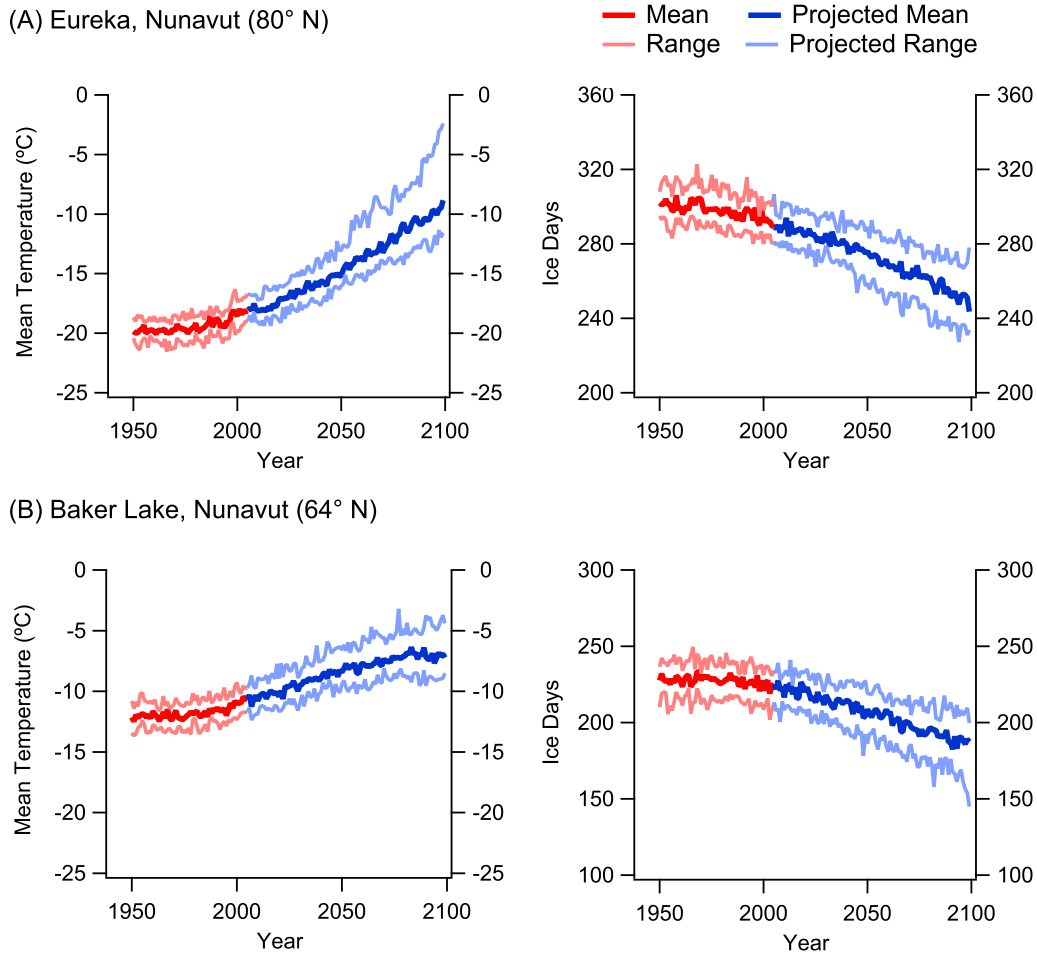


Figure 1.7 Long-term records of mean temperature (°C, y-axes) and number of ice days at High (Eureka, 80° N) and Low (Baker Lake, 64° N) Arctic regions in Canada as a function of time (year, x-axis). Ice days refers to the number of days where the maximum daily temperature is equal to or less than 0 °C. Empirical measurements are denoted by red lines and modelled measurements are denoted by blue lines. Modelled measurements are estimated according to greenhouse gas concentration estimates from Representative Concentration Pathway 8.5. Historical and modelled data are obtained from www.climatedata.ca.

In the High Arctic of Canada, the Queen Elizabeth Islands (QEI) represent approximately 14% of the global glacier area, spanning 104,000 km².⁶⁴ Glaciers on QEI receive low annual precipitation inputs, thus their mass balance is contingent on summer air temperatures.⁶⁴ Sharp et al. indicate that a large mass loss of glaciers is occurring on the QEI, particularly post-2005 due to warmer summer temperatures and longer melting seasons.⁶⁴ For instance, summer air temperatures during 2005-2009 were 0.8 to 2.2 °C higher than those reported during 2000-2004, while a 30-48% mass loss was reported for glaciers on QEI post-2005.⁶⁴ It is suggested that warmer summer temperatures are attributed to atmospheric circulation patterns delivering heat from the northwest Atlantic Ocean to the QEI.⁶⁴ Similar observations are reported by Gascon et al., whereby the delivery of warm air into the QEI promotes warmer summer temperatures and longer melting seasons leading to enhanced surface melting on Devon Ice Cap during 2004-2010.^{65,66} The mass loss of glaciers is also observed from the Lake Hazen watershed (Ellesmere Island, Nunavut, 82° N), particularly post-2006. The mass loss of glaciers, promoted by warmer summer temperatures, enhanced glacial meltwater discharge into Lake Hazen, the largest lake by volume north of the Arctic Circle.⁶⁷ Lehnerr et al. note that enhanced glacier melting during 2007-2012 increased the water level in Lake Hazen by 0.8 m and its outflow discharge from 0.49 to 1.8 km³ relative to a pre-climate warming baseline in 1996-2006.⁶⁷ Warmer summer temperatures in the Lake Hazen region deepen the soil active layer in the Lake Hazen watershed. The active layer is the top layer of soil that undergoes seasonal freeze-thaw cycles, and is underlain by permafrost, which is ground (i.e., soil) that has maintained a temperature of 0 °C for at least two consecutive years.⁶⁸ Permafrost is ubiquitous, ice-rich, and deep in the High Arctic, such that 90% of

its terrain is underlain by permafrost, with an estimated depth exceeding 500 m.⁵⁴ When permafrost soils contain an excess of ice, the thawing of soils and the melting of ice produces a significant quantity of meltwater.⁶⁸ The discharge of ice meltwaters from soils contributes to enhanced surface runoff.⁶⁸ These observations demonstrate that climate warming is an important vector relevant to the freshwater balance in the High Arctic.

1.6.1 Climate Implications for PFAS in the Arctic

Climate warming-induced glacier melting has important implications for PFAA deposition in the High Arctic of Canada. Several studies determine chronological records of PFAA deposition using ice cores from Devon Ice Cap,^{36,37} however, the enhanced production and subsequent percolation of meltwaters into deep snow layers can affect the accuracy of these records, such that snow layers (i.e., annual records of atmospheric deposition) become integrated.^{66,69} An important consequence of climate warming on Devon Ice Cap is the ability to accurately monitor historical changes in atmospheric emissions, particularly within the context of PFAS manufacturing shifts promoted by regulatory initiatives. It is also possible that enhanced glacier melting will impact PFAA deposition in the Lake Hazen watershed. It was suggested that climate warming-induced glacier melting is implicated in the enhanced delivery of sediment and contaminants such as organochlorine pesticides (OCPs) and mercury (Hg) into Lake Hazen.⁶⁷ By analogy, the thawing of permafrost soils and melting of ice contained within them is expected to enhance the discharge of contaminants to freshwater systems via surface runoff in the Lake Hazen watershed. An important consequence of climate warming in this region is

that enhanced glacier and ground ice melting can remobilize contaminants that are historically archived in ice into Lake Hazen,⁶⁷ which in turn may offset current global regulations and enhances exposure of legacy contaminants to wildlife and humans.

1.7 Objectives and Goals

The manufacturing of PFAA since the 1950s has resulted in their ubiquitous, environmental dissemination.^{13,14} The detection of PFAA in remote environments, such as the High Arctic, indicates they are amenable to long-range transport. Long-range atmospheric transport is an important, albeit poorly understood pathway for PFAA to the High Arctic. Some of the most compelling evidence of long-range atmospheric transport is the occurrence of PFAA in high altitude glaciers³⁶⁻³⁸ and landlocked lakes^{47,51,52} in the High Arctic because these areas are uninhabited and are removed from anthropogenic pollution. Thus, environmental monitoring of PFAA in the High Arctic is useful for improving current understanding of long-range atmospheric transport. For instance, glacier ice cores³⁶⁻³⁸ and lake sediment cores^{47,70} are used to establish long-term chronological records of atmospheric PFAA deposition, which is useful for elucidating sources, as well as historical changes in PFAA pollution within the context of global market changes and regulatory initiatives. Indeed, environmental monitoring is useful for improving understanding of long-range transport of PFAA, however, it is currently unknown how climate warming will impact the post-depositional transport and fate of PFAA in the High Arctic. This is a critical knowledge gap because the High Arctic contains a large portion of the global glacier mass and has been responding rapidly to

climate warming over the last decade.⁶⁴⁻⁶⁶ The occurrence of PFAA in glacier ice suggests climate warming will impact their post-depositional transport and fate in the High Arctic.³⁶⁻³⁸ The overall goal of this thesis is to improve current understanding of long-range transport and fate of PFAS in the Arctic, especially in environments that are responding rapidly to the effects of climate change.

The study of PFAS in glacier ice is limited to two studies in the High Arctic of Canada, one of which pre-dates standardized methods for PFAS extraction and analysis such as available isotopically labeled surrogates and instrumentation for reaching low detection limits.^{36,37} To improve current understanding of long-range transport, a 14-year depositional ice record of PFAS on Devon Ice Cap is discussed in Chapter 2. The hypothesis that the long-range transport atmospheric oxidation of volatile precursors is a dominant source of PFAS is tested. This work expands on an earlier study,³⁷ with a greater number of detected analytes, thereby permitting a comprehensive assessment of sources and long-range transport mechanisms on the Devon Ice Cap.

The study of PFAS in sediment cores from the Arctic of Canada is very limited.^{47,51,52,70} In this thesis, three chapters are focused on PFAS measurements in the Lake Hazen area of Ellesmere Island in the High Arctic. The hydrology and bathymetry of the lake are well characterized, and it has been previously studied for mercury, but not organic contaminants. The lake is on Ellesmere Island and far from any human settlements. Further, its northern coast is surrounded by glaciers. In Chapter 3, chronological records of PFAS deposition are discussed for the first time in Lake B35 in the low Arctic of Canada near Hudson Bay and Lake Hazen. The Lake Hazen and Lake B35 regions have been responding to climate warming, thus, the hypothesis that climate

warming enhances PFAS deposition in Lake B35 and Lake Hazen sediments is investigated. The dominant historical sources of PFAS in sediments are also discussed.

In Chapter 4, PFAS are quantified for the first time in annual snow and lake water from the Lake Hazen watershed. The implications of atmospheric particles on the long-range and post-depositional transport and fate of PFAS in snowpacks are discussed, as well as the seasonal impacts of melting snow and glaciers on the delivery of PFAS into the Lake Hazen.

The transport and fate of PFAS in freshwater systems in the High Arctic is poorly understood. In Chapter 5, PFAS are quantified for the first time along a freshwater continuum fed by permafrost thaw streams and snowmelt, as well as in glacier-fed rivers in the Lake Hazen watershed. The transport of PFAS along the freshwater continuum, implications of climate warming on the remobilization of contaminants from ice, and the mass transfer of PFAS by glacier-fed rivers are discussed.

A summary of these results is provided in Chapter 6, and the implications and future outlook on PFAS monitoring in the High Arctic of Canada are discussed.

1.8 Literature Cited

- (1) Buck, R. C.; Franklin, J.; Berger, U.; Conder, J. M.; Cousins, I. T.; Voogt, P. De; Jensen, A. A.; Kannan, K.; Mabury, S. A.; van Leeuwen, S. P. J. Perfluoroalkyl and polyfluoroalkyl substances in the environment: Terminology, classification, and origins. *Integr. Environ. Assess. Manag.* **2011**, *7* (4), 513–541.
- (2) Hurley, M. D.; Wallington, T. J.; Sulbaek Andersen, M. P.; Ellis, D. A.; Martin, J. W.; Mabury, S. A. Atmospheric chemistry of fluorinated alcohols: Reaction with Cl atoms and OH radicals and atmospheric lifetimes. *J. Phys. Chem. A* **2004**, *108* (11), 1973–1979.
- (3) Martin, J. W.; Ellis, D. A.; Mabury, S. A.; Hurley, M. D.; Wallington, T. J. Atmospheric chemistry of perfluoroalkanesulfonamides: Kinetic and product studies of the OH radical and Cl atom initiated oxidation of N-ethyl perfluorobutanesulfonamide. *Environ. Sci. Technol.* **2006**, *40* (3), 864–872.
- (4) Wallington, T. J.; Hurley, M. D.; Xia, J.; Wuebbles, D. J.; Sillman, S.; Ito, A.; Penner, J. E.; Ellis, D. A.; Martin, J.; Mabury, S. A.; Nielsen, O.J., Sulbaek Andersen, M.P. Formation of C₇F₁₅COOH (PFOA) and other perfluorocarboxylic acids during the atmospheric oxidation of 8:2 fluorotelomer alcohol. *Environ. Sci. Technol.* **2006**, *40* (3), 924–930.
- (5) Pan, Y.; Wang, J.; Yeung, L. W. Y.; Wei, S.; Dai, J. Analysis of emerging per- and polyfluoroalkyl substances: Progress and current issues. *Trac. Trends Anal. Chem.* **2020**, *124*, 115481.

- (6) Kissa, E. *Fluorinated Surfactants and Repellents*; 2001.
- (7) Young, C. J.; Mabury, S. A. Atmospheric perfluorinated acid precursors: Chemistry, occurrence, and impacts. *Rev. Environ. Contam. Toxicol.* **2010**, *208*, 1–109.
- (8) Boucher, J. M.; Cousins, I. T.; Scheringer, M.; Hungerbühler, K.; Wang, Z. Toward a Comprehensive Global Emission Inventory of C4-C10 Perfluoroalkanesulfonic Acids (PFSA) and Related Precursors: Focus on the Life Cycle of C6- and C10-Based Products. *Environ. Sci. Technol. Lett.* **2019**, *6* (1), 1–7.
- (9) Wang, Z.; Cousins, I. T.; Scheringer, M.; Buck, R. C.; Hungerbühler, K. Global emission inventories for C4-C14 perfluoroalkyl carboxylic acid (PFCA) homologues from 1951 to 2030, part II: The remaining pieces of the puzzle. *Environ. Int.* **2014**, *69*, 166–176.
- (10) O'Hagan, D. Understanding organofluorine chemistry. An introduction to the C-F bond. *Chem. Soc. Rev.* **2008**, *37* (2), 308–319.
- (11) Wang, Z.; Boucher, J. M.; Scheringer, M.; Cousins, I. T.; Hungerbühler, K. Toward a Comprehensive Global Emission Inventory of C4-C10 Perfluoroalkanesulfonic Acids (PFSA) and Related Precursors: Focus on the Life Cycle of C8-Based Products and Ongoing Industrial Transition. *Environ. Sci. Technol.* **2017**, *51* (8), 4482–4493.
- (12) Wang, Z.; Cousins, I. T.; Scheringer, M.; Buck, R. C.; Hungerbühler, K. Global emission inventories for C4-C14 perfluoroalkyl carboxylic acid (PFCA) homologues from 1951 to 2030, Part I: Production and emissions from quantifiable

- sources. *Environ. Int.* **2014**, *70*, 62–75.
- (13) Butt, C. M.; Berger, U.; Bossi, R.; Tomy, G. T. Levels and trends of poly- and perfluorinated compounds in the arctic environment. *Sci. Total Environ.* **2010**, *408* (15), 2936–2965.
- (14) Rigét, F.; Bignert, A.; Braune, B.; Dam, M.; Dietz, R.; Evans, M.; Green, N.; Gunnlaugsdóttir, H.; Hoydal, K. S.; Kucklick, J.; Letcher, R.; Muir, D.; Schuur, S., Sonne, C., Stern, G., Tomy, G., Vorkamp, K., Wilson, S. Temporal trends of persistent organic pollutants in Arctic marine and freshwater biota. *Sci. Total Environ.* **2019**, *649*, 99–110.
- (15) Wang, Y.; Wang, L.; Chang, W.; Zhang, Y.; Zhang, Y.; Liu, W. Neurotoxic effects of perfluoroalkyl acids: Neurobehavioral deficit and its molecular mechanism. *Toxicol. Lett.* **2019**, *305*, 65–72.
- (16) Ritter, S. K. Fluorochemicals go short. *Chem. Eng. News* **2010**, *88* (5), 12–17.
- (17) US EPA. 2010/15 PFOA Stewardship Program <https://www.epa.gov/assessing-and-managing-chemicals-under-tsca> (accessed May 1, 2017).
- (18) Government of Canada. Perfluorocarboxylic acids and their precursors : environmental performance agreement overview <https://www.canada.ca/en/environment-climate-change/services/environmental-performance-agreements/list/perfluorocarboxylic-acids-overview.html> (accessed Jun 9, 2019).
- (19) Stockholm Convention. PFOS, its salts and PFOSE <http://chm.pops.int/Implementation/IndustrialPOPs/PFOS/Overview/tabid/5221/Default.aspx>.

- (20) The European Commission. Commission Regulation (EU) 2017/1000 concerning the Registration, Evaluation, Authorisation and Restriction of Chemicals as regards perfluorooctanoic acid (PFOA), its salts and PFOA-related substances. *Off. J. Eur. Union* **2017**, L 150 (June), 14–18.
- (21) Gordon, S. C. Toxicological evaluation of ammonium 4,8-dioxa-3H-perfluorononanoate, a new emulsifier to replace ammonium perfluorooctanoate in fluoropolymer manufacturing. *Regul. Toxicol. Pharmacol.* **2011**, 59 (1), 64–80.
- (22) Wang, S.; Huang, J.; Yang, Y.; Hui, Y.; Ge, Y.; Larssen, T.; Yu, G.; Deng, S.; Wang, B.; Harman, C. First report of a Chinese PFOS alternative overlooked for 30 years: Its toxicity, persistence, and presence in the environment. *Environ. Sci. Technol.* **2013**, 47 (18), 10163–10170.
- (23) Gebbink, W. A.; Bossi, R.; Rigét, F. F.; Rosing-Asvid, A.; Sonne, C.; Dietz, R. Observation of emerging per- and polyfluoroalkyl substances (PFASs) in Greenland marine mammals. *Chemosphere* **2016**, 144, 2384–2391.
- (24) Pan, Y.; Zhang, H.; Cui, Q.; Sheng, N.; Yeung, L. W. Y.; Sun, Y.; Guo, Y.; Dai, J. Worldwide Distribution of Novel Perfluoroether Carboxylic and Sulfonic Acids in Surface Water. *Environ. Sci. Technol.* **2018**, 52 (14), 7621–7629.
- (25) Yamashita, N.; Taniyasu, S.; Petrick, G.; Wei, S.; Gamo, T.; Lam, P. K. S.; Kannan, K. Perfluorinated acids as novel chemical tracers of global circulation of ocean waters. *Chemosphere* **2008**, 70 (7), 1247–1255.
- (26) Benskin, J. P.; Muir, D. C. G.; Scott, B. F.; Spencer, C.; De Silva, A. O.; Kylin, H.; Martin, J. W.; Morris, A.; Lohmann, R.; Tomy, G.; Rosenberg, B., Taniyasu, S., Yamashita, N. Perfluoroalkyl acids in the atlantic and Canadian arctic oceans.

Environ. Sci. Technol. **2012**, *46* (11), 5815–5823.

- (27) St. Pierre, K. A.; St. Louis, V. L.; Lehnerr, I.; Schiff, S. L.; Muir, D. C. G.; Poulain, A. J.; Smol, J. P.; Talbot, C.; Ma, M.; Findlay, D. L.; Arnott, S.E, Gardner, A.S. Contemporary limnology of the rapidly changing glacierized watershed of the world's largest High Arctic lake. *Sci. Rep.* **2019**, *9* (1), 1–15.
- (28) Wang, Z.; MacLeod, M.; Cousins, I. T.; Scheringer, M.; Hungerbühler, K. Using COSMOtherm to predict physicochemical properties of poly- and perfluorinated alkyl substances (PFASs). *Environ. Chem.* **2011**, *8* (4), 389–398.
- (29) Burns, D. C.; Ellis, D. A.; Li, X.; McMurdo, C. J.; Webster, E. Experimental pKa determination for perfluorooctanoic acid (PFOA) and the potential impact of pKa concentration dependence on laboratory-measured partitioning phenomena and environmental modeling. *Environ. Sci. Technol.* **2008**, *42*, 9283–9288.
- (30) Bhatarai, B.; Gramatica, P. Prediction of aqueous solubility, vapor pressure and critical micelle concentration for aquatic partitioning of perfluorinated chemicals. *Environ. Sci. Technol.* **2011**, *45* (19), 8120–8128.
- (31) Ellis, D. A.; Martin, J. W.; Mabury, S. A.; Hurley, M. D.; Sulbaek Andersen, M. P.; Wallington, T. J. Atmospheric lifetime of fluorotelomer alcohols. *Environ. Sci. Technol.* **2003**, *37* (17), 3816–3820.
- (32) Wong, F.; Shoeib, M.; Katsoyiannis, A.; Eckhardt, S.; Stohl, A.; Bohlin-Nizzetto, P.; Li, H.; Fellin, P.; Su, Y.; Hung, H. Assessing temporal trends and source regions of per- and polyfluoroalkyl substances (PFASs) in air under the Arctic Monitoring and Assessment Programme (AMAP). *Atmos. Environ.* **2018**, *172*, 65–73.

- (33) Ahrens, L.; Shoeib, M.; Del Vento, S.; Codling, G.; Halsall, C. Polyfluoroalkyl compounds in the Canadian Arctic atmosphere. *Environ. Chem.* **2011**, *8* (4), 399–406.
- (34) Shoeib, M.; Harner, T.; Vlahos, P. Perfluorinated chemicals in the arctic atmosphere. *Environ. Sci. Technol.* **2006**, *40* (24), 7577–7583.
- (35) Rauert, C.; Shoieib, M.; Schuster, J. K.; Eng, A.; Harner, T. Atmospheric concentrations and trends of poly- and perfluoroalkyl substances (PFAS) and volatile methyl siloxanes (VMS) over 7 years of sampling in the Global Atmospheric Passive Sampling (GAPS) network. *Environ. Pollut.* **2018**, *238*, 94–102.
- (36) Pickard, H. M.; Criscitiello, A. S.; Spencer, C.; Sharp, M. J.; Muir, D. C. G.; De Silva, A. O.; Young, C. J. Continuous non-marine inputs of per- and polyfluoroalkyl substances to the High Arctic: A multi-decadal temporal record. *Atmos. Chem. Phys.* **2018**, *18* (7), 5045–5058.
- (37) Young, C. J.; Furdui, V. I.; Franklin, J.; Koerner, R. M.; Muir, D. C. G.; Mabury, S. A. Perfluorinated acids in Arctic snow: New evidence for atmospheric formation. *Environ. Sci. Technol.* **2007**, *41*, 3455–3461.
- (38) Kwok, K. Y.; Yamazaki, E.; Yamashita, N.; Taniyasu, S.; Murphy, M. B.; Horii, Y.; Petrick, G.; Kallerborn, R.; Kannan, K.; Murano, K.; Lam, P.K.S. Transport of Perfluoroalkyl substances (PFAS) from an arctic glacier to downstream locations: Implications for sources. *Sci. Total Environ.* **2013**, *447*, 46–55.
- (39) Wurl, O.; Wurl, E.; Miller, L.; Johnson, K.; Vagle, S. Formation and global distribution of sea-surface microlayers. *Biogeosciences* **2011**, *8* (1), 121–135.

- (40) McMurdo, C. J.; Ellis, D. A.; Webster, E.; Butler, J.; Christensen, R. D.; Reid, L. K. Aerosol enrichment of the surfactant PFO and mediation of the water-air transport of gaseous PFOA. *Environ. Sci. Technol.* **2008**, *42*, 3969–3974.
- (41) Reth, M.; Berger, U.; Broman, D.; Cousins, I. T.; Nilsson, E. D.; McLachlan, M. S. Water-to-air transfer of perfluorinated carboxylates and sulfonates in a sea spray simulator. *Environ. Chem.* **2011**, *8*, 381–388.
- (42) Wania, F. A global mass balance analysis of the source of perfluorocarboxylic acids in the Arctic Ocean. *Environ. Sci. Technol.* **2007**, *41* (13), 4529–4535.
- (43) Armitage, J. M.; McCleod, M.; Cousins, I. T. Modeling the global fate and transport of PFO (A) emitted from direct sources using a multi-species mass balance model. *Environ. Sci. Technol.* **2008**, *43* (4), 1134–1140.
- (44) Yeung, L. W. Y.; Dassuncao, C.; Mabury, S.; Sunderland, E. M.; Zhang, X.; Lohmann, R. Vertical Profiles, Sources, and Transport of PFASs in the Arctic Ocean. *Environ. Sci. Technol.* **2017**, *51* (12), 6735–6744.
- (45) Ellis, D. A.; Martin, J. W.; De Silva, A. O.; Mabury, S. A.; Hurley, M. D.; Sulbaek Andersen, M. P.; Wallington, T. J. Degradation of fluorotelomer alcohols: A likely atmospheric source of perfluorinated carboxylic acids. *Environ. Sci. Technol.* **2004**, *38* (12), 3316–3321.
- (46) D’eon, J. C.; Hurley, M. D.; Wallington, T. J.; Mabury, S. A. Atmospheric chemistry of N-methyl perfluorobutane sulfonamidoethanol, C₄F₉SO₂N(CH₃)CH₂CH₂OH: Kinetics and mechanism of reaction with OH. *Environ. Sci. Technol.* **2006**, *40* (6), 1862–1868.
- (47) Stock, N. L.; Furdui, V. I.; Muir, D. C. G.; Mabury, S. A. Perfluoroalkyl

- contaminants in the Canadian arctic: Evidence of atmospheric transport and local contamination. *Environ. Sci. Technol.* **2007**, *41* (10), 3529–3536.
- (48) Cai, M.; Xie, Z.; Möller, A.; Yin, Z.; Huang, P.; Cai, M.; Yang, H.; Sturm, R.; He, J.; Ebinghaus, R. Polyfluorinated compounds in the atmosphere along a cruise pathway from the Japan Sea to the Arctic Ocean. *Chemosphere* **2012**, *87* (9), 989–997.
- (49) Bossi, R.; Vorkamp, K.; Skov, H. Concentrations of organochlorine pesticides, polybrominated diphenyl ethers and perfluorinated compounds in the atmosphere of North Greenland. *Environ. Pollut.* **2016**, *217*, 4–10.
- (50) Xie, Z.; Wang, Z.; Mi, W.; Möller, A.; Wolschke, H.; Ebinghaus, R. Neutral Poly-/perfluoroalkyl Substances in Air and Snow from the Arctic. *Sci. Rep.* **2015**, *5*, 1–6.
- (51) Lescord, G. L.; Kidd, K. A.; De Silva, A. O.; Williamson, M.; Spencer, C.; Wang, X.; Muir, D. C. G. Perfluorinated and polyfluorinated compounds in lake food webs from the Canadian High Arctic. *Environ. Sci. Technol.* **2015**, *49* (5), 2694–2702.
- (52) Veillette, J.; Muir, D. C. G.; Antoniades, D.; Spencer, C.; Loewen, T. N.; Babaluk, J. A.; Reist, J. D.; Vincent, W. F. Perfluorinated Chemicals in Meromictic Lakes on the Northern Coast of Ellesmere Island, High Arctic Canada. *Arctic* **2014**, *65* (3), 245–256.
- (53) Skaar, J. S.; Ræder, E. M.; Lyche, J. L.; Ahrens, L.; Kallenborn, R. Elucidation of contamination sources for poly- and perfluoroalkyl substances (PFASs) on Svalbard (Norwegian Arctic). *Environ. Sci. Pollut. Res.* **2019**, *26* (8), 7356–7363.

- (54) Cabrerizo, A.; Muir, D. C. G.; De Silva, A. O.; Wang, X.; Lamoureux, S. F.; Lafrenière, M. J. Legacy and Emerging Persistent Organic Pollutants (POPs) in Terrestrial Compartments in the High Arctic: Sorption and Secondary Sources. *Environ. Sci. Technol.* **2018**, *52* (24), 14187–14197.
- (55) Rankin, K.; Mabury, S. A.; Jenkins, T. M.; Washington, J. W. A North American and global survey of perfluoroalkyl substances in surface soils: Distribution patterns and mode of occurrence. *Chemosphere* **2016**, *161*, 333–341.
- (56) Young, C. J.; Furdui, V. I.; Franklin, J.; Koerner, R. M.; Muir, D. C. G.; Mabury, S. A. Perfluorinated acids in arctic snow: New evidence for atmospheric formation. *Environ. Sci. Technol.* **2007**, *41* (10), 3455–3461.
- (57) Cai, M.; Zhao, Z.; Yin, Z.; Ahrens, L.; Huang, P.; Cai, M.; Yang, H.; He, J.; Sturm, R.; Ebinghaus, R.; Xie, Z. Occurrence of perfluoroalkyl compounds in surface waters from the North Pacific to the Arctic Ocean. *Environ. Sci. Technol.* **2012**, *46* (2), 661–668.
- (58) Xie, Z.; Wang, Z.; Mi, W.; Möller, A.; Wolschke, H.; Ebinghaus, R. Neutral Poly-/perfluoroalkyl Substances in Air and Snow from the Arctic. *Sci. Rep.* **2015**, *5*.
- (59) Zhao, Z.; Xie, Z.; Möller, A.; Sturm, R.; Tang, J.; Zhang, G.; Ebinghaus, R. Distribution and long-range transport of polyfluoroalkyl substances in the Arctic, Atlantic Ocean and Antarctic coast. *Environ. Pollut.* **2012**, *170*, 71–77.
- (60) Li, L.; Zheng, H.; Wang, T.; Cai, M.; Wang, P. Perfluoroalkyl acids in surface seawater from the North Pacific to the Arctic Ocean: Contamination, distribution and transportation. *Environ. Pollut.* **2018**, *238*, 168–176.
- (61) Busch, J.; Ahrens, L.; Xie, Z.; Sturm, R.; Ebinghaus, R. Polyfluoroalkyl

- compounds in the East Greenland Arctic Ocean. *J. Environ. Monit.* **2010**, *12* (6), 1242–1246.
- (62) Ahrens, L.; Gerwinski, W.; Theobald, N.; Ebinghaus, R. Sources of polyfluoroalkyl compounds in the North Sea, Baltic Sea and Norwegian Sea: Evidence from their spatial distribution in surface water. *Mar. Pollut. Bull.* **2010**, *60* (2), 255–260.
- (63) Law, K. S.; Stohl, A. Arctic air pollution: Origins and impacts. *Science* **2007**, *315* (5818), 1537–1540.
- (64) Sharp, M.; Burgess, D. O.; Cogley, J. G.; Ecclestone, M.; Labine, C.; Wolken, G. J. Extreme melt on Canada's Arctic ice caps in the 21st century. *Geophys. Res. Lett.* **2011**, *38* (11), L11501.
- (65) Gascon, G.; Sharp, M.; Bush, A. Changes in melt season characteristics on Devon Ice Cap, Canada, and their association with the Arctic atmospheric circulation. *Ann. Glaciol.* **2013**, *54* (63), 101–110.
- (66) Gascon, G.; Sharp, M.; Burgess, D.; Bezeau, P.; Bush, A. B. G. Changes in accumulation-area firn stratigraphy and meltwater flow during a period of climate warming: Devon Ice Cap, Nunavut, Canada. *J. Geophys. Res. Earth Surf.* **2013**, *118* (4), 2380–2391.
- (67) Lehnherr, I.; St. Louis, V. L.; Sharp, M.; Gardner, A.; Smol, J.; Schiff, S.; Muir, D.; Mortimer, C.; Michelutti, N.; Tarnocai, C.; St. Pierre, K.; Emmerton, C.; Wiklund, J.; Köck, G.; Lamoureux, S.; Talbot, C. The world's largest High Arctic lake responds rapidly to climate warming. *Nat. Commun.* **2018**, *9*, 1–9.
- (68) Woo, M. K. *Permafrost hydrology*; 2012.

- (69) Bezeau, P.; Sharp, M.; Burgess, D.; Gascon, G. Firn profile changes in response to extreme 21st-century melting at Devon Ice Cap, Nunavut, Canada. *J. Glaciol.* **2013**, *59* (217), 981–991.
- (70) Benskin, J. P.; Phillips, V.; St. Louis, V. L.; Martin, J. W. Source elucidation of perfluorinated carboxylic acids in remote alpine lake sediment cores. *Environ. Sci. Technol.* **2011**, *45* (17), 7188–7194.

**2 Emerging Investigator Series: A 14-year Depositional Ice
Record of Perfluoroalkyl Substances in the High Arctic**

2.1 Abstract

Snow samples were collected from a snow pit on the Devon Ice Cap in spring 2008 to improve understanding of long-range transport of perfluoroalkyl substances to the High Arctic of Canada. Snow was analyzed for perfluoroalkyl acids (PFAA), including perfluoroalkyl carboxylic acids (PFCA) and perfluoroalkyl sulfonic acids (PFSA), as well as perfluorooctane sulfonamide. PFAA are detected in all samples dated from 1993 to 2007. PFAA fluxes range from <1 to hundreds of $\text{ng m}^{-2} \text{ year}^{-1}$. Ratios of even-odd PFCA congeners in snow are mostly between 1 and 6, corresponding to those expected from the atmospheric oxidation of fluorotelomer alcohols. Concentrations of perfluorobutanoic acid are much higher than other PFCA, suggesting its occurrence on the Devon Ice Cap is linked to additional sources, such as the oxidation of heat transfer fluids. All PFCA fluxes increase with time, while PFSA fluxes generally decrease with time. No correlations are observed between PFAA and the marine aerosol tracer, sodium. Perfluoro-4-ethylcyclohexanesulfonate is detected for the first time in an atmospherically derived sample, and its presence may be attributed to aircraft hydraulic system leakage. Observations of PFAA from these samples provide further evidence that the atmospheric oxidation of volatile precursors is an important source of PFAA to the Arctic environment.

2.2 Introduction

Perfluoroalkyl acids (PFAA) are found ubiquitously in the environment, including remote regions where local emissions are not expected. The prevalence of PFAA in remote locations¹ indicates these compounds can undergo long-range transport. Transport of PFAA can be through the atmosphere, the ocean, or a combination of the two. In the atmosphere, PFAA can be formed in the gas phase as oxidation products of volatile precursors, such as fluorotelomer alcohols (FTOH)² and perfluoroalkane sulfonamido substances (PFSAm), including perfluoroalkane sulfonamides (FASA) and perfluoroalkane sulfonamido ethanols (FASE).³ These precursors have sufficient atmospheric lifetimes to reach remote locations⁴⁻⁶ before subsequent oxidation to PFAA. PFAA are highly acidic organic compounds⁷ present primarily as anions in the aqueous phase under environmental conditions. Transport of PFAA is feasible via ocean currents.⁸⁻¹⁰ Transport of persistent compounds to remote locations via ocean currents is reported to take place on a scale of decades and is slow in comparison to atmospheric transport, which occurs on a scale of days.² Considering PFAA are surface-active compounds, they should be enriched in the surface microlayer (SML). The SML forms at the interface between the atmosphere and the ocean surface, has a thickness between 1–1000 nm, and is rich in organic compounds.¹¹ During wave events, air bubbles containing particles enriched in organic compounds from the SML are formed and subsequently broken. Marine aerosols containing SML components, as well as sea salts, are formed via this bubble bursting mechanism. This mechanism is poorly understood for PFAA and is examined in only two studies.^{12,13}

Elucidation of long-range transport mechanisms can be assisted through remote sample collection. Ice caps receive their contamination solely from atmospheric deposition because of their high elevation (e.g., Devon Ice Cap summit is 1800 m above sea level). PFAA atmospheric deposition to an ice cap in the High Arctic of Canada is reported in a previous work.⁶ Long-chain PFAA, including perfluorooctanoic acid (PFOA), perfluorononanoic acid (PFNA), perfluorodecanoic acid (PFDA), perfluoroundecanoic acid (PFUnDA), and perfluorooctane sulfonic acid (PFOS) are detected in surface snow from multiple locations and a snow pit on the Devon Ice Cap. In this study, a deeper snow pit was sampled on the Devon Ice Cap in 2008. With increased analytical capabilities, it is possible to detect a greater number of analytes to further explore the mechanisms of long-range transport to the High Arctic. Herein, we discuss: (1) PFAA depositional and temporal trends; (2) transport mechanisms to the High Arctic; and (3) environmental implications.

2.3 Methods

2.3.1 Sample Collection

Sampling procedures are described in detail elsewhere.¹⁴ Briefly, samples were collected from the Devon Ice Cap, Devon Island, Nunavut (75° 20 N, 82° 40 W) in spring 2008. A 7 m snow pit was created near the highest point on the ice cap located a few km upwind from the nearest temporary research site. Samples were taken vertically using 4 L polypropylene (PP) bottles every 25 cm continuously along the face of the snow pit for a total of 28 samples. Samples designated for density and major ion chemistry were

collected at 10 cm intervals along the face of the pit. Densities are determined by measuring the mass collected in the volume of a steel corer. Conductivity is measured using an Orion model 135 conductivity meter (Orion Research, Beverly, MA, USA). Major ions (SO_4^{2-} , Cl^- and Na^+) are analyzed by the National Laboratory for Environmental Testing (Environment and Climate Change Canada, Canada Centre for Inland Waters, Burlington, ON, Canada). Duplicate samples, totaling approximately 16 L of snow, were collected at each depth. Products containing fluoropolymer coatings were avoided at the sampling sites. Prior to sampling, the surface layer of the snowpit wall was removed using a stainless-steel scraper. Samples were stored in new, unopened PP bottles and were kept frozen prior to analysis. Field blanks were taken from an unopened bottle of HPLC grade water and placed in PP bottles, which were transported to the sampling site, opened for 10 minutes and transported back to the laboratory with samples. Field blanks are compared to the water that was stored refrigerated in the laboratory in the same PP bottle (i.e., stay blank). A complete summary of quality control is provided in Appendix A (Section A1, Tables A1 and A2).

2.3.2 Sample Analysis

Samples were defrosted the night before extraction and 500 mL of melted sample was used. Melted samples were spiked with 30 μL of a surrogate mixture (Table A3), which acted as the internal standard to monitor recovery. Covered samples were shaken and sonicated for ten minutes and were placed in the lab for 30 minutes to equilibrate at room temperature. Samples were concentrated using an Oasis® weak anion exchange

(WAX) solid phase extraction (SPE) cartridge (6 cm³, 150 mg, 30 μm).¹⁵ Two elution fractions were collected. In the first fraction, FOSA was eluted with 6 mL of methanol, and in the second fraction, PFAA were eluted with 8 mL of 0.1% ammonia in methanol. Both fractions were evaporated to dryness using nitrogen and reconstituted in 0.25 mL of water pre-cleaned using SPE and 0.25 mL methanol (Fisher Brand HPLC Grade, ThermoFisher). An additional isotopically labelled PFAA mixture was added before analysis to monitor matrix effects (Table A3). The data presented here are corrected on the basis of internal standard recovery in sample extracts (Tables A2).

Samples were analyzed using ultra performance liquid chromatography (Waters Acquity UPLC I) with tandem mass spectrometry (Waters Xevo® TQ-S, UPLC-MS/MS) detection operated in electrospray negative ionization mode (Tables A4 and A5). Samples were separated using a C₁₈ column (Acquity UPLC® BEH, 2.1 x 100 mm, 1.7 mm) with a water-methanol 0.1 mM ammonium acetate gradient method (Table A6).

The limit of detection (LOD) and limit of quantitation (LOQ) are defined as compounds having signal-to-noise (S/N) ratios of 3 and 10, respectively. S/N ratios are calculated by dividing analyte peak height by the standard deviation of the blank across compound-specific retention time windows. Values for LOD and LOQ are found in Appendix A (Table A1). Years of PFAS deposition is based on snow density, ion chemistry, and annual snow accumulation data as described in detail by Meyer et al.¹⁴ Net deposition fluxes for each analyte are calculated by multiplying the ng L⁻¹ concentration by the annual accumulation of water equivalent (L cm⁻² year⁻¹). Spearman correlation analysis is performed using StatPlus:mac (V6), with a critical p-value set to 5 %. Temporal trend analysis is conducted using PFAS fluxes and first-order kinetics.

Doubling times (t_2) and half-life ($t_{1/2}$) are determined according to $\ln(2)/k$, where k is the first-order rate constant (year^{-1}) derived from the slope of the linear regression of natural log transformed PFAS flux versus year of deposition.

2.4 Results and Discussion

2.4.1 PFCA on the Devon Ice Cap

PFCA from C_4 (PFBA) to C_{14} (PFTeDA) are detected on the Devon Ice Cap, with concentrations ranging from pg L^{-1} to ng L^{-1} (Table A7). PFCA concentrations on the Devon Ice Cap are comparable to, but generally lower than concentrations in precipitation collected at lower latitudes between 2006 and 2008.¹⁶ Concentrations are higher than those in another snow pit from the Devon Ice Cap collected in 2006 (Figure 2.1).⁶ The discrepancy between snow concentrations could be caused by differences in sampling location or analytical methods. For instance, the 2006 samples used 100 mL sample aliquots, a different SPE sorbent (Hydrophilic-Lipophilic Balance, HLB) and elution solvent (1 mL MeOH), and the extracts were filtered and analyzed using an isocratic liquid chromatography method.⁶ Furthermore, when the 2006 samples were analyzed, the availability of isotopically labelled standards was limited. As a result, there are substantial analytical method improvements in the current study. Many protocols used in this study are also used in current standardized methods, including the use of a selective WAX SPE sorbent, liquid chromatography gradient elution, and isotopically labelled internal standards for each analyte.

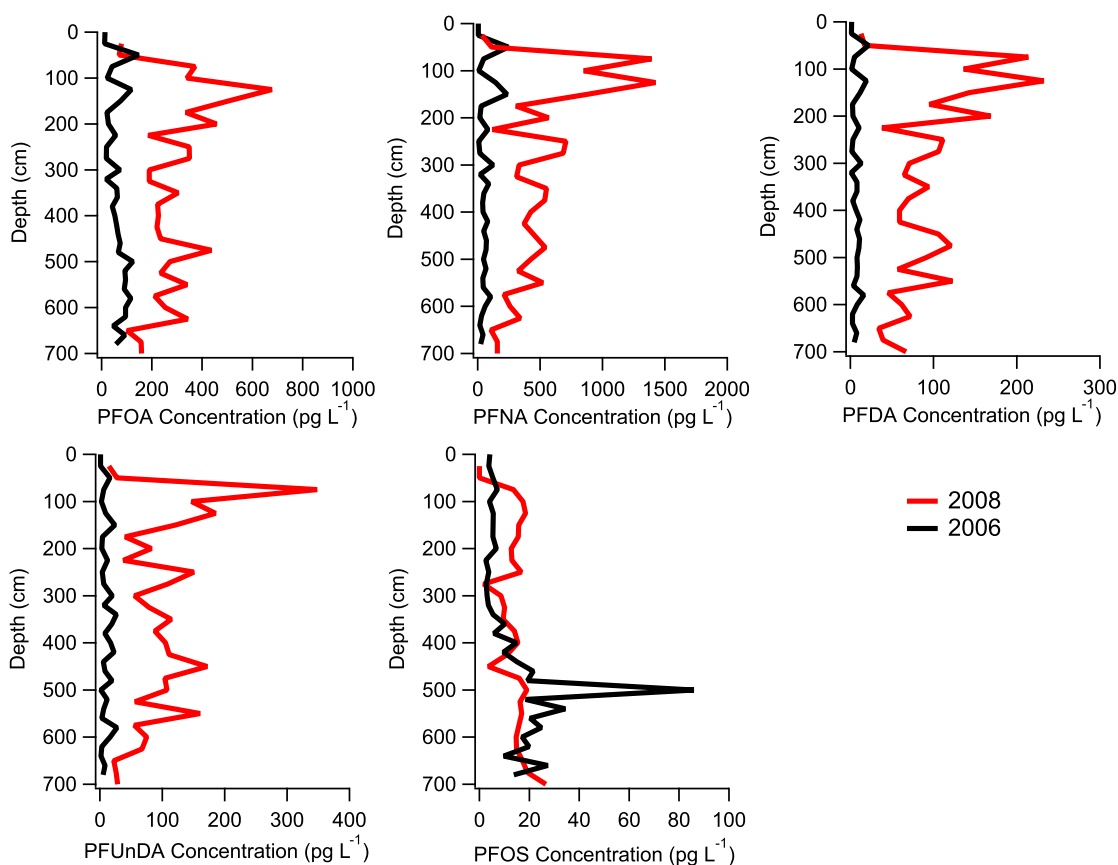


Figure 2.1 Comparison of PFAA concentrations from sampling campaigns at the Devon Ice Cap in 2006⁶ and 2008.

Differences in polybrominated diphenyl ether concentrations are also observed in samples collected at the same locations in 2006 and 2008.¹⁴

Even-odd pairs are a useful metric to examine the role of fluorotelomer atmospheric oxidation on PFCA deposition. Studies indicate that degradation of an $x:2$ FTOH (i.e., containing a $\text{F}(\text{CF}_2)_x(\text{CH}_2)_2\text{OH}$ moiety), will produce even-odd PFCA, with x and $x + 1$ carbons in ratios ranging from 1:1 to 1:6.¹⁷ For example, the atmospheric

oxidation of the 8:2 FTOH is expected to produce PFOA and PFNA. It is expected that there will be some variability in the yields as a result of relative levels of NO_x, peroxy radicals, and atmospheric particles.^{17,18} Even-odd pairs of most PFCA congeners are deposited in similar amounts on the ice cap (Figure 2.2). This is observed for PFOA: PFNA and PFDA: PFUnDA in previous samples from the Devon Ice Cap⁶ and for PFOA: PFNA from an ice core collected from a glacier on Svalbard.¹⁹ In this study, comparisons are made between observed concentrations of the even-odd pairs between C₄ (PFBA) and C₁₃ (PFTrDA). Correlations between even-odd pairs (C₄-C₁₃) are all statistically significant ($r_s \geq 0.42$, $p \leq 0.02$, Table A8). Of the 58 flux measurement ratios for the 4 pairs from PFHxA to PFTrDA, 84% are within a factor of 2 and 98% of the measurement ratios are within a factor of 6. This is consistent with the expected ratios of even and odd PFCA congeners formed from the atmospheric oxidation of FTOH.¹⁷ This is further supported by the flux ratios of PFDA: PFUnDA and PFDoDA: PFTrDA observed at the Devon Ice Cap. These similar fluxes of even-odd congeners are likely the result of atmospheric oxidation of volatile precursors²⁰ 10:2 and 12:2 FTOH for PFDA, PFUnDA and PFDoDA, PFTrDA, respectively. Estimates of the quantities of long-chain PFCA, from PFDA to PFTeDA present in the environment from direct and indirect sources vary substantially but are generally thought to be dominated by indirect sources. This hypothesis is corroborated by the presence of FTOH^{21,22} and their oxidation products in Arctic Canada. These observations suggest the detection of long-chain PFCA on the Devon Ice Cap is consistent with dominant contributions from indirect sources.

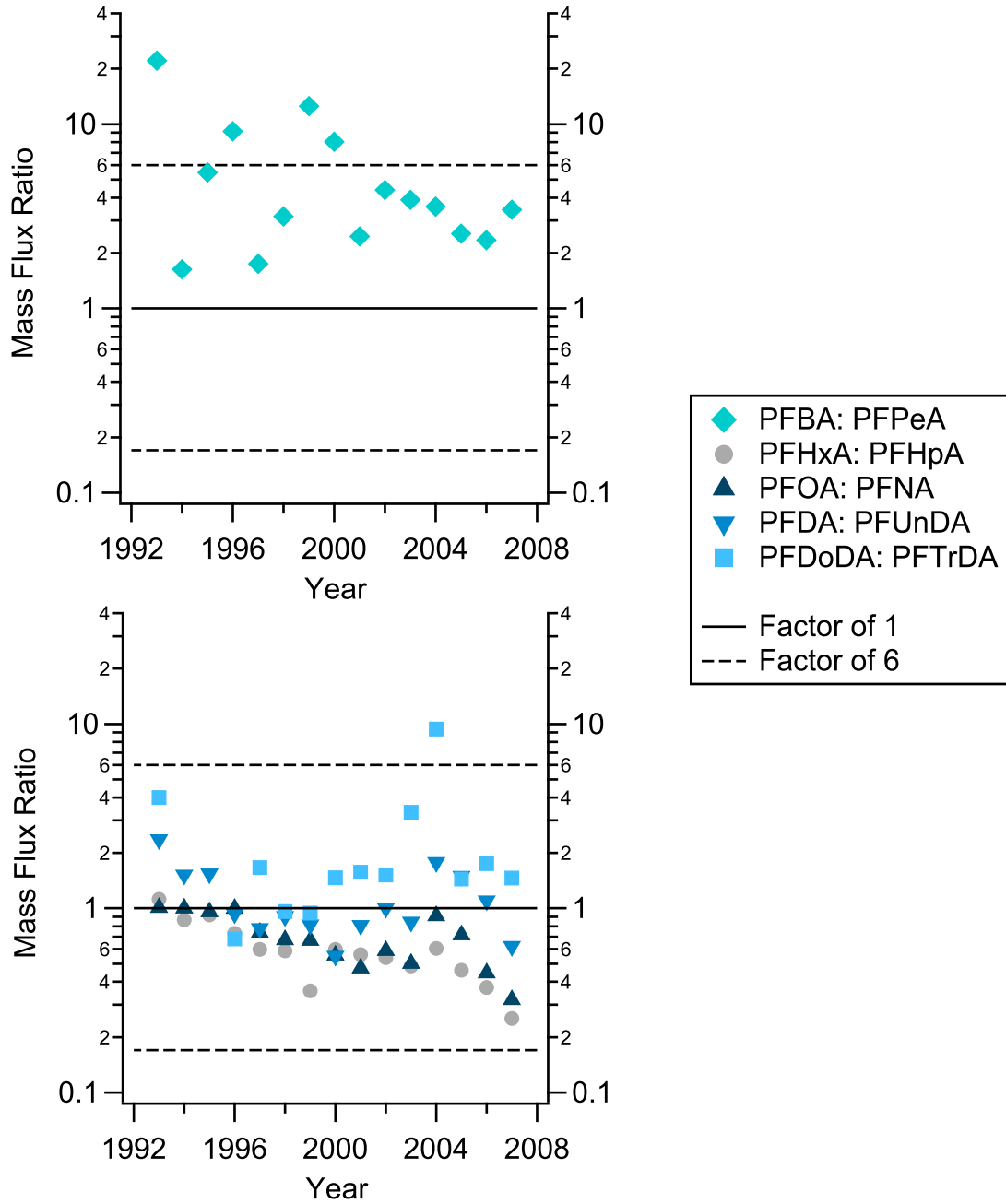


Figure 2.2 Flux ratios of even-odd PFCA as a function of year on the Devon Ice Cap.

The even-odd ratios for PFBA: PFPeA on the Devon Ice Cap suggest these compounds are likely derived from the atmospheric oxidation of 4:2 FTOH, however, several of the observed ratios are much higher than those expected from FTOH oxidation (Figure 2.2). PFSAm oxidation could also lead to the formation of PFBA, although, this source cannot be excluded because our measurements did not include any of these precursor compounds. However, we anticipate contributions of this source will be minor due to the strong correlations for even-odd PFCA noted above, and the lack of correlation observed between PFBA and PFBS ($r_s < 0.01$, $p = 0.98$, Table A8). PFBA deposition is much greater than PFPeA (mean of 6.0 ± 2.1 times larger) and most other congeners (Table A7). This observation is consistent with PFBA measurements from other studies, including Arctic char (*Salvelinus alpinus*) from Svalbard,²³ glacial samples from Svalbard¹⁹ and Italy,^{24,25} snow from Tibet,^{25,26} and sea ice from the Arctic Ocean.²⁷ This is particularly surprising in biota considering the greater bioaccumulation factor for PFPeA than PFBA.²⁸ High concentrations of PFBA in previous studies is attributed to direct emissions of PFBA²⁵ or a shift in fluorotelomer production to short-chain congeners, such as the 4:2 FTOH.²⁶ We argue that observations of high concentrations of PFBA and other short chain PFAA²⁹⁻³³ in environmental samples are consistent with our knowledge of multiple non-fluorotelomer gas phase sources. Known sources of PFBA include hydrofluorocarbons (HFC), such as HFC-329 ($\text{CF}_3(\text{CF}_2)_3\text{H}$),³⁴ and hydrofluoroethers (HFE), such as HFE-7100 ($\text{C}_4\text{F}_9\text{OCH}_3$) and HFE-7200 ($\text{C}_4\text{F}_9\text{OC}_2\text{H}_5$).^{35,36} Mixing ratios of several HFC compounds are reported in the atmosphere, ranging from approximately 5 to 200 parts-per-trillion by volume.³⁷ Levels of many HFC³⁸ and likely HFE, are increasing in the atmosphere, as these compounds are

replacements for stratospheric ozone depleting chlorofluorocarbons and hydrochlorofluorocarbons. Elevated concentrations of PFBA in relation to other PFCA found on the Devon Ice Cap suggest its formation is driven by the atmospheric oxidation of these other compounds. Mixing ratios of HFC in the atmosphere are substantially higher³⁹ than those of FTOH and PFSAm, which are in the range of a few to a few hundred parts-per-quadrillion by volume.⁴⁰ Both the lack of correlation between PFBA and other PFCA on the ice cap and the highly elevated concentrations of PFBA suggest an atmospheric source other than FTOH and PFSAm, such as HFC and/or HFE. In contrast, our results suggest that PFPeA and all other long-chained PFCA are formed predominantly from atmospheric oxidation of FTOH and PFSAm.

Elevated concentrations of PFBA on the Devon Ice Cap are consistent with observations reported in the Arctic abiotic environment (Section 1.5). However, it is important to note that there are analytical challenges associated with PFBA quantitation. For instance, PFBA is often detected using a single precursor-product ion transition (i.e., 213 to 169 m/z), whereas some transitions used for confirmation (e.g., 19 m/z) are often below the mass range of many mass spectrometers (i.e., 50 to 1500 m/z) and are not specific. Furthermore, PFBA and other short-chain PFAA are not retained well or separated on a C₁₈ stationary phase using standardized liquid chromatography methods, which can affect the reliability of their quantitation.⁴¹ Standard addition can be used to validate PFBA quantitation, however, this approach can be labor intensive and may not be practical for samples that are limited in quantity. Alternatively, high-resolution mass spectrometry can be a suitable complementary technique to confirm the detection of PFBA and other short-chain PFAS in environmental samples, while separations

conducted using supercritical fluid chromatography can improve chromatographic resolution of short-chain PFAA.⁴¹

An additional source of PFCA to the Devon Ice Cap could result from the atmospheric oxidation of PFSAm. Studies suggest the dominant oxidation products of N-methyl perfluorobutane sulfonamidoethanol (N-MeFBSE) and N-ethyl perfluorobutane sulfonamide (N-EtFBSA) in the presence of hydroxyl radicals are PFCA.^{3,42} The yield is favorable under low NO_x conditions and is expected to be representative of the Arctic environment. It is possible the oxidation of FOSA could contribute to the occurrence of PFOA and shorter-chain PFCA on the Devon Ice Cap, pursuant to the statistically significant negative correlations observed between FOSA and C₅-C₇ PFCA concentrations ($r_s \geq -0.54$, $p < 0.01$); although, a weak correlation is observed for FOSA and PFOA concentrations ($r_s = -0.25$, $p = 0.22$, Table A8). Source apportionment is very challenging considering the number of volatile precursors and mechanisms involved in long-range atmospheric transport. It is difficult to assess the full extent of atmospheric oxidation of these species considering FOSA was the only PFSAm monitored in this work. Furthermore, the analytical methods used in this study are not optimized for monitoring other precursors or their intermediate degradation products (e.g., FTOH and fluorotelomer unsaturated carboxylic acids, FTUCA). The monitoring of precursors and their intermediate degradation products in snow would provide further evidence of long-range atmospheric transport and oxidation as a mechanism for the occurrence of PFAS in the High Arctic of Canada.⁴³

2.4.2 PFSA and FOSA on the Devon Ice Cap

C₄ (PFBS), C₈ (PFOS), C₁₀ (PFDS), and cyclic C₈ (PFECHS) PFSA, along with FOSA, are detected on the Devon Ice Cap, with concentrations ranging from a few to hundreds of pg L⁻¹ (Table A7). PFSA and FOSA concentrations and detection frequencies are lower than those of PFCA. PFBS, PFOS, PFECHS, and FOSA are detected in most samples, while PFDS is detected in samples corresponding to four years of deposition. No measurements above the LOD are made for C₆ (PFHxS) and C₇ (PFHpS) PFSA. Precipitation collected at lower latitudes between 2006 and 2008 contain similar concentrations of PFBS, PFOS, and FOSA.¹⁶ In general, concentrations of PFBS and FOSA are higher than PFOS. Elevated concentrations of PFBS and FOSA relative to PFOS are also observed in some snow samples collected from the surface of Arctic Ocean sea ice in 2010.²⁷ Concentrations of PFOS are similar to those measured in another Devon Ice Cap snow pit in 2006, with the exception of elevated concentrations in the lowest 2 m of the older core (Figure 2.1).⁶ Differences in concentration could be caused by different sample locations, analytical improvements, or post-depositional melting effects (Section 2.4.3).

Both PFOS and PFBS can be produced through the atmospheric oxidation of volatile precursors.³ However, no correlation is observed between measurements of PFOS and its potential semi-volatile precursor, FOSA ($r_s = -0.03$, $p = 0.89$, Table A8). Precursors to PFSA can also produce PFCA with equal or fewer carbons, however, neither PFOS nor PFBS correlates with PFCA on the Devon Ice Cap (Table A8). The formation of PFBS is observed from oxidation of N-MeFBSE in one study,³ though this was not observed in a FASA oxidation study.⁴² Thus, it is possible that FOSA may not degrade to form PFOS.

From this data, it is difficult to allocate sources of these species to the Devon Ice Cap without complementary volatile precursor measurements and complete knowledge of precursor chemistry.

PFECHS is measured at low ng L⁻¹ concentrations on the Devon Ice Cap, similar to observed levels of PFOS. PFECHS is detected in surface waters in Lake Ontario,⁴⁴ the Arctic,¹⁵ and in aquatic biota downstream from an airport.⁴⁵ This is the first reported detection of PFECHS in an atmospherically derived sample. We note there are no volatile precursors known to degrade in the environment to PFECHS, suggesting deposition must be through direct sources. PFECHS is primarily used as an erosion inhibitor in aircraft hydraulic fluids. However, PFECHS may be released into the environment from additional sources, pursuant to its detection in residential wastewater⁴⁶ and indoor dust.⁴⁷

2.4.3 Temporal Trends

PFAS deposition to the Devon Ice Cap increased or is constant during 1993-2007, with the exception of PFBS, which decreased during 1996-2007 (Table A9). The temporal trends for PFOS, PFBS, and FOSA fluxes are shown in Figure 2.3.

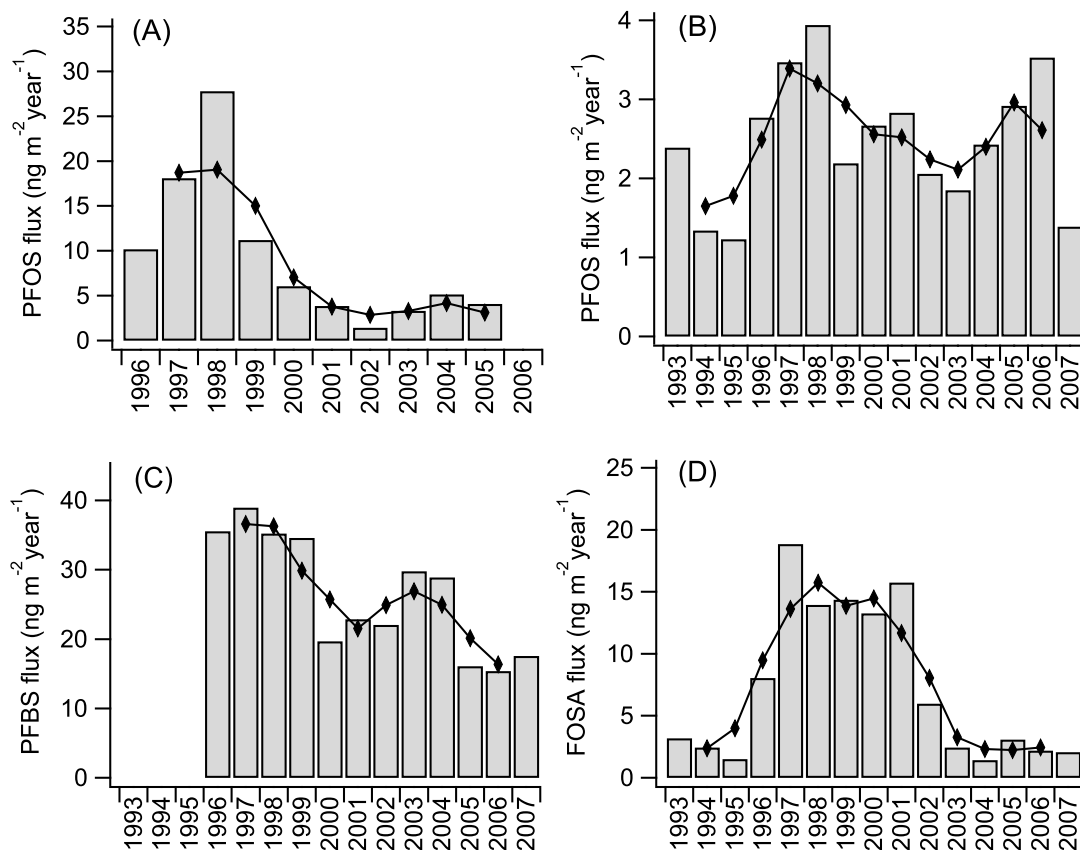


Figure 2.3 PFAS fluxes on the Devon Ice Cap (a) PFOS from Young et al.;⁶ (b) PFOS; (c) PFBS; (d) FOSA. Lines represent three-year moving averages.

Differences are observed between the temporal trends of PFCA and PFOS fluxes from another snow pit on Devon Island collected in 2006, such that PFCA fluxes in this study are generally higher than those reported in 2006.⁶ Calculated fluxes of PFOS are much higher in earlier years (1995–1999) of the 2006 samples (Figure 2.3a), while calculated fluxes from both sample sets are similar in later years (2001 onward). Differences between calculated fluxes are unsurprising because sampling in 2006 accounted for only

30-40% of the vertical face of the snow pit surface, while sampling in 2008 collected the entire vertical face. Melting events within the snowpack may also bias the assignment of fluxes to the Devon Ice Cap. The surface of the Devon Ice Cap is undergoing seasonal melting due to increasing air temperatures,^{48,49} which results in the formation of impermeable ice layers in the snowpack. Subsequent percolating meltwater within a snowpack will refreeze at the ice layer interface.⁴⁹ Consequently, the accumulation of ice in the snowpack makes it challenging to deduce meaningful interpretations for the most recent years of deposition.⁵⁰ This suggests that concentrations measured near the surface layer can result in inaccuracies in estimating PFCA deposition, whereby overestimation occurs in certain years and underestimation in others. A simulated snowpack melting study suggests that short-chain PFAA eluted at a faster rate relative to long-chain PFAA in the presence of percolating meltwater.⁵¹ However, the percolation of meltwater in a snowpack is expected to refreeze within an annual year.⁵² Seasonal cycles of PFAA deposition would be inevitably biased, while annual interpretations of data, such as those presented here, should not be affected. Nevertheless, we present a three-year moving average to minimize impacts of melting (Figure 2.3).

In 2001, 3M, one of the largest global producers of PFAS, voluntarily phased out the production of perfluorooctane sulfonyl fluoride (POSF) and all related products, including PFOS and its volatile precursors, such as FOSA.⁵³ It was proposed that further production would use C₄-based compounds derived from perfluorobutane sulfonyl fluoride (PBSF), which are believed to have lower bioaccumulation and toxicological effects.⁵⁴ Reported production of PBSF in the United States has almost doubled in 2006 compared to production in 2002, while that of POSF decreased by more than two orders

of magnitude between 2000 and 2002, and no production was reported for 2006.⁵⁵

Production of PFOS has increased dramatically in Asia since 2001 and China is now the dominant producer of these compounds.^{56,57}

In a previous study,⁶ PFOS deposition increases on the ice cap up to 1999, after which it decreased (Figure 2.3a). PFOS in these samples also indicates an increase up to 1998 followed by a decline until 2003 (Figure 2.3b). Because transport through the atmosphere is fast, on the order of weeks, if atmospheric oxidation is the dominant source of PFOS to the ice cap, then a fast change in response to the newly adopted syntheses might be observed after 2001. In the previous study, the decrease is thought to indicate a fast response to the production change. As described above, differences in sample collection may provide an explanation for this discrepancy between studies. It is also possible that melting effects in the ice cap prior to sampling could have created a false maximum.⁶ It is also important to note that although both data sets suggest a decline in PFOS flux, when applying first order kinetics, neither data set indicates a statistically significant ($p > 0.05$) declining temporal trend in the period post-1998. FOSA deposition, which is also derived from POSF, increased in the 1990s, peaking around the year 2000, followed by a decrease up to 2007 (Figure 2.3d). The observed behaviour of FOSA is likely in accordance with the voluntary phase-out of the perfluorooctane-based chemistry in 2001. Considering FOSA is much less water-soluble than other PFAA measured in this work, it should be less susceptible to percolating effects within a snowpack,⁵¹ and any observed trends should reflect changes in production. While PFOS is constant over the 1993-2007 period, PFBS decreases. It is reported that the Devon Ice Cap receives air masses originating from Asian sources.⁵⁸ The smaller than expected flux of PFBS to the

Devon Ice Cap may be reflective of Asian air masses enriched in POSF-based product emissions.²⁰ Atmospheric gas and particle measurements made in the Canadian Archipelago in 2005 show elevated levels of electrochemical fluorination (ECF)-derived POSF substances, N-MeFOSE and N-EtFOSE.²¹ These ECF intermediates are not produced using contemporary North American synthetic techniques (i.e., telomerization), which suggest ECF may be presently used in Asia. Recent studies examine PFOA isomer profiles in blood serum⁵⁹ and commercial products⁶⁰ from China and find fractions of branched isomers unique to ECF manufacturing. The presence of ECF derived sulfonyl fluoride substances from Asian air masses in the Canadian Archipelago may provide an explanation for the discrepancy between reported emissions and PFAA profiles on the Devon Ice Cap if perfluorobutane-related chemistries are not fully implemented in Asian manufacturing.

2.4.4 Direct Transport of PFAS to the Arctic

To examine the influence of long-range oceanic transport on PFCA deposition at the Devon Ice Cap, the concentrations of PFAS and Na⁺, a tracer for marine aerosols, are compared.⁶¹ No correlation is observed between concentrations of Na⁺ and PFAA (r_s -0.27 to 0.26, $p \geq 0.21$), suggesting PFAA deposition on the Devon Ice Cap is not primarily influenced by transport of marine aerosols. A similar lack of correlation is seen by Kwok et al. between PFAA and sea-salt derived sulfate in Svalbard.¹⁹ It is interesting to note that a moderate relationship is observed for Na⁺ and FOSA concentrations

($r_s=0.43$, $p=0.04$), which may suggest marine aerosol is a relevant source and/or vector (e.g., as a scavenger in the atmosphere) of FOSA to the Devon Ice Cap.

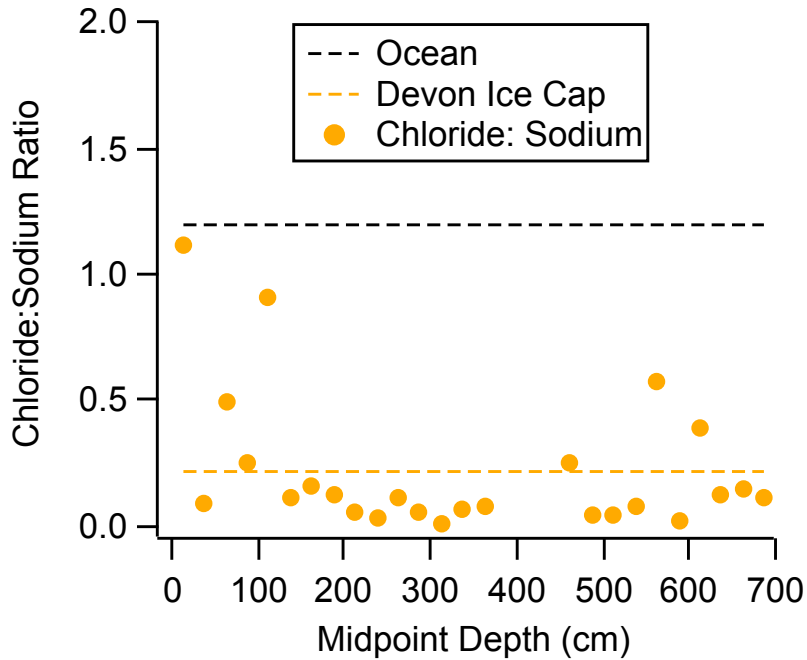


Figure 2.4 Comparison of chloride: sodium molar ratios on the Devon Ice Cap to expected ocean ratios. The dashed orange line corresponds to the average chloride: sodium ratio on the Devon Ice Cap, and the dashed black line corresponds to the expected ocean ratio.⁶¹

In contrast, it is possible that this correlation reflects a commonality in post-depositional transport and fate (e.g., similar mobility in melting snow). The influence of sea spray on the Devon Ice Cap could also be tested by comparing the ratio of Cl^- to Na^+ observed on the ice cap to expected ocean water ratios.⁶¹ The observed molar ratio of Cl^- to Na^+ on the

Devon Ice Cap averages 0.2, while the expected ocean water ratio is 1.2 (Figure 2.4).

However, ratios observed from 2006-2008 begin approaching the expected seawater ratio.

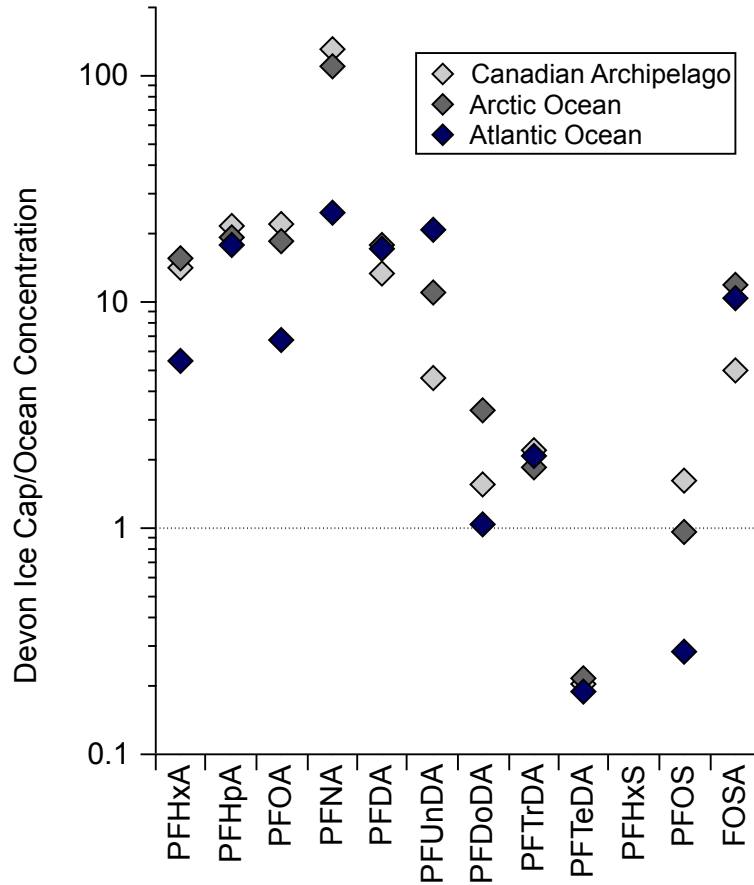


Figure 2.5 Ratios of observed concentrations in the Devon Ice Cap in 2004-2006 compared to levels in the Canadian Archipelago and Arctic Oceans collected in 2005 and to the Atlantic Ocean.⁶³

These observations may be consistent with percolation events within the snowpack, or with decreasing sea ice coverage in the Canadian Archipelago.⁶² Melting of sea ice is

expected to enhance the flux of marine aerosol to the Devon Ice Cap.⁵⁰ Another technique used to assess the influence of marine aerosol deposition of PFAA to the ice cap is a comparison between ocean and ice cap congener patterns. If marine aerosols are a major source of the PFAA on the Devon Ice Cap, then a similar congener profile should be observed in both the ocean and the ice cap. PFCA concentrations on the ice cap are generally higher than those in the ocean, though not for long-chain congeners (Figure 2.5). Concentrations of PFOS and FOSA are higher than some ocean concentrations and lower than others. Concentrations of PFBS are not widely measured in ocean water, therefore a comparison is not possible at this time. PFHxS is not detected on the ice cap, while it is measured in several ocean samples.⁶³⁻⁶⁵ In glacier samples from Svalbard, PFHxS is not detected, though it is detected in surface snow in coastal regions.¹⁹ According to reported usage, the synthetic precursor to PFHxS, perfluorohexane sulfonyl fluoride (PHxSF), is not used for the production of commercial volatile PFSAm compounds.^{66,67} Thus, the detection of PFHxS on the ice cap would confirm the role of direct sources. The absence of PFHxS on the ice cap provides further evidence that marine aerosols are not a significant source of PFAA to the ice cap. The differences in congener profiles between the ice cap and the ocean cannot be accounted for by different surfactant properties. If differences in surfactant properties are leading to different congener patterns, then we would expect a greater enhancement of PFSA relative to PFCA on the ice cap because the former are stronger surfactants. In addition, we would expect longer-chain PFCA to be preferentially enriched.¹³ Discrepancies between Cl⁻: Na⁺ ratios and congener patterns provide further evidence that marine aerosols are not a dominant source of PFAA to the Devon Ice Cap.

The presence of PFECHS on the Devon Ice Cap could be a result of long-range oceanic transport and marine aerosol formation. Although no marine measurements of PFECHS are reported, there is no relationship between the concentrations of Na⁺ and PFECHS ($r_s=0.05$, $p=0.81$, Table A8), suggesting PFECHS deposition is likely dominated by another transport mechanism. The detection of PFECHS in freshwater Arctic lakes¹⁵ is attributed to contamination from a local airport, suggesting contemporary usage of the compound in the area. It is possible local inputs of PFECHS into freshwater Arctic lakes, followed by aerosol formation, could serve as a mechanism of transport for PFECHS to the Devon Ice Cap. It is also possible that PFECHS deposition on the Devon Ice Cap is a result of direct emission of the compound from aircraft during usage. PFECHS is used as an additive in phosphate ester-based hydraulic fluids to reduce metal erosion in commercial aircraft.⁶⁸ In the event of water contamination, phosphate ester hydraulic fluids can undergo hydrolysis, leading to the production of acid products.⁶⁸ The accumulation of acid in hydraulic fluid systems can promote metal corrosion and subsequent leakage. Hydraulic system leakage in commercial aircrafts is an inherent problem in the aviation industry.^{69,70} Considering hydraulic systems in aircraft are under pressure, a small leak could result in large emissions. The persistence of aircraft hydraulic fluid system leakage and the absence of known volatile precursors of commercial relevance may provide an explanation for the presence of PFECHS in the Arctic environment. Regulatory documents in Canada⁷¹ list hydraulic fluid as a potential use for PFOS, suggesting detection of PFECHS on the ice cap indicates the possibility of another direct mechanism for PFOS long-range transport. Evidence of this may be substantiated by a report in 2001, which describes the use of Skydrol®, a PFOS-based hydraulic fluid

employed in commercial aircraft.⁷² Contemporary uses of PFOS as additives in aviation hydraulic fluids are permitted, according to the exemptions listed in the Stockholm Convention.⁷³ The continued usage of these hydraulic fluids in commercial aircrafts could serve as direct emission sources of PFOS on the Devon Ice Cap. An industry report suggests PFECHS and PFOS would be present in different hydraulic fluids.⁷² Thus, lack of correlation between PFOS and PFECHS concentrations on the ice cap ($r_s=0.34$, $p=0.11$, Table A8) cannot be used to infer the validity of hydraulic fluid as a source of PFOS. It is challenging to interrogate aviation sources given their complexity; however, the presence of PFECHS and PFOS in an atmospherically derived sample could provide an explanation for the observations on the Devon Ice Cap.

2.5 Conclusions

There is considerable discussion in the literature regarding long-range transport mechanisms of PFAA. For certain congeners, such as PFOA⁷⁴ and PFOS,¹⁰ both of which were historically produced in large quantities, it is clear that direct transport is the dominant mechanism to remote regions. For other congeners that are produced in lower quantities, the major transport pathways are less clear. Ice caps receive and preserve records of atmospheric pollution, and by sampling ice caps, more clarity can be brought to the role of the atmosphere in the long-range transport of PFAA. Samples collected from the Devon Ice Cap contain concentrations of PFAA that are higher than those in the ocean for many congeners. The patterns and ratios of congener concentrations, as well as the absence of a relationship to an ocean tracer, are consistent with a dominant indirect

source, atmospheric oxidation of volatile precursors, for most PFAA to the ice cap. The first observation of PFECHS in an Arctic atmospheric sample suggests the possibility of a new direct source to remote regions through leakage of airline hydraulic fluids.

2.6 Literature Cited

- (1) Butt, C. M.; Berger, U.; Bossi, R.; Tomy, G. T. Levels and trends of poly- and perfluorinated compounds in the arctic environment. *Sci. Total Environ.* **2010**, *408* (15), 2936–2965.
- (2) Ellis, D. A.; Martin, J. W.; De Silva, A. O.; Mabury, S. A.; Hurley, M. D.; Sulbaek Andersen, M. P.; Wallington, T. J. Degradation of fluorotelomer alcohols: A likely atmospheric source of perfluorinated carboxylic acids. *Environ. Sci. Technol.* **2004**, *38* (12), 3316–3321.
- (3) D'eon, J. C.; Hurley, M. D.; Wallington, T. J.; Mabury, S. A. Atmospheric chemistry of N-methyl perfluorobutane sulfonamidoethanol, C₄F₉SO₂N(CH₃)CH₂CH₂OH: Kinetics and mechanism of reaction with OH. *Environ. Sci. Technol.* **2006**, *40* (6), 1862–1868.
- (4) Ellis, D. A.; Martin, J. W.; Mabury, S. A.; Hurley, M. D.; Sulbaek Andersen, M. P.; Wallington, T. J. Atmospheric lifetime of fluorotelomer alcohols. *Environ. Sci. Technol.* **2003**, *37* (17), 3816–3820.
- (5) Hurley, M. D.; Wallington, T. J.; Sulbaek Andersen, M. P.; Ellis, D. A.; Martin, J. W.; Mabury, S. A. Atmospheric chemistry of fluorinated alcohols: Reaction with Cl atoms and OH radicals and atmospheric lifetimes. *J. Phys. Chem. A* **2004**, *108* (11), 1973–1979.
- (6) Young, C. J.; Furdui, V. I.; Franklin, J.; Koerner, R. M.; Muir, D. C. G.; Mabury, S. A. Perfluorinated acids in Arctic snow: New evidence for atmospheric formation. *Environ. Sci. Technol.* **2007**, *41*, 3455–3461.

- (7) Cheng, J.; Psillakis, E.; Hoffmann, M. R.; Colussi, A. J. Acid dissociation versus molecular association of perfluoroalkyl oxoacids: Environmental implications. *J. Phys. Chem. A* **2009**, *113* (29), 8152–8156.
- (8) Armitage, J. M.; Macleod, M.; Cousins, I. T. Modeling the global fate and transport of perfluorooctanoic acid (PFOA) and perfluorooctanoate (PFO) Emitted from direct sources using a multispecies mass balance model. *Environ. Sci. Technol.* **2009**, *43* (4), 1134–1140.
- (9) Armitage, J. M.; Macleod, M.; Cousins, I. T. Comparative assessment of the global fate and transport pathways of long-chain perfluorocarboxylic acids (PFCAs) and perfluorocarboxylates (PFCs) emitted from direct sources. *Environ. Sci. Technol.* **2009**, *43* (15), 5830–5836.
- (10) Armitage, J. M.; Schenker, U.; Scheringer, M.; Martin, J. W.; Macleod, M.; Cousins, I. T. Modeling the global fate and transport of perfluorooctane sulfonate (PFOS) and precursor compounds in relation to temporal trends in wildlife exposure. *Environ. Sci. Technol.* **2009**, *43* (24), 9274–9280.
- (11) Wurl, O.; Wurl, E.; Miller, L.; Johnson, K.; Vagle, S. Formation and global distribution of sea-surface microlayers. *Biogeosciences* **2011**, *8*, 121–135.
- (12) McMurdo, C. J.; Ellis, D. A.; Webster, E.; Butler, J.; Christensen, R. D.; Reid, L. K. Aerosol enrichment of the surfactant PFO and mediation of the water-air transport of gaseous PFOA. *Environ. Sci. Technol.* **2008**, *42*, 3969–3974.
- (13) Reth, M.; Berger, U.; Broman, D.; Cousins, I. T.; Nilsson, E. D.; McLachlan, M. S. Water-to-air transfer of perfluorinated carboxylates and sulfonates in a sea spray simulator. *Environ. Chem.* **2011**, *8*, 381–388.

- (14) Meyer, T.; Muir, D. C. G.; Teixeira, C.; Wang, X.; Young, T.; Wania, F. Deposition of brominated flame retardants to the Devon Ice Cap, Nunavut, Canada. *Environ. Sci. Technol.* **2012**, *46* (2), 826–833.
- (15) Lescord, G. L.; Kidd, K. A.; De Silva, A. O.; Williamson, M.; Spencer, C.; Wang, X.; Muir, D. C. G. Perfluorinated and polyfluorinated compounds in lake food webs from the Canadian High Arctic. *Environ. Sci. Technol.* **2015**, *49* (5), 2694–2702.
- (16) Kwok, K. Y.; Taniyasu, S.; Yeung, L. W. Y.; Murphy, M. B.; Lam, P. K. S.; Horii, Y.; Kannan, K.; Petrick, G.; Sinha, R. K.; Yamashita, N. Flux of perfluorinated chemicals through wet deposition in Japan, the United States, and several other countries. *Environ. Sci. Technol.* **2010**, *44* (18), 7043–7049.
- (17) Styler, S. A.; Myers, A. L.; Donaldson, D. J. Heterogeneous photooxidation of fluorotelomer alcohols: A new source of aerosol-phase perfluorinated carboxylic acids. *Environ. Sci. Technol.* **2013**, *47* (12), 6358–6367.
- (18) Young, C. J.; Mabury, S. A. Atmospheric perfluorinated acid precursors: Chemistry, occurrence, and impacts. *Rev. Environ. Contam. Toxicol.* **2010**, *208*, 1–110.
- (19) Kwok, K. Y.; Yamazaki, E.; Yamashita, N.; Taniyasu, S.; Murphy, M. B.; Horii, Y.; Petrick, G.; Kallerborn, R.; Kannan, K.; Murano, K.; Lam, P.K.S. Transport of Perfluoroalkyl substances (PFAS) from an arctic glacier to downstream locations: Implications for sources. *Sci. Total Environ.* **2013**, *447*, 46–55.
- (20) Wang, Z.; Cousins, I. T.; Scheringer, M.; Buck, R. C.; Hungerbühler, K. Global emission inventories for C4-C14 perfluoroalkyl carboxylic acid (PFCA)

- homologues from 1951 to 2030, Part I: Production and emissions from quantifiable sources. *Environ. Int.* **2014**, *70*, 62–75.
- (21) Shoeib, M.; Harner, T.; Vlahos, P. Perfluorinated chemicals in the arctic atmosphere. *Environ. Sci. Technol.* **2006**, *40* (24), 7577–7583.
- (22) Stock, N. L.; Furdui, V. I.; Muir, D. C. G.; Mabury, S. A. Perfluoroalkyl contaminants in the Canadian arctic: Evidence of atmospheric transport and local contamination. *Environ. Sci. Technol.* **2007**, *41* (10), 3529–3536.
- (23) Garsjo, M. Perfluorinated alkylated substances (PFAS) in Arctic char (*Salvelinus alpinus*): A case study from Svalbard, Norwegian University of Life Sciences, 2013.
- (24) Kirchgeorg, T.; Dreyer, A.; Gabrielli, P.; Gabrieli, J.; Thompson, L. G.; Barbante, C.; Ebinghaus, R. Seasonal accumulation of persistent organic pollutants on a high altitude glacier in the Eastern Alps. *Environ. Pollut.* **2016**, *218*, 804–812.
- (25) Kirchgeorg, T.; Dreyer, A.; Gabrieli, J.; Kehrwald, N.; Sigl, M.; Schwikowski, M.; Boutron, C.; Gambaro, A.; Barbante, C.; Ebinghaus, R. Temporal variations of perfluoroalkyl substances and polybrominated diphenyl ethers in snow. *Environ. Pollut.* **2013**, *178*, 367–374.
- (26) Wang, X.; Halsall, C.; Codling, G.; Xie, Z.; Xu, B.; Zhao, Z.; Xue, Y.; Ebinghaus, R.; Jones, K. C. Accumulation of perfluoroalkyl compounds in Tibetan mountain snow: Temporal patterns from 1980 to 2010. *Environ. Sci. Technol.* **2014**, *48*, 173–181.
- (27) Cai, M.; Zhao, Z.; Yin, Z.; Ahrens, L.; Huang, P.; Cai, M.; Yang, H.; He, J.; Sturm, R.; Ebinghaus, R.; Xie, Z. Occurrence of perfluoroalkyl compounds in surface

- waters from the North Pacific to the Arctic Ocean. *Environ. Sci. Technol.* **2012**, *46* (2), 661–668.
- (28) Martin, J. W.; Mabury, S. A.; Solomon, K. R.; Muir, D. C. G. Dietary accumulation of perfluorinated acids in juvenile rainbow trout (*Oncorhynchus mykiss*). *Environ. Toxicol. Chem.* **2003**, *22* (1), 189–195.
- (29) Taniyasu, S.; Kannan, K.; Yeung, L. W. Y.; Kwok, K. Y.; Lam, P. K. S.; Yamashita, N. Analysis of trifluoroacetic acid and other short-chain perfluorinated acids (C2-C4) in precipitation by liquid chromatography-tandem mass spectrometry: Comparison to patterns of long-chain perfluorinated acids (C5-C18). *Anal. Chim. Acta* **2008**, *619* (2), 221–230.
- (30) Wujcik, C. E.; Zehavi, D.; Seiber, J. N. Trifluoroacetic acid levels in 1994-1996 fog, rain, snow and surface waters from California and Nevada. *Chemosphere* **1998**, *36* (6), 1233–1245.
- (31) Berg, M.; Müller, S. R.; Mühlemann, J.; Wiedmer, A.; Schwarzenbach, R. P. Concentrations and mass fluxes of trifluoroacetic acid in rain and natural waters in Switzerland. *Environ. Sci. Technol.* **2000**, *34* (13), 2675–2683.
- (32) Scott, B. F.; Moody, C. A.; Spencer, C.; Small, J. M.; Muir, D. C. G.; Mabury, S. A. Analysis for Perfluorocarboxylic Acids/Anions in Surface Waters and Precipitation Using GC-MS and Analysis of PFOA from Large-Volume Samples. *Environ. Sci. Technol.* **2006**, *40*, 6405–6410.
- (33) Scott, B. F.; Spencer, C.; Mabury, S. A.; Muir, D. C. G. Poly and perfluorinated carboxylates in North American precipitation. *Environ. Sci. Technol.* **2006**, *40* (23), 7167–7174.

- (34) Young, C. J.; Hurley, M. D.; Wallington, T. J.; Mabury, S. A. Atmospheric chemistry of $\text{CF}_3\text{CF}_2\text{H}$ and $\text{CF}_3\text{CF}_2\text{CF}_2\text{CF}_2\text{H}$: Kinetics and products of gas-phase reactions with Cl atoms and OH radicals, infrared spectra, and formation of perfluorocarboxylic acids. *Chem. Phys. Lett.* **2009**, *473* (4–6), 251–256.
- (35) Wallington, T. J.; Schneider, W. F.; Sehested, J.; Bilde, M.; Platz, J.; Nielsen, O. J.; Christensen, L. K.; Molina, M. J.; Molina, L. T.; Wooldridge, P. W. Atmospheric Chemistry of HFE-7100 ($\text{C}_4\text{F}_9\text{OCH}_3$): Reaction with OH Radicals, UV Spectra and Kinetic Data for $\text{C}_4\text{F}_9\text{OCH}_2$ and $\text{C}_4\text{F}_9\text{OCH}_2\text{O}_2$. Radicals, and the Atmospheric Fate of $\text{C}_4\text{F}_9\text{OCH}_2\text{O}$. Radicals. *J. Phys. Chem. A* **1997**, *101* (44), 8264–8274.
- (36) Chen, L.; Kutsuna, S.; Tokuhashi, K.; Sekiya, A. Kinetics and mechanisms of $\text{CF}_3\text{CHFOCH}_3$, $\text{CF}_3\text{CHFOC(O)H}$, and FC(O)OCH_3 reactions with OH radicals. *J. Phys. Chem. A* **2011**, *514* (4–6), 207–213.
- (37) Myhre, G.; Shindell, D.; Bréon, F.-M.; Collins, W.; Fuglestvedt, J.; Huang, J.; Koch, D.; Lamarque, J.-F.; Lee, D.; Mendoza, B.; Nakajima, T.; Robock, A.; Stephens, G.; Takemura, T.; Zhang, H. Anthropogenic and Natural Radiative Forcing. In *Climate Change 2013: The Physical Science Basis. Contribution of Working Group I to the Fifth Assessment Report of the Intergovernmental Panel on Climate Change*; Stocker, T. F.; Qin, D.; Plattner, G.-K.; Tignor, M. M. B.; Allen, S. K.; Boschung, J.; Nauels, A.; Xia, Y.; Bex, V.; Midgley, P. M., Eds.; Cambridge University Press, Cambridge, United Kingdom and New York, NY, USA, 2014.
- (38) Yao, B.; Vollmer, M. K.; Zhou, L. X.; Henne, S.; Reimann, S.; Li, P. C.; Wenger,

- A.; Hill, M. In-situ measurements of atmospheric hydrofluorocarbons (HFCs) and perfluorocarbons (PFCs) at the Shangdianzi regional background station, China. *Atmos. Chem. Phys.* **2012**, *12* (11), 10181–10193.
- (39) Montzka, S. A.; Mcfarland, M.; Andersen, S. O.; Miller, B. R.; Fahey, D. W.; Hall, B. D.; Hu, L.; Siso, C.; Elkins, J. W. Recent trends in global emissions of hydrochlorofluorocarbons and hydrofluorocarbons: Reflecting on the 2007 adjustments to the montreal protocol. *J. Phys. Chem. A* **2015**, *119* (19), 4439–4449.
- (40) Cai, M.; Xie, Z.; Möller, A.; Yin, Z.; Huang, P.; Cai, M.; Yang, H.; Sturm, R.; He, J.; Ebinghaus, R. Polyfluorinated compounds in the atmosphere along a cruise pathway from the Japan Sea to the Arctic Ocean. *Chemosphere* **2012**, *87* (9), 989–997.
- (41) Yeung, L. W. Y.; Stadey, C.; Mabury, S. A. Simultaneous analysis of perfluoroalkyl and polyfluoroalkyl substances including ultrashort-chain C2 and C3 compounds in rain and river water samples by ultra performance convergence chromatography. *J. Chromatogr. A* **2017**, *1522*, 78–85.
- (42) Martin, J. W.; Ellis, D. A.; Mabury, S. A.; Hurley, M. D.; Wallington, T. J. Atmospheric chemistry of perfluoroalkanesulfonamides: Kinetic and product studies of the OH radical and Cl atom initiated oxidation of N-ethyl perfluorobutanesulfonamide. *Environ. Sci. Technol.* **2006**, *40* (3), 864–872.
- (43) Yeung, L. W. Y.; Dassuncao, C.; Mabury, S.; Sunderland, E. M.; Zhang, X.; Lohmann, R. Vertical Profiles, Sources, and Transport of PFASs in the Arctic Ocean. *Environ. Sci. Technol.* **2017**, *51* (12), 6735–6744.

- (44) De Silva, A. O.; Spencer, C.; Scott, B. F.; Backus, S.; Muir, D. C. G. Detection of a cyclic perfluorinated acid, perfluoroethylcyclohexane sulfonate, in the great lakes of North America. *Environ. Sci. Technol.* **2011**, *45* (19), 8060–8066.
- (45) De Solla, S. R.; De Silva, A. O.; Letcher, R. J. Highly elevated levels of perfluorooctane sulfonate and other perfluorinated acids found in biota and surface water downstream of an international airport, Hamilton, Ontario, Canada. *Environ. Int.* **2012**, *39* (1), 19–26.
- (46) Karrman, A.; Wang, T.; Kallenborn, R. PFASs in the Nordic environment Screening of Poly- and Perfluoroalkyl Substances (PFASs) and Extractable Organic Fluorine (EOF) in the Nordic Environment. *TemaNord* **2019**, 515, 1–153.
- (47) De Silva, A. O.; Allard, C. N.; Spencer, C.; Webster, G. M.; Shoeib, M. Phosphorus-containing fluorinated organics: Polyfluoroalkyl phosphoric acid diesters (diPAPs), perfluorophosphonates (PFPA), and perfluorophosphinates (PFPIAs) in residential indoor dust. *Environ. Sci. Technol.* **2012**, *46* (22), 12575–12582.
- (48) Sharp, M.; Burgess, D. O.; Cogley, J. G.; Ecclestone, M.; Labine, C.; Wolken, G. J. Extreme melt on Canada's Arctic ice caps in the 21st century. *Geophys. Res. Lett.* **2011**, *38* (11), L11501.
- (49) Bezeau, P.; Sharp, M.; Burgess, D.; Gascon, G. Firn profile changes in response to extreme 21st-century melting at Devon Ice Cap, Nunavut, Canada. *J. Glaciol.* **2013**, *59* (217), 981–991.
- (50) Kinnard, C.; Zdanowicz, C. M.; Fisher, D. A.; Wake, C. P. Calibration of an ice-core glaciochemical (sea-salt) record with sea-ice variability in the Canadian

- Arctic. *Ann. Glaciol.* **2006**, *44*, 383–390.
- (51) Plassmann, M. M.; Meyer, T.; Lei, Y. D.; Wania, F.; McLachlan, M. S.; Berger, U. Laboratory studies on the fate of perfluoroalkyl carboxylates and sulfonates during snowmelt. *Environ. Sci. Technol.* **2011**, *45* (16), 6872–6878.
- (52) Koerner, R. M. Mass balance of glaciers in the Queen Elizabeth Islands, Nunavut, Canada. *Ann. Glaciol.* **2005**, *42*, 417–423.
- (53) 3M Company. *Phase-out plan for POSF-based products*; US Environmental Protection Agency, St. Paul, MN, 2000.
- (54) Stahl, T.; Mattern, D.; Brunn, H. Toxicology of perfluorinated compounds. *Environ. Sci. Eur.* **2011**, *23* (38).
- (55) Wang, Z.; Cousins, I. T.; Scheringer, M.; Buck, R. C.; Hungerbühler, K. Global emission inventories for C4-C14 perfluoroalkyl carboxylic acid (PFCA) homologues from 1951 to 2030, part II: The remaining pieces of the puzzle. *Environ. Int.* **2014**, *69*, 166–176.
- (56) Xie, S.; Wang, T.; Liu, S.; Jones, K. C.; Sweetman, A. J.; Lu, Y. Industrial source identification and emission estimation of perfluorooctane sulfonate in China. *Environ. Int.* **2013**, *52*, 1–8.
- (57) Paul, A. G.; Jones, K. C.; Sweetman, A. J. A first global production, emission, and environmental inventory for perfluorooctane sulfonate. *Environ. Sci. Technol.* **2009**, *43* (2), 386–392.
- (58) Zhang, X.; Meyer, T.; Muir, D. C. G.; Teixeira, C.; Wang, X.; Wania, F. Atmospheric deposition of current use pesticides in the Arctic: Snow core records from the Devon Island Ice Cap, Nunavut, Canada. *Environ. Sci. Process. Impacts*

- 2013, *15*, 2304–2311.
- (59) Jiang, W.; Zhang, Y.; Zhu, L.; Deng, J. Serum levels of perfluoroalkyl acids (PFAAs) with isomer analysis and their associations with medical parameters in Chinese pregnant women. *Environ. Int.* **2014**, *64*, 40–47.
- (60) Jiang, W.; Zhang, Y.; Yang, L.; Chu, X.; Zhu, L. Perfluoroalkyl acids (PFAAs) with isomer analysis in the commercial PFOS and PFOA products in China. *Chemosphere* **2015**, *127*, 180–187.
- (61) Keene, W. C.; Pszenny, A. A. P.; Galloway, J. N.; Hawley, M. E. Sea-salt corrections and interpretation of constituent ratios in marine precipitation. *J. Geophys. Res.* **1986**, *91*, 6647–6658.
- (62) Tivy, A.; Howell, S. E. L.; Alt, B.; McCourt, S.; Chagnon, R.; Crocker, G.; Carrieres, T.; Yackel, J. J. Trends and variability in summer sea ice cover in the Canadian Arctic based on the Canadian Ice Service Digital Archive, 1960-2008 and 1968-2008. *J. Geophys. Res. Ocean.* **2011**, *116* (C3), C06027.
- (63) Benskin, J. P.; Muir, D. C. G.; Scott, B. F.; Spencer, C.; De Silva, A. O.; Kylin, H.; Martin, J. W.; Morris, A.; Lohmann, R.; Tomy, G.; Rosenberg, B; Taniyasu, S; Yamashita, N. Perfluoroalkyl acids in the atlantic and Canadian arctic oceans. *Environ. Sci. Technol.* **2012**, *46* (11), 5815–5823.
- (64) Ahrens, L.; Xie, Z.; Ebinghaus, R. Distribution of perfluoroalkyl compounds in seawater from Northern Europe, Atlantic Ocean, and Southern Ocean. *Chemosphere* **2010**, *78* (8), 1011–1016.
- (65) Sánchez-Avila, J.; Meyer, J.; Lacorte, S. Spatial distribution and sources of perfluorochemicals in the NW Mediterranean coastal waters (Catalonia, Spain).

- Environ. Pollut.* **2010**, 158 (9), 2833–2840.
- (66) Persistent Organic Pollutants Review Committee. *Report of the Persistent Organic Pollutant Review Committee on the work of its sixth meeting*; Geneva, Switzerland, 2010, 5-38.
- (67) OECD. *Survey on the production, use, and release of PFOS, PFAS, PFOA PFCA, their related substances and products/mixtures containing these substances*; Paris, France, 2011, 11-59.
- (68) Smith, T. D. Functional fluid compositions containing perfluoro surfactants. 3,679,587, 1972.
- (69) Leakage Prevention. *Hydraul. Pneum.* **2012**, 1–5.
- (70) The Challenges of Aircraft Hydraulic Design. *Hydraul. Pneum.* **1998**, 1–4.
- (71) Canada Environmental Protection Act: Prohibition of Certain Toxic Substances Regulations P.C. 2012-1714, 13 December, 2012, SOR/2012-285. *Canada Gaz. Part I* **2011**, 147, 19–67.
- (72) Stifel, P. Boeing A&M Environmental Technotes: FLASHJET® Qualification Test Programs Expand Customer Applications. **2001**, 6.
- (73) Secretariat of the Stockholm Convention. *Stockholm Convention on Persistent Organic Pollutants (POPs) as amended in 2009*; 2009.
- (74) Wania, F. A global mass balance analysis of the source of perfluorocarboxylic acids in the Arctic Ocean. *Environ. Sci. Technol.* **2007**, 41 (13), 4529–4535.

**3 Characterization of Perfluoroalkyl Substances in Sediment
Cores from High and Low Arctic Lakes in Canada**

3.1 Abstract

Perfluoroalkyl substances (PFAS) are synthetic environmentally persistent pollutants that are amenable to long-range transport and accumulation in remote Arctic ecosystems. In this study, historical inventories of twenty-three PFAS (i.e., C₄-C₁₄, C₁₆ perfluoroalkane carboxylic acids (PFCA); C₄, C₆-C₈, C₁₀ perfluoroalkane sulfonic acids (PFSA); perfluoro-4-ethyl-cyclohexane sulfonic acid (PFECHS); ammonium 4,8-dioxo-3H-perfluorononanoate (ADONA); 8-chloro-perfluoro-1-octane sulfonic acid (8-Cl-PFOS); chlorinated polyfluorinated ether sulfonic acids (Cl-PFESA) including 9-chlorohexadecafluoro-3-oxanonane-1-sulfonic acid (6:2 Cl-PFESA) and 11-chloroeicosafuoro-3-oxaundecane-1-sulfonic acid (8:2 Cl-PFESA); as well as perfluorooctane sulfonamide (FOSA)) are determined in two intact sediment cores collected from Lake Hazen, located in northern Ellesmere Island at 82° N in 2012 and Lake B35, located in central Nunavut at 64° N in 2009. In Lake Hazen, fluxes of perfluorooctanoic acid (PFOA), perfluorodecanoic acid (PFDA), perfluorobutane sulfonic acid (PFBS), and perfluorooctane sulfonic acid (PFOS) increase during 1963-2011. In Lake B35, fluxes of perfluoroheptanoic acid (PFHpA), PFOA, perfluorononanoic acid (PFNA), and perfluoroundecanoic acid (PFUnDA) increase during 1952-2009. The temporal trends for PFAS in Lake Hazen and Lake B35 sediments are consistent with the continuous annual delivery of PFAS to the Arctic of Canada. Temporal trends in sediment cores appear to follow historical market changes in PFAS manufacturing inventory. The doubling time of PFAS fluxes are faster in Lake Hazen sediments than Lake B35 sediments. In Lake Hazen, this may be attributed to the enhanced delivery of sediment

and historically archived PFAS promoted by climate-induced glacier melting in the Lake Hazen watershed post-2005. Exponentially increasing PFAS temporal trends in High and Low Arctic lakes in Canada stress the importance of developing effective global regulatory policies for PFAS manufacturing and highlights the potential for climate change-induced contaminant release from melting glaciers in the Arctic.

3.2 Introduction

Perfluoroalkyl substances (PFAS) are anthropogenic pollutants that are environmentally persistent, some of which have bioaccumulative properties.¹⁻³ Perfluoroalkane carboxylic acids (PFCA) and perfluoroalkane sulfonic acids (PFSA), collectively known as perfluoroalkyl acids (PFAA) are major classes of PFAS. PFCA are manufactured by electrochemical fluorination (ECF) and telomerization, whereas PFSA are manufactured by ECF.⁴ PFCA are used as processing aids in the manufacture of fluoropolymers and surface treatments, which are used for numerous applications such as oil and water repellency, and durability.^{4,5} PFSA are used as active ingredients in aqueous-film-forming-foams (AFFF) and mist suppressants during electroplating.⁶

Historical PFAS manufacturing shifted in response to industry phase-out initiatives. In 2002, the 3M Company phased-out its global production of perfluorooctane-based chemistry using ECF due to concerns of environmental persistence and bioaccumulation, while perfluorooctanoic acid (PFOA) manufacturing was concurrently set in motion by DuPont using telomerization in the USA.⁵ In 2006, the US EPA invited six major fluorochemical manufacturers to participate in the PFOA Stewardship Program to further reduce PFAS emissions. Under this program, six major fluorochemical manufacturers agreed to reduce PFOA, long-chain PFCA, and precursor emissions from facilities and products with full elimination by 2015.⁷ Several manufacturers committed to reduce or discontinue perfluorooctane-based chemistry, however, several countries resume manufacturing using this chemistry. For example, estimated consumption of ammonium/sodium perfluorooctanoate for the manufacturing

of polytetrafluoroethylene increased in China, India, Poland and Russia from 248 to 347 kt year⁻¹ during 2006-2015, but decreased in Japan, Western Europe and the USA from 320 to 200 kt year⁻¹ during 2006-2015.⁵ Similarly, China was a large-scale producer of perfluorooctane sulfonyl fluoride (POSF) post-2002, with estimated production volumes ranging from 50-250 and 100-250 tons year⁻¹ during 2003-2008 and 2008-2015, respectively.⁶ The global phase-out of perfluorooctane-based chemistry and long-chain PFCA promoted a recent shift towards the manufacturing of PFAS alternatives. For example, ammonium 4,8-dioxa-3H-perfluorononanoate (ADONA), a polyfluoropolyether carboxylic acid, is a replacement for ammonium perfluorooctanoate and is regulated by the European Union REACH initiative with a tonnage band of 1-10 tonnes per annum.^{8,9} Other PFAS alternatives include chlorinated polyfluorinated ether sulfonic acids (Cl-PFESA), such as 9-chlorohexadecafluoro-3-oxanonane-1-sulfonic acid (6:2 Cl-PFESA) and 11-chloroeicosafluoro-3-oxaundecane-1-sulfonic acid (8:2 Cl-PFESA), which are major components of F-53B.¹⁰ F-53B is a mist suppressant replacement for PFOS during metal plating in China,¹¹ with a reported usage of 20-30 tons during 2009.¹² It is expected that sustained manufacturing will contribute to global emissions of legacy and alternative PFAS in the environment.

The detection of PFAS in pristine remote environments, such as the Arctic demonstrates long-range transport.^{1,13-15} PFAS deposition in Arctic regions is possible through the long-range atmospheric transport of aerosols such as sea spray, and the long-range atmospheric transport and oxidation of volatile precursors such as FTOH and perfluoroalkane sulfonamido substances.^{13,16-18}

Environmental archives are used to reconstruct historical periods of PFAS deposition. For example, wildlife tissue bank archives demonstrate PFAS temporal trends in livers from polar bears (*Ursus maritimus*)^{19,20} and ringed seals (*Phoca hispida*).²¹ Recently, a continuous air sampling campaign from 2006 to 2014 in Alert, Nunavut (82° N) demonstrates increasing temporal trends for PFAS concentrations on particles.²²

There are challenges associated with long-term environmental monitoring. Annual sampling for tissue banks or other long-term environmental monitoring is costly and can be logistically challenging for storage integrity. Furthermore, many tissue archives and monitoring datasets are not able to capture emissions during the onset of PFAS manufacturing in the 1950s,^{18–20,22–25} which is useful for establishing and interpreting long-term chronological records of PFAS deposition in the environment. Another challenge with quantifying temporal trends includes changes in analytical methodology over time, which can affect inter-annual comparisons. To circumvent these challenges, chronological records of PFAS deposition determined using sediment and ice cores are advantageous because they can be collected during a single sampling excursion and analyzed using the same analytical methods with fine temporal resolution.^{13,18} Sediment core analyses demonstrate chronological records of PFAS deposition in Tokyo Bay,^{26,27} High Arctic lakes,¹⁴ and the Canadian Rocky Mountains.²⁸ In recent years, knowledge of historical PFAS emission inventories improved based on industry data,^{5,6} which is valuable for comparison of temporal trends in environmental samples.

In this study, chronological records of PFAS deposition are determined using sediment cores collected from the High Arctic Lake Hazen watershed on northern Ellesmere Island at 82° N and in the Low Arctic Lake B35 watershed near Hudson Bay at

64° N. The primary objective of this study is to elucidate the role of long-range atmospheric transport and deposition on PFAS contaminant trends in the Arctic Archipelago. Lake Hazen is suitable in this regard because it is north of 75° N on Ellesmere Island and is far from local human contamination. In addition, the Lake Hazen watershed is unique compared to other watersheds in the High Arctic of Canada in that it receives substantial glacier inputs, providing a unique opportunity to examine PFAS deposition trends in the context of climate warming and the accelerated release of historically archived (i.e., stored in glacier ice) PFAS. The size and accessibility of Lake Hazen are also contributing reasons for selection in this study. Lake B35 is selected also as an Arctic site but is located at a lower latitude and is closer to human settlements on mainland Canada. Lake B35 is also of interest to fill a current data gap for PFAS deposition in the Low Arctic of Canada at 64° N and examine the relationship between climate warming and PFAS deposition in sediments from the Baker Lake region. We present the first chronological record of PFAS deposition in sediments north of 75° N and the most temporally resolved chronological records of PFAS deposition in sediments from the Arctic of Canada.

3.3 Methods

3.3.1 Study Area

Lake Hazen is the largest lake by volume north of the Arctic Circle and is located in Quttinirpaaq National Park on Ellesmere Island, Nunavut, Canada (Appendix B,

Section B1, Table 3.1). The hydrological budget of Lake Hazen is dominated by glacial meltwater inputs and the lake is drained by the Ruggles River into Chandler Fiord.²⁹

Table 3.1 An overview of the Lake Hazen and Lake B35 study areas. Annual precipitation data for Lake Hazen and Lake B35 is reported by Thompson et al.³⁰ and Environment and Climate Change Canada.³¹ *Corresponds to the mid-basin depth due to unknown bathymetry in this lake.

	Lake Hazen	Lake B35
Latitude (°N)	81° 49'	64° 11'
Longitude (°W)	70° 42'	95° 32'
Lake Area (km²)	544	0.0538
Catchment Area (km²)	7516	1.40
Catchment: Lake Area Ratio	14	26
Lake Depth (m)	267	1.3*
Annual Precipitation (mm)	95	250

Lake B35 is a small lake approximately 6 km east of the community of Baker Lake, located near the geographic center of Canada (Table 3.1). The hydrological budget of Lake B35 is dominated by surface runoff and permafrost thaw inputs. Lake B35 is drained into Prince River.

3.3.2 Sampling

Two intact sediment cores were collected on 30 May 2012, while the lake was fully ice-covered, from the deep trench (262 m deep) in Lake Hazen at 81.84° N, 70.51° W using a UWITEC gravity corer with an 8.6 cm inner diameter polyvinyl chloride tube to determine dating chronology and PFAS deposition profiles. Further details of the Lake Hazen sediment core sampling method can be found in Lehnherr et al.²⁹ Cores were extruded and sectioned in the Lake Hazen field laboratory at 0.5 cm (0-15 cm) and 1 cm (15-38 cm) intervals the same day. Each section was placed into polypropylene (PP) screw capped jars, frozen immediately on-site in a propane-powered freezer, and kept frozen until analyzed. Samples were transported to the Canada Centre for Inland Waters (CCIW), Burlington, Ontario for dating and analysis. An intact sediment core of 20 cm length was collected from the eastern basin of Lake B35 on 28 June 2009, at a mid-basin depth of 1.3 m, also using a UWITEC corer. The core was sectioned at 0.5 cm intervals up to 10 cm depth and stored in PP jars for transport and analysis at CCIW, Burlington, ON.

3.3.3 Sample Extraction

Sediments were extracted according to Weber et al.³² with a few modifications. Briefly, 0.5 to 1 g of freeze-dried sediment was spiked with internal standard, consisting of isotopically labeled PFAS and subjected to an ultrasonic assisted basicified methanolic extraction. After triplicate extraction and centrifugation, the supernatants were combined and taken to dryness using nitrogen gas. Residues were reconstituted in acidified methanol and heated before further concentration by nitrogen to a final 1.0 mL volume. A second suite of isotopically labeled standards was added before analysis to monitor matrix effects. PFAS concentrations in sediment are blank, recovery, and matrix corrected. Matrix effects are determined by comparing the peak area of isotopically labeled PFAS standards added after the extraction to the peak areas of PFAS in a solvent standard at equivalent concentrations. Accuracy was evaluated using spike and recovery analysis, as described in detail in Appendix B (Section B4). The analytical laboratory annually participates in the Northern Contaminants Program Interlaboratory Evaluation and has consistently achieved high performance for accuracy based on low z-scores obtained from interlaboratory trials. Accuracy could be further evaluated using standard reference materials available from National Institute of Standards and Technology for sediment. However, sediment reference materials are only validated for PFOS. Analysis was by ultra-high-performance liquid chromatography-tandem mass spectrometry (UPLC-MS/MS). Further details of chemicals, sediment extraction procedure, and QA/QC parameters are presented in Appendix B (Sections B2-B4, Tables B1-B3).

3.3.4 Instrumental Analysis

All extracts were analyzed on an Acquity UPLC I class liquid chromatograph coupled to a XEVO TQ-S tandem mass spectrometer operated in electrospray negative ionization mode (Waters Corporation, Massachusetts, USA) as per previous methods.^{13,18} PFAS were separated on an Acquity UPLC® BEH C₁₈ (2.1 x 100 mm, 1.7 µm) stationary phase (Waters Corporation, Massachusetts, USA) using a 0.1 mM ammonium acetate water-methanol gradient. Details of the UPLC-MS/MS method are presented in Appendix B (Tables B4-B6).

3.3.5 Sediment Dating

Sectioned sediment core sub-samples were freeze-dried, ground, and treated to polonium distillation for alpha counting analysis.¹³⁷Cs was determined by gamma spectroscopy for 47 hours per sample using a high purity germanium spectrometer (DSPEC, Ortec instruments) at CCIW. Dating and sedimentation rates are based on unsupported ²¹⁰Pb results using the Constant Rate of Supply (CRS) model.³³ Unsupported ²¹⁰Pb corresponds to the atmospheric fallout of ²¹⁰Pb that is incorporated into lake sediments resulting from the diffusion and subsequent decay of ²²²Rn from soils.³⁴ The CRS model is chosen for sediment dating in this study because it provides robust dating accuracy by permitting changes in sedimentation rates over time.³³ The Lake Hazen dating was confirmed using the distinctive ¹³⁷Cs peak at 15.5 cm indicative of atmospheric nuclear weapons testing in the early 1960s. The Lake B35 dating was confirmed using ²¹⁰Pb profiles only.¹³⁷Cs and ²¹⁰Pb profiles for Lake Hazen and Lake B35

are presented in Appendix B (Figure B1). Sedimentation rates range from 0.047-6.659 (mean 0.922, median 0.389) $\text{g cm}^{-2} \text{ year}^{-1}$ in Lake Hazen during 1923-2011 and 0.011-0.015 (mean 0.013) $\text{g cm}^{-2} \text{ year}^{-1}$ in Lake B35 during 1940-2009. The limitations of High Arctic sediment sampling are discussed in Appendix B (Section B5, Figure B2).

3.3.6 Data Treatment

The limits of detection (LOD) and quantitation (LOQ) are designated as the concentration corresponding to signal-to-noise ratios (S/N) of 3 and 10 (Table B2).¹³ PFAS with detection frequencies less than 50 % are excluded from temporal trend analyses. For all other PFAS (i.e., C₇-C₁₁ PFCA; C₄ and C₈ PFSA), temporal trends are determined using fluxes derived from sediment concentrations equal to or greater than the LOD. PFAS sedimentation flux (F_{sed}) is calculated according to $F_{\text{sed}} = C_{\text{sed}} \cdot R_{\text{sed}} / \text{FF}$, where C_{sed} is the concentration of PFAS in sediment (ng g^{-1} dry weight, dw), R_{sed} is the sedimentation rate estimated from the CRS model ($\text{g cm}^{-2} \text{ year}^{-1}$), and FF is the focusing factor, as described by Yeung et al.³⁵ Focusing factors of 11 and 1.2 are determined for Lake Hazen and Lake B35 sediments, respectively, according to $\text{FF} = {}^{210}\text{Pb}_{\text{sed}} / {}^{210}\text{Pb}_{\text{soil}}$, where ${}^{210}\text{Pb}_{\text{sed}}$ is the unsupported ${}^{210}\text{Pb}$ inventory in sediment, and ${}^{210}\text{Pb}_{\text{soil}}$ is the local inventory of unsupported ${}^{210}\text{Pb}$ in soil due to atmospheric fallout, as reported by Lockhart et al.³⁶ Statistical analysis on natural log-transformed sediment flux is performed using StatPlus:mac (V6), with a critical value set to 5 % (i.e., $p < 0.05$) for linear regression, Spearman (r_s), and Pearson (r) correlation analysis. Doubling times (t_2) are calculated for PFAS displaying first-order kinetics in sediment according to $t_2 = \ln(2)/k$, where k is the

first order rate constant with units (year^{-1}) obtained from the slope of the linear regression of natural log-transformed PFAS flux ($\text{ng m}^{-2} \text{ year}^{-1}$) versus time (year). The sum of PFAS concentrations (ΣPFAS) corresponds to the sum of all detected PFAS equal to or greater than congener LOD at each depth (i.e., concentrations $<\text{LOD}$ were assigned a value of 0).

3.4 Results and Discussion

3.4.1 Composition of PFAS in Sediments

Thirteen PFAS are detected in Lake Hazen sediments, including $\text{C}_6\text{-C}_{13}$ PFCA, C_4 , C_6 , C_8 PFSA, PFECHS, and FOSA (Table B7). The most consistently detected PFAS in all Lake Hazen sediments are PFOA, PFDA, PFBS, PFOS. Several PFAS are only detected frequently at specific depth intervals in Lake Hazen sediments. For example, PFNA occurs in 3.25-9.25 cm (2002-2009 CE), PFUnDA in 6.25-13.75 cm (1987-2006 CE), PFDoDA in 7.25-9.75 cm (2000-2005 CE), and PFTrDA in 6.25-10.75 cm (1998-2006 CE, Figure 3.1). The detection frequencies of other PFAS including PFHxA, PFHpA, PFECHS, PFHxS, and FOSA are low and inconsistent in Lake Hazen sediments. The highest concentrations of $\text{C}_6\text{-C}_9$ PFCA and C_4 , C_6 , C_8 PFSA in Lake Hazen sediments occur in 0.25-2.25 cm (all 5 sections corresponding to 2011 CE). Diverting from this trend, maximum concentrations of PFDA and FOSA occur at 9.25 cm (2002 CE), whereas maximum concentrations of PFUnDA, PFDoDA, and PFTrDA occur at 7.75 cm (2004 CE). ΣPFAS concentrations range from 0.006-0.161 $\text{ng g}^{-1} \text{ dw}$, with a maximum concentration at 9.25 cm (2002 CE, Figure 3.1). The sum of PFCA concentration

(Σ PFCA) exceeds PFSA, comprising $64 \pm 3\%$ (mean \pm standard error, SE) of all the PFAS quantified throughout the sediment core.

Seven PFAS are detected in Lake B35 sediments, including C₇-C₁₁ PFCA, as well as C₄ and C₈ PFSA (Table B7, Figure 3.1). PFOA and PFNA are detected in all/most sediments in 0.25-3.75 cm (1963-2009 CE), whereas PFHpA, PFDA, and PFUnDA are detected in most sediments in 0.25-2.75 cm (1986-2009 CE). PFOS is only detected at 0.25 cm (2009 CE) and PFBS in 1.25-2.75 cm (1986-2002 CE). The highest individual concentrations of C₇-C₁₁ PFCA and PFOS in Lake B35 sediments occur at 0.25 cm (2009 CE). Σ PFAS concentrations range from 0.044-1.52 ng g⁻¹ dw, with a maximum concentration at 0.5 cm (2009 CE, Figure 3.1). Σ PFCA concentration is $96 \pm 2\%$ of all PFAS quantified throughout the sediment core.

The composition profiles for PFAS in Lake Hazen and Lake B35 sediments demonstrate that these regions are impacted by different emission sources. For example, PFSA are detected more frequently in Lake Hazen sediments than Lake B35 sediments, indicating that ECF-based sources are more impactful in the Lake Hazen region. The general absence of PFHxS in sediments from Lake Hazen and Lake B35 (Figure 3.1) is noteworthy given that PFHxS is a co-contaminant in AFFF formulations with PFBS and PFOS^{37,38} and has a higher partitioning coefficient (i.e., K_d) in sediment than PFBS³⁹ (Figure 3.1). As such, the low detection frequency of PFHxS relative to PFBS and PFOS in Lake Hazen and Lake B35 sediments indicates that PFBS and PFOS are derived from a non-AFFF source. On the other hand, it is possible that the low detection frequency of PFHxS in Lake Hazen and Lake B35 sediments indicates that PFHxS emissions from the

product life-cycles of perfluorohexane sulfonyl fluoride (PH_xSF) and POSF-based products are limited in these regions.⁴⁰

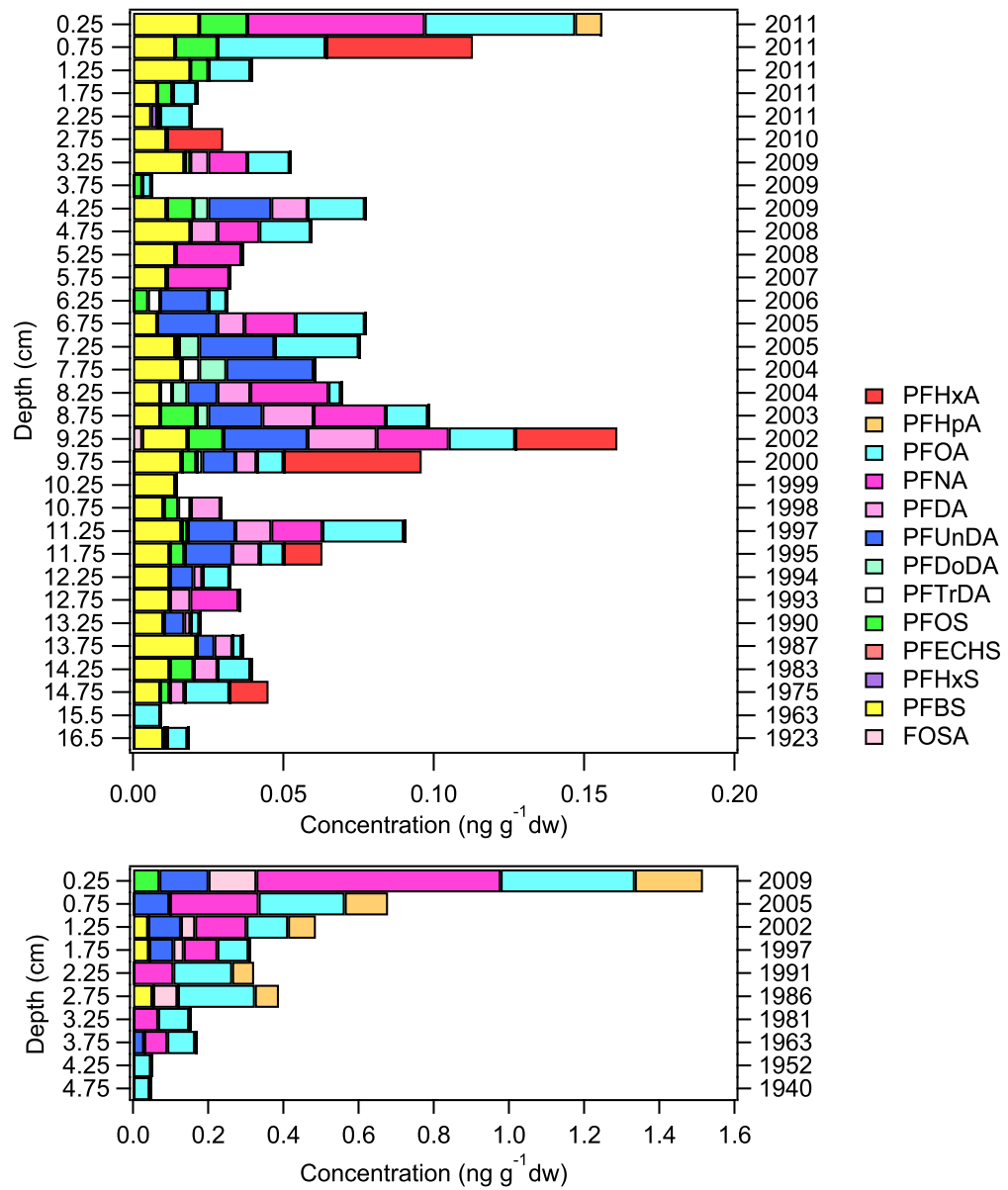


Figure 3.1 Concentration profiles (ng g⁻¹ dw) of PFAS in sediment cores versus midpoint depth (left y-axes, cm) and year (right y-axes) in Lake Hazen (top panel) and Lake B35 (bottom panel). The legend applies to both panels.

3.4.2 Temporal Trends

The Lake Hazen and Lake B35 sediment cores correspond to depositional periods from 1923-2011 and 1940-2009, respectively. Low Σ PFAS flux in sediments prior to the 1950s is regarded as a period that precedes large-scale PFAS manufacturing.²⁸ PFAS deposition prior to the 1950s is omitted from temporal trend analysis to portray the influence of large-scale manufacturing on PFAS deposition in Lake Hazen and Lake B35 sediments (Figure 3.2).

In Lake Hazen, exponentially increasing fluxes ($p < 0.01$) are observed during 1963-2011, with doubling times corresponding to 6.9 years for PFOA, 6.9 years for PFDA, 6.3 years for PFOS, and 7.7 years for PFBS (Tables 3.2 and B8). Exponentially increasing fluxes are also observed in Lake B35 during 1952-2009, with doubling times corresponding to 14 years for PFHpA, 21 years for PFOA, 14 years for PFNA, and 19 years for PFUnDA (Tables 3.2 and B8). A comparison of doubling times in Lake Hazen and Lake B35 sediments with PFAS trends in Arctic wildlife is discussed in Appendix B (Section B6). The doubling times for PFOA in this study are within the range of those reported in a sediment core collected from Lake Oesa in the Canadian Rocky Mountains from 1957-2008 (Table 3.2). Interestingly, FOSA and long-chain PFCA, such as PFDoDA and PFTrDA were detected frequently in sediments from Lake Oesa and Lake Opabin, but not in sediments from Lake Hazen and Lake B35.

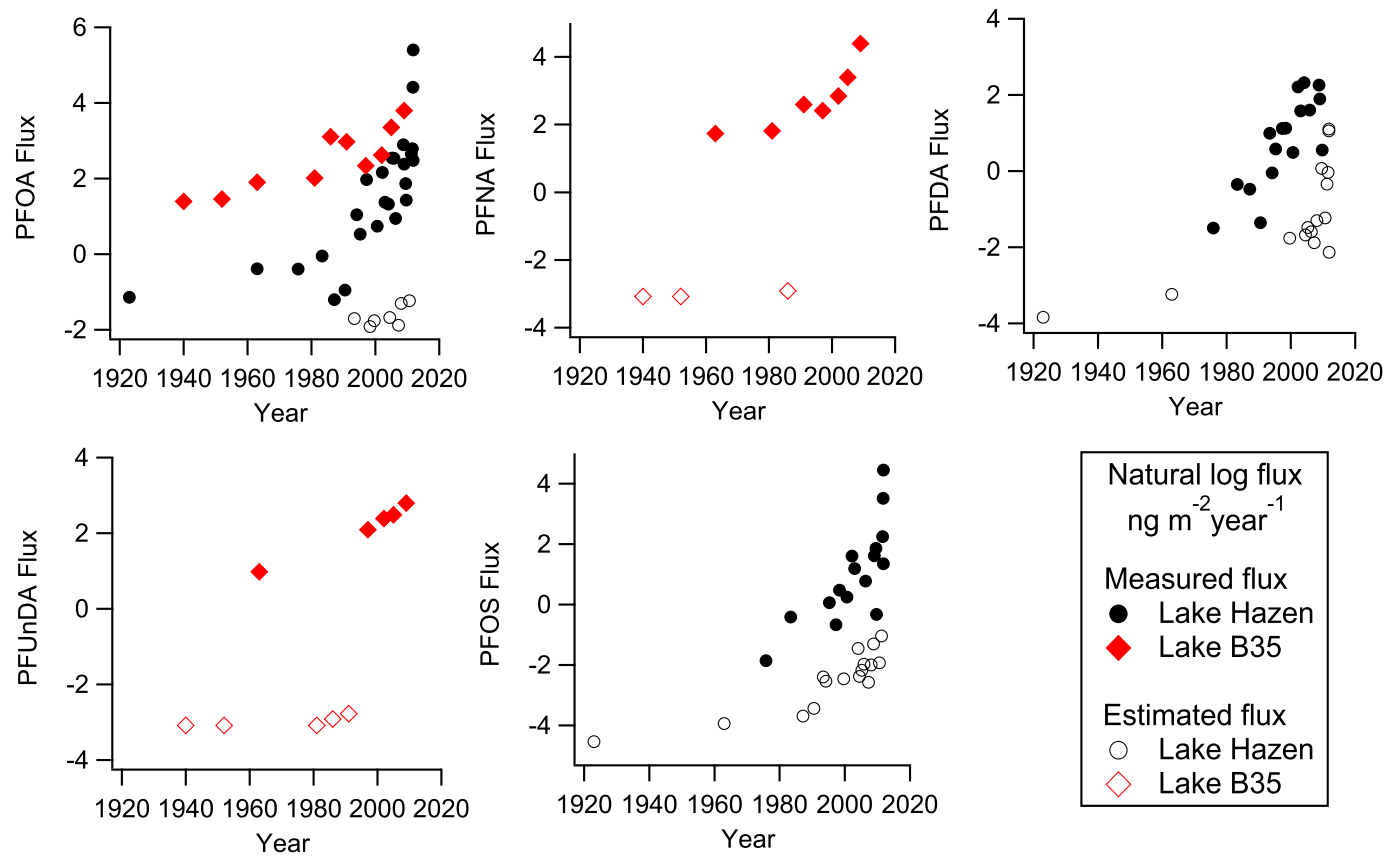


Figure 3.2 Natural log-transformed PFAS fluxes ($\text{ng m}^{-2} \text{year}^{-1}$) into Lake Hazen (solid black circles, 1923-2011), and Lake B35 (solid red squares, 1940-2009) sediments. Fluxes are estimated at Lake Hazen (unfilled circles) and Lake B35 (unfilled squares) using substituted sediment concentrations equal to LOD.

Table 3.2 Comparison of doubling times (and 95% confidence interval) of PFAS fluxes in Lake Hazen and Lake B35 sediments with reported sediment and wildlife bank tissue archives. Doubling times for all sites are calculated using only detected concentrations.

Location	Lake Hazen, Nunavut, Canada	Lake B35, Nunavut, Canada	Lake Oesa, Canadian Rocky Mountains	Lake Ontario, Station 1034	Baffin Island, Nunavut, Canada	Barrow, Alaska, USA	West Greenland	Prince Leopold Island Nunavut, Canada
Reference	This Study	This Study	Benskin et al. ²⁸	Yeung et al. ³⁵	Smithwick et al. ²⁰	Smithwick et al. ²⁰	Riget et al. ¹⁹	Braune and Letcher ²⁴
Matrix	Sediment Core	Sediment Core	Sediment Core	Sediment Core	Polar Bear Liver	Polar Bear Liver	Ringed Seal Liver	Northern Fulmar Eggs
Period	1963-2011	1952-2009	1957-2008	1952-2005	1972-2002	1972-2002	1982-2006	1975-2011
Doubling Time (years)								
PFHpA		14 (7.7-110)						
PFOA	6.9 (5.3-11)	21 (13-49)	11 (7.7-35)	9.9 (8.7-14)	7.3 (4.5-10.1)			
PFNA		14 (8.7-69)			3.6 (2.7-4.5)	5.6 (4.7-6.5)		5.3 (4.3-6.9)
PFDA	6.9 (4.9-11)				4.2 (3.2-5.2)	6.7 (5.0-8.4)	9.9 (6.9-35)	8.7 (5.8-17)
PFUnDA		19 (15-25)	8.7 (6.9-14)		4.1 (2.7-5.5)	6.1 (5.0-7.2)	8.7 (6.9-17)	5.3 (3.8-8.7)
PFBS	7.7 (5.8-11)							
PFOS	6.3 (4.1-11)			14 (11-17)	9.8 (4.7-14.9)	13.1 (9.1-17.1)		

Higher detection frequencies of long-chain PFCA and FOSA in Lake Oesa and Lake Opabin, located at altitudes > 2000 m and 51° N in western Canada, suggest these regions are impacted by different air mass pollution than Lake Hazen and Lake B35.

Annual fluxes of PFOA from 1963-2008 and 1952-2009 in Lake Hazen and Lake B35 sediment cores, respectively, are similar to PFOA fluxes in Lake Oesa located in the Western Canada Rocky Mountains during 1967-2008 (Table 3.3).²⁸

Table 3.3 Comparison of mean PFAS sedimentation fluxes (ng m⁻² year⁻¹) in Lake Hazen and Lake B35 sediments to Lake Ontario sediment sediments.³⁵ Sedimentation rates are expressed in g cm⁻² year⁻¹. Range of fluxes are presented in parentheses.

Location	Lake Hazen, Nunavut, Canada	Lake B35, Nunavut, Canada	Lake Oesa, Canadian Rocky Mountains	Lake Ontario, Canada Station 1004
Matrix	Sediment Core	Sediment Core	Sediment Core	Sediment Core
Period	1963-2008	1952-2009	1957-2008	1953-2004
Sedimentation Rates	0.050-6.659	0.011-0.015	0.029-0.058	0.025-0.038
Analyte	Flux	Flux	Flux	Flux
PFOA	5.0 (<0.29-18)	21 (5.2-54)	9.5 (<LOD-29)	683 (<6-1139)
PFOS	1.7 (<0.039-4.9)	(<0.11-8.7)	<LOD	3087 (292-10410)

In contrast, annual fluxes of PFOA and PFOS in Lake Hazen and Lake B35 sediments during 1963-2008 and 1952-2009, respectively are approximately 100 and 200 times, respectively, lower than annual fluxes in Lake Ontario sediments (Table 3.3).³⁵ It is noteworthy that the magnitude of PFOS deposition in Lake Ontario is greater than Lake Hazen, despite having lower sedimentation rates relative to Lake Hazen, which highlights the impact of local anthropogenic activity in the Lake Ontario watershed on elevating PFOS sediment concentrations relative to Lake Hazen and Lake B35 (Table 3.3).

The doubling times for PFAA are faster in Lake Hazen sediments than Lake B35 sediments. A recent study by Lehnerr et al. noted climate warming in the Lake Hazen watershed resulted in large scale mass losses from glaciers driving inputs of sediment, organic carbon, mercury, and organochlorine pesticides (OCP) into the Lake Hazen watershed.²⁹ Glaciers are also repositories for atmospheric PFAS deposition, consistent with observations in ice cores from the High Arctic of Canada,^{13,17,18} Svalbard,⁴¹ and the European Alps.⁴² Thus, it is reasonable to hypothesize that melting glaciers deliver PFAS into Lake Hazen. In Longyearbyen, Svalbard, Norway (78° N) PFAS concentrations in glacier meltwater are an order of magnitude higher than concentrations in glacial surface snow.⁴¹ Kwok et al. postulated that climate warming accelerated glacier melting, resulting in the mixing of multi-decadal meltwater enriched in PFAS.⁴¹

To investigate the effect of melting glaciers on PFAS deposition, annual glacier meltwater discharge in the Lake Hazen watershed is correlated to fluxes of PFAS in Lake Hazen sediments during 1963-2011. Correlation analysis suggests that PFOA ($r=0.65$, $p=0.01$), PFBS ($r=0.55$, $p=0.02$), and PFOS ($r=0.69$, $p=0.02$) deposition in Lake Hazen sediments is impacted by glacier melting. Climate-induced glacial melting promotes

greater rates of sediment accumulation in Lake Hazen via increasing riverine inputs.²⁹ As such, the variability in glacier meltwater discharge is reflected in the rates of sediment accumulation, particularly post-2005 when glacier melting is most variable. For example, fluxes of PFOA in Lake Hazen sediments are notably consistent with glacier meltwater discharge post-2005, suggesting the increased delivery of sediment and glacier meltwaters post-2005 increased the input of historically archived and surface runoff inputs of PFOA into Lake Hazen (Figure 3.3). Similar observations are reported by Lehnherr et al., whereby higher concentrations of legacy OCP are observed in a Lake Hazen sediment core post-2000 in response to enhanced glacier melting.²⁹ In contrast, fluxes of PFDA in Lake Hazen sediments are not correlated with annual glacier meltwater discharge ($r=0.35$, $p=0.20$), which may suggest the delivery of PFDA into Lake Hazen is governed by snowmelt in the surrounding catchment.

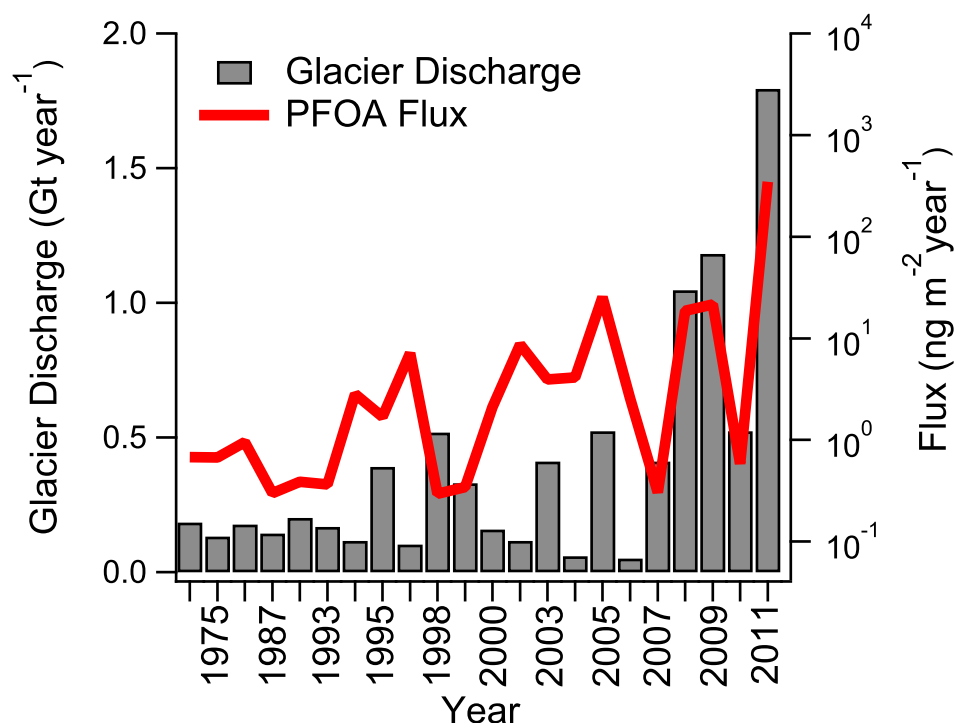


Figure 3.3 Comparison of glacier meltwater discharge (Gt year⁻¹, left y-axis, grey bars) in the Lake Hazen watershed and PFOA fluxes (ng m⁻² year⁻¹, right y-axis, red line) in the Lake Hazen sediment core versus time (bottom x-axis, 1963-2011). PFOA fluxes are estimated for Lake Hazen data <LOD by using LOD-substituted concentrations for flux calculations.

Taken together, melting glaciers in the Lake Hazen watershed are vectors of sediment and historically archived PFAS, particularly post-2005, which can be used to corroborate the faster increasing depositional trends and impact of climate warming on PFAS deposition in Lake Hazen sediments. In contrast, climate analysis in the Baker Lake region, which is close to Lake B35, indicates that mean annual temperature (mean ± SE, -11.8 ± 0.2 °C)

and precipitation (253 ± 7 mm) is fairly constant during 1952-2009,³¹ suggesting these climate factors do not account for the increasing PFAS deposition in Lake B35 sediment.

The increasing temporal trends for PFAS suggest that historical emissions from telomerization and ECF-based sources may impact PFAS deposition in Lake Hazen and Lake B35 sediments. To investigate the influence of telomerization and ECF manufacturing on PFAS deposition in Lake Hazen and Lake B35, PFAS fluxes in sediments are correlated with estimated annual production volumes of FT-based products and POSF. In Lake Hazen, fluxes of PFOA, PFDA, and PFBS are strongly correlated with FT-based production volumes during 1963-2005 ($\rho \geq 0.65$, $p < 0.01$, Table B9). Similarly, strong correlations are observed between FT-based production volumes and all PFCA fluxes in Lake B35 during 1963-2009 ($\rho \geq 0.72$, $p < 0.05$, Table B9). These observations suggest manufacturing via telomerization is a dominant historic source of PFCA to the Arctic of Canada. In contrast, PFAS fluxes in Lake Hazen and Lake B35 sediments are not correlated with estimated POSF production volumes (Table B9). Weak correlations between PFSA fluxes and POSF production volumes indicate that PFSA deposition in Lake Hazen and Lake B35 sediments is not representative of the production trends for POSF.

The composition profiles of PFAS in Lake Hazen and Lake B35 sediments are generally consistent with regulatory phase-out initiatives and historical market changes in PFAS manufacturing. For example, the low detection frequency of PFOS and FOSA in Lake Hazen sediments post-2003 is consistent with the global phase-out of perfluorooctane sulfonyl-based chemistries by the 3M Company in 2001, whereas the high detection frequency of C₈-C₁₂ PFCA in Lake Hazen sediments during 2003-2005 is

consistent with emerging global FT manufacturing using perfluorooctane-based chemistries (Figure 3.1). Similarly, the low detection frequency of C₁₀-C₁₃ PFCA in Lake Hazen sediments post-2006 is consistent with reductions of perfluorooctane-based emissions by FT manufacturers participating in the US EPA PFOA Stewardship Program (Figure 3.1). The detection of PFHxA in Lake Hazen sediments during 2010 and 2011 may also provide evidence of global PFAS manufacturing shifts toward shorter-chain chemistries in recent years due to global phase-out initiatives. However, it is possible that resurgences in global PFAS emissions impact environmental inventories in Lake Hazen and Lake B35 sediments. For example, the detection long-chain PFCA and PFOS in Lake Hazen and Lake B35 sediments post-2006 may provide historical evidence of global emission resurgences due to the sustained production of PFAS by perfluorooctane-based chemistry,⁴³ or reflects emissions during the life-cycle of PFAS products manufactured prior to industry phase-out initiatives. The absence of PFAS alternatives such as 6:2 and 8:2 Cl-PFESA, and ADONA in Lake Hazen and Lake B35 sediments indicates that emissions from the manufacturing of PFAS alternatives are not impactful in the Arctic of Canada. These observations contrast those reported by Gebbink et al., whereby 6:2 Cl-PFESA is detected in livers of polar bears, ringed seals, and killer whales in East Greenland during 2012 and 2013.⁴⁴ Similarly, 6:2 Cl-PFESA is measured in surface waters from rivers and lakes in China, the United States, United Kingdom, Sweden, Germany, Netherlands, and South Korea during 2016,⁴⁵ demonstrating that PFAS alternatives are amenable to global dissemination. Future work should focus on the continued monitoring of legacy and novel PFAS alternatives in Lake Hazen and Lake

B35 to evaluate the efficacy of industry phase-out initiatives and the impact of market changes on PFAS deposition in the Arctic of Canada.

3.4.3 Implications for PFAS Deposition in the Arctic of Canada

The detection of PFAS in remote High and Low Arctic lakes in Canada corroborates evidence of long-range atmospheric transport. Some of the most compelling evidence for long-range transport is the detection of PFCA in High Arctic ice caps, including Devon Island ice cap and Agassiz ice cap on Ellesmere Island, both sampled at 1800 m above sea-level.^{13,17,18} In recent studies, PFCA deposition on the Devon Ice Cap is governed by the long-range atmospheric transport and oxidation of volatile precursors.^{13,17,18} The Devon Ice Cap is located at 75° N, an intermediate latitude between Lake Hazen and Lake B35, implying that these lakes may be influenced by the same air masses as the Devon Ice Cap. To investigate this hypothesis, PFOA and PFOS fluxes from the Devon Ice Cap, Lake Hazen, and Lake B35 are compared (Figure 3.4). Overall, there is a general agreement for PFOA fluxes in Lake B35 (mean ± SE, 1981-2009, 21 ± 5 ng m⁻² year⁻¹), and the Devon Ice Cap (1982-2009, 32 ± 3 ng m⁻² year⁻¹). Interestingly, after 1997, PFOA flux in Lake B35 increased from 14 to 45 ng m⁻² year⁻¹ during 2002-2009, which is consistent with the gradual increase observed on the Devon Ice Cap from 16 to 41 ng m⁻² year⁻¹ during 2003-2008 (Figure 3.4).

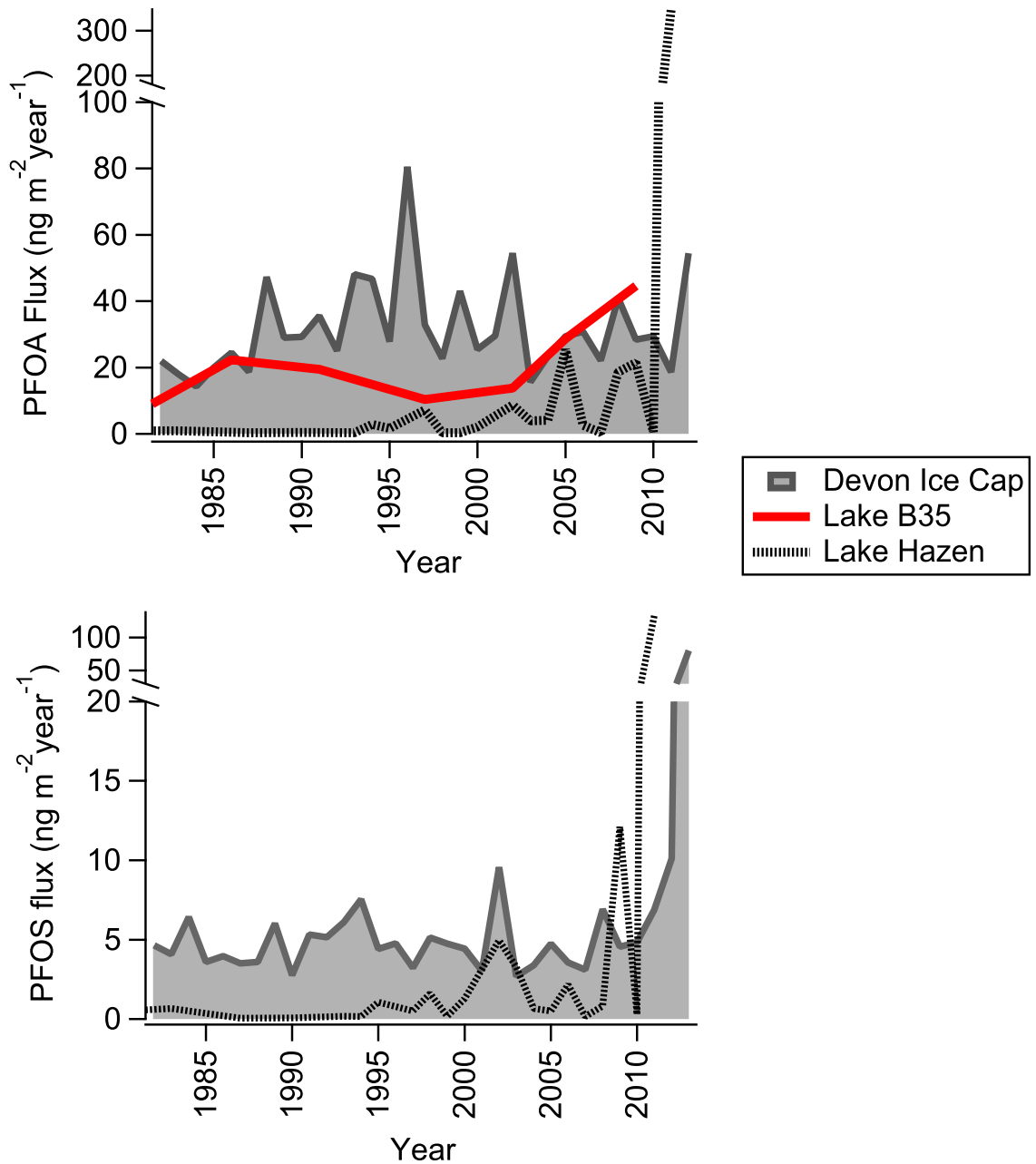


Figure 3.4 Comparison of PFOA and PFOS flux deposition (ng m⁻² year⁻¹, y-axis) in Lake Hazen and Lake B35 sediment to an ice core from the summit of the Devon Ice Cap¹⁸ over a 1982-2011 temporal period. PFAS fluxes are estimated for Lake Hazen data <LOD by using LOD-substituted concentrations for flux calculations.

In contrast, the magnitude of mean PFOA and PFOS fluxes in Lake Hazen is 11 and 3 times lower, respectively, than mean PFOA and PFOS fluxes observed on the Devon Ice Cap during 1983-2004 (Figure 3.4). The maximum flux of PFOA in Lake Hazen is observed during 2011 corresponding to $350 \text{ ng m}^{-2} \text{ year}^{-1}$ and is 19 times greater than the flux on the Devon Ice Cap during 2011. Interestingly, the maximum flux of PFOS observed during 2011 in Lake Hazen ($130 \text{ ng m}^{-2} \text{ year}^{-1}$) is similar to the maximum flux of PFOS reported on the Devon Ice Cap in 2013 ($80.3 \text{ ng m}^{-2} \text{ year}^{-1}$). PFOS is only detected in one sample from Lake B35 in 2009 ($8.7 \text{ ng m}^{-2} \text{ year}^{-1}$), possibly due to limited temporal resolution relative to Lake Hazen and the Devon Ice Cap but is consistent with the maximum flux observed on the Devon Ice Cap during 1982-2009 ($9.57 \text{ ng m}^{-2} \text{ year}^{-1}$).

The general consistency of PFOA deposition in Lake B35 and the Devon Ice Cap suggests these regions are impacted by similar source regions, predominantly via long-range atmospheric transport and deposition. The contrast observed for the magnitude of PFAS deposition during 2011 in Lake Hazen can be attributed to differences in sediment delivery driven by climate-induced glacier melting. It is likely that these study areas are influenced by both North American and Eurasian air masses to some extent given the prevalence of PFAS manufacturing in these countries. The importance of local emission sources on PFAS deposition is currently unknown in Lake Hazen and Lake B35, which may also contribute to the occurrence of PFAS in these areas.

3.5 Conclusions

In this study, exponentially increasing temporal trends are observed for PFAS in High and Low Arctic lakes in Canada, which are consistent with historical market changes in PFAS manufacturing inventory. Faster doubling times of PFAS fluxes in Lake Hazen sediments demonstrates the potential for climate change-induced contaminant release from melting glaciers in the Arctic. The consistency of observations in this study with the Devon Ice Cap suggests the Arctic will continue to act as a sink for contemporary PFAS pollution in lower latitudes, which highlights the importance of developing effective global regulatory policy for PFAS.

3.6 Literature Cited

- (1) Butt, C. M.; Berger, U.; Bossi, R.; Tomy, G. T. Levels and trends of poly- and perfluorinated compounds in the arctic environment. *Sci. Total Environ.* **2010**, *408* (15), 2936–2965.
- (2) Campo, J.; Lorenzo, M.; Pérez, F.; Picó, Y.; Farré, M. la; Barceló, D. Analysis of the presence of perfluoroalkyl substances in water, sediment and biota of the Jucar River (E Spain). Sources, partitioning and relationships with water physical characteristics. *Environ. Res.* **2016**, *147*, 503–512.
- (3) Ahrens, L.; Gashaw, H.; Sjöholm, M.; Gebrehiwot, S. G.; Getahun, A.; Derbe, E.; Bishop, K.; Åkerblom, S. Poly- and perfluoroalkylated substances (PFASs) in water, sediment and fish muscle tissue from Lake Tana, Ethiopia and implications for human exposure. *Chemosphere* **2016**, *165*, 352–357.
- (4) Buck, R. C.; Franklin, J.; Berger, U.; Conder, J. M.; Cousins, I. T.; Voogt, P. De; Jensen, A. A.; Kannan, K.; Mabury, S. A.; van Leeuwen, S. P. J. Perfluoroalkyl and polyfluoroalkyl substances in the environment: Terminology, classification, and origins. *Integr. Environ. Assess. Manag.* **2011**, *7* (4), 513–541.
- (5) Wang, Z.; Cousins, I. T.; Scheringer, M.; Buck, R. C.; Hungerbühler, K. Global emission inventories for C4-C14 perfluoroalkyl carboxylic acid (PFCA) homologues from 1951 to 2030, Part I: Production and emissions from quantifiable sources. *Environ. Int.* **2014**, *70*, 62–75.
- (6) Wang, Z.; Boucher, J. M.; Scheringer, M.; Cousins, I. T.; Hungerbühler, K. Toward a Comprehensive Global Emission Inventory of C4-C10

- Perfluoroalkanesulfonic Acids (PFSA) and Related Precursors: Focus on the Life Cycle of C8-Based Products and Ongoing Industrial Transition. *Environ. Sci. Technol.* **2017**, *51* (8), 4482–4493.
- (7) USEPA. 2010/15 PFOA Stewardship Program <https://www.epa.gov/assessing-and-managing-chemicals-under-tsca> (accessed May 1, 2017).
- (8) Gordon, S. C. Toxicological evaluation of ammonium 4,8-dioxa-3H-perfluorononanoate, a new emulsifier to replace ammonium perfluorooctanoate in fluoropolymer manufacturing. *Regul. Toxicol. Pharmacol.* **2011**, *59* (1), 64–80.
- (9) ECHA. *Committee for Risk Assessment (RAC) Committee for Socio-economic Analysis (SEAC) Background document*; 2018; Vol. 1.
- (10) Liu, Y.; Ruan, T.; Lin, Y.; Liu, A.; Yu, M.; Liu, R.; Meng, M.; Wang, Y.; Liu, J.; Jiang, G. Chlorinated Polyfluoroalkyl Ether Sulfonic Acids in Marine Organisms from Bohai Sea, China: Occurrence, Temporal Variations, and Trophic Transfer Behavior. *Environ. Sci. Technol.* **2017**, *51* (8), 4407–4414.
- (11) Wang, S.; Huang, J.; Yang, Y.; Hui, Y.; Ge, Y.; Larssen, T.; Yu, G.; Deng, S.; Wang, B.; Harman, C. First report of a Chinese PFOS alternative overlooked for 30 years: Its toxicity, persistence, and presence in the environment. *Environ. Sci. Technol.* **2013**, *47* (18), 10163–10170.
- (12) Shi, Y.; Vestergren, R.; Zhou, Z.; Song, X.; Xu, L.; Liang, Y.; Cai, Y. Tissue distribution and whole body burden of the chlorinated polyfluoroalkyl ether sulfonic acid F-53B in crucian carp (*Carassius carassius*): evidence for a highly bioaccumulative contaminant of emerging concern. *Environ. Sci. Technol.* **2015**, *49* (24), 14156–14165.

- (13) MacInnis, J. J.; French, K.; Muir, D. C. .; Spencer, C.; Criscitiello, A.; De Silva, A. O.; Young, C. J. Emerging investigator series: a 14-year depositional ice record of perfluoroalkyl substances in the High Arctic. *Environ. Sci. Process. Impacts* **2017**, *19* (1), 22–30.
- (14) Stock, N. L.; Furdui, V. I.; Muir, D. C. G.; Mabury, S. A. Perfluoroalkyl contaminants in the Canadian Arctic: Evidence of atmospheric transport and local contamination. *Environ. Sci. Technol.* **2007**, *41*, 3529–3536.
- (15) Yeung, L. W. Y.; Dassuncao, C.; Mabury, S.; Sunderland, E. M.; Zhang, X.; Lohmann, R. Vertical Profiles, Sources, and Transport of PFASs in the Arctic Ocean. *Environ. Sci. Technol.* **2017**, *51* (12), 6735–6744.
- (16) Ellis, D. A.; Martin, J. W.; Mabury, S. A.; Hurley, M. D.; Sulbaek Andersen, M. P.; Wallington, T. J. Atmospheric lifetime of fluorotelomer alcohols. *Environ. Sci. Technol.* **2003**, *37* (17), 3816–3820.
- (17) Young, C. J.; Furdui, V. I.; Franklin, J.; Koerner, R. M.; Muir, D. C. G.; Mabury, S. A. Perfluorinated acids in Arctic snow: New evidence for atmospheric formation. *Environ. Sci. Technol.* **2007**, *41*, 3455–3461.
- (18) Pickard, H. M.; Criscitiello, A. S.; Spencer, C.; Sharp, M. J.; Muir, D. C. G.; Silva, A. O. De; Young, C. J. Continuous Non-Marine Inputs of Per- and Polyfluoroalkyl Substances to the High Arctic : A Multi-Decadal Temporal Record. *Atmos. Chem. Phys. Discuss.* **2018**, *18* (7), 5045–5058.
- (19) Rigét, F.; Bossi, R.; Sonne, C.; Vorkamp, K.; Dietz, R. Trends of perfluorochemicals in Greenland ringed seals and polar bears: Indications of shifts to decreasing trends. *Chemosphere* **2013**, *93* (8), 1607–1614.

- (20) Smithwick, M.; Norstrom, R. J.; Mabury, S. A.; Solomon, K.; Evans, T. J.; Stirling, I.; Taylor, M. K.; Muir, D. C. G. Temporal trends of perfluoroalkyl contaminants in polar bears (*Ursus maritimus*) from two locations in the North American Arctic, 1972-2002. *Environ. Sci. Technol.* **2006**, *40* (4), 1139–1143.
- (21) Rotander, A.; Kärman, A.; Bavel, B. van; Polder, A.; Rigét, F.; Audunsson, G. A.; Víkingsson, G.; Gabrielsen, G. W.; Bloch, D.; Dam, M. Increasing levels of long-chain perfluorocarboxylic acids (PFCAs) in Arctic and North Atlantic marine mammals, 1984-2009. *Chemosphere* **2012**, *86* (3), 278–285.
- (22) Wong, F.; Shoeib, M.; Katsoyiannis, A.; Eckhardt, S.; Stohl, A.; Bohlin-Nizzetto, P.; Li, H.; Fellin, P.; Su, Y.; Hung, H. Assessing temporal trends and source regions of per- and polyfluoroalkyl substances (PFASs) in air under the Arctic Monitoring and Assessment Programme (AMAP). *Atmos. Environ.* **2018**, *172*, 65–73.
- (23) Reiner, J. L.; O’Connell, S. G.; Moors, A. J.; Kucklick, J. R.; Becker, P. R.; Keller, J. M. Spatial and temporal trends of perfluorinated compounds in beluga whales (*Delphinapterus leucas*) from Alaska. *Environ. Sci. Technol.* **2011**, *45* (19), 8129–8136.
- (24) Braune, B. M.; Letcher, R. J. Perfluorinated sulfonate and carboxylate compounds in eggs of seabirds breeding in the Canadian Arctic: Temporal trends (1975-2011) and interspecies comparison. *Environ. Sci. Technol.* **2013**, *47* (1), 616–624.
- (25) Dassuncao, C.; Hu, X. C.; Zhang, X.; Bossi, R.; Dam, M.; Mikkelsen, B.; Sunderland, E. M. Temporal Shifts in Poly- and Perfluoroalkyl Substances (PFASs) in North Atlantic Pilot Whales Indicate Large Contribution of

- Atmospheric Precursors. *Environ. Sci. Technol.* **2017**, *51* (8), 4512–4521.
- (26) Zushi, Y.; Tamada, M.; Kanai, Y.; Masunaga, S. Time trends of perfluorinated compounds from the sediment core of Tokyo Bay, Japan (1950s-2004). *Environ. Pollut.* **2010**, *158* (3), 756–763.
- (27) Ahrens, L.; Yamashita, N.; Yeung, L. W. Y.; Taniyasu, S.; Horii, Y.; Lam, P. K. S.; Ebinghaus, R. Partitioning behavior of per- and polyfluoroalkyl compounds between pore water and sediment in two sediment cores from Tokyo Bay, Japan. *Environ. Sci. Technol.* **2009**, *43* (18), 6969–6975.
- (28) Benskin, J. P.; Phillips, V.; St. Louis, V. L.; Martin, J. W. Source elucidation of perfluorinated carboxylic acids in remote alpine lake sediment cores. *Environ. Sci. Technol.* **2011**, *45* (17), 7188–7194.
- (29) Lehnerr, I.; St. Louis, V. L.; Sharp, M.; Gardner, A.; Smol, J.; Schiff, S.; Muir, D.; Mortimer, C.; Michelutti, N.; Tarnocai, C.; St. Pierre, K.; Emmerton, C.; Wiklund, J.; Köck, G.; Lamoureux, S.; Talbot, C. The world's largest High Arctic lake responds rapidly to climate warming. *Nat. Commun.* **2018**, *9*, 1–9.
- (30) Thompson, W. Climate. In *Resource description and analysis: Ellesmere Island, National Park Reserve*; Parks Canada: National Resource Conservation Section, Prairie and Northern Region: Winnipeg, Canada, 1994; p 78.
- (31) Environment and Climate Change Canada. Climate Normals 1981-2010 Baker Lake
http://climate.weather.gc.ca/climate_normals/results_1981_2010_e.html?stnID=1709&lang=e&StationName=Baker+Lake&SearchType=Contains&stnNameSubmit=go&dCode=1&dispBack=1 (accessed Mar 6, 2018).

- (32) Weber, A. K.; Barber, L. B.; Leblanc, D. R.; Sunderland, E. M.; Vecitis, C. D. Geochemical and Hydrologic Factors Controlling Subsurface Transport of Poly- and Perfluoroalkyl Substances, Cape Cod, Massachusetts. *Environ. Sci. Technol.* **2017**, *51* (8), 4269–4279.
- (33) Appleby, P. G.; Oldfield, F. The calculation of lead-210 dates assuming a constant rate of supply of unsupported Pb-210 in the sediment. *Catena* **1978**, *5* (1), 1–8.
- (34) Appleby, P. G. *Dating recent sediment by 210Pb: problems and solutions*; 1998.
- (35) Yeung, L. W. Y.; De Silva, A. O.; Loi, E. I. H.; Marvin, C. H.; Taniyasu, S.; Yamashita, N.; Mabury, S. A.; Muir, D. C. G.; Lam, P. K. S. Perfluoroalkyl substances and extractable organic fluorine in surface sediments and cores from Lake Ontario. *Environ. Int.* **2013**, *59* (2013), 389–397.
- (36) Lockhart, W. L.; Wilkinson, P.; Billeck, B. N.; Danell, R. A.; Hunt, R. V.; Brunskill, G. J.; Delaronde, J.; St. Louis, V. Fluxes of mercury to lake sediments in central and northern Canada inferred from dated sediment cores. *Biogeochemistry* **1998**, *40* (2), 163–173.
- (37) D’Agostino, L. A.; Mabury, S. A. Certain Perfluoroalkyl and Polyfluoroalkyl Substances Associated with Aqueous Film Forming Foam Are Widespread in Canadian Surface Waters. *Environ. Sci. Technol.* **2017**, *51* (23), 13603–13613.
- (38) Backe, W. J.; Day, T. C.; Field, J. A. Zwitterionic, cationic, and anionic fluorinated chemicals in aqueous film forming foam formulations and groundwater from U.S. military bases by nonaqueous large-volume injection HPLC-MS/MS. *Environ. Sci. Technol.* **2013**, *47* (10), 5226–5234.
- (39) Zhu, Z.; Wang, T.; Wang, P.; Lu, Y.; Giesy, J. P. Perfluoroalkyl and

- polyfluoroalkyl substances in sediments from South Bohai coastal watersheds, China. *Mar. Pollut. Bull.* **2014**, *85* (2), 619–627.
- (40) Boucher, J. M.; Cousins, I. T.; Scheringer, M.; Hungerbühler, K.; Wang, Z. Toward a Comprehensive Global Emission Inventory of C4 –C10 Perfluoroalkanesulfonic Acids (PFASs) and Related Precursors: Focus on the Life Cycle of C6- and C10-Based Products. *Environ. Sci. Technol. Lett.* **2019**, *6* (1), 1-7.
- (41) Kwok, K. Y.; Yamazaki, E.; Yamashita, N.; Taniyasu, S.; Murphy, M. B.; Horii, Y.; Petrick, G.; Kallerborn, R.; Kannan, K.; Murano, K.; Lam, P.K.S. Transport of Perfluoroalkyl substances (PFAS) from an arctic glacier to downstream locations: Implications for sources. *Sci. Total Environ.* **2013**, *447*, 46–55.
- (42) Kirchgeorg, T.; Dreyer, A.; Gabrieli, J.; Kehrwald, N.; Sigl, M.; Schwikowski, M.; Boutron, C.; Gambaro, A.; Barbante, C.; Ebinghaus, R. Temporal variations of perfluoroalkyl substances and polybrominated diphenyl ethers in alpine snow. *Environ. Pollut.* **2013**, *178*, 367–374.
- (43) Ruan, T.; Wang, Y.; Wang, T.; Zhang, Q.; Ding, L.; Liu, J.; Wang, C.; Qu, G.; Jiang, G. Presence and partitioning behavior of polyfluorinated iodine alkanes in environmental matrices around a fluorochemical manufacturing plant: Another possible source for perfluorinated carboxylic acids? *Environ. Sci. Technol.* **2010**, *44* (15), 5755–5761.
- (44) Gebbink, W. A.; Bossi, R.; Rigét, F. F.; Rosing-Asvid, A.; Sonne, C.; Dietz, R. Observation of emerging per- and polyfluoroalkyl substances (PFASs) in Greenland marine mammals. *Chemosphere* **2016**, *144*, 2384–2391.

- (45) Pan, Y.; Zhang, H.; Cui, Q.; Sheng, N.; Yeung, L. W. Y.; Sun, Y.; Guo, Y.; Dai, J. Worldwide Distribution of Novel Perfluoroether Carboxylic and Sulfonic Acids in Surface Water. *Environ. Sci. Technol.* **2018**, *52* (14), 7621–7629.

4 Fate and Transport of Perfluoroalkyl Substances from Snowpacks into a Lake in the High Arctic of Canada

4.1 Abstract

The delivery of perfluoroalkyl substances (PFAS) from snowpacks into Lake Hazen, located on Ellesmere Island (Nunavut, Canada, 82° N) indicates that annual atmospheric deposition is a major source of PFAS that undergoes complex cycling in the High Arctic. Perfluoroalkyl carboxylic acids (PFCA) in snowpacks display even-odd concentration ratios characteristic of long-range atmospheric transport and oxidation of volatile precursors. Major ion analysis in snowpacks suggests that sea spray, mineral dust, and combustion aerosol are all relevant to the fate of PFAS in the Lake Hazen watershed. Distinct drifts of light and dark snow (enriched with light absorbing particles, LAP) facilitate the study of particle loads on the fate of PFAS in the snowpack. Total PFAS (Σ PFAS, ng m^{-2}) loads are lower in snowpacks enriched with LAP and are attributed to reductions in snowpack albedo combined with enhanced post-depositional melting. Elevated concentrations of PFCA are observed in the top 5 m of the water column during snowmelt periods compared to ice-covered or ice-free periods. PFAS concentrations in deep waters of the Lake Hazen water column are consistent between snowmelt, ice-free, and ice-covered periods, which is ascribed to the delivery of dense and turbid glacier meltwaters mixing PFAS throughout the Lake Hazen water column. These observations highlight the underlying mechanisms in PFAS cycling in High Arctic lakes, particularly in the context of increased particle loads and melting.

4.2 Introduction

Perfluoroalkyl substances (PFAS) are environmentally ubiquitous chemicals that were manufactured since the 1950s.¹ PFAS are incorporated into coating layers of many commercial products such as textiles, furniture, and food-contact paper to impart oil, water, and stain repellency.² Due to concerns over environmental persistence and bioaccumulation, long-chain perfluoroalkyl acids (i.e. >C₆, PFAA), including perfluoroalkyl carboxylic acids (PFCA) and perfluoroalkyl sulfonic acids (PFSA), are regulated in Canada and many other countries.³⁻⁵

The discovery of PFAS in the High Arctic provides evidence of their long-range transport ability.^{1,6-10} It is hypothesized, for example, that indirect sources of PFAS to the High Arctic include the long-range atmospheric transport of volatile precursors such as fluorotelomer alcohols (FTOH) and perfluoroalkane sulfonamido substances,^{7,8} all of which undergo atmospheric oxidation in regions with low NO_x: HO₂ ratios such as the Arctic. Direct sources of PFAS to the High Arctic include the long-range atmospheric transport of PFAS on particles.¹⁰⁻¹²

The measurement of PFAS in snow can provide insights into long-range atmospheric transport in the High Arctic of Canada.⁶⁻⁹ In a recent study, PFAS are reported in a snow core from the summit of the Devon Ice Cap that encapsulate the period 1977-2015.⁸ The continuous annual accumulation of PFAS on the Devon Ice Cap is attributed to the long-range atmospheric transport and oxidation of volatile precursors such as FTOH, consistent with results from a 2006-2014 air monitoring campaign at Alert (Nunavut, Canada, 82° N). This demonstrates the continuous annual delivery of volatile

precursors and particle-bound PFAA to the High Arctic of Canada.¹⁰ The accumulation of atmospherically-supplied PFAS in snow is also observed on the Melville, Agassiz, and Meighen Ice Caps (Nunavut, Canada, 75-80° N) in 2005-2006,⁶ demonstrating that snow is a repository for PFAS in the High Arctic of Canada.

Indeed, snowmelt is a source of PFAS to freshwater ecosystems.¹³⁻¹⁵ For example, in the Krycklan watershed (northern Sweden, 64° N), 0.11-0.48 ng L⁻¹ perfluorohexanoic acid (PFHxA), 0.20-0.68 ng L⁻¹ perfluoroheptanoic acid (PFHpA), 0.12-0.81 ng L⁻¹ perfluorooctanoic acid (PFOA), 0.09-0.79 ng L⁻¹ perfluorononanoic acid (PFNA) and 0.03-0.45 ng L⁻¹ perfluorodecanoic acid (PFDA) are measured in snowmelt.¹³ Similar observations are reported in an urban watershed in Highland Creek (Ontario, Canada, 44° N) where approximately one-fifth of the increasing riverine flux of PFAS in early spring is attributed to snowmelt.¹⁴ More recently, Skaar et al. report high total concentrations of PFAS (Σ PFAS, mean 1.4 ng L⁻¹, 0.1-4.1 ng L⁻¹) in glacial- and snowmelt-impacted surface waters from Lake Linnévatnet (Svalbard, Norway, 78° N) in 2014 and 2015, dominated by PFBA (mean 0.6 ng L⁻¹, <0.08-1.4 ng L⁻¹) and PFOA (mean 0.3 ng L⁻¹, <0.06-1.8 ng L⁻¹).¹⁶ These observations highlight the importance of snowmelt as a vector for PFAS into freshwater ecosystems.

The study of PFAS in lakes from the High Arctic of Canada is used to compare long-range transport mechanisms to local contamination from human activity.^{11,15,17} For example, low concentrations of PFAS in water from landlocked lakes on Cornwallis Island (Nunavut, Canada, 74° N) such as Lake Amituk (10 ± 2 ng L⁻¹) and Char Lake (16 ± 4 ng L⁻¹) in 2003 and 2005 is postulated to demonstrate long-range atmospheric transport and deposition.¹¹ Local sources of PFAS may also be present such as higher

PFAS concentrations in Resolute Lake linked to aqueous film forming foam (AFFF) use at an active airport.¹¹ For example, perfluorohexane sulfonic acid (PFHxS), PFOS, PFHpA, and PFOA in Resolute Lake are 127, 28, 32, and 4 times greater than in Amituk and Char Lakes. More recently, Lescord et al. also find that Σ PFAS concentrations are higher in Arctic lakes such as Meretta ($153 \pm 14 \text{ ng L}^{-1}$) and Resolute ($112 \pm 20 \text{ ng L}^{-1}$), relative to Char ($1.9 \pm 0.48 \text{ ng L}^{-1}$), Small ($2.4 \pm 0.40 \text{ ng L}^{-1}$), North ($1.9 \pm 0.81 \text{ ng L}^{-1}$), and 9 Mile ($1.9 \pm 0.42 \text{ ng L}^{-1}$) lakes during 2010-2011.¹⁷ In Lake A, a meromictic lake on northern Ellesmere Island (Nunavut, Canada, 83° N) $\sim 1000 \text{ km}$ north of Cornwallis Island, Σ PFAS concentrations in May and August 2008 ($0.025\text{-}0.45 \text{ ng L}^{-1}$) are lower than those in Amituk and Char lakes in 2003 and 2005, possibly due to the large distance from source regions, smaller catchment area, and its perennial lake ice cover.¹⁵

The objective of this study is to determine PFAS in High Arctic snow, combined with that of lake waters and hydrology, to discern the sources and transport of PFAS to remote freshwater ecosystems. In this study, PFAS are quantified in snow and water samples collected in the Lake Hazen watershed on northern Ellesmere Island (Nunavut, Canada, 82° N) to elucidate the composition, sources, and seasonal depositional trends relevant to the long-range transport and fate of PFAS. We quantify concentrations and loads of PFAS in snowpack samples with different enrichments of light-absorbing particles (LAP), as well as concentrations of PFAS throughout the water column of Lake Hazen, the largest lake by volume north of the Arctic Circle, during the spring and summer to assess the impact of seasonal melting on the transport and fate of PFAS in this High Arctic freshwater ecosystem.

4.3 Methods

4.3.1 Study Area

Lake Hazen (81° 49' N, 70° 42' W) is located in Quttinirpaaq National Park on Ellesmere Island, Nunavut, Canada. Lake Hazen is the world's largest lake by volume (51.4 km³) entirely above the Arctic Circle, with a surface area of 544 km² and maximum depth of 267 m (Figure 4.1). The Lake Hazen region is a polar semi-desert, receiving only 95 mm of precipitation per year.¹⁸ Approximately 41% of the 7156 km² watershed is covered by the Northern Ellesmere Icefield and its outlet glaciers, which flow downstream up to 42 km before draining into Lake Hazen.¹⁹ It is estimated that Lake Hazen receives 1.09 km³ of hydrological inputs, of which approximately 0.120 km³ is derived from snowmelt and 0.979 km³ from melting glaciers.¹⁹ The Henrietta Nesmith, Very, and Gilman glacier-fed rivers collectively account for ~70% of glacier meltwater inputs into Lake Hazen, with maximum discharges ranging from 122-377 m³ s⁻¹.¹⁹ Lake Hazen is drained by the Ruggles River into Chandler Fiord.²⁰ Lake Hazen is supplied by snowmelt runoff from late-May to early-June, and by permafrost thaw and glacier melt runoff from mid-June to late-August. The surface of Lake Hazen is ice-covered for 9-10 months per year beginning in September when glacier meltwater discharge ceases.¹⁹ An overview of the hydrological cycle in the Lake Hazen watershed is provided in Appendix C (Table C1). The lake ice surface acts as a temporary repository for snow and atmospheric pollution. Under the ice, Lake Hazen has reverse temperature stratification, with oxygen depletion at its deepest point (267 m), but following ice melt, Lake Hazen is un-stratified, with mixing facilitated by the delivery of dense and turbid glacial

meltwater.²¹ Further details of the study area are presented in a detailed mercury (Hg) mass balance analysis in Lake Hazen by St. Pierre et al.¹⁹

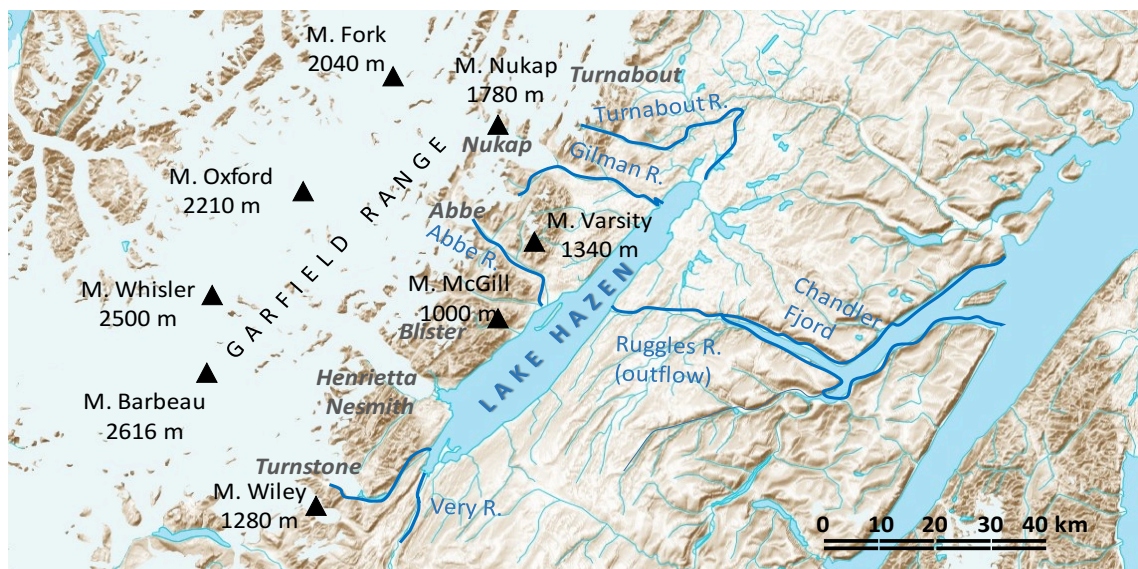


Figure 4.1 Map of Lake Hazen and surrounding area in Quttinirpaaq National Park, Ellesmere Island, Canada. Triangles indicate peaks and corresponding elevations, labels in grey italics correspond to glaciers and in blue are major rivers. Map adapted from Toporama (<https://atlas.gc.ca/toporama/en/index.html>). Toporama is a public on-line mapping service developed by Natural Resources Canada and is licensed under the Open Government Licence of Canada.

4.3.2 Sampling

In May 2013, integrated snowpack samples (i.e., 3 snow cores per site) were collected from the ice-covered Lake Hazen surface (n=6 sites) and on the surrounding landscape (n=2 sites) using a stainless-steel corer (4.3 cm inner diameter, I.D.). Integrated snowpack samples were stored in high-density polyethylene containers and kept frozen until analysis. Additional snowpack samples were collected into Ziploc plastic freezer bags for water chemistry analyses. The winter was exceptionally dry in 2013-2014 resulting in little snow accumulation on the landscape and facilitated dust transport creating distinct drifts of light and dark (i.e., highly enriched with LAP) snow that were sampled in June 2014 along the ice surface of Lake Hazen (Figure C1).¹⁹ This presented a unique opportunity to investigate PFAS inputs from LAP through sampling and analysis of the dark snow (designated as “dark snowpacks”) compared to light snow (designated as “light snowpacks”).¹⁹ Integrated light snowpacks (n=9 sites) were collected along the surface of Lake Hazen using the stainless steel corer, while integrated dark snowpacks (n=9 sites) were collected using a cleaned stainless steel spatula with a known surface area due to limited snowpack depth.

The water column of Lake Hazen was sampled using a pre-cleaned 10 or 12 L General Oceanics Niskin PTFE-free water sampler during ice-covered periods on 15-18 May 2013 (2-250 m) and 19-22 May 2014 (3-250 m), during snowmelt on lake ice on 2-4 June 2012 (0.5, 20, 80, 200, 258 m) and 29-30 May 2014 (0-225 m), as well as during an ice-free open water period on 27-29 July 2015 (0-250 m). Water samples were then transferred into 1 L pre-cleaned polypropylene containers. A list of sampling periods is presented in the Appendix C (Table C2).

4.3.3 Sample Extraction

PFAS were extracted from snow (melted overnight at room temperature in the lab) and water samples using previously outlined methods.^{7,8} Briefly, 500 mL sub-samples were equilibrated to room temperature before the addition of 30 μ L of an internal standard mixture (Table C3). All samples were concentrated and extracted using Oasis® weak anion exchange solid phase extraction (WAX SPE, cartridge: 6 cm³, 150 mg, 30 μ m). In the first fraction, perfluorooctane sulfonamide (FOSA) was eluted using 6 mL of methanol (MeOH), while PFAA were eluted in the second fraction using 8 mL of 0.1% ammonia in MeOH. Samples were evaporated to dryness using nitrogen and reconstituted in 0.25 mL SPE-polished water (i.e. HPLC Grade water cleaned by Oasis® WAX SPE) and 0.25 mL MeOH. A second suite of isotopically labeled standards was added before analysis to monitor matrix effects (Table C3). An overview of chemicals and QA/QC can be found in Appendix C (Sections C1 and C2, Tables C4 and C5). As with all PFAS analysis, efforts were taken to avoid the use of glass due to sorption of PFCA and PFSA to glass from aqueous solution. Thus sampling, standards preparation, sample preparation, and extraction used high density polypropylene and polyethylene vessels and equipment. Further, care was taken to eliminate fluoropolymers such as polytetrafluoroethylene (PTFE), during sampling and the liquid chromatograph was adapted to replace standard PTFE parts with non-fluoropolymer components supplied by the vendor.

4.3.4 Instrumental Analysis

Extracted samples were analyzed on an Acquity UPLC I class liquid chromatograph coupled to a XEVO TQ-S tandem mass spectrometer operated in electrospray negative ionization mode (Waters Corporation, Massachusetts, USA).^{7,8} PFAS congeners were separated on an Acquity UPLC® BEH C18 (2.1 x 100 mm, 1.7 µm) stationary phase (Waters Corporation, Massachusetts, USA) using a water-MeOH 0.1 mM ammonium acetate gradient. Details of the UPLC-MS/MS method can be found in Appendix C (Tables C6-C8). Major ions were analyzed on a Dionex DX-600 Ion Chromatograph, following US EPA Method 300.1 at the accredited Biogeochemical Analytical Service Laboratory (BASL) at the University of Alberta. Particulate carbon (PC) and nitrogen (PN) were analyzed using a CE-440 Elemental Analyzer (Exeter Analytical Inc.), following a modified version of EPA Method 440.0 at the BASL. Major ion, PC, and PN analyses were limited to 2014 snowpack samples.

4.3.5 Data Treatment

All PFAS concentrations are blank-corrected (Table C4). The LOD and LOQ correspond to concentrations yielding a signal-to-noise ratio of 3 and 10, respectively (Table C4).⁷ A natural log transformation is applied prior to statistical analysis using StatPlus:mac (V6), with a critical p-value set to 5%. Spearman rank correlation (r_s) analysis is limited to PFAS concentrations equal to or greater than the LOQ for congeners with detection frequencies equal to or greater than 50%. Areal water volume (AWV, L m⁻²) is calculated for snowpacks using the average weight of three snowpack cores at each

site (kg, where 1 kg melted snow =1 L water) and dividing by the coring area (m²). Total PFAS snowpack loads (Σ PFAS, ng m⁻²) are calculated by multiplying site-specific AWV by PFAS concentrations (ng L⁻¹). Kruskal-Wallis and *post-hoc* Mann-Whitney U tests are used to evaluate differences between Σ PFAS loads (95% confidence interval) in light and dark snowpacks. Concentrations, AWV, and snowpack depth in the next section are presented as 95% confidence interval mean \pm standard error (SE) unless otherwise noted.

4.4 Results and Discussion

4.4.1 Concentrations and Loads of PFAS in Snowpacks

A comparison of PFAS concentrations in snowpacks from the Lake Hazen watershed between 2013 and 2014 is presented in Table 4.1. C₄-C₁₂ PFCA and PFOS are found in all snowpacks (Table C9). PFBA is the dominant PFCA, with concentrations ranging from 1.2-52 ng L⁻¹ in 2013 and 1.8-3.8 ng L⁻¹ in 2014 in light snowpacks, and 2.3-11 ng L⁻¹ in dark snowpacks in 2014. PFSA concentrations are generally an order of magnitude less than PFCA concentrations, with PFOS being the dominant PFSA. PFOS concentrations range from 0.0090-1.0 ng L⁻¹ and 0.0090-0.051 ng L⁻¹ in light snowpacks in 2013 and 2014, respectively, and 0.035-0.44 ng L⁻¹ in dark snowpacks in 2014.

Table 4.1 Concentrations of PFAS (ng L⁻¹) in light and dark snowpacks collected from the Lake Hazen region during 2013 and 2014 (this study) and literature survey of other locations. Compounds not measured are designated as N.M.

Site	Lake Hazen Light Snowpacks	Lake Hazen Light Snowpacks	Lake Hazen Dark Snowpacks	Krycklan Surface Snow	Arctic Sea Ice Surface Snow	Longyearbyen Surface Snow
Reference	This Study	This Study	This Study	Codling et al. ⁴⁹	Yeung et al. ⁹	Kwok et al. ²⁷
Year	2013	2014	2014	2009	2012	2006
Latitude	81°N	81°N	81°N	64°N	81 - 88°N	78°N
Location	Nunavut	Nunavut	Nunavut	Northern Sweden	Arctic Ocean	Norway
PFBA	8.9 (1.2-52)	2.7 (1.8-3.8)	4.8 (2.3-11)	(0.017-0.823)	N.M	0.1085
PFPeA	0.35 (0.097-1.6)	0.14 (0.083-0.21)	0.67 (0.18-1.5)	(<LOD-0.589)	N.M	0.0302
PFHxA	0.40 (0.12-1.3)	0.25 (0.16-0.38)	0.89 (0.36-1.6)	(0.0175-0.154)	0.060 (0.026-0.109)	0.0758
PFHpA	1.1 (0.38-4.3)	0.45 (0.29-0.70)	1.5 (0.54-2.9)	(<LOD-0.0422)	0.029 (0.014-0.049)	0.0171
PFOA	2.2 (0.35-10)	0.71 (0.46-1.1)	2.2 (0.92-4.9)	(<LOD-0.122)	0.15 (0.072-0.294)	0.1125
PFNA	1.2 (0.39-3.1)	0.59 (0.37-0.94)	2.3 (0.76-5.3)	(0.0054-0.252)	0.12 (0.033-0.253)	0.0505
PFDA	0.21 (0.082-0.56)	0.14 (0.086-0.24)	0.68 (0.16-1.7)	(0.0037-0.149)	0.075 (0.033-0.142)	0.0218
PFUnDA	0.087 (0.048-0.17)	0.10 (0.052-0.17)	0.37 (0.088-0.80)	(0.0021-0.266)	0.053 (0.021-0.092)	<LOQ
PFDoDA	0.022 (0.012-0.051)	0.046 (0.0097-0.12)	0.14 (0.020-0.31)	(<LOD-0.0852)	(<LOD-0.088)	0.00669
PFTTrDA	<0.0020	0.0070 (<0.0020-0.010)	0.035 (<0.0020-0.10)	(<LOD-0.040)	N.M	N.M
PFTeDA	0.011 (<0.0030-0.023)	(<0.0030-0.0065)	0.014 (<0.0030-0.019)	(<LOD-0.0167)	N.M	<LOQ
PFBS	(<0.0020-0.40)	0.0058 (<0.0020-0.011)	0.013 (<0.0030-0.024)	(<LOD-2.163)	<LOD	N.M
PFHxS	(0.00070-0.44)	<0.00070	(<0.00070-0.0043)	(<LOD-0.651)	(<LOD-0.018)	<LOQ
PFOS	0.19 (0.0090-1.0)	0.029 (0.0090-0.051)	0.18 (0.035-0.44)	(0.0026-0.253)	0.14 (0.034-0.343)	0.0339
PFECHS	0.031 (<0.0010-0.059)	0.0083 (<0.0010-0.022)	0.0066 (<0.0010-0.0088)	N.M	N.M	N.M

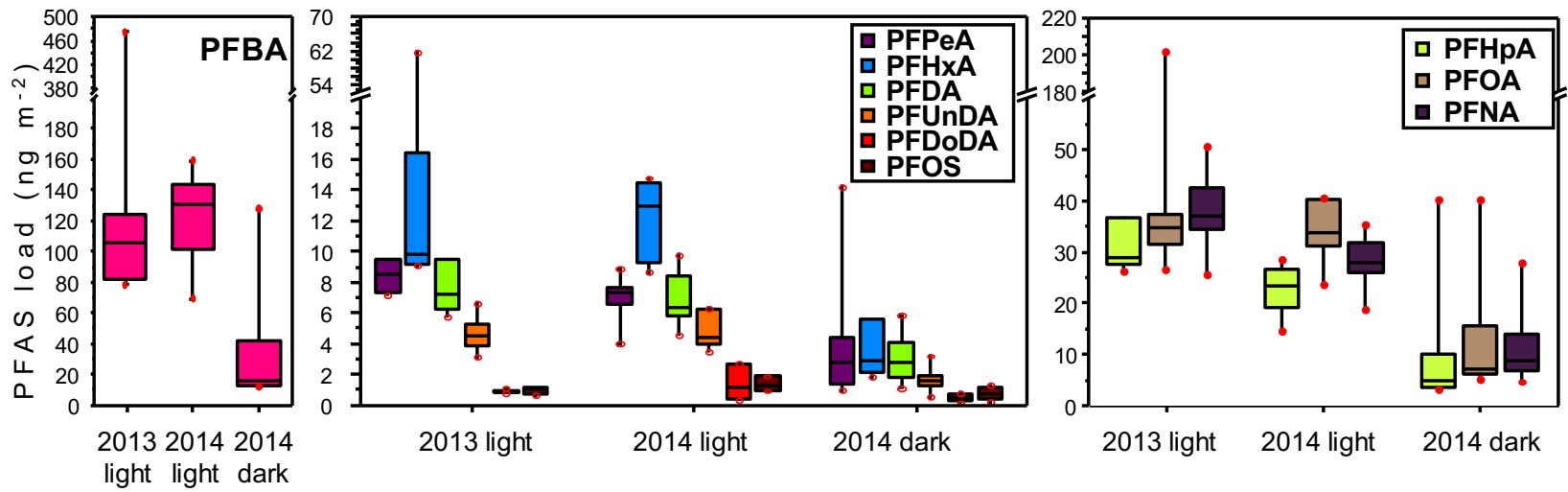


Figure 4.2 PFAS loads in snowpacks collected in 2013 (n=6 sites) and in paired light and dark snowpacks in 2014 (n=8 sites) from the ice surface of Lake Hazen. Box is 25-75% range, line is the median and whiskers are the 95% confidence interval.

PFAS loads are comparable in light snowpacks in 2013 (Σ PFAS $290 \pm 44 \text{ ng m}^{-2}$) and 2014 (Σ PFAS $203 \pm 24 \text{ ng m}^{-2}$, Mann-Whitney U test, $p=0.92$), suggesting similar air mass pollution during this period. However, PFAS loads are significantly lower in dark snowpacks (Σ PFAS $77 \pm 29 \text{ ng m}^{-2}$, Mann-Whitney U test, $p<0.03$, Figure 4.2).

To understand the lower PFAS loads in the dark snowpacks, the influence of LAP on the snowpack must be considered. Deposition of LAP on a snowpack (i.e., dirty snow) reduces snowpack albedo, enhances the absorption of solar radiation, and accelerates snowpack melting.^{22,23} During snowpack melting, LAP, such as black carbon (BC) and mineral dust, are retained on the snowpack surface.^{22,24} In effect, this can initiate a positive feedback melting cycle where LAP are enriched at the snowpack surface, thereby enhancing the absorption of solar radiation and snowpack melting.²² LAP can also be enriched on a snowpack via sublimation.²⁵

The structural features of light and dark snowpacks are different in the Lake Hazen region. The AWW for dark snowpacks is $14 \pm 6 \text{ L m}^{-2}$, approximately three times lower than paired light snowpacks with AWW of $49 \pm 3 \text{ L m}^{-2}$. Similarly, the depth of dark snowpacks is shallower, $6.0 \pm 1.4 \text{ cm}$, compared to the depth of the light snowpacks, $15.2 \pm 0.6 \text{ cm}$. For comparison, the AWW is $63 \pm 3 \text{ L m}^{-2}$ and the depth is $30 \pm 1 \text{ cm}$ in 2013 light snowpacks. The lower AWW and depth in dark snowpacks compared to light snowpacks from the same region further supports that LAP in dark snowpacks are vectors for enhanced snowpack melting. We attribute the lower PFAS loads in dark snowpacks to the influence of LAP through post-depositional snowpack melting, whereby PFAS are lost from the snowpack (i.e., as percolation or sequestered into lake ice) during the accelerated melting. Alternatively, it is possible that the retention of PFAS in dark

snowpacks is due to concentration effects occurring during sublimation of the snowpacks, such that as the snow sublimates, PFAS and LAP residues are retained. Skaar et al. note that post-depositional snowpack melting contributes to the retention of PFOS and PFOA and the depletion of PFBA in aged snowpacks from the Lake Linnévatnet catchment in 2015.¹⁶ Our observations demonstrate that snowpack albedo interactions are relevant to the fate of PFAS in the Lake Hazen region.

4.4.2 Indirect Sources of PFAS in Snowpacks

Correlation analysis of natural log-transformed PFAS concentrations in light and dark snowpacks from the Lake Hazen region in 2013 and 2014 is used here to elucidate common emission sources and environmental dynamics (Tables C10-C12). In this context, environmental dynamics refer to PFAS having commonality in (1) transport and formation (e.g., are transported and formed via long-range transport and atmospheric oxidation of volatile precursors), (2) removal from the atmosphere (e.g., scavenged by particles or snow), and/or (3) post-depositional effects (e.g., preferential elution during snowmelt). In general, most PFAS positively correlate with each other in snowpacks (Tables C10-C12). Strong positive correlations are observed for PFHxA-PFHpA ($r_s \geq 0.89$, $p < 0.01$), PFOA-PFNA ($r_s \geq 0.81$, $p \leq 0.01$), and PFDA-PFUnDA ($r_s \geq 0.95$, $p < 0.01$) in all snowpacks (Tables C10-C12). Interestingly, most PFCA congeners (i.e., PFHpA through PFUnDA) positively correlate with PFOS ($R_s \geq 0.69$, $p \leq 0.04$) in snowpacks. Taken together, correlation analysis of PFAS concentrations in snowpacks from the Lake Hazen region in 2013 and 2014 suggests most PFAS undergo similar environmental dynamics

and/or derive from common sources. This is generally consistent with observations from snow collected on Livingston Island (maritime Antarctica), where PFOA concentrations are positively correlated with PFHxA, PFHpA, and PFNA-PFTrDA concentrations²⁶ and on Svalbard, Norway where PFOA concentrations in snow are positively correlated with PFBA, PFPeA, PFHpA, PFNA, PFDA, and PFDoDA.²⁷ Similar observations are also reported in snow from the Antarctic Fildes Peninsula, whereby PFHxA-PFOA and PFPeA-PFOA concentrations are positively correlated.²⁸

It is possible to estimate contributions from indirect sources on the occurrence of PFCA in snowpacks from the Lake Hazen region using knowledge of volatile precursor atmospheric chemistry.²⁹⁻³¹ For example, oxidation products of $x:2$ FTOH (i.e., $F(CF_2)_x(CH_2OH)$) in the presence of hydroxyl/chlorine radicals are dominated by PFCA with x and $x+1$ carbons.²⁹⁻³¹ Similarly, dominant degradation products from the photooxidation of $6:2$ FTOH with heterogeneous particles are PFHxA and PFPeA with PFHxA:PFPeA mass ratios ranging from 1:1 to 6:1.³² The variability in the ratio of even-odd PFCA congener pairs from the oxidation of FTOH is expected when the illumination and heterogeneity of particle surfaces (e.g., ash and mineral dust) vary.³² As such, a comparison of even-odd PFCA congener mass concentration ratios in snowpacks from the Lake Hazen region, combined with knowledge of smog chamber chemistry, can be used to estimate contributions from the atmospheric oxidation of volatile precursors.

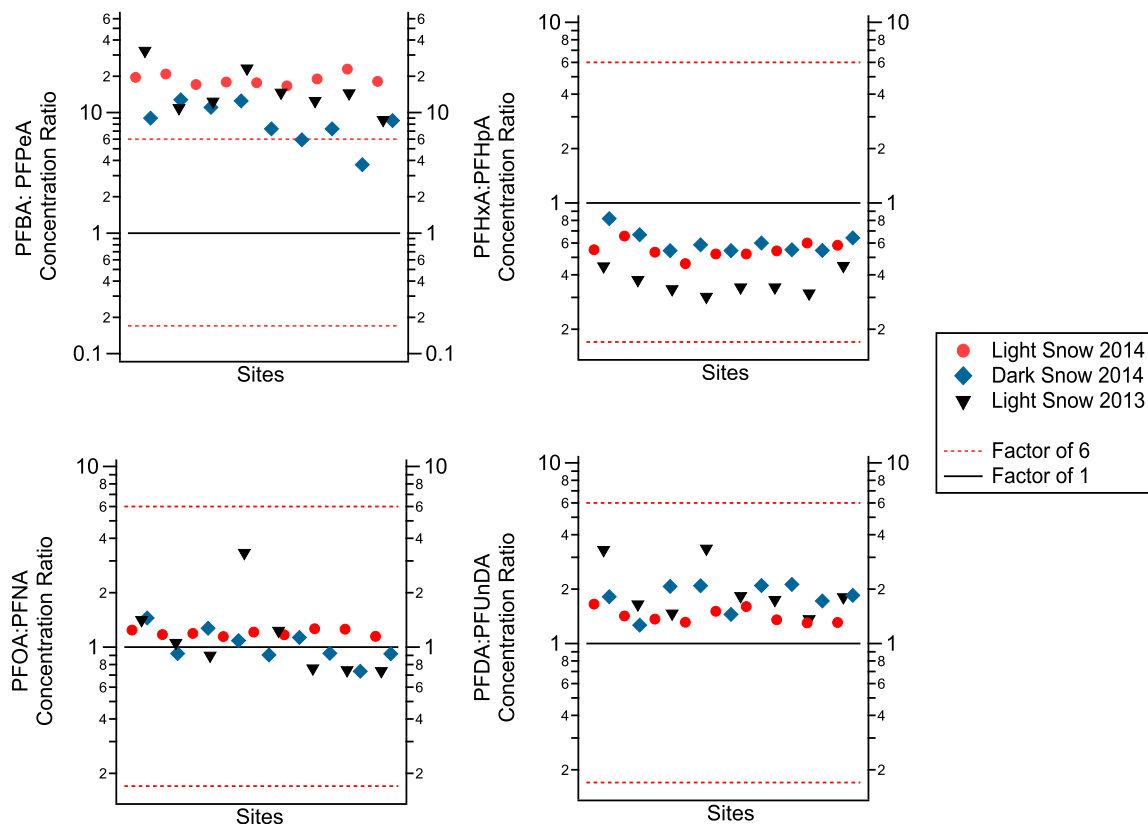


Figure 4.3 Even-odd PFCA concentration ratios in light and dark snowpacks from the Lake Hazen region during 2013-2014. Ratios in light snowpacks collected during 2013 are represented by black triangles, while light and dark snowpacks collected during 2014 are represented by red circles and blue diamonds, respectively. Solid black lines correspond to even-odd ratios within a factor of 1, while the dashed red lines correspond to even-odd ratios within a factor of 6, which represents the range of ratios expected from the oxidation of FTOH in the presence of heterogeneous particles.³²

Here, the even-odd mass concentration ratios of PFBA: PFPeA, PFHxA: PFHpA, PFOA: PFNA, and PFDA: PFOA are used as a proxy for the oxidation products of 4:2, 6:2, 8:2, and 10:2 FTOH, respectively. Even-odd PFCA congener mass concentration ratios in light and dark snowpacks are presented in Figure 4.3. In total, 78 mass ratios are calculated for even-odd pairs for PFHxA through PFOA in light and dark snowpacks collected in 2013 and 2014, of which 85% are within a factor of 2, and 100% within a factor of 6, suggesting fluorotelomer precursors such as 6:2, 8:2 and 10:2 FTOH are sources of PFCA to the Lake Hazen region.

Mass concentration ratios of PFBA: PFPeA, however, are much greater than ratios expected from the oxidation of FTOH in snowpacks from the Lake Hazen region (Figure 4.3). Elevated mass ratios of PFBA: PFPeA are also found in ice from the Devon Ice Cap, which are attributed to the oxidation of heat transfer fluids containing short-chain perfluoroalkyl moieties, such as hydrofluoroether-7100 (HFE, C₄F₉OCH₃), HFE-7200 (C₄F₉OC₂H₅), and hydrofluorocarbon-329 (HFC, CF₃(CF₂)₃H).⁷ Oxidation of heat transfer fluids is likely the predominant source of PFBA to the High Arctic, considering these substances are present in the atmosphere at approximately an order of magnitude greater concentration than volatile fluorotelomer PFCA precursors.¹⁰⁻¹² Global mixing ratios of many HFC are on the order of several to tens of parts-per-trillion by volume and doubled from 2005 to 2011.³³

The long-range atmospheric transport and oxidation of perfluoroalkane sulfonamido substances is a possible indirect source of PFAS in Lake Hazen snowpacks.^{10,11} The atmospheric oxidation of perfluoroalkane sulfonamido substances are studied using smog chamber experiments.³⁴ Oxidation of N-methyl perfluorobutane

sulfonamido ethanol (N-MeFBSE) in the presence of chlorine radicals yields a complete suite of PFCA (i.e., C₂-C₄) and PFBS.³⁴ An extension of N-MeFBSE oxidation is applied to N-methyl perfluorooctane sulfonamido ethanol (N-MeFOSE), considering the atmospheric chemistry is independent of perfluoroalkyl chain length.³⁴ As such, the oxidation of N-MeFOSE is expected to yield PFOS and a complete suite of PFCA (i.e., C₂-C₈). N-MeFBSE is measured in particle and gas phase samples from Cornwallis Island in Arctic Canada in 2004, with concentrations ranging from <LOD-5.4 pg m⁻³ and <LOD-34.0 pg m⁻³, respectively.¹¹ Similarly, perfluorooctane sulfonamido substances are elsewhere in the High Arctic at Alert on Ellesmere Island during 2006-2014, with concentrations ranging from <LOD-2.7 pg m⁻³ N-MeFOSE and <LOD-3.9 pg m⁻³ N-ethyl perfluorooctane sulfonamidoethanol (N-EtFOSE).¹⁰ The elevated concentrations of PFBA in snowpacks from the Lake Hazen region are unlikely to be accounted for by the oxidation of perfluorobutane sulfonamido substances given the low to non-detect concentrations of these volatile precursors in the High Arctic atmosphere;^{10,11} however, this source cannot be excluded considering concentrations of PFBS and PFBA correlate in dark snowpacks ($r_s=0.81$, $p=0.03$). Complimentary atmospheric measurements are necessary to confirm the presence of perfluorobutane sulfonamido substances at Lake Hazen. It is interesting that PFOS concentrations in snowpacks positively correlate with PFHpA and PFOA, and several short-chain PFCA in all samples, an outcome expected from perfluorooctane sulfonamido oxidation (Tables C10-C12).

4.4.3 Direct Sources of PFAS in Snowpacks

Major ions in atmospheric samples are often used to elucidate the role of direct emission sources on PFAS deposition in pristine environments.⁸ Major ions such as Na^+ , K^+ , and Ca^{2+} are used as tracers for sea spray, biomass burning, and mineral dust aerosol, respectively, in the Arctic;^{8,35} however, it is necessary to distinguish major ions that are native to multiple environmental compartments. For example, K^+ , Ca^{2+} , and Mg^{2+} are components of mineral dust and sea spray aerosol.⁸ To estimate contributions from sea spray aerosol, molar concentration ratios of major ions in atmospheric samples are compared to expected molar concentration ratios of major ions in ocean water. In this work, molar concentration ratios for major ions in snowpacks from the Lake Hazen region are used to identify environmental sources.^{36,37} We find that molar concentration ratios of $\text{Mg}^{2+}:\text{Na}^+$, $\text{K}^+:\text{Na}^+$, $\text{SO}_4^{2-}:\text{Na}^+$, $\text{Cl}^+:\text{SO}_4^{2-}$, and $\text{Ca}^{2+}:\text{Mg}^{2+}$ in light and dark snowpacks are not consistent with those in the ocean water (Figure C2). This suggests that these major ions are derived primarily from non-marine sources. Elevated molar concentration ratios of $\text{Mg}^{2+}:\text{Na}^+$ and $\text{Ca}^{2+}:\text{Na}^+$ are consistent with mineral dust aerosol signatures, which are also postulated as a source of aerosol in snow from the Devon Ice Cap.⁸ Elevated molar concentration ratios of $\text{K}^+:\text{Na}^+$ and $\text{SO}_4^{2-}:\text{Na}^+$ are consistent with signatures of natural and anthropogenic combustion aerosol. Forest fires and the continuous burning of sulfur-rich lignite deposits in the Smoking Hills, located in the Canadian Northwest Territories, are identified as natural sources of combustion aerosols whereas local emissions of combustion aerosol such as garbage burning and vehicle traffic are reported in the High Arctic at Alert.³⁵ Local emissions in the Lake Hazen region are not expected to be a major source of PFAS given the area is uninhabited from

early August to late May. Taken together, these observations suggest that mineral dust and combustion aerosol are possible sources of atmospheric PFAS.

Correlation analysis is applied to PFAS and major ion concentrations to investigate the role of sea spray, mineral dust, and combustion aerosol on PFAS deposition in snowpacks from the Lake Hazen region in 2014. Most PFAS are not correlated with major ions in light snowpacks in 2014 (Table C13). Exceptions are observed for PFDODA, PFECHS, and PFOS, which all positively correlate with SO_4^{2-} , Na^+ , Ca^{2+} , Mg^{2+} , PN, and PC. Other notable positive correlations are observed for PFDODA and PFOS with K^+ and Cl^- . In contrast, most PFAS positively correlate with major ions in dark snowpacks (Table C14). The contrast in correlation analysis of PFAS with major ions in light and dark snowpacks are ascribed to differences in post-depositional snowpack melting. This is also based on the observation of structural features of light versus dark snowpacks governed by the differences in snowpack melting. As such, it is possible that the positive correlations in dark snowpacks reflect similar partitioning (i.e., preferential elution) of PFAS and major ions under enhanced melting conditions.

Overall, these observations suggest that PFAS and major ions are derived from common, primarily non-marine sources and/or undergo similar environmental dynamics. Stock et al., note that the presence of long-chain PFCA (C_{10} - C_{14}) in atmospheric particles from Cornwallis Island is attributed to the long-range transport and oxidation of volatile precursors, such that PFAA partition to particles following atmospheric oxidation.¹¹ This partitioning phenomena is confirmed experimentally using particles collected from urban and rural locations, as well as mineral-rich particles.³⁸ The partitioning of PFCA to

particles proceeds only under conditions of moderate relative humidity (RH, >30%),³⁸ suggesting atmospheric particles can act as a sink for PFAS. It is also suggested that atmospheric particle concentrations modulate Hg partitioning at Alert.³⁹ For example, high concentrations of particle-bound Hg are observed at Alert from 2002 to 2011 during the months of March-April, a period characterized by the enhanced delivery of sea spray aerosol and particles from Arctic haze.³⁹ Steffen et al. suggest that enhanced spring atmospheric particle loads facilitate partitioning by providing a surface for reactive gaseous Hg.³⁹ By analogy, it is possible that atmospheric particles facilitate PFAS partitioning (i.e., particle scavenging) in the Lake Hazen region. We postulate that wind storms in the Lake Hazen region facilitated the transport of particles into the atmosphere due to the low snow accumulation on the landscape during the 2013-2014 winter,¹⁹ thus, local particle emissions could facilitate PFAS partitioning following atmospheric oxidation.

It is not possible to preclude the long-range atmospheric transport of particle bound PFAS to the Lake Hazen region. In a recent study, a complete suite of PFAA (i.e., C₄-C₁₈) is reported in air samples from Alert during 2006-2014¹⁰, suggesting the direct transport of PFAS on atmospheric particles is a possible mode of transport to the High Arctic. It is not possible to confirm the extent of particle scavenging or direct transport mechanisms in this study, however, our observations suggest atmospheric particles (i.e., LAP) are relevant to the long-range transport, removal, and fate of PFAS in Lake Hazen snowpacks. Future study of the impact of spring particle loads and the effects on PFAS partitioning under representative conditions of the Arctic atmosphere is warranted.

4.4.4 Seasonal Melting Inputs of PFAS into the Lake Hazen Water Column

Unless it becomes glacial ice, snow is a short-term repository for atmospheric PFAS pollution and a vector for PFAS deposition into freshwater ecosystems upon spring melt.¹³⁻¹⁵ To investigate melting inputs, the Lake Hazen water column was sampled seasonally (i.e., before, during, and after melt) for PFAS.

PFAS with the highest detection frequencies at all depths throughout the water column during snowmelt periods are the series of PFCA with four to nine carbons: PFBA, PFHxA, PFHpA, PFOA, and PFNA (Table C9, Figures 4.4 and C3). PFSA and FOSA are infrequently detected in the Lake Hazen water column during snowmelt in 2014, which is consistent with observations in 2014 Lake Hazen snowpacks. For example, PFHxS is detected in only one snowpack sample, but not in the water column, whereas PFDS and FOSA are not detected in snowpacks or the water column during snowmelt (Table C9). Similar observations are reported in snowmelt from the Krycklan Catchment in Sweden, where PFHxS and PFDS have detection frequencies of 22% and 0%, respectively.¹³ The low proportion and concentrations of PFSA in the Lake Hazen water column during snowmelt are also consistent with low to non-detect concentrations in other remote lakes^{11,15,17} and PFSA volatile precursors in atmospheric samples from the High Arctic of Canada.¹⁰⁻¹² Conversely, Kwok et al. report a greater contribution of PFOS in snow and water sampled near the Longyearbreen glacier in the coastal area of Longyearbyen (Svalbard, Norway, 78° N). In that study, 118 ± 51 pg L⁻¹ PFOS in snow are similar to 396 ± 161 pg L⁻¹ PFOA and 245 ± 112 pg L⁻¹ PFNA in the same samples.²⁷ In our study, 2014 Lake Hazen snowpack samples contain 29 ± 5 pg L⁻¹ PFOS, 711 ± 82 pg L⁻¹ PFOA, and 593 ± 69 pg L⁻¹ PFNA.

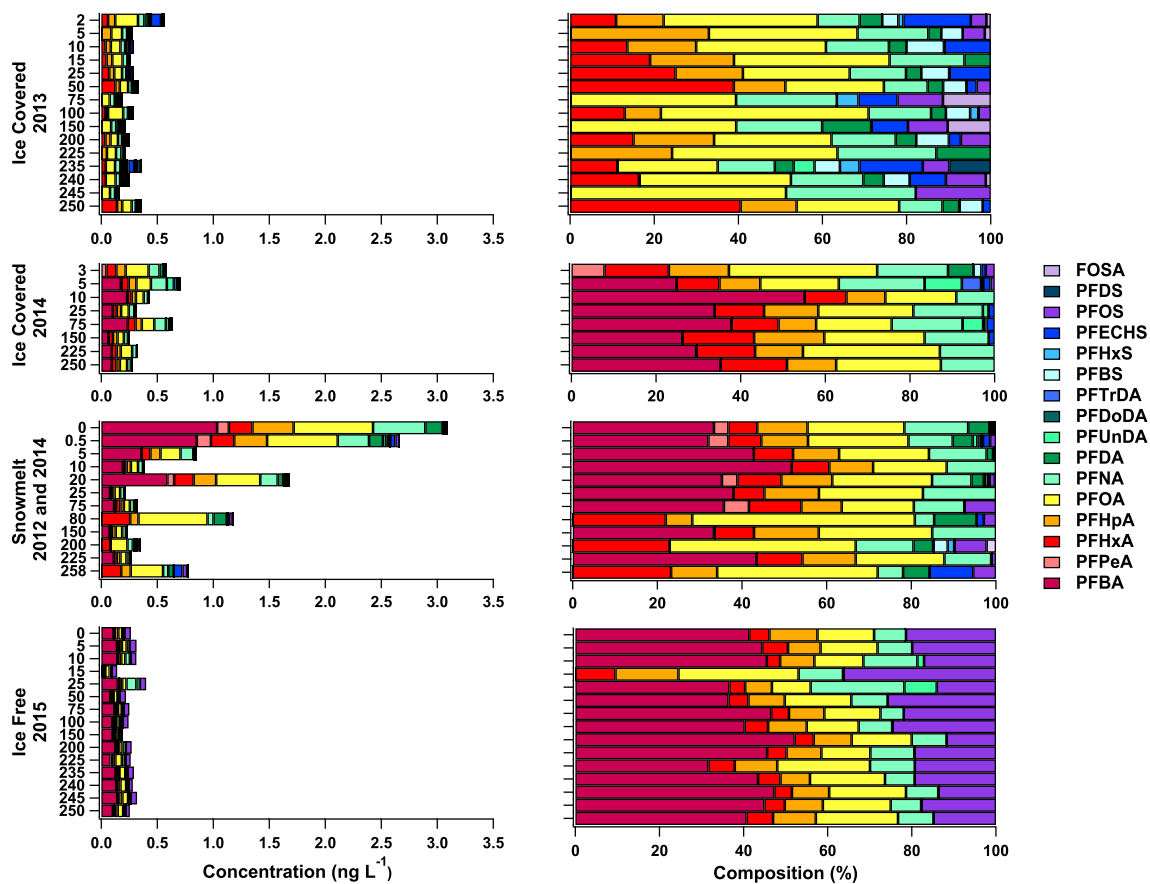


Figure 4.4 PFAS depth profiles in the Lake Hazen water column during ice-covered periods on 15-18 May 2013 and 19-22 May 2014; during snowmelt on 2-4 June 2012 (0.5, 20, 80, 200, 258 m depths) and during an ice-free period on 27-29 July 2015. Concentrations (left panels, ng L^{-1}) and composition (right panels, % of ΣPFAS) profiles correspond to depths between 0 to 258 m.

This discrepancy may be due to the older 2006 sampling period in Kwok et al., the closer proximity of the Svalbard site to marine influences, and/or local anthropogenic emissions from skiing activities and industrial discharge in Svalbard.²⁷ Skaar et al. also report high contributions and concentrations of PFOS in soils (90-92% of the Σ PFAS profile, >280 ng g⁻¹ dw PFOS) from Ny-Ålesund in 2016 and meltwaters (55-58% of the Σ PFAS profile, >100 ng L⁻¹ PFOS) from Longyearbyen in 2015. This prevalence of PFOS is ascribed to local emissions from fire-fighting training operations at an airport.¹⁶ Thus, it is likely local emission sources are more prominent in the Norwegian High Arctic.^{16,27}

It is interesting that PFOS and PFECHS are detected sporadically in the Lake Hazen water column during snowmelt compared to snowpacks on the ice surface of Lake Hazen in 2014. For example, PFOS and PFECHS are detected in 100% and 50% of all snowpack samples but are only detected in 57% and 0% of water column samples during snowmelt in 2014. Of note, however, is that PFOS and PFECHS are consistently in the Lake Hazen water column during the 2-4 June 2012 snowmelt period (Figure 4.4). It is possible that lower detection frequencies of PFOS and PFECHS in the Lake Hazen water column during the snowmelt period in 2014 relative to 2012 is due to: 1) an overall decline in PFOS and PFECHS emissions; 2) reduced melting inputs (i.e., snow in spring 2014 and/or glacier meltwaters in summer 2013); 3) reduced snow accumulation; or 4) snowmelt interactions with lake ice. For example, it is possible that meltwaters enriched in PFAS re-freeze at the lake ice-surface boundary following snowmelt (i.e., before full ice-off). Similar observations are reported by Cai et al. in a sea ice core collected from the Arctic Ocean in August 2010 (site I2, 80° N).⁴⁰ In that study, concentrations of PFBS are

approximately 38 times higher in the surface ice core layer (i.e., 0-15 cm) than in overlying snow,⁴⁰ demonstrating that ice is a repository for PFAS following snowmelt. On the other hand, it is possible that residual LAP remaining on the lake ice surface from the light and dark snowpacks act as a repository for PFAS. It is expected that the melting of lake ice will vector ice- and LAP-sequestered PFAS into the Lake Hazen water column.

The highest concentrations of PFAS congeners are typically near the surface waters (i.e., <5 m depth) in Lake Hazen during snowmelt periods (Figure 4.4, Figure C3). Deeper waters (10-250 m) show similar Σ PFAS concentrations (mean \pm SD) before (0.4 ± 0.1 ng L⁻¹) and during (0.27 ± 0.07 ng L⁻¹) snowmelt in 2014. These observations suggest that snowmelt enhances surface water concentrations of PFBA, PFHxA, PFHpA, PFOA, and PFNA in the Lake Hazen water column through percolation in lake ice. St. Pierre et al. suggest snowmelt is a source of mercury into Lake Hazen, wherein mercury concentrations tripled in the upper 5 m of the water column during snowmelt. The snowmelt period in Lake Hazen results in melt pools on the surface of the ice for a week before meltwater enters the lake through pressure cracks in the ice.

The composition profiles of PFCA in the Lake Hazen water column during ice-covered and ice-free periods are generally consistent, however, PFSA are not. For example, PFHxA, PFHpA, PFOA, PFNA, and PFOS are detected frequently in both water columns, but other PFSA congeners (PFBS, PFHxS, PFECHS, PFDS) and FOSA are only detected in the ice-covered water column (Figure 4.4). Σ PFAS concentrations (mean \pm SD) are similar at all depths of the Lake Hazen water column during ice-covered (0.28 ± 0.09 ng L⁻¹) and ice-free (0.27 ± 0.06 ng L⁻¹) periods (Figure 4.4). To provide a

rationale for these trends, we consider the water budget within Lake Hazen.

Approximately 88% of the water entering Lake Hazen each year is via melting glaciers between mid-June to late August. Beginning in September, the surface of Lake Hazen freezes, and all hydrological inputs from melting glaciers during the summer redistribute throughout the lake over the winter. The discharge of glacier meltwaters into Lake Hazen promotes dense and turbid underflows,^{21,41} which mixes the water column during the summer, and has a lasting effect throughout the winter. Thus, the consistency of ΣPFAS concentrations in deep waters of the Lake Hazen water column during all melting periods supports that melting glaciers are relevant to the fate of PFAS in Lake Hazen. These observations are consistent with our earlier study of PFAS in a Lake Hazen sediment core.⁴² As reviewed by Rigét et al., there are decreasing trends in PFOS in biota throughout the circumpolar Arctic,⁴³ whereas we note increasing PFOS and other PFAS sedimentary fluxes from 1963 to 2011. These elevated PFAS fluxes in Lake Hazen sediments are attributed to the enhanced delivery of sediment and glacier meltwaters promoted by climate warming.⁴² The consistency of the PFCA composition profiles during ice-covered and ice-free periods suggests Lake Hazen is impacted by analogous melting inputs of PFCA in 2012 and 2015. In contrast, lower detection frequencies of PFSA in the ice-free water column in 2015 is attributed to a reduction in PFSA emissions and/or different meltwater and sediment⁴² inputs relative to 2012. Given the predominance of glacier melt to Lake Hazen's hydrological budget compared to snowmelt, whereby glacier melt delivered 0.979 km³ water compared to 0.120 km³ via snowmelt in 2015, the delivery of PFAS to Lake Hazen via glaciers requires further attention.¹⁹

4.5 Conclusions

Our results suggest that the long-range atmospheric transport and oxidation of volatile precursors is a primary source of PFAS in the Lake Hazen region, pursuant to even-odd PFCA ratios in snowpacks and correlation analysis. Local particle scavenging occurs in the Lake Hazen region when reduced snow accumulation on the landscape and wind storms enhance atmospheric particle loads and PFAS partitioning following atmospheric oxidation. Indirect sources are dominant in the Lake Hazen region, however, the detection of PFECHS confirms a direct source, considering it has no known volatile precursors.^{7,17,45} We present the first report that LAP are relevant to the transport and fate of PFAS by enhancing snowpack melting in the High Arctic. Seasonal profiling of the Lake Hazen water column demonstrates that snowmelt enhances near surface PFAS concentrations and melting glaciers govern PFAS mixing in Lake Hazen.

4.6 Literature Cited

- (1) Butt, C. M.; Berger, U.; Bossi, R.; Tomy, G. T. Levels and trends of poly- and perfluorinated compounds in the arctic environment. *Sci. Total Environ.* **2010**, *408* (15), 2936–2965.
- (2) Buck, R. C.; Franklin, J.; Berger, U.; Conder, J. M.; Cousins, I. T.; Voogt, P. De; Jensen, A. A.; Kannan, K.; Mabury, S. A.; van Leeuwen, S. P. J. Perfluoroalkyl and polyfluoroalkyl substances in the environment: Terminology, classification, and origins. *Integr. Environ. Assess. Manag.* **2011**, *7* (4), 513–541.
- (3) Government of Canada. *Perfluorooctane Sulfonate and its Salts and Certain Other Compounds*; 2016; pp 1–10.
- (4) Ritter, S. K. Fluorochemicals go short. *Chem. Eng. News* **2010**, *88* (5), 12–17.
- (5) US EPA. 2010/15 PFOA Stewardship Program <https://www.epa.gov/assessing-and-managing-chemicals-under-tsca> (accessed May 1, 2017).
- (6) Young, C. J.; Furdui, V. I.; Franklin, J.; Koerner, R. M.; Muir, D. C. G.; Mabury, S. A. Perfluorinated acids in Arctic snow: New evidence for atmospheric formation. *Environ. Sci. Technol.* **2007**, *41*, 3455–3461.
- (7) MacInnis, J. J.; French, K.; Muir, D. C. .; Spencer, C.; Criscitiello, A.; De Silva, A. O.; Young, C. J. Emerging investigator series: a 14-year depositional ice record of perfluoroalkyl substances in the High Arctic. *Environ. Sci. Process. Impacts* **2017**, *19* (1), 22–30.
- (8) Pickard, H. M.; Criscitiello, A. S.; Spencer, C.; Sharp, M. J.; Muir, D. C. G.; Silva, A. O. De; Young, C. J. Continuous Non-Marine Inputs of Per- and Polyfluoroalkyl

- Substances to the High Arctic : A Multi-Decadal Temporal Record. *Atmos. Chem. Phys. Discuss.* **2018**, *18* (7), 5045–5058.
- (9) Yeung, L. W. Y.; Dassuncao, C.; Mabury, S.; Sunderland, E. M.; Zhang, X.; Lohmann, R. Vertical Profiles, Sources, and Transport of PFASs in the Arctic Ocean. *Environ. Sci. Technol.* **2017**, *51* (12), 6735–6744.
- (10) Wong, F.; Shoeib, M.; Katsoyiannis, A.; Eckhardt, S.; Stohl, A.; Bohlin-Nizzetto, P.; Li, H.; Fellin, P.; Su, Y.; Hung, H. Assessing temporal trends and source regions of per- and polyfluoroalkyl substances (PFASs) in air under the Arctic Monitoring and Assessment Programme (AMAP). *Atmos. Environ.* **2018**, *172*, 65–73.
- (11) Stock, N. L.; Furdui, V. I.; Muir, D. C. G.; Mabury, S. A. Perfluoroalkyl contaminants in the Canadian Arctic: Evidence of atmospheric transport and local contamination. *Environ. Sci. Technol.* **2007**, *41*, 3529–3536.
- (12) Shoeib, M.; Harner, T.; Vlahos, P. Perfluorinated chemicals in the arctic atmosphere. *Environ. Sci. Technol.* **2006**, *40* (24), 7577–7583.
- (13) Filipovic, M.; Laudon, H.; McLachlan, M. S.; Berger, U. Mass Balance of Perfluorinated Alkyl Acids in a Pristine Boreal Catchment. *Environ. Sci. Technol.* **2015**, *49* (20), 12127–12135.
- (14) Meyer, T.; De Silva, A. O.; Spencer, C.; Wania, F. Fate of perfluorinated carboxylates and sulfonates during snowmelt within an urban watershed. *Environ. Sci. Technol.* **2011**, *45* (19), 8113–8119.
- (15) Veillette, J.; Muir, D.; Antoniadis, D.; Small, J. M.; Spencer, C.; Loewen, T. N.; Babaluk, J. A.; Reist, J. D.; Vincent, W. F. Perfluorinated chemicals in meromictic

- lakes on the northern coast of Ellesmere Island, High Arctic Canada. *Arctic* **2012**, *65*, 245–256.
- (16) Skaar, J. S.; Ræder, E. M.; Lyche, J. L.; Ahrens, L.; Kallenborn, R. Elucidation of contamination sources for poly- and perfluoroalkyl substances (PFASs) on Svalbard (Norwegian Arctic). *Environ. Sci. Pollut. Res.* **2019**, *26* (8), 7356–7363.
- (17) Lescord, G. L.; Kidd, K. A.; De Silva, A. O.; Williamson, M.; Spencer, C.; Wang, X.; Muir, D. C. G. Perfluorinated and polyfluorinated compounds in lake food webs from the Canadian High Arctic. *Environ. Sci. Technol.* **2015**, *49* (5), 2694–2702.
- (18) Thompson, W. Climate. In *Resource description and analysis: Ellesmere Island, National Park Reserve*; Parks Canada: National Resource Conservation Section, Prairie and Northern Region: Winnipeg, Canada, 1994; p 78.
- (19) St. Pierre, K. A.; St. Louis, V. L.; Lehnherr, I.; Gardner, A. S.; Serbu, J. A.; Mortimer, C. A.; Muir, D. C. G.; Wiklund, J. A.; Lemire, D.; Szostek, L.; Talbot, C. Drivers of Mercury Cycling in the Rapidly Changing Glacierized Watershed of the High Arctic's Largest Lake by Volume (Lake Hazen, Nunavut, Canada). *Environ. Sci. Technol.* **2019**, *53* (3), 1175–1185.
- (20) Emmerton, C. A.; Louis, V. L. S.; Lehnherr, I.; Graydon, J. A.; Kirk, J. L.; Rondeau, K. J. The importance of freshwater systems to the net atmospheric exchange of carbon dioxide and methane with a rapidly changing high Arctic watershed. *Biogeosciences* **2016**, *13* (20), 5849–5863.
- (21) Lehnherr, I.; St. Louis, V. L.; Sharp, M.; Gardner, A.; Smol, J.; Schiff, S.; Muir, D.; Mortimer, C.; Michelutti, N.; Tarnocai, C.; St. Pierre, K.; Emmerton, C.;

- Wiklund, J.; Köck, G.; Lamoureaux, S.; Talbot, C. The world's largest High Arctic lake responds rapidly to climate warming. *Nat. Commun.* **2018**, *9*, 1–9.
- (22) Qian, Y.; Yasunari, T. J.; Doherty, S. J.; Flanner, M. G.; Lau, W. K. M.; Ming, J.; Wang, H.; Wang, M.; Warren, S. G.; Zhang, R. Light-absorbing particles in snow and ice: Measurement and modeling of climatic and hydrological impact. *Adv. Atmos. Sci.* **2015**, *32* (1), 64–91.
- (23) Skiles, S. M.; Flanner, M.; Cook, J. M.; Dumont, M.; Painter, T. H. Radiative forcing by light-absorbing particles in snow. *Nat. Clim. Chang.* **2018**, *8*, 964–971.
- (24) Schmale, J.; Flanner, M.; Kang, S.; Sprenger, M.; Zhang, Q.; Guo, J.; Li, Y.; Schwikowski, M.; Farinotti, D. Modulation of snow reflectance and snowmelt from Central Asian glaciers by anthropogenic black carbon. *Sci. Rep.* **2017**, *7*, 1–10.
- (25) Aoki, T.; Matoba, S.; Yamaguchi, S.; Tanikawa, T.; Niwano, M.; Kuchiki, K.; Adachi, K.; Uetake, J.; Motoyama, H.; Hori, M. Light-absorbing snow impurity concentrations measured on Northwest Greenland ice sheet in 2011 and 2012. *Bull. Glaciol. Res.* **2014**, *32* (1), 21–31.
- (26) Casal, P.; Zhang, Y.; Martin, J. W.; Pizarro, M.; Jiménez, B.; Dachs, J. Role of Snow Deposition of Perfluoroalkylated Substances at Coastal Livingston Island (Maritime Antarctica). *Environ. Sci. Technol.* **2017**, *51* (15), 8460–8470.
- (27) Kwok, K. Y.; Yamazaki, E.; Yamashita, N.; Taniyasu, S.; Murphy, M. B.; Horii, Y.; Petrick, G.; Kallerborn, R.; Kannan, K.; Murano, K.; Lam, P.K.S. Transport of Perfluoroalkyl substances (PFAS) from an arctic glacier to downstream locations: Implications for sources. *Sci. Total Environ.* **2013**, *447*, 46–55.

- (28) Cai, M.; Yang, H.; Xie, Z.; Zhao, Z.; Wang, F.; Lu, Z.; Sturm, R.; Ebinghaus, R. Per- and polyfluoroalkyl substances in snow, lake, surface runoff water and coastal seawater in Fildes Peninsula, King George Island, Antarctica. *J. Hazard. Mater.* **2012**, *209–210*, 335–342.
- (29) Ellis, D. A.; Martin, J. W.; De Silva, A. O.; Mabury, S. A.; Hurley, M. D.; Sulbaek Andersen, M. P.; Wallington, T. J. Degradation of fluorotelomer alcohols: A likely atmospheric source of perfluorinated carboxylic acids. *Environ. Sci. Technol.* **2004**, *38* (12), 3316–3321.
- (30) Ellis, D. A.; Martin, J. W.; Mabury, S. A.; Hurley, M. D.; Sulbaek Andersen, M. P.; Wallington, T. J. Atmospheric lifetime of fluorotelomer alcohols. *Environ. Sci. Technol.* **2003**, *37* (17), 3816–3820.
- (31) Wallington, T. J.; Hurley, M. D.; Xia, J.; Wuebbles, D. J.; Sillman, S.; Ito, A.; Penner, J. E.; Ellis, D. A.; Martin, J.; Mabury, S. A.; et al. Formation of C₇F₁₅COOH (PFOA) and other perfluorocarboxylic acids during the atmospheric oxidation of 8:2 fluorotelomer alcohol. *Environ. Sci. Technol.* **2006**, *40* (3), 924–930.
- (32) Styler, S. A.; Myers, A. L.; Donaldson, D. J. Heterogeneous photooxidation of fluorotelomer alcohols: A new source of aerosol-phase perfluorinated carboxylic acids. *Environ. Sci. Technol.* **2013**, *47* (12), 6358–6367.
- (33) Myhre, G.; Shindell, D.; Bréon, F.-M.; Collins, W.; Fuglestedt, J.; Huang, J.; Koch, D.; Lamarque, J.-F.; Lee, D.; Mendoza, B.; Nakajima, T.; Robock, A.; Stephens, G.; Takemura, T.; Zhang, H. Anthropogenic and Natural Radiative Forcing. In *Climate Change 2013: The Physical Science Basis. Contribution of*

Working Group I to the Fifth Assessment Report of the Intergovernmental Panel on Climate Change; Stocker, T. F.; Qin, D.; Plattner, G.-K.; Tignor, M. M. B.; Allen, S. K.; Boschung, J.; Nauels, A.; Xia, Y.; Bex, V.; Midgley, P. M., Eds.; Cambridge University Press, Cambridge, United Kingdom and New York, NY, USA, 2014.

- (34) D'eon, J. C.; Hurley, M. D.; Wallington, T. J.; Mabury, S. A. Atmospheric chemistry of N-methyl perfluorobutane sulfonamidoethanol, C₄F₉SO₂N(CH₃)CH₂CH₂OH: Kinetics and mechanism of reaction with OH. *Environ. Sci. Technol.* **2006**, *40* (6), 1862–1868.
- (35) Leaitch, W. R.; Russell, L. M.; Liu, J.; Kolonjari, F.; Toom, D.; Huang, L.; Sharma, S.; Chivulescu, A.; Veber, D.; Zhang, W. Organic functional groups in the submicron aerosol at 82.5° N, 62.5° W from 2012 to 2014. *Atmos. Chem. Phys.* **2018**, *18* (5), 3269–3287.
- (36) De Caritat, P.; Hall, G.; Gislason, S.; Belsey, W.; Braun, M.; Goloubeva, N. I.; Olsen, H. K.; Scheie, J. O.; Vaive, J. E. Chemical composition of arctic snow: Concentration levels and regional distribution of major elements. *Sci. Total Environ.* **2005**, *336* (1–3), 183–199.
- (37) Church, T. M.; Tramontano, J. M.; Scudlark, J. R.; Jickells, T. D.; Tokos, J. J.; Knap, A. H.; Galloway, J. N. The wet deposition of trace metals to the western atlantic ocean at the mid-atlantic coast and on Bermuda. *Atmos. Environ.* **1984**, *18* (12), 2657–2664.
- (38) Arp, H. P. H.; Goss, K. U. Gas/particle partitioning behavior of perfluorocarboxylic acids with terrestrial aerosols. *Environ. Sci. Technol.* **2009**, *43*

- (22), 8542–8547.
- (39) Steffen, A.; Bottenheim, J.; Cole, A.; Ebinghaus, R.; Lawson, G.; Leitch, W. R. Atmospheric mercury speciation and mercury in snow over time at Alert, Canada. *Atmos. Chem. Phys.* **2014**, *14* (5), 2219–2231.
- (40) Cai, M.; Zhao, Z.; Yin, Z.; Ahrens, L.; Huang, P.; Cai, M.; Yang, H.; He, J.; Sturm, R.; Ebinghaus, R.; et al. Occurrence of perfluoroalkyl compounds in surface waters from the North Pacific to the Arctic Ocean. *Environ. Sci. Technol.* **2012**, *46* (2), 661–668.
- (41) Crookshanks, S.; Gilbert, R. Continuous, diurnally fluctuating turbidity currents in Kluane Lake, Yukon Territory. *Can. J. Earth Sci.* **2008**, *45*, 1123–1138.
- (42) MacInnis, J. J.; Lehnerr, I.; Muir, D. C. G.; Quinlan, R.; De Silva, A. O. Characterization of Perfluoroalkyl Substances in Sediment Cores from High and Low Arctic Lakes in Canada. *Sci. Total Environ.* **2019**, *666*, 414–422.
- (43) Rigét, F.; Bignert, A.; Braune, B.; Dam, M.; Dietz, R.; Evans, M.; Green, N.; Gunnlaugsdóttir, H.; Hoydal, K. S.; Kucklick, J.; et al. Temporal trends of persistent organic pollutants in Arctic marine and freshwater biota. *Sci. Total Environ.* **2019**, *649*, 99–110.
- (44) Hand, V. L.; Capes, G.; Vaughan, D. J.; Formenti, P.; Haywood, J. M.; Coe, H. Evidence of internal mixing of African dust and biomass burning particles by individual particle analysis using electron beam techniques. *J. Geophys. Res. Atmos.* **2010**, *115* (D13), 1–11.
- (45) De Silva, A. O.; Spencer, C.; Scott, B. F.; Backus, S.; Muir, D. C. G. Detection of a cyclic perfluorinated acid, perfluoroethylcyclohexane sulfonate, in the great lakes

- of North America. *Environ. Sci. Technol.* **2011**, *45* (19), 8060–8066.
- (46) Xu, B.; Cao, J.; Joswiak, D. R.; Liu, X.; Zhao, H.; He, J. Post-depositional enrichment of black soot in snow-pack and accelerated melting of Tibetan glaciers. *Environ. Res. Lett.* **2012**, *7* (1), 1–6.
- (47) Li, C.; Bosch, C.; Kang, S.; Andersson, A.; Chen, P.; Zhang, Q.; Cong, Z.; Chen, B.; Qin, D.; Gustafsson, Ö. Sources of black carbon to the Himalayan-Tibetan Plateau glaciers. *Nat. Commun.* **2016**, *7*, 1–7.
- (48) Wang, X.; Halsall, C.; Codling, G.; Xie, Z.; Xu, B.; Zhao, Z.; Xue, Y.; Ebinghaus, R.; Jones, K. C. Accumulation of perfluoroalkyl compounds in Tibetan mountain snow: Temporal patterns from 1980 to 2010. *Environ. Sci. Technol.* **2014**, *48*, 173–181.
- (49) Codling, G.; Halsall, C.; Ahrens, L.; Del Vento, S.; Wiberg, K.; Bergknut, M.; Laudon, H.; Ebinghaus, R. The fate of per- and polyfluoroalkyl substances within a melting snowpack of a boreal forest. *Environ. Pollut.* **2014**, *191*, 190–198.

**5 Permafrost and Glacier Melt as Sources of Perfluoroalkyl
Substances to Freshwater Ecosystems of the High Arctic of
Canada**

5.1 Abstract

Perfluoroalkyl substances (PFAS) are anthropogenic contaminants with unique physicochemical properties, ubiquitous environmental presence, and extraordinary persistence. The sources, fate, and transport of PFAS are complex, particularly in the Arctic given their legacy and contemporary emissions from local and distant sources superimposed upon an ecosystem experiencing changes in land development, ship traffic, and climate change. In this study, PFAS are measured in water samples collected along a freshwater continuum (i.e., streams-lake-ponds-wetland-creek) and in glacial rivers to investigate the role of permafrost thaw and glacier melt on the fate and transport of PFAS to freshwater ecosystems within the Lake Hazen watershed in 2015. Streams derived from subsurface soils consisting of permafrost thaw and snowmelt are collectively identified as sources of C₄, C₆-C₁₀, C₁₄ perfluoroalkyl carboxylic acids (PFCA), and C₄, C₆, C₈ perfluoroalkyl sulfonic acids (PFSA). Low detection frequencies of long-chain PFCA (i.e., C₉-C₁₄) in streams are linked to the enhanced partitioning of these compounds to subsurface soil. Concentrations and detection frequencies of PFAS change along the continuum, whereby PFAS are lower downstream of a meadow wetland relative to upstream locations. These observations suggest PFAS partition to vegetation and/or soil in meadow wetlands in the High Arctic. Glacial rivers are identified as sources of C₄-C₁₁ PFCA and C₄, C₈ PFSA within the Lake Hazen watershed. The mass transfer of total PFAS (i.e., ΣPFAS) by glacial rivers into Lake Hazen is estimated at 1.6 ± 0.7 kg, whereas the output of ΣPFAS from Lake Hazen is estimated at 0.64 kg in 2015. A positive net balance of 0.96 kg indicates PFAS have notable residence times in Lake

Hazen. The results of this study provide insight into the transport and fate of PFAS in High Arctic freshwater ecosystems.

5.2 Introduction

Perfluoroalkyl substances (PFAS) are anthropogenic chemicals that are used in surface treatments (e.g., for stain, oil, and water repellency), aqueous-film-forming-foams, as aids in fluoropolymer manufacturing, and mist suppressants during electroplating.¹ The persistence and bioaccumulative properties of several PFAS, such as long-chain perfluoroalkyl carboxylic acids (PFCA, i.e., seven or more perfluorinated carbons) and perfluoroalkyl sulfonic acids (PFSA, i.e., six or more perfluorinated carbons) promoted regulatory efforts to reduce their environmental inventories.² For example, the global phase-out of perfluorooctane-based chemistries by the 3M Company in 2001 was followed by several international global regulatory initiatives to reduce perfluorooctane-based emissions during manufacturing.³⁻⁵ Despite these regulatory efforts, ongoing perfluorooctane-based emissions from PFAS products manufactured prior to phase-out initiatives (i.e., through usage and disposal) and contemporary manufacturing using perfluorooctane-based chemistries continue to release PFAS to the environment.⁶⁻⁸

The detection of PFAS in freshwater and terrestrial ecosystems in the High Arctic is attributed to long-range and local transport of PFAS these environments.⁹⁻¹³ Most recently Skaar et al. report $1.4 \pm 0.2 \text{ ng L}^{-1}$ Σ PFAS in Lake Linnévatnet water (Svalbard, Norway) during April to June 2015.¹⁰ In the same study, Skaar et al. attribute high Σ PFAS concentrations in run-off waters ($113\text{-}119 \text{ ng L}^{-1}$) and soil ($211\text{-}800 \text{ ng g}^{-1}$ dry weight, dw) to local fire-fighting training activities in Ny-Ålesund (High Arctic of Norway) in 2016.¹⁰ Cabrerizo et al. report similar findings in western Arctic Canada in 2015 and 2016, where lower Σ PFAS concentrations are reported (0.20 to 2.0 ng g^{-1} dw) in

soil around two lakes on the uninhabited, Melville Island (Nunavut, Canada) relative to soil around Meretta Lake (9.52 ng g⁻¹ dw) on Cornwallis Island (Nunavut, Canada), which is impacted by local airport activity.¹¹

Current efforts are directed towards understanding the fate and transport of PFAS in High Arctic ecosystems that are responding to climate warming. In particular, the Lake Hazen watershed is the focus of recent studies on the effects of climate warming on PFAS deposition^{14,15} in the High Arctic because the glaciers surrounding the north coast of Lake Hazen are retreating.^{16,17} The large-scale mass loss of glaciers has important hydrological consequences in Lake Hazen, such as increasing water levels and freshwater discharge to the Arctic Ocean.^{16,17} Melting glaciers are also implicated in the enhanced delivery of sediment, nutrients, and contaminants,^{16–18} including PFAS,^{14,15} to Lake Hazen. We observe exponentially increasing PFAS fluxes in a Lake Hazen sediment core from 1963 to 2011,¹⁴ which is attributed to the enhanced delivery of glacial meltwaters and sediments promoted by climate warming. More recently, we hypothesize that light-absorbing particles accelerate snowpack and glacier melting in the Lake Hazen watershed.¹⁵ An important consequence of climate warming on accelerated melting is the release of historically archived PFAS from glacial ice and the mixing of meltwaters from different time periods that are discharged into freshwater ecosystems.¹⁴ Through this mechanism, it is possible that historically archived PFAS can be released from old ground ice into freshwater ecosystems in the Lake Hazen watershed. Lehnherr et al. note that climate warming deepens the soil active layer in the Lake Hazen watershed,¹⁶ a consequence of which is the thawing of soils that were once perennially frozen (i.e., permafrost) and the melting of old ground ice contained within. Thus, investigation of

permafrost thaw streams in the Lake Hazen region may provide insights into the effects of climate warming on the release of historically archived PFAS from ice contained in permafrost soils into freshwater ecosystems.

These studies highlight the importance of elucidating post-depositional processes governing the transport and fate of PFAS in a changing Arctic climate. While snow¹⁵ is identified as a source for PFAS into Lake Hazen and glacier melt is postulated as a source,^{14,15} the quantitative assessment of other hydrological sources is currently unknown. In this study, PFAS are measured in water samples collected along a freshwater continuum and glacial rivers within the Lake Hazen watershed to investigate the role of ground thaw and glacial melt on the fate and transport of PFAS to freshwater ecosystems in the High Arctic of Canada.

5.3 Methods

5.3.1 Study Area

The Lake Hazen watershed is located within Quttinirpaaq National Park on northern Ellesmere Island, Nunavut, Canada. Lake Hazen is the largest lake by volume (51.4 km³) north of the Arctic Circle, with a maximum depth of 267 m.¹⁶ The Lake Hazen catchment is sheltered from polar winds on the northwest by the Garfield Mountain Range. Within the Lake Hazen watershed exists innumerable, small non-glacierized sub-catchments. These sub-catchments receive stream waters derived from subsurface soils that consist of soil active layer/permafrost thaw and snowmelt. We sampled one of these representative sub-catchments, hereafter the Skeleton Continuum, located near the Lake

Hazen base camp, along the northwestern shore of Lake Hazen (Figure 5.1, Table D1, Appendix D). During the summer, hydrological inputs along the Skeleton Continuum are largely supplied by snowmelt from the landscape and streams (Figure 5.1, Figure D1). Snowmelt and stream water enters Skeleton Lake (1.9 ha, max. depth = 4.7 m, 299 m.a.s.l.),¹⁹ which drains into two small downstream ponds (<1 ha, < 2.5 m deep), a riparian and meadow wetland, and finally, the sparsely vegetated Skeleton Creek before discharging into Lake Hazen (Figure 5.1). The riparian wetland is surrounded by vegetation including alpine foxtail (*Alopecurus alpinus*), arctic willow (*Salix arctica*), cotton grass (*Eriophorum spp.*), two-flowered rush (*Juncus biglumis*), and water sedge (*Carex aquatilis*).²⁰ The shallow meadow wetland along the Skeleton Continuum is characterized by a relatively homogeneous cover of water sedge, cotton grass, bryophytes, and graminoids.²¹ Skeleton Creek is a summer habitat for juvenile Arctic char (*Salvelinus alpinus*).¹⁷

Lake Hazen is primarily supplied by hydrological inputs from melting glaciers (~88%). The glacier melting period in the Lake Hazen watershed occurs during the months of June-August, and the delivery of meltwaters and sediments by glacial rivers into Lake Hazen promotes water column mixing via dense and turbid underflows.¹⁷ Annual glacial runoff is increasing in recent years due to climate warming. For example, annual glacier runoff was 0.064 km³ in 2013, 0.083 km³ in 2014, and 0.979 km³ in 2015.¹⁷ Annual glacial runoff in the Lake Hazen watershed in 2015 is dominated by inputs from the Henrietta Nesmith River (0.291 km³, 30%), Gilman River (0.192 km³, 20%), Very River (0.165 km³, 17%), Turnabout River (0.082 km³, 8%), Abbé River (0.061 km³, 6%), and Snowgoose River (0.026 km³, 3%). Lake Hazen is drained by the

Ruggles River into Chandler Fiord.¹⁶ The annual output by the Ruggles River was 1.093 km³ in 2015.¹⁷ Further information on tributaries in the Lake Hazen watershed is presented in Appendix D (Table D2).

5.3.2 Sampling

Five sites designated S1 through S5, along the Skeleton Continuum were sampled between 9 July and 1 August 2015, as follows: Subsurface-derived streams were sampled directly from an upland seep located along the side of Mount McGill (site S1, Figure D1). Surface water samples were collected from the southeastern bank of Skeleton Lake (site S2), downstream of the pond network (site S3) and meadow wetland (site S4), as well as Skeleton Creek (site S5) at approximately 0.2 km before its outlet into Lake Hazen (Figure 5.1). Rivers in the Lake Hazen watershed (i.e., Henrietta Nesmith River, Abbé River, Turnabout River, Very River, and Ruggles River) were sampled by helicopter on 15 July 2015, while Blister Creek and Snowgoose River were sampled by foot, on a weekly basis during July 2015. Water was collected in pre-cleaned 1000 mL polypropylene bottles at all sites, and subsequently stored at ~5 °C until shipped to the Canada Centre for Inland Waters (Burlington, Ontario) for analysis. A weather data logger (CR10X, Campbell Scientific) was mounted on a raft in Lake Hazen for hourly temperature and wind speed measurements during the sampling period. The mean daily temperature in July was above 4 °C and daily maximum temperatures were as high as 17 °C (Figure D2).

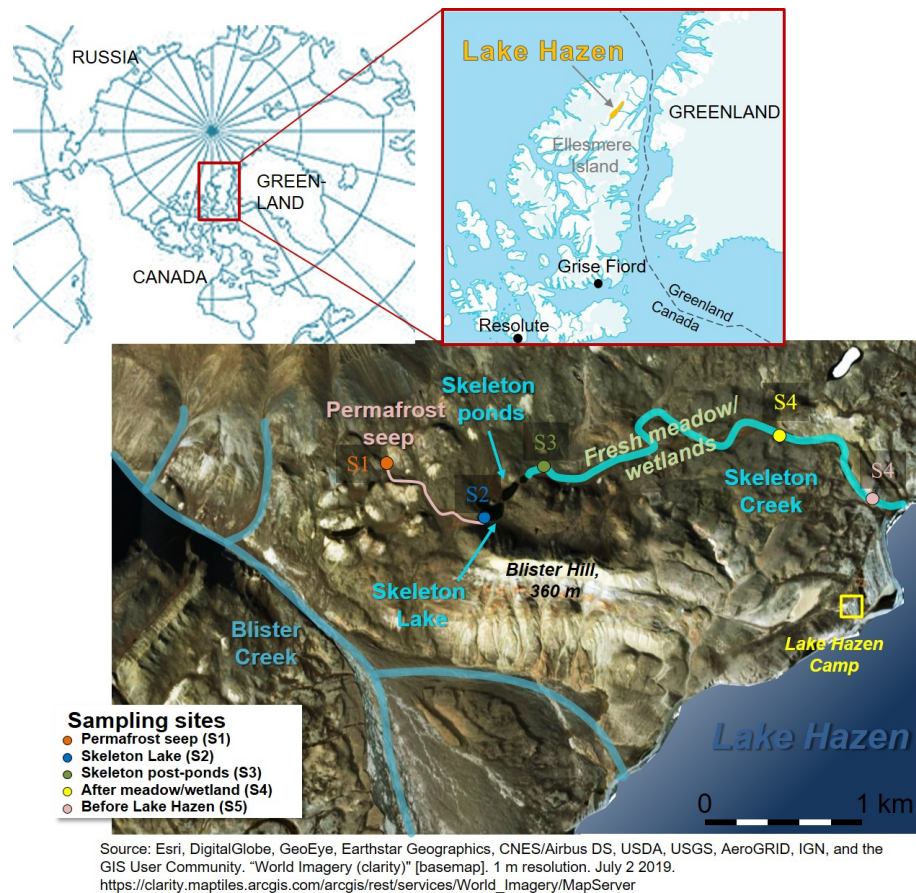


Figure 5.1 Overview of sites along the Skeleton Continuum. Sampling sites S1 through S5 are represented by coloured circles and legend. Location of the Lake Hazen base camp and the glacier-fed river, Blister Creek are also shown. Map source: ESRI World Imagery base map. Inset map presents location of Lake Hazen on Ellesmere Island and the two closest human settlements: Grise Fiord (population 129) on Ellesmere Island and Resolute (population 198) on Cornwallis Island. Inset map source: Toporama (atlas.gc.ca), a topographic reference product produced by Natural Resources Canada using CanVec data.

5.3.3 Sample Extraction

Water samples were extracted using a weak anion exchange solid-phase extraction method as described previously.^{14,22,23} Isolation of PFAS was conducted using two fractions. The first fraction consisted of methanol and eluted perfluorooctane sulfonamide (FOSA) and the second was basicified methanol to elute PFCA and PFSA. Extracts were concentrated to dryness and reconstituted in 0.5 mL of 1:1 SPE-cleaned water: methanol. Further details on chemicals and QA/QC is presented in Appendix D (Sections D1 and D2, Tables D3 and D4).

5.3.4 Instrument and Data Analysis

Water samples were analyzed on an Acquity UPLC I class liquid chromatograph coupled to a XEVO TQ-S tandem mass spectrometer operated in electrospray negative ionization mode (Waters Corporation, Massachusetts, USA) as described before (Tables D5 and D6).^{14,22,23} PFAS were separated on an Acquity UPLC® BEH C18 (2.1 x 100 mm, 1.7 μ m) stationary phase (Waters Corporation, Massachusetts, USA) using a water-methanol gradient (Table D7). The limits of detection (LOD) and quantitation (LOQ) correspond to concentrations with signal-to-noise ratios of 3 and 10, respectively (Table D4).^{14,15,22} Total PFAS concentrations (i.e., Σ PFAS) correspond to the sum of PFAS with concentrations above LOD. Mann-Whitney U-tests were performed using StatPlus:mac (V6) to compare PFAS concentrations, with a critical p-value set to 5%. PFAS concentrations are reported in the following sections according to the mean \pm standard deviation unless specified differently.

5.4 Results and Discussion

5.4.1 Composition of PFAS along the Skeleton Continuum

The concentration ranges and detection frequencies of PFAS along the Skeleton Continuum are shown in Table 5.1. PFBA, PFBS, and PFOA are detected at all sites along the continuum. Other PFAS are specific to zones within and closest to the seep. For example, PFHxA, PFHpA, and PFOS are detected at the seep, Skeleton Lake, and post-ponds with detection frequencies corresponding to 60 to 100% but are only present in 0 to 33% samples further downstream. Conversely, PFNA and PFHpS are only detected frequently at Skeleton Lake, post-ponds, and Skeleton Creek. Maximum PFAS (Σ and individual) concentrations along the continuum occur at the seep and Skeleton Lake.

PFAS profiles are dominated by PFBA and PFBS, with concentration ranges of 1.1-3.8 ng L⁻¹ and 0.18-0.41 ng L⁻¹, respectively (Figure 5.2). Σ PFAS concentrations are of the same magnitude at the seep (3.7 ± 0.7 ng L⁻¹), Skeleton Lake (4.1 ± 0.4 ng L⁻¹), and post-ponds (3.5 ± 0.4 ng L⁻¹), however, concentrations are attenuated by a factor of 2 in the last two zones of the continuum. For instance, Σ PFAS concentrations are 1.78 ± 0.06 ng L⁻¹ after the meadow wetland and 1.6 ± 0.1 ng L⁻¹ at Skeleton Creek. Σ PFAS concentrations along the Skeleton Continuum are much higher than those in waters from Lake A (Ellesmere Island, Nunavut, 0.027-0.456 ng L⁻¹),¹² and waters from Lake Hazen during the same sampling period (0-10 m, 0.29 ± 0.03 ng L⁻¹).¹⁵

Table 5.1 Concentration ranges (ng L⁻¹) and detection frequencies (%) of PFAS along the Skeleton Continuum and in glacial rivers during July-August 2015. Detection frequencies are calculated as the percent number of samples out of the sampling dates (*n*) with concentrations equal to or greater than the LOD and are presented in bold text in parentheses. PFDoDA, PFHxDA, and PFDS are <LOD in all samples.

Site	Seep	Skeleton Lake	After Ponds	After Meadow Wetland	Skeleton Creek	Glacial Rivers
<i>n</i>	5	5	3	3	3	12
PFBA	1.9-3.7 (100)	2.8-3.8 (100)	2.5-3.0 (100)	1.3-1.5 (100)	1.1-1.4 (100)	0.62-3.3 (100)
PFPeA	<0.010 (0)	<0.010 (0)	<0.010 (0)	<0.010 (0)	<0.010 (0)	<0.010-0.10 (67)
PFHxA	0.11-0.18 (100)	0.17-0.23 (100)	0.14-0.24 (100)	<0.005-0.029 (33)	<0.005 (0)	0.050-0.20 (100)
PFHpA	0.060-0.094 (100)	0.12-0.17 (100)	0.075-0.13 (100)	<0.002 (0)	<0.002-0.044 (33)	0.044-0.28 (100)
PFOA	0.074-0.10 (100)	0.094-0.15 (100)	0.069-0.13 (100)	0.025-0.039 (100)	0.034-0.047 (100)	0.10-0.33 (100)
PFNA	<0.002-0.004 (20)	0.017-0.061 (100)	<0.002-0.038 (66)	<0.002 (0)	<0.002-0.014 (66)	0.037-0.26 (100)
PFDA	<0.003-0.003 (40)	<0.003-0.007 (20)	<0.003-0.005 (33)	<0.003 (0)	<0.003-0.032 (33)	<0.003-0.11 (58)
PFUnDA	<0.003 (0)	<0.003 (0)	<0.003 (0)	<0.003 (0)	<0.003 (0)	<0.003-0.009 (17)
PFTTrDA	<0.002 (0)	<0.002-0.004 (20)	<0.002 (0)	<0.002 (0)	<0.002 (0)	<0.002 (0)
PFTeDA	<0.003-0.003 (20)	<0.003-0.004 (20)	<0.003 (0)	<0.003 (0)	<0.003 (0)	<0.003 (0)
PFBS	0.36-0.41 (100)	0.25-0.26 (100)	0.30-0.31 (100)	0.21-0.25 (100)	0.18-0.24 (100)	<0.002-0.053 (75)
PFHxS	0.037-0.051 (100)	<0.0007 (0)	<0.0007 (0)	<0.0007-0.014 (33)	<0.0007 (0)	<0.0007 (0)
PFHpS	<0.0009 (0)	0.097-0.12 (100)	0.045-0.060 (100)	<0.0009-0.054 (33)	0.038-0.044 (100)	<0.0009 (0)
PFOS	<0.001-0.047 (60)	0.013-0.020 (100)	<0.001-0.019 (66)	<0.001-0.21 (33)	<0.001-0.017 (33)	<0.001-0.046 (83)
PFECHS	<0.001-0.001 (20)	<0.001-0.002 (20)	<0.001 (0)	<0.001 (0)	<0.001 (0)	<0.001 (0)
FOSA	<0.0002 (0)	<0.0002-0.029 (20)	<0.0002 (0)	<0.0002 (0)	<0.0002 (0)	<0.0002 (0)

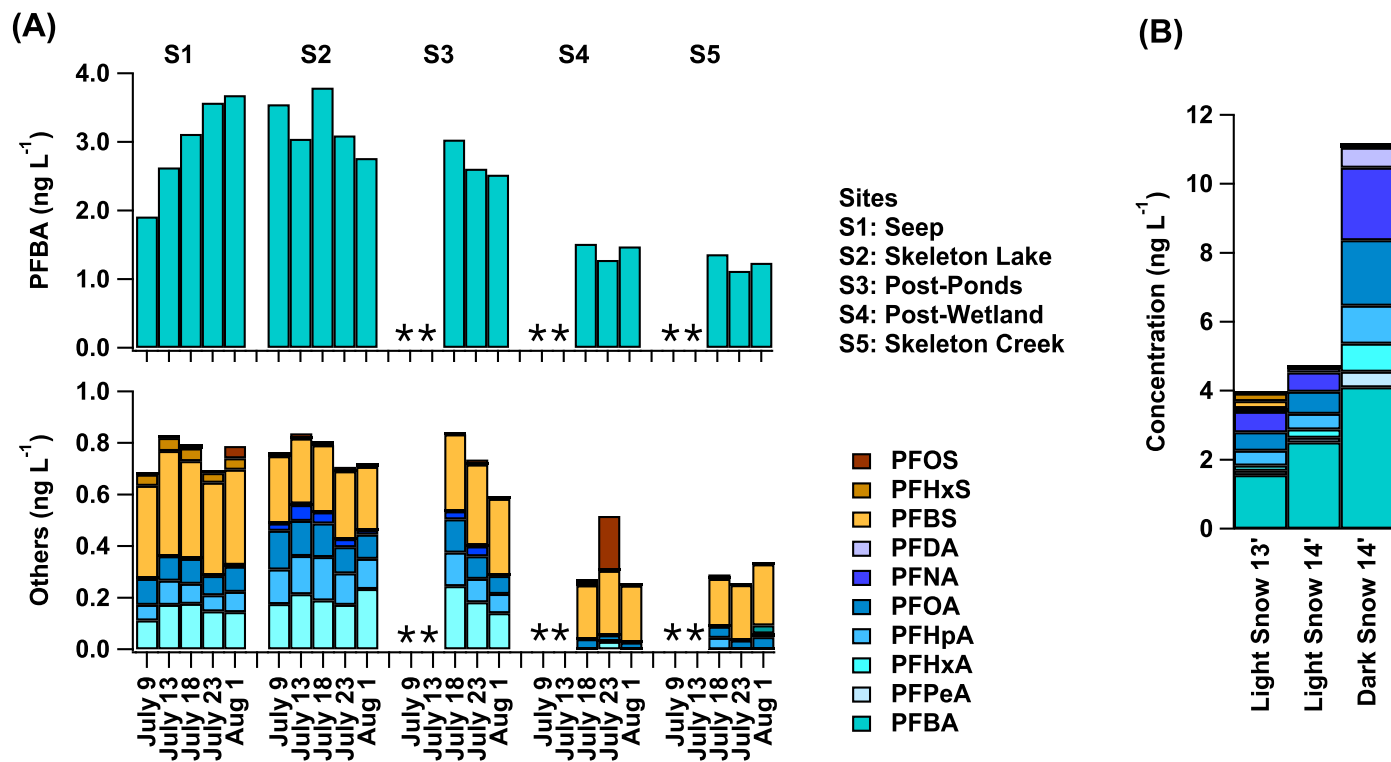


Figure 5.2 Concentrations (ng L⁻¹) of PFBA and other PFAS along the Skeleton Continuum (A) from July 9 to August 1 2015. * indicates no sampling was conducted because Skeleton Creek began flowing on July 18. Lake Hazen snow from May 2013 and June 2014 are shown in (B).

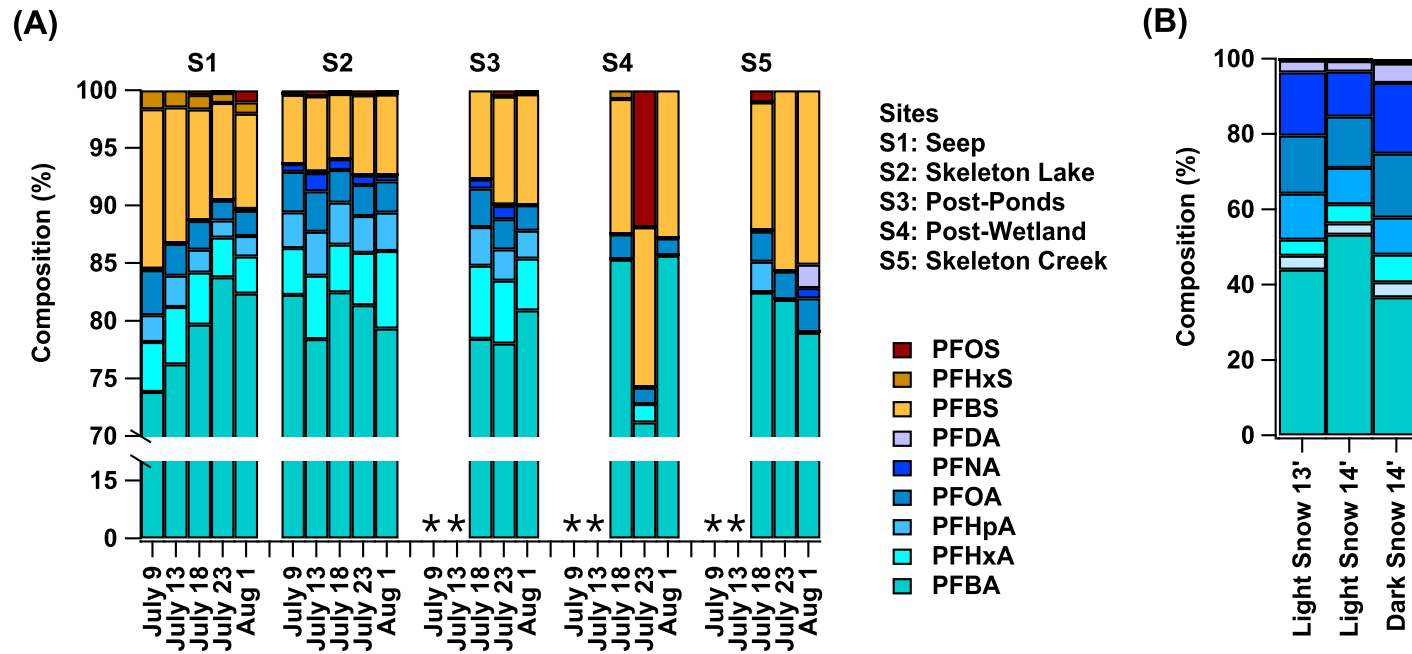


Figure 5.3 PFAS composition (%) along the Skeleton Continuum (A) from July 9 to Aug 1 2015 and Lake Hazen snow (B)

sampled during May 2013 and June 2013. * indicates no sampling was conducted because Skeleton Creek began flowing on July

18.

However, Σ PFAS concentrations in waters from the Skeleton uplands are similar to those in light snowpacks from the Lake Hazen region (median 3.6-4.7 ng L⁻¹, Figure 5.2b).¹⁵

The composition profile of PFAS along the Skeleton Continuum suggests this region is impacted by different hydrological and atmospheric sources. For instance, PFHxS is detected frequently only at the seep, but not in the recipient Skeleton Lake or downstream (Figure 5.3b). It is unlikely that the absence of PFHxS within Skeleton Lake is due to sorption and sedimentation given the similarity of sorption coefficients with PFHpA and PFOA. For example, the organic carbon-normalized sorption coefficient (log K_{oc}) is 2.05-3.7 for PFHxS, 1.63-2.1 for PFHpA, and 1.89-3.5 for PFOA²⁴ and PFHpA, and PFOA are detected frequently within Skeleton Lake. It is possible that the absence of PFHxS in Skeleton Lake is attributed to the partitioning of this compound to soil during the transport of seep waters to Skeleton Lake and/or dilution because Skeleton Lake is supplied by multiple seeps and snowmelt inputs from the landscape. In contrast, concentrations of PFHxA and PFHpA, which are frequently detected in Lake Hazen snowpacks,¹⁵ are higher in Skeleton Lake than the seep ($p \leq 0.03$), while higher detection frequencies are observed for other PFAS (i.e., PFNA, PFTrDA, PFHpS, FOSA). These observations indicate that integrated hydrological inputs from seeps and snowmelt results in higher detection frequencies and concentrations of PFAS in Skeleton Lake relative to the single seep sampled in this study (Table 5.1, Figures 5.2 and 5.3). Of note, however, is that PFHpS is not detected in Lake Hazen snowpacks,¹⁵ sediments,¹⁴ or water.¹⁵ As such, the occurrence of PFHpS, as well as elevated concentrations and detection frequencies of other PFAS in Skeleton Lake, may be attributed to atmospheric sources of local and/or distant origin. The sites along the Skeleton Continuum are ice-free from mid-

June until late-August, facilitating direct atmospheric deposition of particles and gases. The Lake Hazen base camp (Figure 5.1) is a possible local source of PFAS via human activity including emissions from weatherproofing gear (e.g., garments and tents) and waste burning. If the Skeleton Continuum receives inputs from the base camp, then these would be magnified due to low flow; however, the sites along the continuum closest to the camp were not pronounced with PFAS. Further investigation of local contamination from the base camp is warranted.

The source of PFHxS and PFBS to the Skeleton Continuum is intriguing since these are not major PFAS in Lake Hazen snowpacks (Figure 5.3).^{14,15} The low detection frequency of PFHxS along the Skeleton Continuum is consistent with our studies of annual atmospheric deposition in the High Arctic in Devon Island^{22,23} and our 2013-2014 Lake Hazen snowpack^{14,15} analysis where PFHxS is predominantly <LOD. A recent report from the Norwegian Environment Agency indicates that PFHxS may be present in fire-fighting foam, food-contact paper, weather-proofing additives, and cleaning agents, however, 30 global chemical companies report that they are not producing or using the substance.²⁵ In our earlier research, we did not observe a historical trend for PFHxS in a Lake Hazen sediment core because PFHxS is only detected in near surface sediment at 2.25 cm depth, corresponding to 2011.¹⁴ On the other hand, PFBS is detected in 91% of Lake Hazen sediments between 0.25-15.5 cm depths, with a doubling time of 7.7 years from 1963 to 2011.¹⁴ In the latter study, maximum concentrations and fluxes of most PFAS, including PFHxS and PFBS, occur in near surface sediments.¹⁴ This is attributed to enhanced climate warming-induced glacier melting because 2011 was unusually warm and resulted in high glacial meltwater discharge. For reference, glacial meltwater

discharge was 0.2 ± 0.1 Gt year⁻¹ during 1963-2004 compared to 1.8 Gt year⁻¹ in 2011. A corollary of enhanced glacier melting is the release and mixing of glacial meltwaters from different time periods, resulting in the discharge of historically archived PFAS into Lake Hazen. The occurrence of PFHxS and PFBS at the seep may be attributed to a historical hydrological source through this mechanism. For example, it is possible that higher temperatures promoted the release of archived PFAS from the thawing of active layer/permafrost soils and the melting of ice contained within those soils, considering 2015 was a strong melt year.¹⁷ Alternatively, the origin of water at the seep may reflect integrated inputs from permafrost and contemporary snowmelt that infiltrated soils. This provides a rationale for the unique PFHxS and PFBS profiles at the seep relative to Lake Hazen snowpacks,^{14,15} and the similarities of Σ PFAS concentrations at the seep with Lake Hazen light snowpacks and Skeleton Lake, which is fed primarily by snowmelt. We acknowledge that it is not possible to preclude 2015 snowmelt as a primary source of PFHxS and PFBS at the seep without having snowpack samples. However, if 2015 snowmelt is the primary source of water at the seep, then we would expect similar PFHxS and PFBS profiles at the seep and Skeleton Lake. In fact, PFHxS is not detected at Skeleton Lake, while concentrations of PFBS are lower in Skeleton Lake (0.257 ± 0.008 ng L⁻¹) than those at the seep (0.37 ± 0.02 ng L⁻¹, $p < 0.01$). This suggests that PFHxS and PFBS inputs from seep waters are diluted primarily by 2015 snowmelt in Skeleton Lake.

5.4.2 Transport and Partitioning of PFAS along the Skeleton Continuum

PFAS profiles along the Skeleton Continuum provide insight into the transport and partitioning behavior of PFAS in High Arctic freshwater ecosystems. For example, the detection of PFAS at the seep indicates that seep water is a source of PFAS; however, the low detection frequency of long-chain PFCA (i.e., C₉-C₁₄) may be attributed to the enhanced hydrophobic interactions with subsurface soils. This may also provide a rationale for the delayed delivery of PFOS to the seep (Figure 5.2). Similar observations are reported in the Krycklan Catchment (northern Sweden, 64° N), wherein the mobility of PFUnDA and PFDoDA within a groundwater system is limited by PFAS partitioning within soils.²⁶

It is interesting that C₆-C₈ PFCA and C₄, C₆ PFSA concentration profiles are similar at the seep during July (Figure 5.2). These observations suggest that subsurface transport and partitioning are similar for these PFAS, which is consistent with their similarity in log K_{oc}.²⁴ In contrast, a distinct profile is observed for PFBA, such that concentrations increase from 1.9 ng L⁻¹ to 3.7 ng L⁻¹ over the 9 July to 1 August sampling period (Figure 5.2). A rationale for this distinctive trend may be related to the progressive melting of ice contained in permafrost soils during the summer, which may have enhanced PFBA concentrations at the seep due to its high water solubility and low log K_{oc}.²⁴ Further research is required to improve understanding of PFAS subsurface transport in the High Arctic.

Overall, concentrations and detection frequencies of PFAS are comparable at the seep, Skeleton Lake, and post-ponds, suggesting that there is only limited PFAS partitioning (e.g., to soils or lake/pond sediments) across these sites (Table 5.1, Figures 5.2 and 5.3). On the other hand, lower concentrations and detection frequencies are

typically observed for PFAS after the meadow wetland and Skeleton Creek, which may be attributed to the partitioning of PFAS to vegetation and/or soil in the meadow wetland. Müller et al. report uptake and depuration kinetics of PFAS in vegetation using a hydroponic plant model system.²⁷ In that study, high equilibrium concentrations of PFNA ($317 \pm 16 \text{ ng g}^{-1}$), PFDA ($771 \pm 35 \text{ ng g}^{-1}$), PFOS ($766 \pm 68 \text{ ng g}^{-1}$), and PFBA ($275 \pm 14 \text{ ng g}^{-1}$) are reported in plant roots, however, faster uptake and depuration kinetics are reported for PFNA, PFDA, and PFOS relative to PFBA.²⁷ Müller et al. attribute slower uptake and depuration kinetics of PFBA to its enhanced translocation ability throughout the plant system due to its high water solubility.²⁷ This may provide a rationale for lower PFBA concentrations after the meadow wetland because PFBA has a low K_{OC} (1.88)²⁴ and is less likely to partition to soils in the meadow wetland relative to long-chain PFAS. Alternatively, lower concentrations and detection frequencies of other PFAS after the meadow wetland with higher K_{OC} may be attributed to plant uptake and soil partitioning in the meadow wetland. Other studies demonstrate the utility of constructed wetlands to remove and store PFAS from waters in the environment.^{28,29} In contrast, concentrations and detection frequencies of PFAS are similar after the meadow wetland and downstream in Skeleton Creek, suggesting limited PFAS partitioning along the sparsely vegetated rocky streambed. We also consider that lower PFAS concentrations in downstream locations may be due to dilution effects from hydrological sources other than Skeleton Lake waters, however, we believe this is unlikely because this region (1) receives little precipitation, (2) is not fed by glacier melt, and (3) has fewer seeps than the Skeleton uplands.

It is possible that meadow wetlands have a mitigating effect on PFAS transport to habitats for juvenile Arctic char along the Skeleton Continuum. Recently, St. Pierre et al., report 0.025 ± 0.003 ng L⁻¹ methyl mercury (MeHg) in Skeleton Creek and noted that this region may be the initial site of MeHg exposure in Arctic food webs.¹⁷ We might therefore also expect Skeleton Creek and the multitude of similar streams along the Lake Hazen shoreline to be initial sites of PFAS exposure for juvenile Arctic char. Lescord et al. report long-chain PFCA (e.g., PFOA, PFNA, PFTrDA) and PFOS in whole body homogenates of juvenile Arctic char in lakes from the High Arctic,¹³ demonstrating that PFAS can partition and bioaccumulate in juvenile Arctic char.³⁰ Our results suggest that meadow wetlands are sinks for PFAS and may therefore mitigate PFAS exposure in juvenile Arctic char inhabiting locations like Skeleton Creek.

5.4.3 PFAS in Rivers from the Lake Hazen Watershed

PFAS profiles in glacial rivers in the Lake Hazen watershed are presented in Figure 5.4. C₄-C₁₁ PFCA as well as PFBS and PFOS are detected in glacial rivers. C₄, C₆-C₉ PFCA have 100% detection frequency, while PFBS and PFOS have detection frequencies of 75% and 83%, respectively (Table 5.1). PFBA is most abundant in glacial rivers with concentrations ranging from 0.62-3.3 ng L⁻¹, accounting for 52-83% of ΣPFAS concentrations. ΣPFAS concentrations are highest in order of Blister Creek (3.7 ± 0.8 ng L⁻¹), Turnabout (2.4 ng L⁻¹), Very (1.8 ng L⁻¹), Snowgoose (1.6 ± 0.4 ng L⁻¹), Henrietta Nesmith (1.3 ng L⁻¹), and Abbé (1.1 ng L⁻¹) Rivers.

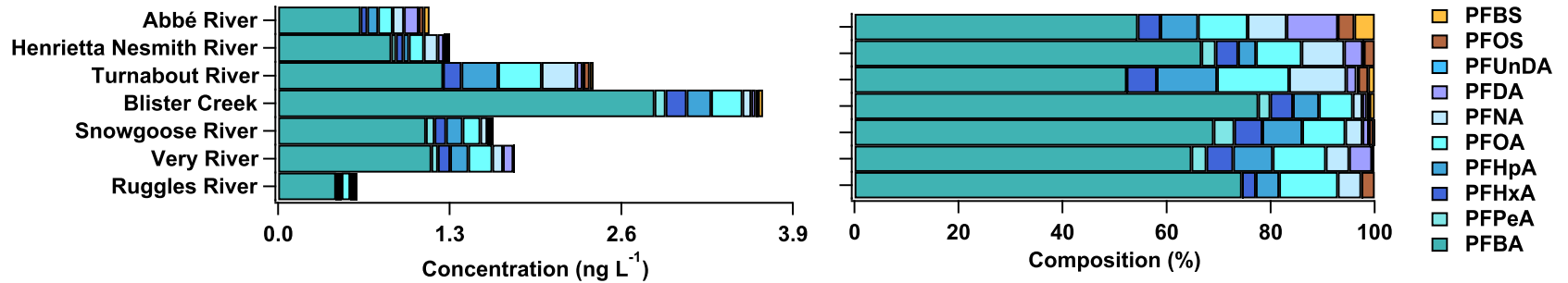
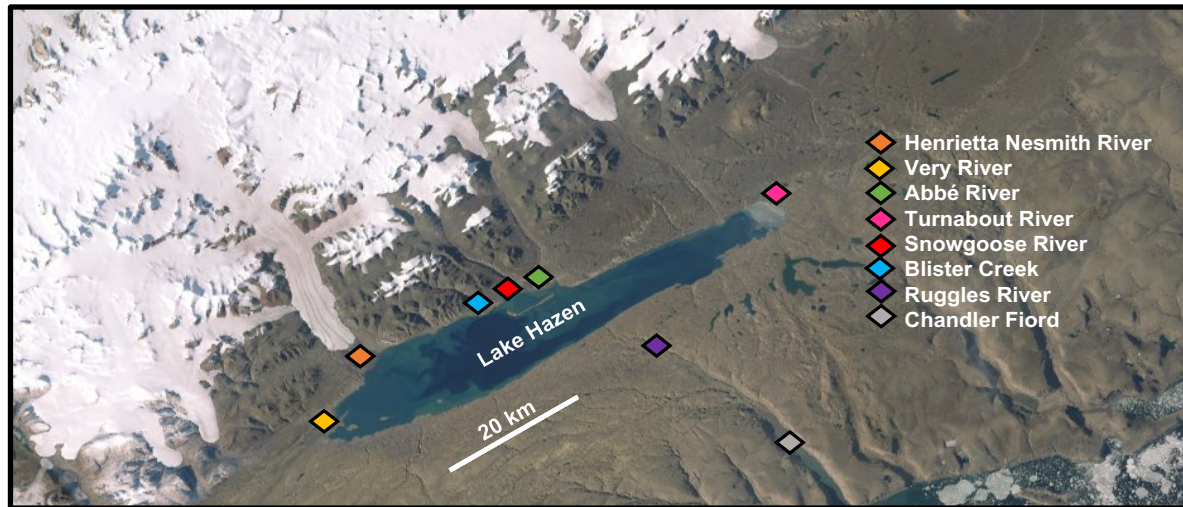


Figure 5.4 Map (top), concentration (ng L^{-1}) and composition (% , bottom) of PFAS in rivers from the Lake Hazen watershed in July 2015. Map source: ESRI.

Σ PFAS concentrations in glacial rivers are higher than those in surface waters, suggesting melting glaciers increase levels of PFAS in Lake Hazen. Chen et al. note similar findings, whereby glacial rivers in the Tibetan Plateau are implicated in the enhanced delivery of PFAS to Lake Nam Co.³¹ Σ PFAS concentrations in glacial rivers from the Lake Hazen watershed in 2015 are similar to those reported in the glacier-fed Qugaqie River in the Tibetan Plateau during 2017 (0.653-1.630 ng L⁻¹)³¹ and meltwaters from the Longyearbreen glacier in the High Arctic of Norway in 2006 (1.575 ng L⁻¹).³²

PFAS are detected in the outflow of Lake Hazen (i.e., the Ruggles River), which include C₄, C₆-C₉ PFCA and PFOS (Figure 5.4). PFBA (0.44 ng L⁻¹) and PFOA (0.066 ng L⁻¹) are most abundant, collectively accounting for 85% of the Σ PFAS concentration (0.59 ng L⁻¹). The Σ PFAS concentration in the Ruggles River is comparable to those in surface waters from Lake Hazen. Similar observations are reported in a recent study, where concentrations of MeHg and THg are similar in surface waters of Lake Hazen and the mouth of the Ruggles River.¹⁷

Glacial riverine fluxes are estimated to understand temporal variations in PFAS during the glacier melting season using a United States Geological Survey LOADEST log-linear model,¹⁷ produced by relating measured PFAS concentrations in all glacial rivers to their corresponding flow rates on the day of sampling. Σ PFAS glacial riverine fluxes are presented in Figure D3. The temporal profiles for Σ PFAS fluxes are similar in all glacial rivers, such that high Σ PFAS fluxes occur during the onset of glacier melting in mid-July, while low Σ PFAS fluxes occur before and after this period (Figure D3).

Our findings are similar to those reported by Chen et al. In that study, enhanced glacier melting is linked to higher Σ PFAS fluxes in the Qugaqie River.³¹ Glacial riverine

fluxes for Σ PFAS in the Qugaqie River (0.027-0.68 g day⁻¹) are similar to those at Blister Creek (0.00042-0.51 g day⁻¹, median 0.067 g day⁻¹) during July 2015, but are lower than Σ PFAS fluxes in other glacial rivers in the Lake Hazen watershed. For reference, glacial river fluxes for Σ PFAS during July are 1.0-44 g day⁻¹ at Henrietta Nesmith River, 0.90-16 g day⁻¹ at Very River, 0.072-14 g day⁻¹ at Turnabout River, 0.012-11 g day⁻¹ at Abbé River, and 0.0046-5.4 g day⁻¹ at Snowgoose River.

5.4.4 Glacial Riverine Discharge of PFAS into Lake Hazen

A recent study demonstrates the significant contribution of melting glaciers on the transport and fate of contaminants in the Lake Hazen watershed. For example, St. Pierre et al. use a mass balance model to demonstrate that Lake Hazen is a sink for MeHg and THg inputs that are primarily derived from melting glaciers.¹⁷ By analogy, it is likely that Lake Hazen is a sink for PFAS, considering PFAS are consistently detected throughout its water column¹⁵ and sediments.¹⁴

In this study, an approach adapted from St. Pierre et al.¹⁷ is used to estimate net PFAS inputs by glacial rivers into Lake Hazen and the output of PFAS by the Ruggles River according to Equation 2:

$$\Delta_{PFAS} = \sum_i^n C_i V_i - C_{Ruggles} V_{Ruggles} \text{ Equation 2}$$

where Δ_{PFAS} is the net PFAS input from glacial rivers (kg) into Lake Hazen, $\sum C_i V_i$ is the input of PFAS to Lake Hazen via glacier rivers based on the product of PFAS concentration in glacier river i , C_i , and volume of annual runoff for glacier river i , V_i ,

$C_{Ruggles}$ and $V_{Ruggles}$ are the PFAS concentration and annual volume of runoff in the Ruggles River.¹⁷

Table 5.2 Glacial inputs (kg) and the net change (Δ_{PFAS} , kg) of total PFAS, PFCA, and PFSA in the Lake Hazen watershed during 2015. Glacial inputs are calculated as the sum of daily glacial riverine fluxes during the 2015 glacier melting season from 1 June to 19 August. Fluxes are estimated using a LOADEST log-linear model. Uncertainty is represented by standard error.

Glacial River	ΣPFAS (kg)	ΣPFCA (kg)	ΣPFSA (kg)
Abbé River	0.13 ± 0.06	0.13 ± 0.06	0.003 ± 0.003
Blister Creek	0.006 ± 0.003	0.006 ± 0.002	0.0001 ± 0.0001
Gilman River	0.4 ± 0.2	0.3 ± 0.2	0.008 ± 0.007
Henrietta Nesmith River	0.5 ± 0.2	0.5 ± 0.2	0.01 ± 0.01
Snowgoose River	0.06 ± 0.03	0.06 ± 0.03	0.001 ± 0.001
Turnabout River	0.17 ± 0.08	0.17 ± 0.07	0.004 ± 0.003
Very River	0.3 ± 0.1	0.3 ± 0.1	0.007 ± 0.007
Total Glacial Input[†]	1.6 ± 0.7	1.6 ± 0.7	0.03 ± 0.03
Ruggles River Output	0.64	0.62	0.02
Δ_{PFAS}	0.96	0.98	0.01

[†]Glacial rivers sampled correspond to 84% of watershed area. A factor of 1.19 was applied to scale the total glacial input to the entire watershed.

The total input of PFAS by glacial rivers into Lake Hazen is estimated at 1.6 ± 0.7 kg, whereas the discharge of PFAS from the Ruggles River is estimated at 0.64 kg (Table 5.2). These results indicate a positive net change of 0.96 kg, suggesting PFAS glacial inputs have notable residence times in Lake Hazen.

PFAS inputs by glacial rivers into Lake Hazen are higher than those reported by Chen et al. in Lake Nam Co on the Tibetan Plateau. In that study, glacial rivers account for 27% of the 1.81 kg annual input of PFAS into Lake Namco (i.e., 0.49 kg).³¹ The contrast observed with our study is reflective of differences in hydrological inputs because Lake Nam Co receives less glacial meltwater runoff than Lake Hazen. For perspective, Lake Nam Co is supplied by 0.365 km³ of glacial runoff compared to 0.979 km³ in Lake Hazen during 2015. Chen et al. also note that precipitation inputs (29%, 0.52 kg) are similar to glacial runoff inputs into Lake Namco. As a point of comparison, we estimate PFAS inputs from 2014 snowpacks into Lake Hazen according to Equation 3:

$$\text{Input}_{\text{Snow}} = \Sigma\text{PFAS}_{\text{Dark}} \times \text{Area}_{\text{Dark}} + \Sigma\text{PFAS}_{\text{Light}} \times \text{Area}_{\text{Light}} \quad \text{Equation 3}$$

where $\text{Input}_{\text{Snow}}$ is the total snow input of PFAS into Lake Hazen (kg), $\Sigma\text{PFAS}_{\text{Dark}}$ and $\Sigma\text{PFAS}_{\text{Light}}$ are the average total PFAS loads (kg km⁻², converted from ng m⁻²) in dark and light snowpacks, while $\text{Area}_{\text{Dark}}$ and $\text{Area}_{\text{Light}}$ are areas of dark and light snowpacks on the ice surface of Lake Hazen (km²). Our analysis of light and dark snowpacks in 2014 was limited to the ice surface of Lake Hazen (544 km²), of which 55.3% (301 km²) was covered by dark snowpacks and 44.7% (243 km²) by light snowpacks.¹⁷ Given average total PFAS loads in dark (1.6×10^{-4} kg km⁻²) and light (2.4×10^{-4} kg km⁻²) snowpacks,^{14,15} estimated PFAS inputs from dark and light snowpacks are 0.040 kg and 0.058 kg, corresponding to a total of 0.098 kg. These estimates indicate that the total annual input of PFAS from 2014 snowpacks into Lake Hazen is approximately 16-times lower than those of glacial rivers, which highlights the importance of melting glaciers on the delivery of PFAS to freshwater ecosystems in the Lake Hazen watershed.

Our glacial mass balance for PFAS also contrasts a recent Lake Hazen study, whereby 95% of THg inputs by glacial rivers (16.4 kg) are sequestered in Lake Hazen.¹⁷ St. Pierre et al. note that Lake Hazen is a sink for Hg due to the enhanced delivery of particles via glacial rivers and turbid underflows, which transport Hg to the bottom of the lake.¹⁷ The contrasting mass balances for Hg and PFAS is likely due to differences in physicochemical properties because some PFAS have high water solubilities and are less likely to partition to particles in the water column and accumulate in lake sediments than Hg.

5.5 Conclusions

The results in this study provide unique insights into the sources, as well as the post-depositional transport and fate, of PFAS in High Arctic freshwater ecosystems in Canada. The composition profiles of PFAS along the Skeleton Continuum suggests this region receives inputs from snowmelt, ice contained in permafrost soils, and the atmosphere. The attenuation of PFAS in downstream sites along the Skeleton Continuum suggests plants and soils in High Arctic wetlands remove and store PFAS from water, which may have important implications on mitigating PFAS exposure to Arctic biota inhabiting these regions. This study demonstrates that melting glaciers are primary sources of PFAS in Lake Hazen. Elevated glacial inputs of legacy PFCA (i.e., PFOA and PFNA) into Lake Hazen provides further evidence that contemporary^{14,15} and historically archived¹⁴ emissions are prevalent in the High Arctic of Canada. It is expected that continued climate warming in the Lake Hazen watershed will enhance permafrost and

glacial inputs of PFAS into Lake Hazen and the export of PFAS to Arctic marine waters. These observations highlight the role of snow and ice melting on the transport and fate of PFAS in freshwater lakes from the High Arctic of Canada.

5.6 Literature Cited

- (1) Buck, R. C.; Franklin, J.; Berger, U.; Conder, J. M.; Cousins, I. T.; Voogt, P. De; Jensen, A. A.; Kannan, K.; Mabury, S. A.; van Leeuwen, S. P. J. Perfluoroalkyl and polyfluoroalkyl substances in the environment: Terminology, classification, and origins. *Integr. Environ. Assess. Manag.* **2011**, *7* (4), 513–541.
- (2) Butt, C. M.; Berger, U.; Bossi, R.; Tomy, G. T. Levels and trends of poly- and perfluorinated compounds in the arctic environment. *Sci. Total Environ.* **2010**, *408* (15), 2936–2965.
- (3) 3M Company. *Phase-out plan for POSF-based products*; US Environmental Protection Agency: St. Paul, MN, 2000.
- (4) USEPA. 2010/15 PFOA Stewardship Program <https://www.epa.gov/assessing-and-managing-chemicals-under-tsca> (accessed May 1, 2017).
- (5) Environment and Climate Change Canada. Environmental Performance Agreement (“Agreement”) Respecting Perfluorinated Carboxylic Acids (PFCAs) and their Precursors in Perfluorochemical Products Sold in Canada <http://ec.gc.ca/epe-epa/default.asp?lang=En&n=81AE80CE-1> (accessed Feb 13, 2018).
- (6) Wang, Z.; Cousins, I. T.; Scheringer, M.; Buck, R. C.; Hungerbühler, K. Global emission inventories for C₄-C₁₄ perfluoroalkyl carboxylic acid (PFCA) homologues from 1951 to 2030, Part I: Production and emissions from quantifiable sources. *Environ. Int.* **2014**, *70*, 62–75.
- (7) Wang, Z.; Boucher, J. M.; Scheringer, M.; Cousins, I. T.; Hungerbühler, K. Toward a Comprehensive Global Emission Inventory of C₄-C₁₀

- Perfluoroalkanesulfonic Acids (PFASs) and Related Precursors: Focus on the Life Cycle of C₈-Based Products and Ongoing Industrial Transition. *Environ. Sci. Technol.* **2017**, *51* (8), 4482–4493.
- (8) Boucher, J. M.; Cousins, I. T.; Scheringer, M.; Hungerbühler, K.; Wang, Z. Toward a Comprehensive Global Emission Inventory of C₄–C₁₀ Perfluoroalkanesulfonic Acids (PFASs) and Related Precursors: Focus on the Life Cycle of C₆- and C₁₀-Based Products. *Environ. Sci. Technol. Lett.* **2019**, *6*, 1–7.
- (9) Yeung, L. W. Y.; Dassuncao, C.; Mabury, S.; Sunderland, E. M.; Zhang, X.; Lohmann, R. Vertical Profiles, Sources, and Transport of PFASs in the Arctic Ocean. *Environ. Sci. Technol.* **2017**, *51* (12), 6735–6744.
- (10) Skaar, J. S.; Ræder, E. M.; Lyche, J. L.; Ahrens, L.; Kallenborn, R. Elucidation of contamination sources for poly- and perfluoroalkyl substances (PFASs) on Svalbard (Norwegian Arctic). *Environ. Sci. Pollut. Res.* **2019**, *26* (8), 7356–7363.
- (11) Cabrerizo, A.; Muir, D. C. G.; De Silva, A. O.; Wang, X.; Lamoureux, S. F.; Lafrenière, M. J. Legacy and Emerging Persistent Organic Pollutants (POPs) in Terrestrial Compartments in the High Arctic: Sorption and Secondary Sources. *Environ. Sci. Technol.* **2018**, *52* (24), 14187–14197.
- (12) Veillette, J.; Muir, D.; Antoniades, D.; Small, J. M.; Spencer, C.; Loewen, T. N.; Babaluk, J. A.; Reist, J. D.; Vincent, W. F. Perfluorinated chemicals in meromictic lakes on the northern coast of Ellesmere Island, High Arctic Canada. *Arctic* **2012**, *65*, 245–256.
- (13) Lescord, G. L.; Kidd, K. A.; De Silva, A. O.; Williamson, M.; Spencer, C.; Wang, X.; Muir, D. C. G. Perfluorinated and polyfluorinated compounds in lake food

- webs from the Canadian High Arctic. *Environ. Sci. Technol.* **2015**, *49* (5), 2694–2702.
- (14) MacInnis, J. J.; Lehnherr, I.; Muir, D. C. G.; Quinlan, R.; De Silva, A. O. Characterization of perfluoroalkyl substances in sediment cores from High and Low Arctic lakes in Canada. *Sci. Total Environ.* **2019**, *666*, 414–422.
- (15) MacInnis, J. J.; Lehnherr, I.; Muir, D. C. G.; St. Pierre, K. A.; St. Louis, V. L.; Spencer, C.; De Silva, A. O. Fate and transport of perfluoroalkyl substances from snowpacks into a lake in the High Arctic of Canada. *Environ. Sci. Technol.* **2019**, *53* (18), 10753–10762.
- (16) Lehnherr, I.; St. Louis, V. L.; Sharp, M.; Gardner, A.; Smol, J.; Schiff, S.; Muir, D.; Mortimer, C.; Michelutti, N.; Tarnocai, C.; St. Pierre, K.; Emmerton, C.; Wiklund, J.; Köck, G.; Lamoureux, S.; Talbot, C. The world's largest High Arctic lake responds rapidly to climate warming. *Nat. Commun.* **2018**, *9*, 1–9.
- (17) St. Pierre, K. A.; St. Louis, V. L.; Lehnherr, I.; Gardner, A. S.; Serbu, J. A.; Mortimer, C. A.; Muir, D. C. G.; Wiklund, J. A.; Lemire, D.; Szostek, L.; Talbot, C. Drivers of Mercury Cycling in the Rapidly Changing Glacierized Watershed of the High Arctic's Largest Lake by Volume (Lake Hazen, Nunavut, Canada). *Environ. Sci. Technol.* **2019**, *53* (3), 1175–1185.
- (18) St. Pierre, K. A.; St. Louis, V. L.; Lehnherr, I.; Schiff, S. L.; Muir, D. C. G.; Poulain, A. J.; Smol, J. P.; Talbot, C.; Ma, M.; Findlay, D. L.; Arnott, S.E.; Gardner, A.S. Contemporary limnology of the rapidly changing glacierized watershed of the world's largest High Arctic lake. *Sci. Rep.* **2019**, *9* (1), 1–15.
- (19) Emmerton, C. A.; Louis, V. L. S.; Lehnherr, I.; Graydon, J. A.; Kirk, J. L.;

- Rondeau, K. J. The importance of freshwater systems to the net atmospheric exchange of carbon dioxide and methane with a rapidly changing high Arctic watershed. *Biogeosciences* **2016**, *13* (20), 5849–5863.
- (20) Lehnherr, I.; St. Louis, V. L.; Kirk, J. L. Methylmercury cycling in high arctic wetland ponds: Controls on sedimentary production. *Environ. Sci. Technol.* **2012**, *46* (19), 10523–10531.
- (21) Emmerton, C. A.; St. Louis, V. L.; Humphreys, E. R.; Gamon, J. A.; Barker, J. D.; Pastorello, G. Z. Net ecosystem exchange of CO₂ with rapidly changing high Arctic landscapes. *Glob. Chang. Biol.* **2016**, *22* (3), 1185–1200.
- (22) MacInnis, J. J.; French, K.; Muir, D. C. G.; Spencer, C.; Criscitiello, A.; De Silva, A. O.; Young, C. J. Emerging investigator series: a 14-year depositional ice record of perfluoroalkyl substances in the High Arctic. *Environ. Sci. Process. Impacts* **2017**, *19* (1), 22–30.
- (23) Pickard, H. M.; Criscitiello, A. S.; Spencer, C.; Sharp, M. J.; Muir, D. C. G.; Silva, A. O. De; Young, C. J. Continuous Non-Marine Inputs of Per- and Polyfluoroalkyl Substances to the High Arctic : A Multi-Decadal Temporal Record. *Atmos. Chem. Phys. Discuss.* **2018**, *18* (7), 5045-5058.
- (24) Campos Pereira, H.; Ullberg, M.; Kleja, D. B.; Gustafsson, J. P.; Ahrens, L. Sorption of perfluoroalkyl substances (PFASs) to an organic soil horizon – Effect of cation composition and pH. *Chemosphere* **2018**, *207*, 183-191.
- (25) Norwegian Environment Agency. *Investigation of sources to PFHxS in the environment Investigation of sources to PFHxS in the environment Final Report*; Oslo, Norway, 2018.

- (26) Filipovic, M.; Laudon, H.; McLachlan, M. S.; Berger, U. Mass Balance of Perfluorinated Alkyl Acids in a Pristine Boreal Catchment. *Environ. Sci. Technol.* **2015**, *49* (20), 12127–12135.
- (27) Müller, C. E.; Lefevre, G. H.; Timofte, A. E.; Hussain, F. A.; Sattely, E. S.; Luthy, R. G. Competing mechanisms for perfluoroalkyl acid accumulation in plants revealed using an Arabidopsis model system. *Environ. Toxicol. Chem.* **2016**, *35* (5), 1138–1147.
- (28) Chen, Y.C.; Lo, S.L.; Lee, Y.C. Distribution and fate of perfluorinated compounds (PFCs) in a pilot constructed wetland. *Desalin. Water Treat.* **2011**, 178–184.
- (29) Yin, T.; Chen, H.; Reinhard, M.; Yi, X.; He, Y.; Gin, K. Y. H. Perfluoroalkyl and polyfluoroalkyl substances removal in a full-scale tropical constructed wetland system treating landfill leachate. *Water Res.* **2017**, *125*, 418–426.
- (30) Sinnatamby, R. N.; Babaluk, J. A.; Power, G.; Reist, J. D.; Power, M. Summer habitat use and feeding of juvenile Arctic charr, *Salvelinus alpinus*, in the Canadian High Arctic. *Ecol. Freshw. Fish* **2012**, *21* (2), 309–322.
- (31) Chen, M.; Wang, C.; Wang, X.; Fu, J.; Gong, P.; Yan, J.; Yu, Z.; Yan, F.; Nawab, J. Release of perfluoroalkyl substances from melting glacier of the Tibetan Plateau: Insights into the impact of global warming on the cycling of emerging pollutants. *J. Geophys. Res. Atmos.* **2019**, *124* (13), 7442–7456.
- (32) Kwok, K. Y.; Yamazaki, E.; Yamashita, N.; Taniyasu, S.; Murphy, M. B.; Horii, Y.; Petrick, G.; Kallerborn, R.; Kannan, K.; Murano, K.; Lam, P.K.S. Transport of Perfluoroalkyl substances (PFAS) from an arctic glacier to downstream locations: Implications for sources. *Sci. Total Environ.* **2013**, *447*, 46–55.

6 Conclusions

6.1 Summary

This work demonstrates that remote sample collection is an effective practice for understanding the long-range transport of PFAS to the Arctic. In particular, ice caps and landlocked Arctic lakes are useful for understanding long-range atmospheric transport because these areas are uninhabited, removed from anthropogenic pollution, and accumulate atmospheric PFAS pollution over time. This work highlights that PFAS are amenable to post-depositional transport in Arctic environments that are responding to climate warming. The findings of this work that improve current understanding of long-range atmospheric transport, as well as the post-depositional transport and fate of PFAS to and within the Arctic are summarized below.

In Chapter 2, an ice record on the Devon Ice Cap indicates that PFAS are continuously transported to the High Arctic and are increasing from 1993 to 2007. The analysis of PFCA in snow on the Devon Ice Cap suggests this region is primarily impacted by indirect sources via the long-range atmospheric transport and oxidation of FTOH; however, the unique presence of PFECHS on the Devon Ice Cap indicates a direct source, such as emissions from commercial aircraft.

In Chapter 3, sediment records in Lake Hazen and Lake B35 indicate that PFAS are transported to the Arctic of Canada and are increasing since the 1950s. PFCA deposition in Arctic sediments is consistent with fluorotelomer production over time, suggesting emissions from fluorotelomer-based products are primary historical sources. PFAS deposition is faster to Lake Hazen sediments than Lake B35 sediments, which is attributed to the influence of climate warming-induced glacier melting enhancing the

delivery of sediment and glacial meltwater into Lake Hazen. A general consistency is observed for PFOA deposition to Lake B35 sediments and the Devon Ice Cap, and PFOS deposition to Lake Hazen sediments and the Devon Ice Cap, which suggests these regions are influenced by similar atmospheric sources.

In Chapter 4, the analysis of snowpacks from the Lake Hazen region demonstrates that snow is a short-term repository for atmospheric PFAS pollution, pursuant to the role of LAP on accelerating snowpack melting and remobilizing PFAS into surface waters of Lake Hazen. PFAS pollution is derived from the long-range atmospheric transport and oxidation of fluorotelomer and PFSAm precursors. The seasonal analysis of the Lake Hazen water column demonstrates that melting glaciers govern the mixing of PFAS in Lake Hazen.

In Chapter 5, the analysis of water along the Skeleton Continuum in the Lake Hazen watershed indicates for the first time that climate warming is a vector for the remobilization of PFAS historically archived in permafrost, and meadow wetlands remove and store PFAS from water in the High Arctic. The analysis of glacial rivers in the Lake Hazen watershed demonstrates glaciers are dominant sources of PFAS in Lake Hazen.

6.2 Future Outlook

6.2.1 Atmospheric Transport and Fate of PFAS in the Arctic

The observation of PFAS in ice caps and landlocked lakes in Arctic Canada demonstrates long-range atmospheric transport, however, the mechanisms are not fully

understood. While it is confirmed that volatile precursors can undergo long-range atmospheric transport to the Arctic,¹⁻⁶ the underlying mechanisms for this mode of transport are not well understood, considering FTOH and FOSE are detected in gas and particle phase samples in the Arctic atmosphere.^{5,6} By extension, the atmospheric fate of their oxidation products (i.e., PFAA) is unclear, as they partition to^{4,6} and/or are produced within particles,⁷ all of which may occur during long-range atmospheric transport or locally within the Arctic. Furthermore, while several experiments have examined PFAS partitioning^{7,8} and oxidation⁷ within mineral dust and ash particles, the particles in those studies may not be representative of particles in the Arctic atmosphere. Particles in the Arctic atmosphere are chemically complex, considering they are derived from local and long-range sources (e.g., Arctic haze) and are subjected to reactions with gases and other particles (aging and coagulation).⁹ We observe a positive association of PFAS with sea spray, mineral dust, and combustion aerosol tracers in light and dark snowpacks from the Lake Hazen region, which suggests aged particles may scavenge PFAS in the atmosphere. Future studies should focus on examining the partitioning behavior of PFAS to aged particles under representative conditions of the Arctic atmosphere (i.e., sub-zero temperatures and low relative humidity). These studies will provide insights into the role of Arctic haze on the transport and fate of PFAS in the Arctic.

6.2.2 Implications of Climate Warming on PFAS in the Arctic

Our study on the Devon Ice Cap indicates that ice cores are useful for reconstructing historical records of atmospheric pollution because ice caps preserve

atmospheric deposition over time. We note that increasing temperatures on the Devon Ice Cap can bias the seasonal assignment of PFAS deposition due to post-depositional melting effects, whereas annual assignments should not be affected because meltwater refreezes within an annual snow layer. However, ice cores may become unsuitable for reconstructing historical records of atmospheric pollution in the future with continued climate warming. For instance, if temperatures in the Arctic increase, then it is possible enhanced melting on ice caps will result in the integration of meltwaters from different annual time periods. We observe enhanced melting and the integration of meltwaters from different time periods in the Lake Hazen watershed, pursuant to the observation of elevated PFAS fluxes in Lake Hazen sediments and the unique presence of PFBS and PFHxS in permafrost thaw streams during strong melting years. Our results suggest that climate warming is an important vector for the remobilization of stored PFAS in glaciers in the High Arctic of Canada. This suggests climate warming can render remote environmental archives unsuitable for tracking historical market trends in PFAS manufacturing and the efficacy of phase-out initiatives in the future. It is expected that climate warming-induced glacier melting will enhance freshwater inventories and the exposure of PFAS to Arctic foodwebs.

Climate warming is expected to promote local anthropogenic pollution in the Arctic. For example, increasing temperatures enhance sea ice and ground ice melting in the Arctic, which leads to increasing ship traffic and land development related to the extraction of natural resources (e.g., oil and gas).⁹ An important environmental consequence of these activities is the emission of gases and particles that alter the albedo of ice and snow in the Arctic. We note that LAP enhance snow and glacier melting in the

Lake Hazen watershed and are relevant to the scavenging and transport of PFAS in the atmosphere. Thus, increasing emissions of LAP in the Arctic may enhance snow and glacier ice melting and PFAS scavenging from the Arctic atmosphere. Particle loads are highest in the Arctic atmosphere during the late winter and early spring (i.e., Arctic haze).⁹ However, it is possible that sustained year-round local pollution will enhance particle loads and local PFAS scavenging in the Arctic atmosphere. Future work should focus on the continued monitoring of PFAS in Arctic environments that are responding to climate change.

The results presented in this thesis provide unique insights into the role of climate warming on the release of stored PFAS from the global cryosphere.

6.3 Literature Cited

- (1) Young, C. J.; Furdui, V. I.; Franklin, J.; Koerner, R. M.; Muir, D. C. G.; Mabury, S. A. Perfluorinated acids in Arctic snow: New evidence for atmospheric formation. *Environ. Sci. Technol.* **2007**, *41*, 3455–3461.
- (2) MacInnis, J. J.; French, K.; Muir, D. C. .; Spencer, C.; Criscitiello, A.; De Silva, A. O.; Young, C. J. Emerging investigator series: a 14-year depositional ice record of perfluoroalkyl substances in the High Arctic. *Environ. Sci. Process. Impacts* **2017**, *19* (1), 22–30.
- (3) Pickard, H. M.; Criscitiello, A. S.; Spencer, C.; Sharp, M. J.; Muir, D. C. G.; Silva, A. O. De; Young, C. J. Continuous Non-Marine Inputs of Per- and Polyfluoroalkyl Substances to the High Arctic: A Multi-Decadal Temporal Record. *Atmos. Chem. Phys. Discuss.* **2018**, *18* (7), 5045–5058.
- (4) Wong, F.; Shoeib, M.; Katsoyiannis, A.; Eckhardt, S.; Stohl, A.; Bohlin-Nizzetto, P.; Li, H.; Fellin, P.; Su, Y.; Hung, H. Assessing temporal trends and source regions of per- and polyfluoroalkyl substances (PFASs) in air under the Arctic Monitoring and Assessment Programme (AMAP). *Atmos. Environ.* **2018**, *172*, 65–73.
- (5) Shoeib, M.; Harner, T.; Vlahos, P. Perfluorinated chemicals in the arctic atmosphere. *Environ. Sci. Technol.* **2006**, *40* (24), 7577–7583.
- (6) Stock, N. L.; Furdui, V. I.; Muir, D. C. G.; Mabury, S. A. Perfluoroalkyl contaminants in the Canadian Arctic: Evidence of atmospheric transport and local contamination. *Environ. Sci. Technol.* **2007**, *41*, 3529–3536.

- (7) Styler, S. A.; Myers, A. L.; Donaldson, D. J. Heterogeneous photooxidation of fluorotelomer alcohols: A new source of aerosol-phase perfluorinated carboxylic acids. *Environ. Sci. Technol.* **2013**, *47* (12), 6358–6367.
- (8) Arp, H. P. H.; Goss, K. U. Gas/particle partitioning behavior of perfluorocarboxylic acids with terrestrial aerosols. *Environ. Sci. Technol.* **2009**, *43* (22), 8542–8547.
- (9) Willis, M. D.; Leitch, W. R.; Abbatt, J. P. D. Processes Controlling the Composition and Abundance of Arctic Aerosol. *Rev. Geophys.* **2018**, *56* (4), 621–671.

Appendix A Supporting Information for Chapter 2

Section A1 Chemicals and QA/QC

Targeted analytes on the Devon Ice Cap include: perfluorobutanoic acid (PFBA), perfluoropentanoic acid (PFPeA), perfluorohexanoic acid (PFHxA), perfluoroheptanoic acid (PFHpA), perfluorooctanoic acid (PFOA), perfluorononanoic acid (PFNA), perfluorodecanoic acid (PFDA), perfluoroundecanoic acid (PFUnDA), perfluorododecanoic acid (PFDoDA), perfluorotridecanoic acid (PFTrDA), perfluorotetradecanoic acid (PFTeDA), perfluorohexadecanoic acid (PFHxDA), perfluorooctadecanoic acid (PFOcDA), perfluorobutane sulfonic acid (PFBS), perfluorohexane sulfonic acid (PFHxS), perfluoroheptane sulfonic acid (PFHpS), perfluorooctane sulfonic acid (PFOS), perfluoro-4-ethylcyclohexane sulfonic acid (PFECHS), perfluorodecane sulfonic acid (PFDS), and perfluorooctane sulfonamide (FOSA). PFAS standards were obtained from Wellington Laboratories (Guelph, Ontario, Canada). These analytes were selected for analysis because standardized methods are developed for this series of PFAS in the analytical laboratory. The PFECHS standard used in this study is composed of cis/trans isomers and other minor impurities such as perfluoro-4,4-dimethylcyclohexane sulfonate, perfluoro-3-ethyl-3-methylcyclopentane sulfonate, and perfluoro-3-propylcyclopentane sulfonate. PFECHS was quantified in samples by integrating all peaks (i.e., cis/trans isomers and impurities) across their retention time window. Contamination is rarely observed in cartridge blanks. Due to the common presence of trace PFAA in purchased reagent water, water (Fisher Brand HPLC Grade, ThermoFisher) used in the mobile phase was subjected to additional cleaning through Oasis® WAX SPE.

Table A1 PFAS concentrations (ng L⁻¹) in field, stay, and method blanks, as well as the limits of detection (LOD) and quantitation (LOQ). Stay and field blanks consist of 500 mL of HPLC grade water.

PFAS	LOD	LOQ	Stay Blank	Field Blanks	Method Blanks
PFBA	0.010	0.050	<0.010	<0.010	0.042-0.058
PFPeA	0.007	0.020	<0.007	<0.007	<0.007
PFHxA	0.001	0.004	0.476	0.255-0.265	<0.001
PFHpA	0.002	0.005	0.037	0.045-0.046	<0.002
PFOA	0.002	0.006	0.332	0.34-0.36	0.002-0.005
PFNA	0.002	0.006	0.061	0.061-0.063	<0.002
PFDA	0.001	0.004	0.158	0.15-0.16	<0.001
PFUnDA	0.001	0.005	0.016	0.012-0.019	<0.001
PFDoDA	0.001	0.004	0.028	0.026-0.030	<0.001
PFTTrDA	0.001	0.004	<0.001	<0.001	<0.001
PFTeDA	0.002	0.005	<0.002	<0.002	<0.002
PFHxDA	0.006	0.020	<0.006	<0.006	<0.006
PFOcDA	0.010	0.040	<0.010	<0.010	<0.010
PFECHS	0.0003	0.001	<0.0003	<0.0003	<0.0003
PFBS	0.004	0.010	0.002	0.002-0.003	<0.004
PFHxS	0.001	0.004	<0.001	<0.001	<0.001
PFHpS	0.001	0.004	<0.001	<0.001	<0.001
PFOS	0.001	0.004	0.018	0.014-0.018	<0.001
PFDS	0.002	0.007	<0.002	<0.002	<0.002
FOSA	0.001	0.003	<0.001	<0.001	0.022-0.025

Table A2 Recovery of internal and instrument performance standards in sample extracts.

Internal standards are added before extraction to monitor recovery and instrument performance standards are added after extraction prior to analysis to monitor matrix effects. Recovery is based on a comparison of internal standard peak area in sample extracts to the peak area in a solvent standard at equivalent concentrations. Mean (standard error) recovery reported for n=18 samples from the Devon Ice Cap.

Internal Standard	Recovery (%)	Instrument Performance	Recovery (%)
¹³ C ₄ PFBA	64 (3)	¹³ C ₃ PFBA	98 (3)
¹³ C ₅ PFPeA	71 (4)	¹³ C ₃ PFPeA	98 (1)
¹³ C ₂ PFHxA	73 (3)	¹³ C ₅ PFHxA	100 (1)
¹³ C ₄ PFHpA	74 (3)		
¹³ C ₄ PFOA	89 (3)	¹³ C ₂ PFOA	105 (1)
¹³ C ₅ PFNA	86 (3)	¹³ C ₉ PFNA	97 (1)
¹³ C ₂ PFDA	83 (2)	¹³ C ₆ PFDA	95 (1)
¹³ C ₇ PFUnDA	99 (1)	¹³ C ₂ PFUnDA	86 (1)
¹³ C ₂ PFDoDA	74 (1)		
¹³ C ₂ PFTeDA	50 (3)		
¹³ C ₂ PFHxDA	98 (9)		
¹³ C ₄ PFOS 99	98 (1)	¹³ C ₈ PFOS 99	100 (1)
¹³ C ₄ PFOS 80	97 (1)	¹³ C ₈ PFOS 80	101 (1)
¹⁸ O ₂ PFHxS 103	102 (1)	¹³ C ₃ PFHxS 99	104 (1)
¹⁸ O ₂ PFHxS 84	103 (1)		

Table A3 Overview of native, internal, and instrument performance PFAS standards.

Native Standard	Internal Standard	Instrument Performance
PFBA	¹³ C ₄ PFBA	¹³ C ₃ PFBA
PFPeA	¹³ C ₅ PFPeA	¹³ C ₃ PFPeA
PFHxA	¹³ C ₂ PFHxA	¹³ C ₅ PFHxA
PFHpA	¹³ C ₄ PFHpA	
PFOA	¹³ C ₄ PFOA	¹³ C ₂ PFOA
PFNA	¹³ C ₅ PFNA	¹³ C ₉ PFNA
PFDA	¹³ C ₂ PFDA	¹³ C ₆ PFDA
PFUnDA	¹³ C ₂ PFUnDA	¹³ C ₇ PFUnDA
PFDoDA	¹³ C ₂ PFDoDA	
PFTTrDA	¹³ C ₂ PFTTrDA	
PFTeDA	¹³ C ₂ PFTeDA	
PFHxDA	¹³ C ₂ PFHxDA	
PFOcDA	¹³ C ₂ PFOcDA	
PFBS	¹⁸ O ₂ PFHxS	
PFHxS	¹⁸ O ₂ PFHxS	¹³ C ₃ PFHxS
PFHpS	¹⁸ O ₂ PFHxS	
PFOS	¹³ C ₄ PFOS	¹³ C ₈ PFOS
PFDS	¹³ C ₄ PFOS	
PFECHS	¹⁸ O ₂ PFHxS	
FOSA	¹³ C ₈ FOSA	

Table A4 Overview of precursor/product ion mass-to-charge ratios (m/z), cone voltages (V), and collision energies (eV) for PFAS analysis on the Devon Ice Cap. Product ion scans for PFCA target perfluoroalkyl moieties (i.e., $F(CF_2)_xCO_2^-$ to $F(CF_2)_x$), while product ion scans for PFSA target sulfonic acid moieties (i.e., $F(CF_2)_xSO_3^-$ to FSO_3^- or SO_3^-). The product ion scan for FOSA targets a SO_2N moiety (i.e., $CF_3(CF_2)_7SO_2NH_2$ to SO_2N).

Congener	Quantifier m/z	Cone Voltage	Collision Energy	Qualifier m/z	Cone Voltage	Collision Energy
PFBA	213/169	6	10			
PFPeA	263/219	6	15			
PFHxA	313/269	6	10	313/119	6	17
PFHpA	363/319	8	10	363/119	8	18
PFOA	413/369	16	11	413/169	16	18
PFNA	463/419	16	10	463/219	16	17
PFDA	513/469	16	10	513/219	16	17
PFUnDA	563/519	18	10	563/319	18	17
PFDoDA	613/569	18	12	613/169	18	28
PFTTrDA	663/619	18	12	663/169	18	30
PFTeDA	713/669	26	12	713/169	26	30
PFHxDA	813/769	36	14	813/169	36	36
PFBS	299/80	42	30	299/99	42	30
PFHxS	399/80	42	32	399/99	42	32
PFHpS	449/80	42	44	449/99	42	36
PFOS	499/80	46	40	499/99	46	36
PFDS	599/80	42	46	599/99	42	44
PFECHS	461/381	42	30	461/99	42	26
FOSA	498/78	46	30			

Table A5 Overview of precursor/product ion mass-to-charge ratios, cone voltages (V), and collision energies (eV) for internal and instrument performance PFAS standard analysis.

Internal Standard		Cone Voltage	Collision Energy
¹³ C ₄ PFBA	217/172	6	10
¹³ C ₅ PFPeA	268/223	6	15
¹³ C ₂ PFHxA	315/270	6	10
¹³ C ₄ PFHpA	367/322	8	10
¹³ C ₄ PFOA	417/372	16	10
¹³ C ₅ PFNA	468/423	16	14
¹³ C ₂ PFDA	515/470	16	16
¹³ C ₂ PFUnDA	565/520	18	10
¹³ C ₂ PFDoDA	615/570	18	12
¹³ C ₂ PFTeDA	715/670	26	12
¹³ C ₂ PFHxDA	815/770	36	14
¹⁸ O ₂ PFHxS	403/84	42	38
¹⁸ O ₂ PFHxS	403/103	42	32
¹³ C ₄ PFOS	503/80	46	48
¹³ C ₈ FOSA	506/78	46	28
Instrument Performance		Cone Voltage	Collision Energy
¹³ C ₃ PFBA	216/172	6	10
¹³ C ₃ PFPeA	266/222	6	15
¹³ C ₅ PFHxA	318/273	6	10
¹³ C ₂ PFOA	415/370	16	10
¹³ C ₉ PFNA	472/427	16	14
¹³ C ₆ PFDA	519/474	16	12
¹³ C ₇ PFUnDA	570/525	18	10
¹³ C ₃ PFHxS	402/99	42	32
¹³ C ₈ PFOS	507/99	46	36

Table A6 Summary of chromatographic, mass spectrometric, and inlet conditions.

Liquid Chromatograph Gradient Elution				Mass Spectrometer/Inlet	
Time (min)	Flow Rate (mL min⁻¹)	H₂O (%)	MeOH (%)	Ionization mode: electrospray negative	
0	0.400	75	25		
0.5	0.400	75	25	Capillary Voltage (kV)	0.5
5.0	0.400	15	85	Source Temperature (°C)	150
5.1	0.400	0	100	Desolvation Gas Temperature (°C)	450
5.6	0.400	0	100	Cone Gas Flow (L hr ⁻¹)	150
7.0	0.550	0	100	Desolvation Gas Flow (L hr ⁻¹)	650
9.0	0.400	75	25	Collision Gas Flow (mL min ⁻¹)	0.15
12.0	0.400	75	25	Nebulizer Pressure (bar)	7
Inlet parameters					
Column Temperature (°C)				50	
Injection Volume (μL)				9	

Table A7 Overview of PFAS concentrations (pg L^{-1}) in the snowpit from the Devon Ice Cap. Detection frequency (%) is calculated as the number samples equal to or greater than the LOD, divide by the sample size, and multiply by 100.

Congener	Median (pg L^{-1})	Range (pg L^{-1})	Frequency (%)
PFBA	290	120 – 2000	100
PFPeA	100	34 – 460	100
PFHxA	130	<1 – 410	93
PFHpA	190	<2 – 690	96
PFOA	240	69 – 680	100
PFNA	400	35 – 1400	100
PFDA	71	13 – 230	100
PFUnDA	85	14 – 350	100
PFDoDA	7	<1 – 32	75
PFTTrDA	6	<1 – 26	64
PFTeDA	<2	<2 – 8	14
PFHxDA	<6	<6	0
PFOcDA	<10	<10	0
PFBS	110	<4 – 230	89
PFHxS	<1	<1	0
PFHpS	<1	<1	0
PFOS	15	<1 – 27	89
PFECHS	10	<0.3 – 20	89
PFDS	<2	<2 – 9	14
FOSA	35	<1 – 130	93

Table A8 Spearman rank correlation analysis of natural log-transformed PFAS concentrations (ng L⁻¹) in snow collected from the Devon Ice Cap ($n=28$) from 1993 to 2007. Spearman rank correlation coefficients (r_s) is used to evaluate correlation strength on PFAS concentrations equal to or greater than the LOQ for congeners with detection frequencies equal to or greater than 50%.

		PFBA	PFPeA	PFHxA	PFHpA	PFOA	PFNA	PFDA	PFUnDA	PFDoDA	PFTTrDA	PFOS	PFBS	PFECHS	FOSA	
PFPeA	r_s	0.42														
	p	0.02														
PFHxA	r_s	0.51	0.90													
	p	<0.01	<0.01													
PFHpA	r_s	0.33	0.87	0.84												
	p	0.09	<0.01	<0.01												
PFOA	r_s	-0.10	0.22	0.14	0.55											
	p	0.61	0.26	0.50	<0.01											
PFNA	r_s	-0.22	<0.01	-0.17	0.35	0.88										
	p	0.26	0.98	0.40	0.07	<0.01										
PFDA	r_s	-0.07	0.15	-0.02	0.45	0.91	0.91									
	p	0.70	0.45	0.90	0.02	<0.01	<0.01									
PFUnDA	r_s	-0.26	-0.19	-0.40	0.13	0.75	0.90	0.80								
	p	0.19	0.32	0.04	0.51	<0.01	<0.01	<0.01								
PFDoDA	r_s	-0.50	-0.24	-0.26	<0.01	0.35	0.62	0.43	0.83							
	p	0.02	0.30	0.27	0.98	0.11	<0.01	<0.05	<0.01							
PFTTrDA	r_s	-0.15	-0.06	-0.17	0.03	0.37	0.40	0.52	0.52	0.61						
	p	0.55	0.80	0.50	0.91	0.13	0.10	0.03	0.02	0.01						
PFOS	r_s	-0.27	0.01	0.11	-0.05	0.03	-0.07	<0.01	-0.13	-0.08	-0.22					
	p	0.19	0.96	0.59	0.82	0.88	0.75	1.00	0.52	0.74	0.37					
PFBS	r_s	<0.01	0.20	0.19	0.05	-0.03	-0.32	-0.22	-0.22	-0.33	-0.16	0.17				
	p	0.98	0.35	0.39	0.80	0.89	0.12	0.30	0.28	0.15	0.53	0.45				
PFECHS	r_s	0.02	-0.20	0.01	-0.41	-0.50	-0.63	-0.61	-0.54	-0.21	-0.39	0.34	0.21			
	p	0.90	0.35	0.95	<0.05	0.01	<0.01	<0.01	<0.01	0.38	0.11	0.11	0.34			
FOSA	r_s	-0.37	-0.54	-0.54	-0.64	-0.25	-0.19	-0.30	0.08	0.19	0.09	-0.03	0.23	0.36		
	p	0.06	<0.01	<0.01	<0.01	0.22	0.35	0.14	0.69	0.42	0.72	0.89	0.29	0.10		
Na ⁺	r_s	-0.18	-0.13	-0.27	-0.19	0.21	0.20	0.10	0.12	-0.08	-0.20	0.11	0.26	0.05	0.43	
	p	0.39	0.53	0.21	0.38	0.30	0.35	0.64	0.58	0.74	0.47	0.64	0.25	0.81	0.04	

Table A9 First-order kinetics of natural log-transformed PFAS fluxes on the Devon Ice Cap during 1993-2007. Temporal trends are determined using natural log-transformed PFAS mass flux ($\text{ng m}^{-2} \text{ year}^{-1}$) for congeners with detection frequencies $\geq 50\%$. Doubling times (t_2) and half-life ($t_{1/2}$) are calculated using the first-order rate (k) obtained from the slope of a linear regression of natural log-transformed mass flux versus year of deposition. Standard error is used to represent the uncertainty of k , while a 95% confidence interval (CI) represents the uncertainty for t_2 and $t_{1/2}$. The temporal trend for PFBS spans a period of 1996-2007 due to concentrations $< \text{LOD}$ in samples. Statistically significant ($p < 0.05$) temporal trends are not observed for PFBA, PFHxA, PFTrDA, PFOS, PFECHS, and FOSA.

Congener	r^2	p	k (year^{-1})	t_2 or $t_{1/2}$ (year)	95% CI (year)
PFBA	0.02	0.60	0.03 ± 0.05		
PFPeA	0.33	0.03	0.09 ± 0.03	7.9	4.2 – 56
PFHxA	0.05	0.40	0.03 ± 0.04		
PFHpA	0.42	< 0.01	0.11 ± 0.03	6.5	3.8 – 22
PFOA	0.49	< 0.01	0.12 ± 0.03	5.7	3.5 – 15
PFNA	0.64	< 0.01	0.18 ± 0.04	3.8	2.6 – 7.0
PFDA	0.59	< 0.01	0.14 ± 0.03	5.1	3.4 – 10
PFUnDA	0.50	< 0.01	0.17 ± 0.05	4.1	2.6 – 10
PFDoDA	0.40	0.02	0.12 ± 0.04	5.8	3.2 – 30
PFTrDA	0.23	0.08	0.15 ± 0.08		
PFBS	0.64	< 0.01	-0.07 ± 0.02	9.3	6.1 – 19
PFOS	0.02	0.65	0.01 ± 0.02		
PFECHS	< 0.01	0.84	-0.01 ± 0.04		
FOSA	0.06	0.37	-0.05 ± 0.06		

Appendix B Supporting Information for Chapter 3

Section B1 Study Area

Lake Hazen is the largest lake by volume north of the Arctic Circle (51.4 km³). The Lake Hazen watershed is classified as a polar semi-desert, receiving 95 mm of precipitation annually.¹ The Lake Hazen catchment includes portions of the Garfield Range, extending to 2500 m above sea level, which effectively shelters the Lake Hazen catchment area from polar winds. For this reason, the Lake Hazen region is considered a thermal oasis within a polar desert.² Water in the Lake Hazen basin undergoes mixing during the summer months, facilitated by the delivery of dense turbid glacial meltwater. The surface of Lake Hazen is ice-covered for approximately ten months per year, although lake ice extent and frequency of full ice-off is changing recently due to climate warming.³

Section B2 Chemicals

Twenty-three PFAS were targeted in Lake Hazen and Lake B35 sediments including: perfluorobutanoic acid (PFBA), perfluoropentanoic acid, (PFPeA), perfluorohexanoic acid (PFHxA), perfluoroheptanoic acid (PFHpA), perfluorooctanoic acid (PFOA), perfluorononanoic acid (PFNA), perfluorodecanoic acid (PFDA), perfluoroundecanoic acid (PFUnDA), perfluorododecanoic acid (PFDoDA), perfluorotridecanoic acid (PFTrDA), perfluorotetradecanoic acid (PFTeDA), perfluorohexadecanoic acid (PFHxDA), perfluorobutane sulfonic acid (PFBS), perfluorohexane sulfonic acid (PFHxS), perfluoroheptane sulfonic acid (PFHpS), perfluorooctane sulfonic acid (PFOS), perfluoro-4-ethylcyclohexane sulfonic acid

(PFECHS), perfluorodecane sulfonic acid (PFDS), ammonium 4,8-dioxa-3H-perfluorononanoate (ADONA), 8-chloroperfluoro-1-octane sulfonic acid (8-Cl-PFOS), 9-chlorohexadecafluoro-3-oxanonane-1-sulfonic acid (6:2 Cl-PFESA), 11-chloroeicosafuoro-3-oxaundecane-1-sulfonic acid (8:2 Cl-PFESA), and perfluorooctane sulfonamide (FOSA). All native and isotopically labeled PFAS were purchased from Wellington Laboratories (Guelph, Ontario), with the exception of PFECHS, which was purchased from Chiron AS (Trondheim, Norway). PFECHS was quantified as outlined in Appendix A (Section A1). These analytes were selected for analysis because standardized methods are developed for this series of PFAS in the analytical laboratory. Ammonia (NH₃, Suprapur® 25 %) was purchased from Merck (New Jersey, USA), methanol (MeOH, Optima™ Grade) and water (Optima™ Grade) was purchased from Fisher Scientific (New Hampshire, USA), glacial acetic acid (ACS Grade) was purchased from EMD (Etobicoke, Ontario), and ammonium acetate (>98%) was purchased from Sigma Aldrich (Missouri, USA).

Section B3 Sediment Extraction

30 µL of an isotopically labeled internal standard mixture was added to 0.5-1 g of sediment dry weight to correct for recovery and matrix effects during analysis. For Lake Hazen sediments, 3 mL of 0.1% ammonia in methanol (NH₃-MeOH) was added, then the sediment mixture was vortexed for 5 seconds, followed by sonication for 15 minutes, and placed on a rotating table for 30 minutes. Samples were centrifuged for 20 minutes at 2057·g_f and the supernatant were transferred to a new polypropylene (PP) centrifuge tube. This procedure was repeated twice, and all supernatant was combined into one PP

centrifuge tube, corresponding to a total extraction volume of 9 mL of 0.1 % NH₃-MeOH. This procedure was repeated for Lake B35 sediments, however, 4 mL of 0.1 % NH₃-MeOH was used for the extraction, corresponding to a total extraction volume of 12 mL 0.1 % NH₃-MeOH. The sediment samples were evaporated to dryness using nitrogen and were reconstituted in 1.5 mL of 0.1 % glacial acetic acid in MeOH, vortexed for 5 seconds, and heated for 30 minutes at 50 °C in a hot water bath. Extracts were reduced to 1 mL using nitrogen and were passed through a 0.45 µm nylon syringe filter (Chromatographic Specialties Inc., Brockville, Ontario). An isotopically labeled instrument performance standard was added prior to instrumental analysis to evaluate matrix effects. 1 mL acidified MeOH extracts were analyzed using ultra-high-performance liquid chromatography-tandem mass spectrometry. Due to low concentrations observed in Lake Hazen sediment extracts, the sediment samples were reanalyzed by reducing the extract to dryness and reconstituting in a 1:1 (v/v) solid phase extraction (SPE)-cleaned HPLC grade water (cleaned via Oasis® WAX SPE)/MeOH 0.5 mL extract. A final concentration of ~1 ng g⁻¹ for each isotopically labeled surrogate in 0.5 mL extracts was used for analysis. Lake B35 sediments were subjected to an additional clean-up procedure due to prominent matrix effects in the original sediment sample extracts. 1 mL acidified MeOH sediment extracts were diluted to 50 mL using SPE-cleaned HPLC grade water and were subjected to a WAX SPE method (6 cm³, 150 mg, 30 µm) using previously established methods.⁴⁻⁶ Briefly, SPE cartridges were pre-conditioned with 5 mL of 0.1 % NH₃-MeOH, 5 mL MeOH, and 5 mL of SPE-cleaned water. After loading the sample onto the cartridge at 0.5 mL min⁻¹, the cartridge was

washed with 4 mL of an ammonium acetate buffer solution (made with SPE-cleaned HPLC grade water) following sample loading. The cartridge was centrifuged at $2057 \cdot g_f$ to remove residual water then eluted using 8 mL 0.1 % NH_3 -MeOH to recover the PFCA and PFSA. Samples were evaporated to just dryness using nitrogen and reconstituted in a 1:1 (v/v) SPE-cleaned HPLC grade water/MeOH 0.5 mL extract.

Section B4 QA/QC

PFAS were quantified using a 15-point calibration curve, with concentrations ranging from 0.006 - 10 ng mL^{-1} . Spike and recovery experiments were conducted on Lake Hazen and Lake B35 sediments by spiking $20 \mu\text{L}$ of a native PFAS standard mixture onto sediments. These fortified samples were extracted in parallel with sediment samples. The recovery of PFAS in sediments were calculated by comparing analyte peak area in sediment extracts to analyte peak area in a solvent standard at equivalent concentrations. The recoveries of isotopically-labelled PFAS internal standards in Lake Hazen sediments are comparable to the those reported in sediments from Lake A, which reported recoveries of ^{13}C PFOA, ^{13}C PFNA, ^{13}C PFDA, ^{13}C PFUnDA, ^{13}C PFDoDA, and ^{13}C PFOS corresponding to $67 \pm 20\%$, $53 \pm 17\%$, $52 \pm 16\%$, $52 \pm 16\%$, $43 \pm 20\%$, and $50 \pm 16\%$, respectively.⁷ In contrast, the recoveries of PFAS internal standards in Lake Hazen and Lake B35 sediments are lower than those reported in Lake Ontario sediments, which are typically greater than 70% .⁸ It is possible additional clean-up procedures implemented in the latter study contributed to higher recoveries due to the enhanced removal and breakdown of matrix components in sediments.⁸ Method blanks were used to evaluate

positive biases during the extraction and analysis. The method blanks used during sediment extractions consisted of spiking 30 μL of a PFAS internal standard mixture into a PP centrifuge tube without a sediment matrix and carried through the full extraction procedure. PFOA was detected most abundantly of all PFAS in sediment extraction method blanks (0.031-0.062 ng g^{-1} dw, assuming a theoretical sample mass of 1 g), which is consistent with reported sediment extraction methods.⁹⁻¹¹ Sediment PFAS concentrations were blank, recovery, and matrix-corrected. Matrix effects were evaluated by comparing the peak area of isotopically labeled PFAS standards added after the extraction to the peak areas of PFAS in a solvent standard at equivalent concentrations.

The detection of PFAS in sediments preceding manufacturing periods in this study (i.e., <1950) is consistent with observations by Benskin et al., where PFCA are present in Lake Opabin and Lake Oesa sediments before 1948.¹² The presence of PFAS in sediments preceding manufacturing in Lake Hazen and Lake B35 is most likely attributed to biases during extraction and analysis and/or sediment dating errors; however, these data were not included in temporal trend analysis.

Section B5 Determining Sedimentation Rates in the High Arctic

Accurate dating in the High Arctic is challenging as a result of low fluxes of ^{210}Pb delivered from lower latitudes. The accurate dating and derivation of sedimentation rates using ^{210}Pb in Lake Hazen is further complicated by the presence of melting glaciers, considering they are vectors of atmospheric ^{210}Pb and sediment. As such, the temporal trends for PFAS in Lake Hazen should be interpreted with caution, considering these

trends are driven by the ^{210}Pb -derived sedimentation rates. Furthermore, the temporal trends depicted in this study are representative of depositional trends from one sediment core. Future work should involve collecting multiple sediment cores for PFAS analysis from different depositional zones in Lake Hazen.

Section B6 Temporal Trends in Lake Hazen and Lake B35 Sediments, and Wildlife Bank Tissue Archives

The doubling times for PFAS in Lake Hazen sediments are broadly consistent with those reported in Arctic biota (Table 3.1). In contrast, the doubling times of PFAS in Lake B35 sediments are longer than those reported in Arctic biota (Table 3.1). It is possible the longer doubling times for PFAS in Lake B35 sediments are attributed to dynamic historical emissions over time. For example, concentrations of PFOA in Lake B35 sediments increase from 0.047 to 0.206 ng g⁻¹ dw during 1952-1986, decrease from 0.206 to 0.083 ng g⁻¹ dw during 1986-1997, and increase from 0.083 to 0.357 ng g⁻¹ dw during 1997-2009, indicating this region is impacted by different emission sources over time. It is challenging to compare and contrast temporal trends using doubling times between abiotic and biotic samples due to differences in the fate and transport dynamics governing PFAS deposition in each medium. Biological temporal trends can be impacted by shifts in food web dynamics caused by changes in dietary strategies, shifts in habitat niche, and introduction of invasive species. Abiotic media are affected by a different set of factors. For example, elevated fluxes of PFAS in Lake Hazen sediments post-2005 is attributed to enhanced glacier melting, which remobilized PFAS archived in glacial ice

into the lake. Thus, the increased input of PFAS into Lake Hazen (and its biota) could render a temporal trend in Lake Hazen that is not directly comparable to Arctic seabirds from Prince Leopold Island. Nevertheless, the temporal trends for PFAS in Lake Hazen and Lake B35 sediments are consistent with the continuous annual delivery of PFAS to the Arctic of Canada and trends in Arctic biota. For example, increasing temporal trends have been reported for PFOS and C₉-C₁₁ PFCA in polar bear livers from Baffin Island, Nunavut during 1972-2002;¹³ C₉-C₁₅ PFCA in ringed seal livers from Arviat and Resolute Bay, Nunavut during 1992-2005 and 1993-2005, respectively;¹⁴ C₉-C₁₁ PFCA in eggs of non-migratory northern fulmars (*Fulmarus glacialis*, i.e., Arctic sea birds) from Prince Leopold Island during 1975-201;¹⁵ and PFOS in muscle of landlocked arctic char (*Salvelinus alpinus*) from Char Lake, Nunavut during 1993-2011.

Table B1 Overview of native, internal, and instrument performance PFAS standards.

Native	Internal Standard	Instrument Performance
PFBA	¹³ C ₄ PFBA	¹³ C ₃ PFBA
PFPeA	¹³ C ₅ PFPeA	¹³ C ₃ PFPeA
PFHxA	¹³ C ₂ PFHxA	¹³ C ₅ PFHxA
PFHpA	¹³ C ₄ PFHpA	
PFOA	¹³ C ₄ PFOA	¹³ C ₂ PFOA
PFNA	¹³ C ₅ PFNA	¹³ C ₉ PFNA
PFDA	¹³ C ₂ PFDA	¹³ C ₆ PFDA
PFUnDA	¹³ C ₂ PFUnDA	¹³ C ₇ PFUnDA
PFDoDA	¹³ C ₂ PFDoDA	
PFTTrDA	¹³ C ₂ PFTTrDA	
PFTeDA	¹³ C ₂ PFTeDA	
PFHxDA	¹³ C ₂ PFHxDA	
PFBS	¹³ C ₃ PFBS	
PFHxS	¹⁸ O ₂ PFHxS	¹³ C ₃ PFHxS
PFHpS	¹⁸ O ₂ PFHpS	
PFOS	¹³ C ₄ PFOS	¹³ C ₈ PFOS
PFDS	¹³ C ₄ PFOS	
PFECHS	¹⁸ O ₂ PFHxS	
FOSA	¹³ C ₈ FOSA	
8-Cl PFOS	¹³ C ₄ PFOS	
ADONA	¹³ C ₅ PFNA	
6:2 Cl-PFESA	¹³ C ₄ PFOS	
8:2 Cl-PFESA	¹³ C ₄ PFOS	

Table B2 Summary of PFAS concentrations (pg g⁻¹ dw) in method blanks, with corresponding LOD and LOQ. FOSA is not measured (N.M) in Lake B35 samples.

Congener	LOD	LOQ	SPE Method Blanks	Lake B35 Method Blanks	Lake Hazen Method Blanks
PFBA	6	20	<6 – 37	<6	<6
PFPeA	7	20	<7	<7	<20
PFHxA	2	9	<2	9 – 13	7 – 18
PFHpA	1	3	<1	6	13 – 25
PFOA	1	5	<1	36 – 41	31 – 62
PFNA	1	4	<1 – 4	<1 – 4	<1 – 8
PFDA	1	5	<1	1 – 3	<1 – 13
PFUnDA	1	4	<1	2 – 5	<1 – 3
PFDoDA	1	3	<1	<1	<1 – 6
PFTTrDA	1	3	<1 – 4	<1 – 3	<3
PFTeDA	2	5	<2	<2 – 2	<2 – 5
PFHxDA	6	20	<6	<20	<20
PFOS	0.5	1	<0.5 – 1	9 – 10	4 – 14
PFDS	0.3	1	<0.3	<0.3	<0.3
PFECHS	0.5	1	2 – 7	11 – 24	3 – 7
PFHxS	0.3	1	<0.3	1 – 4	<0.3 – 1
PFHpS	0.4	1	<0.4 – 1	<0.4 – 3	<0.4
PFBS	1	3	<1	<1	<1 – 4
FOSA	0.1	0.3	N.M	N.M	4 – 19
ADONA	0.1	0.5	<0.1	<0.1	<0.1
8-Cl-PFOS	0.4	0.1	<0.1	<0.4	<0.4
6:2 Cl-PFESA	0.2	0.6	<0.2	<0.2	<0.2
8:2 Cl-PFESA	0.4	1	<0.4	<0.4	<0.4

Table B3 Recoveries of internal, instrument performance standards, and native spike and recovery experiments in Lake Hazen and Lake B35 sediments. Internal standards are added before extraction to monitor recovery and instrument performance standards are added after extraction prior to analysis to monitor matrix effects. Recovery is based on a comparison of internal standard peak area in sample extracts to the peak area in a solvent standard at equivalent concentrations. The uncertainty is represented by standard deviation. FOSA is not measured (N.M) in Lake B35 samples.

Congener	Lake Hazen Recovery (%)			Lake B35 Recovery (%)		
	Internal Standard	Instrument Performance	Native	Internal Standard	Instrument Performance	Native
PFBA	45 ± 2	56 ± 3	72 ± 2	17 ± 3	17 ± 2	28 ± 3
PFPeA	56 ± 2	72 ± 3	92 ± 1	27 ± 3	37 ± 6	50 ± 3
PFHxA	52 ± 2	61 ± 3	90 ± 0	21 ± 3	27 ± 5	38 ± 4
PFHpA	49 ± 2		81 ± 2	21 ± 4		34 ± 4
PFOA	44 ± 2	51 ± 3	76 ± 0	21 ± 5	27 ± 6	33 ± 5
PFNA	37 ± 3	42 ± 4	63 ± 4	19 ± 5	24 ± 7	33 ± 4
PFDA	41 ± 3	47 ± 3	67 ± 3	18 ± 5	22 ± 7	28 ± 5
PFUnDA	41 ± 3	47 ± 3	69 ± 2	15 ± 6	18 ± 7	27 ± 2
PFDoDA	29 ± 3		43 ± 3	8 ± 4		20 ± 4
PFTrDA			50 ± 2			21 ± 4
PFTeDA	35 ± 3		56 ± 0	16 ± 6		29 ± 5
PFHxDA	20 ± 5		26 ± 4	20 ± 7		30 ± 7
PFOS	49 ± 1	57 ± 2	99 ± 0	39 ± 7	46 ± 8	57 ± 4
PFDS			93 ± 0			65 ± 4
PFECHS			92 ± 0			69 ± 4
PFHxS	51 ± 2	64 ± 2	100 ± 0	42 ± 7	51 ± 8	69 ± 4
PFHpS			100 ± 0			65 ± 4
PFBS	54 ± 2		103 ± 1	49 ± 7		74 ± 5
FOSA	17 ± 4		40 ± 4	N.M	N.M	N.M
ADONA			82 ± 1			30 ± 3
8-Cl-PFOS			97 ± 1			60 ± 3
6:2 Cl-PFESA			98 ± 1			65 ± 4
8:2 Cl-PFESA			100 ± 2			57 ± 3

Table B4 Overview of precursor/product ion mass-to-charge ratios (m/z), cone voltages (V), and collision energies (eV) for PFAS analysis in Arctic sediments. Product ion scans for PFCA target perfluoroalkyl moieties (i.e., $F(CF_2)_xCO_2^-$ to $F(CF_2)_x$), while product ion scans for PFSA target sulfonic acid moieties (i.e., $F(CF_2)_xSO_3^-$ to FSO_3^- or SO_3^-). The product ion scan for FOSA targets a SO_2N moiety (i.e., $CF_3(CF_2)_7SO_2NH_2$ to SO_2N) and product ion scans for ADONA and Cl-PFESA target perhalogenated alkoxy moieties (i.e., $CF_3O(CF_2)_3OCHF_2CO_2^-$ to CF_3O or $CF_3O(CF_2)_3O$ for ADONA and $ClCF_2(CF_2)_5O(CF_2)_2SO_3^-$ to $ClCF_2(CF_2)_5O$ for 6:2 Cl-PFESA).

PFAS	Quantifier m/z	Cone Voltage	Collision Energy	Qualifier m/z	Cone Voltage	Collision Energy
PFBA	213/169	6	10			
PFPeA	263/219	6	15			
PFHxA	313/269	6	10	313/119	6	17
PFHpA	363/319	8	10	363/119	8	18
PFOA	413/369	16	11	413/169	16	18
PFNA	463/419	16	10	463/219	16	17
PFDA	513/469	16	10	513/219	16	17
PFUnDA	563/519	18	10	563/319	18	17
PFDoDA	613/569	18	12	613/169	18	28
PFTTrDA	663/619	18	12	663/169	18	30
PFTeDA	713/669	26	12	713/169	26	30
PFHxDA	813/769	36	14	813/169	36	36
PFBS	299/99	42	30	299/80	42	30
PFHxS	399/99	42	32	399/80	42	32
PFHpS	449/99	42	36	449/80	42	44
PFOS	499/99	46	36	499/80	46	40
PFDS	599/99	42	44	599/80	42	46
PFECHS	461/381	42	30	461/99	42	26
FOSA	498/78	46	30			
ADONA	377/85	10	26	377/251	10	12
6:2 Cl-PFESA	531/351	42	20	531/83	42	20
8:2 Cl-PFESA	631/451	42	20	631/83	42	20
8-Cl-PFOS	515/99	42	38	515/80	42	41

Table B5 Overview of precursor/product ion mass-to-charge ratios, cone voltages (V), and collision energies (eV) for internal and instrument performance PFAS standard analysis.

Internal Standard		Cone Voltage	Collision Energy
¹³ C ₄ PFBA	217/172	6	10
¹³ C ₅ PFPeA	268/223	6	15
¹³ C ₂ PFHxA	315/270	6	10
¹³ C ₄ PFHpA	367/322	8	10
¹³ C ₄ PFOA	417/372	16	10
¹³ C ₅ PFNA	468/423	16	14
¹³ C ₂ PFDA	515/470	16	16
¹³ C ₂ PFUnDA	565/520	18	10
¹³ C ₂ PFDoDA	615/570	18	12
¹³ C ₂ PFTeDA	715/670	26	12
¹³ C ₂ PFHxDA	815/770	36	14
¹³ C ₃ PFBS	302/99	42	30
¹⁸ O ₂ PFHxS	403/84	42	38
¹⁸ O ₂ PFHxS	403/103	42	32
¹³ C ₄ PFOS	503/80	46	48
¹³ C ₈ FOSA	506/78	46	28
Instrument Performance		Cone Voltage	Collision Energy
¹³ C ₃ PFBA	216/172	6	10
¹³ C ₃ PFPeA	266/222	6	15
¹³ C ₅ PFHxA	318/273	6	10
¹³ C ₂ PFOA	415/370	16	10
¹³ C ₉ PFNA	472/427	16	14
¹³ C ₆ PFDA	519/474	16	12
¹³ C ₇ PFUnDA	570/525	18	10
¹³ C ₃ PFHxS	402/99	42	32
¹³ C ₈ PFOS	507/99	46	36

Table B6 Overview of liquid chromatograph, mass spectrometric, and inlet parameters used for PFAS sediment analysis.

Liquid Chromatograph Gradient Elution				Mass Spectrometer/Inlet	
Time (min)	Flow Rate (mL min⁻¹)	H₂O (%)	MeOH (%)	Ionization mode: electrospray negative	
0	0.400	75	25		
0.5	0.400	75	25	Capillary Voltage (kV)	0.6
5.0	0.400	15	85	Source Temperature (°C)	150
5.1	0.400	0	100	Desolvation Gas Temperature (°C)	450
5.6	0.400	0	100	Cone Gas Flow (L hr ⁻¹)	150
7.0	0.550	0	100	Desolvation Gas Flow (L hr ⁻¹)	800
9.0	0.400	75	25	Collision Gas Flow (mL min ⁻¹)	0.15
13.0	0.400	75	25	Nebulizer Pressure (bar)	7
Inlet parameters					
Column Temperature (°C)				50	
Injection Volume (μL)				9	

Table B7 Overview of blank-, extraction-, and matrix-corrected PFAS concentrations (pg g⁻¹ dw) in Lake B35 and Lake Hazen sediments. Detection frequency (%) is calculated as the number samples equal to or greater than the LOD, divide by the sample size, and multiply by 100.

Congener	Lake B35 Sediments		Lake Hazen Sediments	
	Range (pg g ⁻¹ dw)	Frequency (%)	Range (pg g ⁻¹ dw)	Frequency (%)
PFBA	<6	0	<6	0
PFPeA	<7	0	<7	0
PFHxA	<2	0	<2 – 49	19
PFHpA	<1 – 180	50	<1 – 9	3
PFOA	44 – 360	100	<1 – 50	78
PFNA	<1 – 650	70	<1 – 59	34
PFDA	<1 – 130	40	<1 – 23	53
PFUnDA	<1 – 130	50	<1 – 29	44
PFDoDA	<1	0	<1 – 9	19
PFTTrDA	<1	0	<1 – 6	13
PFTeDA	<2	0	<2	0
PFHxDA	<6	0	<6	0
PFOS	<0.5 – 70	10	<0.5 – 16	50
PFDS	<0.3	0	<0.3	0
PFECHS	<0.5	0	<0.5 – 1	9
PFHxS	<0.3	0	<0.3 – 2	3
PFHpS	<0.4	0	<0.4	0
PFBS	<1 – 51	30	<1 – 22	91
FOSA			<0.1 – 3	3
ADONA	<0.1	0	<0.1	0
8-Cl-PFOS	<0.4	0	<0.4	0
6:2 Cl-PFESA	<0.2	0	<0.2	0
8:2 Cl-PFESA	<0.4	0	<0.4	0

Table B8 First-order kinetics of natural log-transformed PFAS fluxes in Lake Hazen sediments from a 0-16 cm depth and Lake B35 from a 0.0-4.5 cm depth, corresponding to depositional periods of 1963-2011 and 1952-2009, respectively. Temporal trends are determined using natural log-transformed PFAS mass flux ($\text{ng m}^{-2} \text{ year}^{-1}$) for congeners with detection frequencies $\geq 50\%$. Doubling times (t_2) are calculated using the first-order rate (k) obtained from the slope of a linear regression of natural log-transformed mass flux versus year of deposition. Standard error is used to represent the uncertainty of k , while a 95% confidence interval (CI) represents the uncertainty for t_2 . Statistical significance is set to 5%. Temporal trends for PFOA, PFDA, PFBS, and PFOS span a temporal period of 1963-2011, 1975-2009, 1975-2011, and 1975-2011, respectively due to concentrations $< \text{LOD}$ in samples. For Lake B35, temporal trends for PFHpA, PFOA, PFNA, and PFUnDA span a temporal period from 1986-2009, 1952-2009, 1963-2009, and 1963-2009, respectively, due to concentrations $< \text{LOD}$ in samples.

Lake Hazen 1963-2011	r^2	p	k (year^{-1})	t_2 (year)	95% CI t_2
PFOA	0.59	<0.01	0.10 ± 0.02	6.9	5.3 – 11
PFDA	0.68	<0.01	0.10 ± 0.02	6.9	4.9 – 11
PFBS	0.60	<0.01	0.09 ± 0.01	7.7	5.8 – 11
PFOS	0.58	<0.01	0.11 ± 0.03	6.3	4.1 – 11
Lake B35 1952-2009	r^2	p	k (year^{-1})	t_2 (year)	95% CI t_2
PFHpA	0.81	0.04	0.05 ± 0.01	14	7.7 – 110
PFOA	0.71	<0.01	0.033 ± 0.008	21	13 – 49
PFNA	0.71	0.02	0.05 ± 0.01	14	8.7 – 69
PFUnDA	0.98	<0.01	0.037 ± 0.003	19	15 – 25

Table B9 Spearman rank correlation analysis (r_s) of paired (n) natural log-transformed PFAA fluxes in Lake Hazen and Lake B35 sediments with natural-log transformed fluorotelomer-based (FT) and perfluorooctane sulfonyl fluoride (POSF) production volumes (ton year⁻¹).^{16,17} Correlation analysis is applied to natural log-transformed PFAA fluxes and production volumes during 1963-2005 and 1963-2009 in Lake Hazen and Lake B35, respectively.

Lake Hazen	<i>n</i>	<i>r_s</i>	<i>p</i>
FT vs. PFOA	13	0.76	<0.001
FT vs. PFDA	14	0.82	<0.001
FT vs. PFBS	15	0.65	<0.01
FT vs. PFOS	8	0.65	0.08
POSF vs. PFOA	10	0.15	0.69
POSF vs. PFDA	11	0.29	0.39
POSF vs. PFBS	12	0.24	0.45
POSF vs. PFOS	7	0.04	0.94
Lake B35	<i>n</i>	<i>r_s</i>	<i>p</i>
FT vs. PFHpA	5	0.95	0.01
FT vs. PFOA	8	0.72	0.04
FT vs. PFNA	7	0.90	<0.01
FT vs. PFUnDA	5	0.95	0.01
POSF vs. PFHpA	5	-0.80	0.10
POSF vs. PFOA	8	-0.24	0.57
POSF vs. PFNA	7	-0.46	0.29
POSF vs. PFUnDA	5	-0.50	0.39

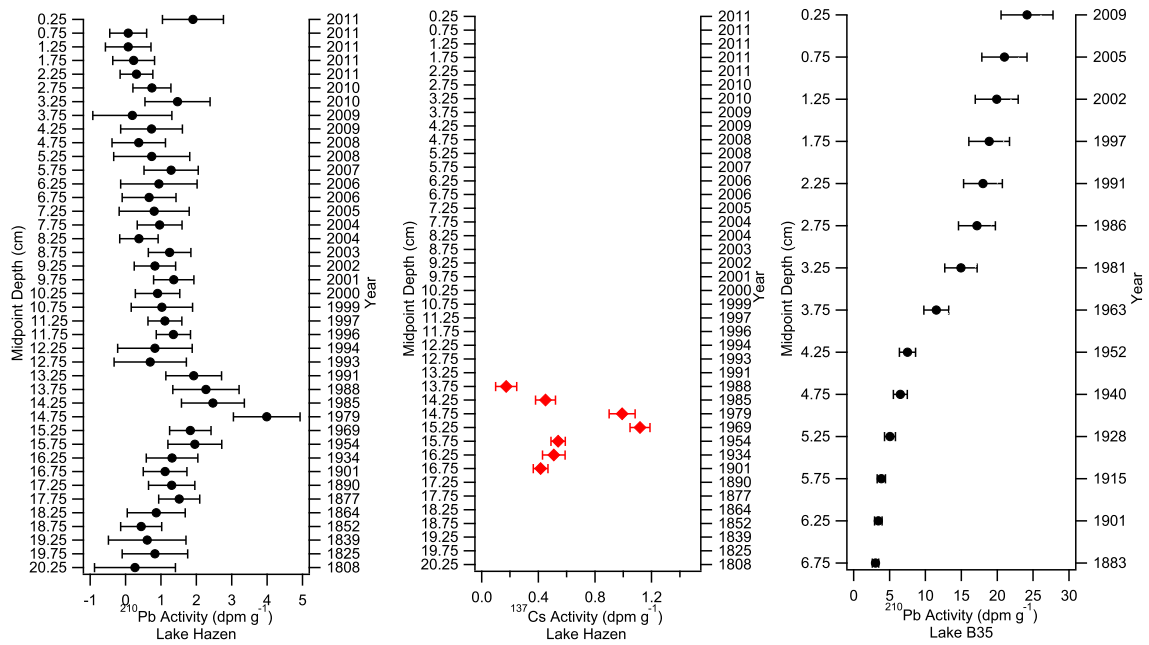


Figure B1 Activity profiles (x-axes, disintegrations per minute per gram, dpm g^{-1}) of unsupported ^{210}Pb (black circles) and ^{137}Cs (red squares) in Lake Hazen and Lake B35 sediments. Depth (midpoint, cm) and corresponding yearly interval are plotted on the left and right y axes, respectively. Error bars correspond to the uncertainty of ^{210}Pb and ^{137}Cs analysis.

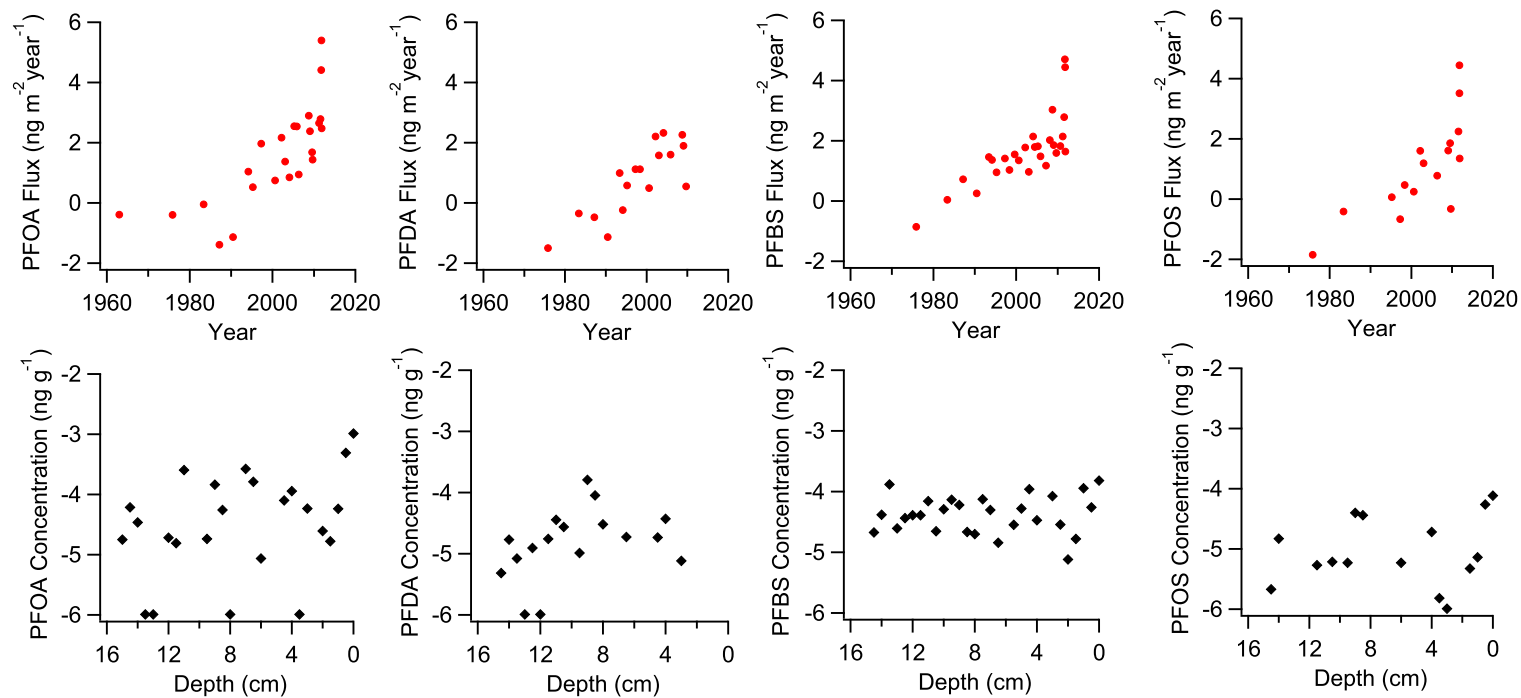


Figure B2 Natural-log transformed PFAA fluxes (ng m⁻² year⁻¹, red circles) and concentrations (ng g⁻¹ dw, black squares) in Lake Hazen sediments as a function of year and depth (cm), respectively.

Literature Cited

- (1) Thompson, W. Climate. In *Resource description and analysis: Ellesmere Island, National Park Reserve*; Parks Canada: National Resource Conservation Section, Prairie and Northern Region: Winnipeg, Canada, 1994; p 78.
- (2) Köck, G.; Muir, D.; Yang, F.; Wang, X.; Talbot, C.; Gantner, N.; Moser, D. Bathymetry and sediment geochemistry of Lake Hazen (Quttinirpaaq National Park, Ellesmere Island, Nunavut). *Arctic* **2012**, *65* (1), 56–66.
- (3) Lehnherr, I.; St. Louis, V. L.; Sharp, M.; Garnder, A.; Smol, J.; Schiff, S.; Muir, D.; Mortimer, C.; Michelutti, N.; Tarnocai, C.; St. Pierre, K.; Emmerton, C.; Wiklund, J.; Köck, G.; Lamoureux, S.; Talbot, C. The world's largest High Arctic lake responds rapidly to climate warming. *Nat. Commun.* **2018**, *9*, 1–9.
- (4) MacInnis, J. J.; French, K.; Muir, D. C. .; Spencer, C.; Criscitiello, A.; De Silva, A. O.; Young, C. J. Emerging investigator series: a 14-year depositional ice record of perfluoroalkyl substances in the High Arctic. *Environ. Sci. Process. Impacts* **2017**, *19* (1), 22–30.
- (5) Lescord, G. L.; Kidd, K. A.; De Silva, A. O.; Williamson, M.; Spencer, C.; Wang, X.; Muir, D. C. G. Perfluorinated and polyfluorinated compounds in lake food webs from the Canadian High Arctic. *Environ. Sci. Technol.* **2015**, *49* (5), 2694–2702.
- (6) Pickard, H. M.; Criscitiello, A. S.; Spencer, C.; Sharp, M. J.; Muir, D. C. G.; Silva, A. O. De; Young, C. J. Continuous Non-Marine Inputs of Per- and Polyfluoroalkyl Substances to the High Arctic : A Multi-Decadal Temporal

- Record. *Atmos. Chem. Phys. Discuss.* **2018**, *18* (7), 5045-5058.
- (7) Veillette, J.; Muir, D.; Antoniadis, D.; Small, J. M.; Spencer, C.; Loewen, T. N.; Babaluk, J. A.; Reist, J. D.; Vincent, W. F. Perfluorinated chemicals in meromictic lakes on the northern coast of Ellesmere Island, High Arctic Canada. *Arctic* **2012**, *65*, 245–256.
- (8) Yeung, L. W. Y.; De Silva, A. O.; Loi, E. I. H.; Marvin, C. H.; Taniyasu, S.; Yamashita, N.; Mabury, S. A.; Muir, D. C. G.; Lam, P. K. S. Perfluoroalkyl substances and extractable organic fluorine in surface sediments and cores from Lake Ontario. *Environ. Int.* **2013**, *59* (2013), 389–397.
- (9) Labadie, P.; Chevreuil, M. Partitioning behaviour of perfluorinated alkyl contaminants between water, sediment and fish in the Orge River (nearby Paris, France). *Environ. Pollut.* **2011**, *159* (2), 391–397.
- (10) Munoz, G.; Giraudel, J. L.; Botta, F.; Lestremau, F.; D??vier, M. H.; Budzinski, H.; Labadie, P. Spatial distribution and partitioning behavior of selected poly- and perfluoroalkyl substances in freshwater ecosystems: A French nationwide survey. *Sci. Total Environ.* **2015**, *517*, 48–56.
- (11) Zushi, Y.; Tamada, M.; Kanai, Y.; Masunaga, S. Time trends of perfluorinated compounds from the sediment core of Tokyo Bay, Japan (1950s-2004). *Environ. Pollut.* **2010**, *158* (3), 756–763.
- (12) Benskin, J. P.; Phillips, V.; St. Louis, V. L.; Martin, J. W. Source elucidation of perfluorinated carboxylic acids in remote alpine lake sediment cores. *Environ. Sci. Technol.* **2011**, *45* (17), 7188–7194.
- (13) Smithwick, M.; Norstrom, R. J.; Mabury, S. A.; Solomon, K.; Evans, T. J.;

- Stirling, I.; Taylor, M. K.; Muir, D. C. G. Temporal trends of perfluoroalkyl contaminants in polar bears (*Ursus maritimus*) from two locations in the North American Arctic, 1972-2002. *Environ. Sci. Technol.* **2006**, *40* (4), 1139–1143.
- (14) Butt, C. M.; Muir, D. C. G.; Stirling, I.; Kwan, M.; Mabury, S. A. Rapid response of arctic ringed seals to changes in perfluoroalkyl production. *Environ. Sci. Technol.* **2007**, *41* (1), 42–49.
- (15) Braune, B. M.; Letcher, R. J. Perfluorinated sulfonate and carboxylate compounds in eggs of seabirds breeding in the Canadian Arctic: Temporal trends (1975-2011) and interspecies comparison. *Environ. Sci. Technol.* **2013**, *47* (1), 616–624.
- (16) Wang, Z.; Boucher, J. M.; Scheringer, M.; Cousins, I. T.; Hungerbühler, K. Toward a Comprehensive Global Emission Inventory of C4-C10 Perfluoroalkanesulfonic Acids (PFSA) and Related Precursors: Focus on the Life Cycle of C8-Based Products and Ongoing Industrial Transition. *Environ. Sci. Technol.* **2017**, *51* (8), 4482–4493.
- (17) Wang, Z.; Cousins, I. T.; Scheringer, M.; Buck, R. C.; Hungerbühler, K. Global emission inventories for C4-C14 perfluoroalkyl carboxylic acid (PFCA) homologues from 1951 to 2030, Part I: Production and emissions from quantifiable sources. *Environ. Int.* **2014**, *70*, 62–75.

Appendix C Supporting Information for Chapter 3

Section C1 Chemicals

Targeted PFAS in Lake Hazen snow and water include: perfluorobutanoic acid (PFBA), perfluoropentanoic acid, (PFPeA), perfluorohexanoic acid (PFHxA), perfluoroheptanoic acid (PFHpA), perfluorooctanoic acid (PFOA), perfluorononanoic acid (PFNA), perfluorodecanoic acid (PFDA), perfluoroundecanoic acid (PFUnDA), perfluorododecanoic acid (PFDoDA), perfluorotridecanoic acid (PFTrDA), perfluorotetradecanoic acid (PFTeDA), perfluorohexadecanoic acid (PFHxDA), perfluorobutane sulfonic acid (PFBS), perfluorohexane sulfonic acid (PFHxS), perfluoroheptane sulfonic acid (PFHpS), perfluorooctane sulfonic acid (PFOS), perfluoro-4-ethylcyclohexane sulfonic acid (PFECHS), perfluorodecane sulfonic acid (PFDS), and perfluorooctane sulfonamide (FOSA). All native and isotopically labeled PFAS were purchased from Wellington Laboratories (Guelph, Ontario), with the exception of PFECHS, which was purchased from Chiron AS (Trondheim, Norway). PFECHS was quantified as outlined in Appendix A (Section A1). These analytes were selected for analysis because standardized methods are developed for this series of PFAS in the analytical laboratory. Ammonia (NH₃, Suprapur® 25 %) was purchased from Merck (New Jersey, USA), methanol (MeOH, Optima™ Grade) and water (Optima™ Grade) was purchased from Fisher Scientific (New Hampshire, USA), glacial acetic acid (ACS Grade) was purchased from EMD (Etobicoke, Ontario), and ammonium acetate (>98%) was purchased from Sigma Aldrich (Missouri, USA).

Section C2 QA/QC

Spike and recovery experiments were conducted by spiking 30 μL of a native PFAS standard mixture into composite water samples from Lake Hazen. These samples were extracted in parallel with water samples. The recovery of PFAS in water was calculated by comparing analyte peak area in water extracts to analyte peak area in a solvent standard at equivalent concentrations. Method blanks were used to evaluate positive biases during the extraction and analysis, which consisted of spiking 30 μL of a PFAS internal standard mixture into an Oasis® WAX SPE cartridge and carried through the extraction procedure. Sampling blanks were collected to evaluate biases from transportation, which consisted of transporting 500 mL HPLC grade water to the field sites. Field blanks were exposed to the atmosphere for ten seconds and were returned to the laboratory for analysis. Concentrations of PFAS in field blanks were compared to concentrations in HPLC grade water that remained in the laboratory, designated as a stay blank. In general, concentrations of PFAS in field blanks were comparable to concentrations in stay blanks, suggesting sampling and transportation are not sources of contamination. As such, concentrations of PFAS in snow and water samples were not corrected for sampling blanks, but were corrected for method (extraction) blanks, recovery, and matrix effects. Matrix effects were evaluated by comparing the peak area of isotopically labeled PFAS standards added after the extraction to the peak areas of PFAS in a solvent standard at equivalent concentrations.

Table C1 Hydrological cycle in the Lake Hazen watershed, adapted from St. Pierre et al. 2019.¹

Month	Sunlight	Precipitation	Hydrological events	2015	2016	
Sept		95 mm precipitation per year, 80-85% from Sept to May as snow	Freeze up begins, glacial rivers stop flowing, Lake Hazen freezes over	Freeze up	Freeze up	
Oct						
Nov			Lake Hazen surface is frozen; snow accumulates (0.120 km ³ water volume equivalent)	Frozen + snow accumulating	Frozen + snow accumulating	
Dec						
Jan						
Feb						
March						
Apr	24 hour sunlight April 6 to Sept 4		Late May/early June: snowmelt and meltwater flow in glacial river valleys	Glacial rivers water volume into Lake Hazen 0.948 km ³	Glacial rivers water volume into Lake Hazen 0.281 km ³	
May						
June						
July				Late July/early Aug: Lake Hazen is completely ice free	Aug 4: Complete ice off	Aug 8: complete ice off
Aug			No precipitation			

Hydrological year

Table C2 Snow and water column sampling in the Lake Hazen watershed.

Year	Date	Location	Sample type	Number of sites
2014	May 14 - 15	Lake Hazen surface	Snow	9
2013	May 13-14	Lake Hazen surface	Snow	9
2014	May 19-22	Lake Hazen	Under-ice water column	1 site, 15 depths
2013	May 15-18	Lake Hazen	Under ice water column	1 site, 15 depths
2012	June 1-3	Lake Hazen	Under ice water column during snow melt	1 site, 15 depths
2014	May 29-31	Lake Hazen	Under-ice water column during snow melt	1 site, 15 depths
2015	July 27-29	Lake Hazen	Ice free water column	1 site, 15 depths

Table C3 Overview of native, internal, and instrument performance PFAS standards.

Native Standard	Internal Standard	Instrument Performance
PFBA	¹³ C ₄ PFBA	¹³ C ₃ PFBA
PFPeA	¹³ C ₅ PFPeA	¹³ C ₃ PFPeA
PFHxA	¹³ C ₂ PFHxA	¹³ C ₅ PFHxA
PFHpA	¹³ C ₄ PFHpA	
PFOA	¹³ C ₄ PFOA	¹³ C ₂ PFOA
PFNA	¹³ C ₅ PFNA	¹³ C ₉ PFNA
PFDA	¹³ C ₂ PFDA	¹³ C ₆ PFDA
PFUnDA	¹³ C ₂ PFUnDA	¹³ C ₇ PFUnDA
PFDoDA	¹³ C ₂ PFDoDA	
PFTTrDA	¹³ C ₂ PFTTrDA	
PFTeDA	¹³ C ₂ PFTeDA	
PFHxDA	¹³ C ₂ PFHxDA	
PFBS	¹³ C ₃ PFBS	
PFHxS	¹⁸ O ₂ PFHxS	¹³ C ₃ PFHxS
PFHpS	¹⁸ O ₂ PFHpS	
PFOS	¹³ C ₄ PFOS	¹³ C ₈ PFOS
PFDS	¹³ C ₄ PFOS	
PFECHS	¹⁸ O ₂ PFHxS	
FOSA	¹³ C ₈ FOSA	

Table C4 Summary of native PFAS concentrations (ng L⁻¹) in HPLC-grade water transported to the field site (field blank), HPLC grade water kept in the lab (stay blank), and method blanks. Method blanks correspond to Oasis® WAX SPE cartridge blanks.

Congener	LOD	LOQ	Field	Stay	SPE
PFBA	0.010	0.040	<0.010–1.2	<0.020	<0.010-0.040
PFPeA	0.010	0.050	<0.010	<0.010	<0.010
PFHxA	0.005	0.020	<0.005–0.059	<0.005	<0.005
PFHpA	0.002	0.007	<0.002–0.019	<0.002	<0.002
PFOA	0.003	0.010	0.008–0.031	0.008–0.017	<0.003 – 0.018
PFNA	0.002	0.008	<0.002–0.005	<0.002–0.008	<0.002
PFDA	0.003	0.010	<0.003–0.030	<0.003	<0.003
PFUnDA	0.003	0.009	<0.003	<0.003	<0.003
PFDoDA	0.002	0.007	<0.002	<0.002	<0.002
PFTTrDA	0.002	0.006	<0.002	<0.002	<0.002
PFTeDA	0.003	0.010	<0.003	<0.003	<0.003
PFHxDA	0.010	0.040	<0.010	<0.010	<0.010
PFOS	0.001	0.003	<0.001	<0.001	<0.001– 0.005
PFDS	0.0006	0.002	<0.0006	<0.0006	<0.0006
PFECHS	0.001	0.003	<0.001–0.002	<0.001	<0.001
PFHxS	0.0007	0.002	<0.0007	<0.0007	<0.0007
PFHpS	0.0009	0.003	<0.0009–0.001	<0.0009	<0.0009
PFBS	0.002	0.007	<0.002–0.013	<0.002	<0.002 – 0.020
FOSA	0.0002	0.0007	<0.0002	<0.0002	<0.0002 – 0.023

Table C5 Summary of mean \pm standard error recovery of internal, instrument performance standards, and native spike and recovery experiments in Lake Hazen water samples. The recovery of internal and instrument performance standards in Lake Hazen water samples is calculated by comparing analyte peak area in water extracts to analyte peak area in a solvent standard at equivalent concentration. N/A refers analytes without an available corresponding isotopically labeled standard.

Congener	Internal Standard	Instrument Performance	Native
PFBA	89 \pm 3	102 \pm 3	116 \pm 3
PFPeA	94 \pm 3	107 \pm 3	108 \pm 2
PFHxA	80 \pm 5	90 \pm 6	104 \pm 6
PFHpA	93 \pm 2	N/A	109 \pm 2
PFOA	97 \pm 2	103 \pm 2	109 \pm 4
PFNA	97 \pm 2	103 \pm 2	107 \pm 2
PFDA	92 \pm 2	102 \pm 2	106 \pm 2
PFUnDA	88 \pm 2	103 \pm 2	105 \pm 3
PFDoDA	76 \pm 3	N/A	100 \pm 6
PFTrDA	N/A	N/A	77 \pm 6
PFTeDA	55 \pm 3	N/A	93 \pm 14
PFHxDA	100 \pm 6	N/A	108 \pm 4
PFOS	90 \pm 2	98 \pm 2	102 \pm 2
PFDS	N/A	N/A	91 \pm 4
PFECHS	N/A	N/A	99 \pm 1
PFHxS	94 \pm 2	98 \pm 2	109 \pm 2
PFHpS	N/A	N/A	100 \pm 3
PFBS	N/A	N/A	107 \pm 3
FOSA	32 \pm 5	N/A	106 \pm 1

Table C6 Overview of precursor/product ion mass-to-charge ratios (m/z), cone voltages (V), and collision energies (eV) for native PFAS analysis. Product ion scans for PFCA target perfluoroalkyl moieties (i.e., $F(CF_2)_xCO_2^-$ to $F(CF_2)_x$), while product ion scans for PFSA target sulfonic acid moieties (i.e., $F(CF_2)_xSO_3^-$ to FSO_3^- or SO_3^-). The transition for FOSA targets a SO_2N moiety (i.e., $CF_3(CF_2)_7SO_2NH_2$ to SO_2N).

PFAS	Quantifier m/z	Cone Voltage	Collision Energy	Qualifier m/z	Cone Voltage	Collision Energy
PFBA	213/169	6	10			
PFPeA	263/219	6	15			
PFHxA	313/269	6	10	313/119	6	17
PFHpA	363/319	8	10	363/119	8	18
PFOA	413/369	16	11	413/169	16	18
PFNA	463/419	16	10	463/219	16	17
PFDA	513/469	16	10	513/219	16	17
PFUnDA	563/519	18	10	563/319	18	17
PFDoDA	613/569	18	12	613/169	18	28
PFTTrDA	663/619	18	12	663/169	18	30
PFTeDA	713/669	26	12	713/169	26	30
PFHxDA	813/769	36	14	813/169	36	36
PFBS	299/99	42	30	299/80	42	30
PFHxS	399/99	42	32	399/80	42	32
PFHpS	449/99	42	36	449/80	42	44
PFOS	499/99	46	36	499/80	46	40
PFDS	599/99	42	44	599/80	42	46
PFECHS	461/381	42	30	461/99	42	26
FOSA	498/78	46	30			

Table C7 Overview of precursor/product ion mass-to-charge ratios, cone voltages (V), and collision energies (eV) for internal and instrument performance PFAS standard analysis.

Internal Standard		Cone Voltage	Collision Energy
¹³ C ₄ PFBA	217/172	6	10
¹³ C ₅ PFPeA	268/223	6	15
¹³ C ₂ PFHxA	315/270	6	10
¹³ C ₄ PFHpA	367/322	8	10
¹³ C ₄ PFOA	417/372	16	10
¹³ C ₅ PFNA	468/423	16	14
¹³ C ₂ PFDA	515/470	16	16
¹³ C ₂ PFUnDA	565/520	18	10
¹³ C ₂ PFDoDA	615/570	18	12
¹³ C ₂ PFTeDA	715/670	26	12
¹³ C ₂ PFHxDA	815/770	36	14
¹³ C ₃ PFBS	302/99	42	30
¹⁸ O ₂ PFHxS	403/84	42	38
¹⁸ O ₂ PFHxS	403/103	42	32
¹³ C ₄ PFOS	503/80	46	48
¹³ C ₈ FOSA	506/78	46	28
Instrument Performance		Cone Voltage	Collision Energy
¹³ C ₃ PFBA	216/172	6	10
¹³ C ₃ PFPeA	266/222	6	15
¹³ C ₅ PFHxA	318/273	6	10
¹³ C ₂ PFOA	415/370	16	10
¹³ C ₉ PFNA	472/427	16	14
¹³ C ₆ PFDA	519/474	16	12
¹³ C ₇ PFUnDA	570/525	18	10
¹³ C ₃ PFHxS	402/99	42	32
¹³ C ₈ PFOS	507/99	46	36

Table C8 Overview of liquid chromatograph, mass spectrometric, and inlet parameters used for PFAS quantitation in Lake Hazen snow and water samples.

Liquid Chromatograph Gradient Elution				Mass Spectrometer/Inlet	
Time (min)	Flow Rate (mL min⁻¹)	H₂O (%)	MeOH (%)	Ionization mode: Electrospray negative	
0	0.400	75	25		
0.5	0.400	75	25	Capillary Voltage (kV)	0.6
5.0	0.400	15	85	Source Temperature (°C)	150
5.1	0.400	0	100	Desolvation Gas Temperature (°C)	450
5.6	0.400	0	100	Cone Gas Flow (L hr ⁻¹)	150
7.0	0.550	0	100	Desolvation Gas Flow (L hr ⁻¹)	800
9.0	0.400	75	25	Collision Gas Flow (mL min ⁻¹)	0.15
13.0	0.400	75	25	Nebulizer Pressure (bar)	7
Inlet parameters					
				Column Temperature (°C)	50
				Injection Volume (μL)	9

Table C9 Detection frequencies for PFAS in snow and water. Detection frequency (%) is calculated as the number samples equal to or greater than the LOQ, divide by the sample size, and multiply by 100.

	Lake Hazen Snowpacks			Lake Hazen Water Columns			
	Light Snow	Light Snow	Dark Snow	Ice covered	Ice covered	Snowmelt	Ice free
Year	2013	2014	2014	2013	2014	2014	2015
PFBA	100	100	100	0	87	100	93
PFPeA	100	100	100	0	12	29	0
PFHxA	100	100	100	67	100	100	100
PFHpA	100	100	100	67	100	100	100
PFOA	100	100	100	100	100	100	100
PFNA	100	100	100	100	100	100	100
PFDA	100	100	100	87	12	29	0
PFUnDA	100	100	100	7	37	14	13
PFDoDA	100	100	100	0	0	0	0
PFTTrDA	0	33	89	0	12	0	0
PFTeDA	75	22	44	0	0	0	0
PFHxDA	0	0	0	0	0	0	0
PFOS	100	100	100	67	25	57	100
PFDS	0	0	0	7	0	0	0
PFECHS	87	55	44	67	62	0	0
PFHxS	25	0	11	27	0	0	0
PFHpS	0	0	0	0	0	0	0
PFBS	25	44	78	67	37	29	0
FOSA	0	0	0	33	0	0	0

Table C10 Spearman rank correlation (r_s) analysis of natural log-transformed PFAS concentrations (ng L^{-1}) in light snowpacks collected from the Lake Hazen watershed during May 2013. PFAS concentrations equal to or greater than the LOQ for congeners with detection frequencies equal to or greater than 50% are included in correlation analysis.

		PFBA	PFPeA	PFHxA	PFHpA	PFOA	PFNA	PFDA	PFUnDA	PFDoDA	PFTeDA	PFOS
PFPeA	r_s	0.71										
	p	0.05										
PFHxA	r_s	0.46	0.85									
	p	0.25	<0.01									
PFHpA	r_s	0.69	0.97	0.89								
	p	0.06	<0.01	<0.01								
PFOA	r_s	0.38	0.83	0.94	0.83							
	p	0.35	0.01	<0.01	0.01							
PFNA	r_s	0.42	0.78	0.71	0.75	0.81						
	p	0.30	0.02	<0.05	0.03	0.01						
PFDA	r_s	0.51	0.88	0.77	0.83	0.84	0.95					
	p	0.19	<0.01	0.02	0.01	<0.01	<0.01					
PFUnDA	r_s	0.48	0.81	0.65	0.73	0.71	0.96	0.95				
	p	0.23	0.01	0.08	0.04	0.05	<0.01	<0.01				
PFDoDA	r_s	0.16	0.65	0.83	0.70	0.77	0.86	0.81	0.75			
	p	0.71	0.08	0.01	0.05	0.03	<0.01	0.01	0.03			
PFTeDA	r_s	0.14	0.72	0.91	0.77	0.77	0.41	0.41	0.43	0.56		
	p	0.79	0.10	0.01	0.07	0.07	0.42	0.42	0.40	0.25		
PFOS	r_s	0.38	0.75	0.83	0.74	0.90	0.81	0.77	0.83	0.70	0.71	
	p	0.35	0.03	0.01	0.04	<0.01	0.01	0.03	0.01	0.05	0.11	
PFECHS	r_s	0.38	0.65	0.71	0.72	0.45	0.41	0.46	0.39	0.63	0.77	0.36
	p	0.40	0.11	0.07	0.07	0.31	0.36	0.29	0.38	0.13	0.07	0.43

Table C11 Spearman rank correlation (r_s) analysis of natural log-transformed PFAS concentrations (ng L⁻¹) in light snowpacks collected from Lake Hazen ice during June 2014. PFAS concentrations equal to or greater than the LOQ for congeners with detection frequencies equal to or greater than 50% are included in correlation analysis.

		PFBA	PFPeA	PFHxA	PFHpA	PFOA	PFNA	PFDA	PFUnDA	PFDoDA	PFOS
PFPeA	r_s	0.96									
	p	<0.01									
PFHxA	r_s	0.90	0.85								
	p	<0.01	<0.01								
PFHpA	r_s	0.92	0.88	0.97							
	p	<0.01	<0.01	<0.01							
PFOA	r_s	0.96	0.95	0.86	0.89						
	p	<0.01	<0.01	<0.01	<0.01						
PFNA	r_s	0.97	0.98	0.87	0.90	0.98					
	p	<0.01	<0.01	<0.01	<0.01	<0.01					
PFDA	r_s	0.95	0.93	0.87	0.92	0.98	0.97				
	p	<0.01	<0.01	<0.01	<0.01	<0.01	<0.01				
PFUnDA	r_s	0.96	0.89	0.87	0.90	0.97	0.94	0.98			
	p	<0.01	<0.01	<0.01	<0.01	<0.01	<0.01	<0.01			
PFDoDA	r_s	0.74	0.62	0.70	0.73	0.79	0.69	0.83	0.89		
	p	0.02	0.07	0.03	0.03	0.01	0.04	<0.01	<0.01		
PFOS	r_s	0.74	0.61	0.83	0.81	0.78	0.69	0.82	0.87	0.94	
	p	0.02	0.08	<0.01	<0.01	0.01	0.04	<0.01	<0.01	<0.01	
PFECHS	r_s	0.32	0.30	0.97	0.90	0.30	0.30	0.50	0.50	0.41	0.87
	p	0.60	0.62	0.04	0.04	0.62	0.62	0.39	0.39	0.49	0.05

Table C12 Spearman rank correlation (r_s) analysis of natural log-transformed PFAS concentrations (ng L^{-1}) in dark snowpacks collected from Lake Hazen ice during June 2014. PFAS concentrations equal to or greater than the LOQ for congeners with detection frequencies equal to or greater than 50% are included in correlation analysis.

		PFBA	PFPeA	PFHxA	PFHpA	PFOA	PFNA	PFDA	PFUnDA	PFDoDA	PFTrDA	PFOS
PFPeA	r_s	0.87										
	p	<0.01										
PFHxA	r_s	0.81	0.85									
	p	<0.01	<0.01									
PFHpA	r_s	0.86	0.95	0.97								
	p	<0.01	<0.01	<0.01								
PFOA	r_s	0.88	0.93	0.89	0.97							
	p	<0.01	<0.01	<0.01	<0.01							
PFNA	r_s	0.82	0.87	0.69	0.84	0.92						
	p	0.01	<0.01	0.04	<0.01	<0.01						
PFDA	r_s	0.82	0.87	0.69	0.84	0.92	1.00					
	p	0.01	<0.01	0.04	<0.01	<0.01	<0.01					
PFUnDA	r_s	0.70	0.82	0.61	0.76	0.83	0.97	0.97				
	p	0.04	<0.01	0.08	0.02	<0.01	<0.01	<0.01				
PFDoDA	r_s	0.67	0.84	0.63	0.78	0.83	0.94	0.94	0.95			
	p	<0.05	<0.01	0.07	0.01	<0.01	<0.01	<0.01	<0.01			
PFTrDA	r_s	-0.17	-0.09	-0.13	-0.03	0.05	0.28	0.29	0.38	0.19		
	p	0.69	0.82	0.76	0.93	0.91	0.49	0.49	0.35	0.65		
PFOS	r_s	0.65	0.83	0.59	0.75	0.80	0.93	0.93	0.95	0.99	0.19	
	p	0.06	<0.01	0.10	0.02	<0.01	<0.01	<0.01	<0.01	<0.01	0.65	
PFBS	r_s	0.81	0.70	0.70	0.73	0.68	0.70	0.70	0.58	0.69	-0.05	0.67
	p	0.03	0.08	0.08	0.06	0.09	0.08	0.08	0.17	0.08	0.91	0.10

Table C13 Spearman rank correlation (r_s) analysis of natural log-transformed PFAS (ng L⁻¹) and major ion (µg L⁻¹ or mg L⁻¹) concentrations in light snowpacks collected from Lake Hazen ice during June 2014. Correlation analysis is limited to PFAS concentrations equal to or greater than the LOQ for congeners with detection frequencies equal to or greater than 50%.

		PFBA	PFPeA	PFHxA	PFHpA	PFOA	PFNA	PFDA	PFUnDA	PFDoDA	PFECHS	PFOS
PN	rs	0.39	0.35	0.59	0.52	0.52	0.43	0.57	0.56	0.71	1.00	0.79
	p	0.29	0.35	0.10	0.15	0.15	0.24	0.11	0.12	0.03	<0.01	0.01
PC	rs	0.38	0.35	0.53	0.50	0.53	0.43	0.60	0.58	0.75	0.90	0.79
	p	0.32	0.35	0.14	0.17	0.14	0.24	0.09	0.10	0.02	0.04	0.01
Cl⁻	rs	0.41	0.21	0.54	0.39	0.35	0.29	0.38	0.48	0.67	0.60	0.73
	p	0.28	0.59	0.13	0.30	0.35	0.46	0.32	0.18	<0.05	0.28	0.02
SO₄²⁻	rs	0.36	0.23	0.60	0.55	0.41	0.30	0.47	0.53	0.74	1.00	0.85
	p	0.34	0.55	0.08	0.12	0.27	0.43	0.20	0.14	0.02	<0.01	<0.01
Na⁺	rs	0.32	0.17	0.59	0.52	0.33	0.24	0.41	0.47	0.70	0.97	0.83
	p	0.41	0.66	0.09	0.15	0.38	0.54	0.28	0.20	0.04	<0.01	<0.01
K⁺	rs	0.39	0.20	0.63	0.54	0.35	0.29	0.42	0.50	0.67	0.82	0.82
	p	0.29	0.61	0.07	0.14	0.35	0.45	0.25	0.17	<0.05	0.09	<0.01
Ca²⁺	rs	0.27	0.15	0.47	0.45	0.37	0.23	0.43	0.48	0.75	0.90	0.82
	p	0.48	0.70	0.20	0.22	0.33	0.55	0.24	0.18	0.02	0.04	<0.01
Mg²⁺	rs	0.38	0.24	0.63	0.57	0.42	0.32	0.48	0.54	0.74	1.00	0.86
	p	0.31	0.53	0.07	0.11	0.26	0.40	0.19	0.13	0.02	<0.01	<0.01

Table C14 Spearman rank correlation (r_s) analysis of natural log-transformed PFAS (ng L⁻¹) and major ion (μg L⁻¹ or mg L⁻¹) concentrations in dark snowpacks collected from Lake Hazen ice during June 2014. Correlation analysis is limited to PFAS concentrations equal to or greater than the LOQ for congeners with detection frequencies equal to or greater than 50%.

		PFBA	PFPeA	PFHxA	PFHpA	PFOA	PFNA	PFDA	PFUnDA	PFDoDA	PFTTrDA	PFOS	PFBS
PN	rs	0.43	0.70	0.54	0.67	0.67	0.68	0.68	0.63	0.82	-0.12	0.82	0.61
	p	0.24	0.03	0.13	<0.05	<0.05	0.04	0.04	0.07	<0.01	0.78	<0.01	0.14
PC	rs	0.42	0.67	0.54	0.65	0.65	0.67	0.67	0.62	0.80	-0.09	0.78	0.70
	p	0.26	<0.05	0.13	0.06	0.06	<0.05	<0.05	0.08	<0.01	0.82	0.01	0.08
Cl⁻	rs	0.62	0.67	0.79	0.71	0.57	0.37	0.37	0.32	0.39	-0.52	0.35	0.77
	p	0.08	<0.05	0.01	0.03	0.11	0.33	0.33	0.41	0.29	0.18	0.35	0.04
SO₄²⁻	rs	0.67	0.73	0.89	0.80	0.67	0.45	0.45	0.42	0.44	-0.33	0.40	0.68
	p	<0.05	0.02	<0.01	<0.01	<0.05	0.22	0.22	0.26	0.23	0.42	0.29	0.09
Na⁺	rs	0.73	0.75	0.90	0.82	0.70	0.48	0.48	0.43	0.42	-0.33	0.38	0.68
	p	0.02	0.02	<0.01	<0.01	0.03	0.19	0.19	0.24	0.26	0.42	0.31	0.09
K⁺	rs	0.77	0.87	0.86	0.86	0.78	0.67	0.67	0.67	0.67	-0.12	0.63	0.72
	p	0.01	<0.01	<0.01	<0.01	0.01	<0.05	<0.05	<0.05	<0.05	0.78	0.07	0.07
Ca²⁺	rs	0.67	0.85	0.79	0.83	0.77	0.72	0.72	0.77	0.76	0.05	0.73	0.65
	p	<0.05	<0.01	0.01	<0.01	0.01	0.03	0.03	0.02	0.02	0.91	0.02	0.11
Mg²⁺	rs	0.74	0.90	0.88	0.89	0.76	0.57	0.57	0.52	0.60	-0.39	0.57	0.75
	p	0.04	<0.01	<0.01	<0.01	0.03	0.14	0.14	0.18	0.12	0.38	0.14	0.08

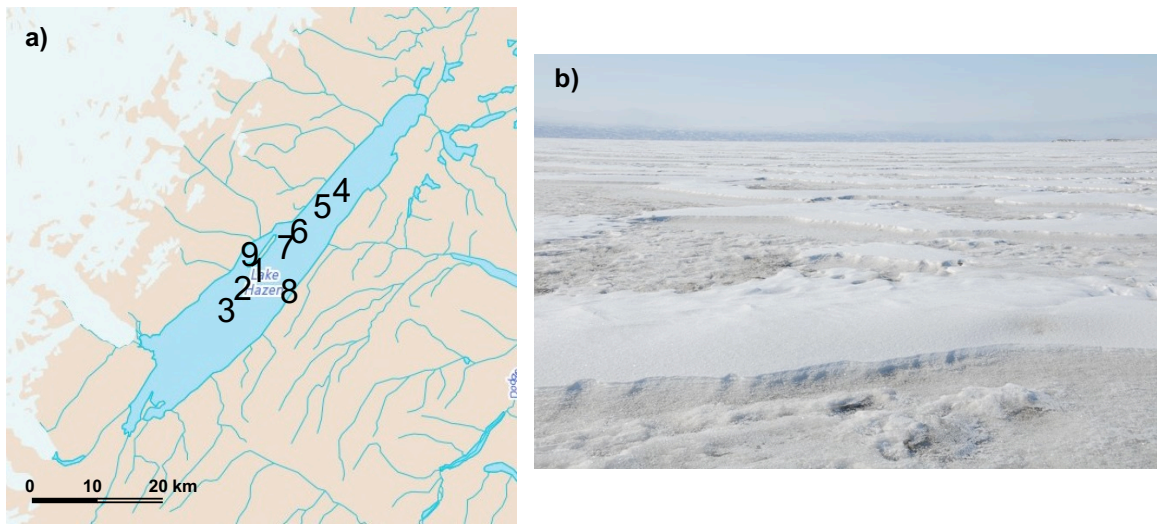


Figure C1 Lake Hazen study area: a) 2014 sampling sites for paired light and dark snowpacks and b) photograph of ice surface of Lake Hazen during 2014. Frequent windstorms in the Lake Hazen region created distinct snow drifts with different enrichments of particles.

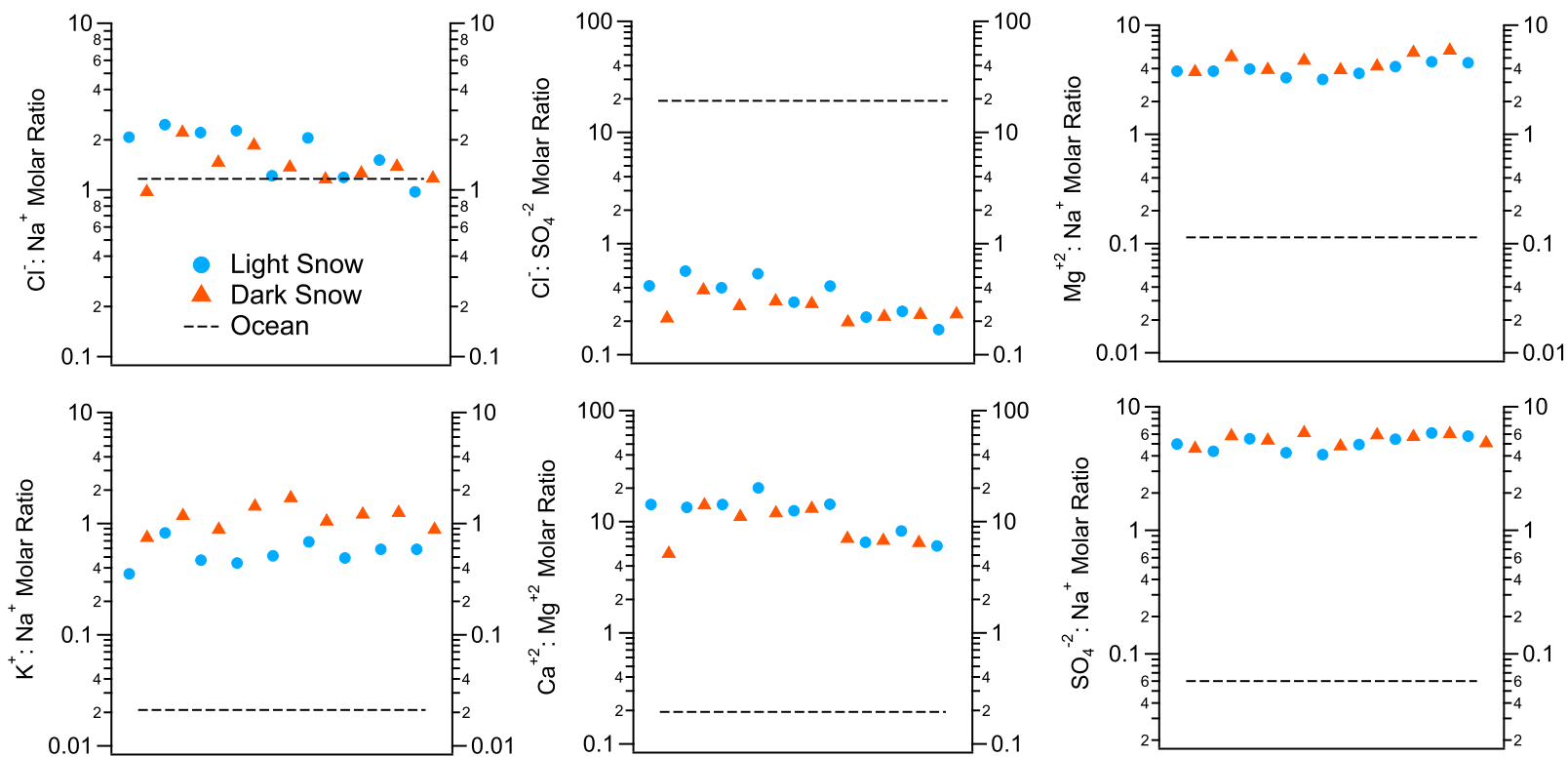


Figure C2 Comparison of molar ratios (left and right y axes) of major ions in paired light (blue circles) and dark (orange triangles) snowpacks collected from Lake Hazen ice during 2014. Expected molar ratios of major ions in ocean water are represented by a dashed line.^{2,3}

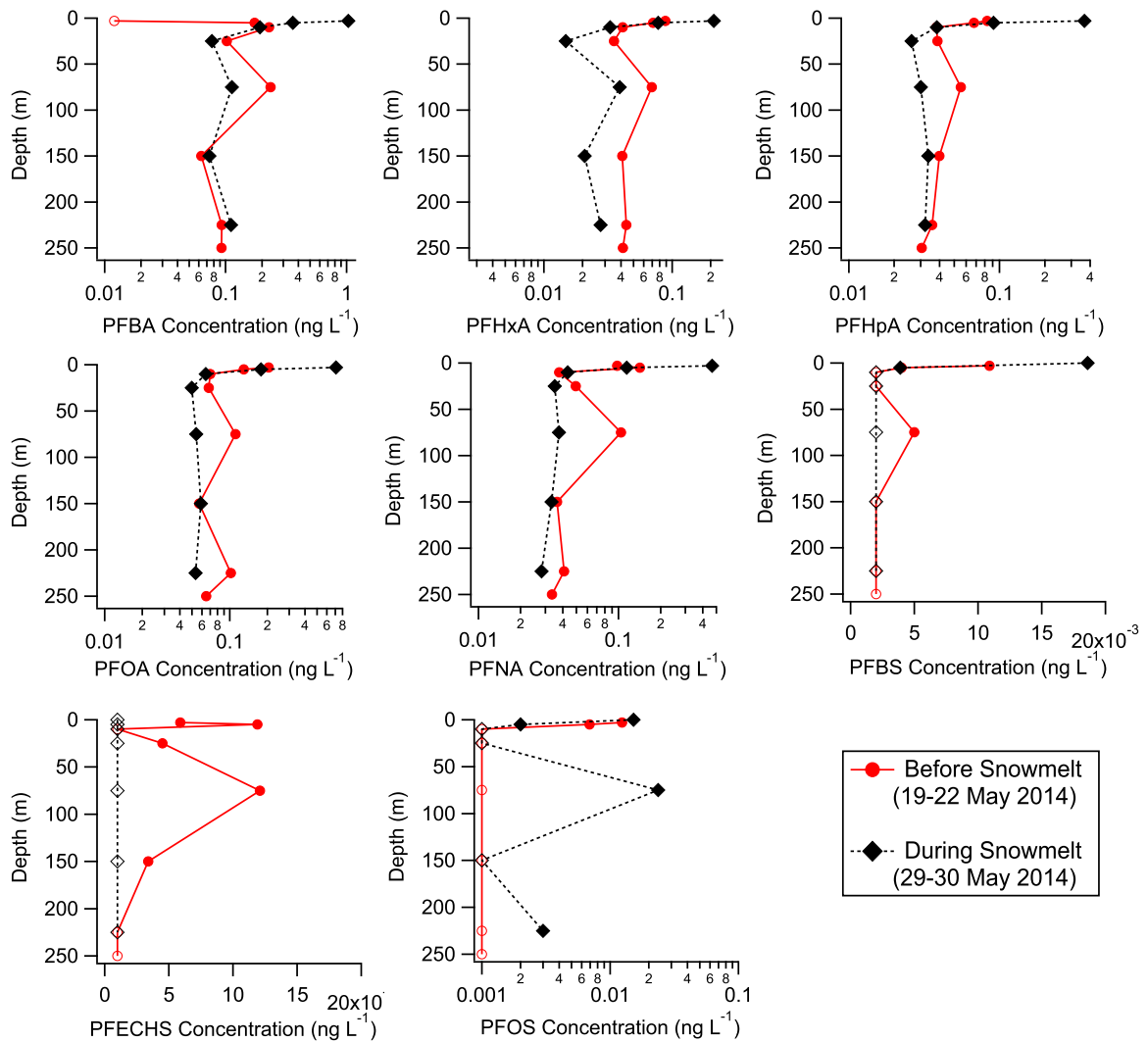


Figure C3 PFAS depth profiles in the Lake Hazen water column before (red circles) and during (black squares) snowmelt in May 2014. Concentration (ng L^{-1}) profiles correspond to depths between 0 to 250 m. Concentrations less than the LOD are substituted with LOD concentrations before (unfilled circles) and during snowmelt (unfilled squares).

Literature Cited

- (1) St. Pierre, K. A.; St. Louis, V. L.; Lehnherr, I.; Gardner, A. S.; Serbu, J. A.; Mortimer, C. A.; Muir, D. C. G.; Wiklund, J. A.; Lemire, D.; Szostek, L.; Talbot, C. Drivers of Mercury Cycling in the Rapidly Changing Glacierized Watershed of the High Arctic's Largest Lake by Volume (Lake Hazen, Nunavut, Canada). *Environ. Sci. Technol.* **2019**, *53* (3), 1175–1185.
- (2) De Caritat, P.; Hall, G.; Gislason, S.; Belsey, W.; Braun, M.; Goloubeva, N. I.; Olsen, H. K.; Scheie, J. O.; Vaive, J. E. Chemical composition of arctic snow: Concentration levels and regional distribution of major elements. *Sci. Total Environ.* **2005**, *336* (1–3), 183–199.
- (3) Church, T. M.; Tramontano, J. M.; Scudlark, J. R.; Jickells, T. D.; Tokos, J. J.; Knap, A. H.; Galloway, J. N. The wet deposition of trace metals to the western atlantic ocean at the mid-atlantic coast and on Bermuda. *Atmos. Environ.* **1984**, *18* (12), 2657–2664.

Appendix D Supporting Information for Chapter 4

Section D1 Chemicals

PFAS analyzed along the Skeleton Continuum and in glacial rivers are: perfluorobutanoic acid (PFBA), perfluoropentanoic acid (PFPeA), perfluorohexanoic acid (PFHxA), perfluoroheptanoic acid (PFHpA), perfluorooctanoic acid (PFOA), perfluorononanoic acid (PFNA), perfluorodecanoic acid (PFDA), perfluoroundecanoic acid (PFUnDA), perfluorododecanoic acid (PFDoDA), perfluorotridecanoic acid (PFTrDA), perfluorotetradecanoic acid (PFTeDA), perfluorohexadecanoic acid (PFHxDA), perfluorobutane sulfonic acid (PFBS), perfluorohexane sulfonic acid (PFHxS), perfluoroheptane sulfonic acid (PFHpS), perfluorooctane sulfonic acid (PFOS), perfluoro-4-ethylcyclohexane sulfonic acid (PFECHS), perfluorodecane sulfonic acid (PFDS), and perfluorooctane sulfonamide (FOSA). PFAS standards (i.e., native and isotopically labeled) were purchased from Wellington Laboratories (Guelph, Ontario) and Chiron AS (Trondheim, Norway). PFECHS was quantified as outlined in Appendix A (Section A1). These analytes were selected for analysis because standardized methods are developed for this series of PFAS in the analytical laboratory. Methanol and water (Optima™ Grade) were purchased from Fisher Scientific (New Hampshire, USA), glacial acetic acid (ACS Grade) was purchased from EMD (Etobicoke, Ontario), ammonium acetate (>98%) was purchased from Sigma Aldrich (Missouri, USA), and ammonia (Suprapur® 25 %) was purchased from Merck (New Jersey, USA).

Section D2 QA/QC

Before laboratory analysis, water samples were spiked with 30 µL of an internal standard mixture and concentrated using Oasis® WAX SPE (6 cm³, 150 mg, 30 µm). Method performance was evaluated by spiking a native PFAS standard mixture into water samples. These samples were analyzed concurrently with other Lake Hazen water samples. Extraction blanks were used to evaluate positive biases during the laboratory analysis. This consisted of extracting an Oasis® WAX SPE cartridge spiked with 30 µL of a PFAS internal standard mixture. Field blanks were collected to evaluate biases from sampling and transport. Field blank collection was conducted by transporting 500 mL of HPLC grade water to the Lake Hazen region, and exposing these samples to the atmosphere for ten seconds. PFAS concentrations in field blanks were similar to those in HPLC grade water from the laboratory (i.e., stay blank), indicating sampling and transportation are not sources of contamination. PFAS concentrations in samples were method blank, recovery, and matrix corrected.

Table D1 Location of sampling sites along the Skeleton Continuum.

Site	Latitude (°N)	Longitude (°W)
Seep	81.832317	-71.522100
Skeleton Lake	81.829283	-71.479700
After ponds	81.831917	-71.465183
Meadow Wetland	81.834267	-71.363850
Skeleton Creek	81.830567	-71.330550

267

Table D2 Hydrological overview of glacier-fed tributaries in the Lake Hazen watershed.¹ Uncertainty is denoted by the standard error estimated daily from July 1 to August 15 2015.

	Glacier Area	River Length	River Discharge	Watershed Area	Runoff Volume 2015	Runoff Volume 2015
	km²	km	m³ s⁻¹	km²	x10⁵ m³ km⁻² year⁻¹	km³
Henrietta Nesmith River	1041	4.3	76 ± 16	1274	2.29	0.29
Gilman River	708	21.2	51 ± 12	992	1.93	0.19
Very River	269	42.5	43 ± 6.0	1035	1.60	0.17
Turnabout River	259	55.3	23 ± 4.8	678	1.20	0.081
Abbé River	204	20.9	17 ± 3.6	390	1.56	0.061
Snowgoose River	87	15.6	17 ± 3.6	222	1.18	0.026
Blister Creek	6	11.2				0.002

Table D3 Overview of native, internal, and instrument performance PFAS standards.

Internal standards are added before extraction to monitor recovery and instrument performance standards are added after extraction prior to analysis to monitor matrix effects.

Native Standard	Internal Standard	Instrument Performance
PFBA	¹³ C ₄ PFBA	¹³ C ₃ PFBA
PFPeA	¹³ C ₅ PFPeA	¹³ C ₃ PFPeA
PFHxA	¹³ C ₂ PFHxA	¹³ C ₅ PFHxA
PFHpA	¹³ C ₄ PFHpA	
PFOA	¹³ C ₄ PFOA	¹³ C ₂ PFOA
PFNA	¹³ C ₅ PFNA	¹³ C ₉ PFNA
PFDA	¹³ C ₂ PFDA	¹³ C ₆ PFDA
PFUnDA	¹³ C ₂ PFUnDA	¹³ C ₇ PFUnDA
PFDoDA	¹³ C ₂ PFDoDA	
PFTTrDA	¹³ C ₂ PFTTrDA	
PFTeDA	¹³ C ₂ PFTeDA	
PFHxDA	¹³ C ₂ PFHxDA	
PFBS	¹³ C ₃ PFBS	
PFHxS	¹⁸ O ₂ PFHxS	¹³ C ₃ PFHxS
PFHpS	¹⁸ O ₂ PFHpS	
PFOS	¹³ C ₄ PFOS	¹³ C ₈ PFOS
PFDS	¹³ C ₄ PFOS	
PFECHS	¹⁸ O ₂ PFHxS	
FOSA	¹³ C ₈ FOSA	

Table D4 Limits of detection and quantification, and PFAS concentrations (ng L⁻¹) in field and stay blanks.

Congener	LOD	LOQ	Field	Stay
PFBA	0.010	0.040	<0.010-1.2	0.019
PFPeA	0.010	0.050	<0.010	<0.010
PFHxA	0.005	0.020	0.011-0.059	<0.005
PFHpA	0.002	0.007	<0.002-0.019	<0.002
PFOA	0.003	0.010	0.014-0.031	0.0077
PFNA	0.002	0.008	<0.002	<0.002
PFDA	0.003	0.010	<0.003-0.030	<0.003
PFUnDA	0.003	0.009	<0.003	<0.003
PFDoDA	0.002	0.007	<0.002	<0.002
PFTTrDA	0.002	0.006	<0.002	<0.002
PFTeDA	0.003	0.010	<0.003	<0.003
PFHxDA	0.010	0.040	<0.010	<0.010
PFOS	0.001	0.003	<0.001	<0.001
PFDS	0.0006	0.002	<0.0006	<0.0006
PFECHS	0.001	0.003	<0.001	<0.001
PFHxS	0.0007	0.002	<0.0007	<0.0007
PFHpS	0.0009	0.003	<0.0009	<0.0009
PFBS	0.002	0.007	<0.002	<0.002
FOSA	0.0002	0.0007	<0.0002	<0.0002

Table D5 Overview of precursor/product ion mass-to-charge ratios (m/z), cone voltages (V), and collision energies (eV) for native PFAS analysis. Product ion scans for PFCA target perfluoroalkyl moieties (i.e., $F(CF_2)_xCO_2^-$ to $F(CF_2)_x$), while product ion scans for PFSA target sulfonic acid moieties (i.e., $F(CF_2)_xSO_3^-$ to FSO_3^- or SO_3^-). The transition for FOSA targets a SO_2N moiety (i.e., $CF_3(CF_2)_7SO_2NH_2$ to SO_2N).

PFAS	Quantifier m/z	Cone Voltage	Collision Energy	Qualifier m/z	Cone Voltage	Collision Energy
PFBA	213/169	6	10			
PFPeA	263/219	6	15			
PFHxA	313/269	6	10	313/119	6	17
PFHpA	363/319	8	10	363/119	8	18
PFOA	413/369	16	11	413/169	16	18
PFNA	463/419	16	10	463/219	16	17
PFDA	513/469	16	10	513/219	16	17
PFUnDA	563/519	18	10	563/319	18	17
PFDoDA	613/569	18	12	613/169	18	28
PFTTrDA	663/619	18	12	663/169	18	30
PFTeDA	713/669	26	12	713/169	26	30
PFHxDA	813/769	36	14	813/169	36	36
PFBS	299/99	42	30	299/80	42	30
PFHxS	399/99	42	32	399/80	42	32
PFHpS	449/99	42	36	449/80	42	44
PFOS	499/99	46	36	499/80	46	40
PFDS	599/99	42	44	599/80	42	46
PFECHS	461/381	42	30	461/99	42	26
FOSA	498/78	46	30			

Table D6 Overview of precursor/product ion mass-to-charge ratios, cone voltages (V), and collision energies (eV) for internal and instrument performance PFAS standard analysis.

Internal Standard		Cone Voltage	Collision Energy
¹³ C ₄ PFBA	217/172	6	10
¹³ C ₅ PFPeA	268/223	6	15
¹³ C ₂ PFHxA	315/270	6	10
¹³ C ₄ PFHpA	367/322	8	10
¹³ C ₄ PFOA	417/372	16	10
¹³ C ₅ PFNA	468/423	16	14
¹³ C ₂ PFDA	515/470	16	16
¹³ C ₂ PFUnDA	565/520	18	10
¹³ C ₂ PFDoDA	615/570	18	12
¹³ C ₂ PFTeDA	715/670	26	12
¹³ C ₂ PFHxDA	815/770	36	14
¹³ C ₃ PFBS	302/99	42	30
¹⁸ O ₂ PFHxS	403/84	42	38
¹⁸ O ₂ PFHxS	403/103	42	32
¹³ C ₄ PFOS	503/80	46	48
¹³ C ₈ FOSA	506/78	46	28
Instrument Performance		Cone Voltage	Collision Energy
¹³ C ₃ PFBA	216/172	6	10
¹³ C ₃ PFPeA	266/222	6	15
¹³ C ₅ PFHxA	318/273	6	10
¹³ C ₂ PFOA	415/370	16	10
¹³ C ₉ PFNA	472/427	16	14
¹³ C ₆ PFDA	519/474	16	12
¹³ C ₇ PFUnDA	570/525	18	10
¹³ C ₃ PFHxS	402/99	42	32
¹³ C ₈ PFOS	507/99	46	36

Table D7 Overview of liquid chromatograph gradient elution, mass spectrometric, and inlet parameters used for PFAS quantitation along the Skeleton Continuum and in glacial rivers.

Liquid Chromatograph Gradient Elution				Mass Spectrometer/Inlet	
Time (min)	Flow Rate (mL min⁻¹)	H₂O (%)	MeOH (%)	Ionization mode: Electrospray negative	
0	0.400	75	25		
0.5	0.400	75	25	Capillary Voltage (kV)	0.6
5.0	0.400	15	85	Source Temperature (°C)	150
5.1	0.400	0	100	Desolvation Gas Temperature (°C)	450
5.6	0.400	0	100	Cone Gas Flow (L hr ⁻¹)	150
7.0	0.550	0	100	Desolvation Gas Flow (L hr ⁻¹)	800
9.0	0.400	75	25	Collision Gas Flow (mL min ⁻¹)	0.15
13.0	0.400	75	25	Nebulizer Pressure (bar)	7
Inlet parameters					
				Column Temperature (°C)	50
				Injection Volume (μL)	9



Figure D1 Photo of water flowing from a seep in the uplands of the Skeleton Continuum in the Lake Hazen watershed.

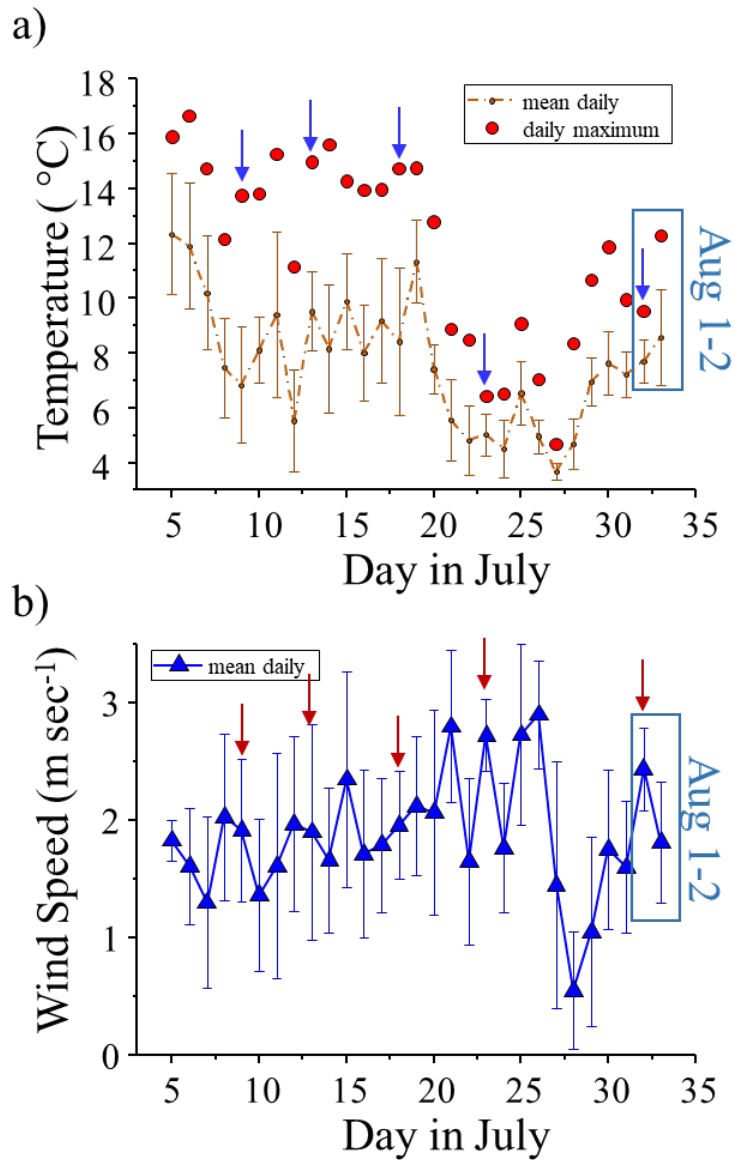


Figure D2 Meteorological conditions at Lake Hazen: a) mean \pm standard deviation daily temperature and maximum daily temperature and b) mean \pm standard deviation daily wind speed, based on hourly recording from July 5 to August 2 using a CR10X Weather logger (Campbell Scientific).

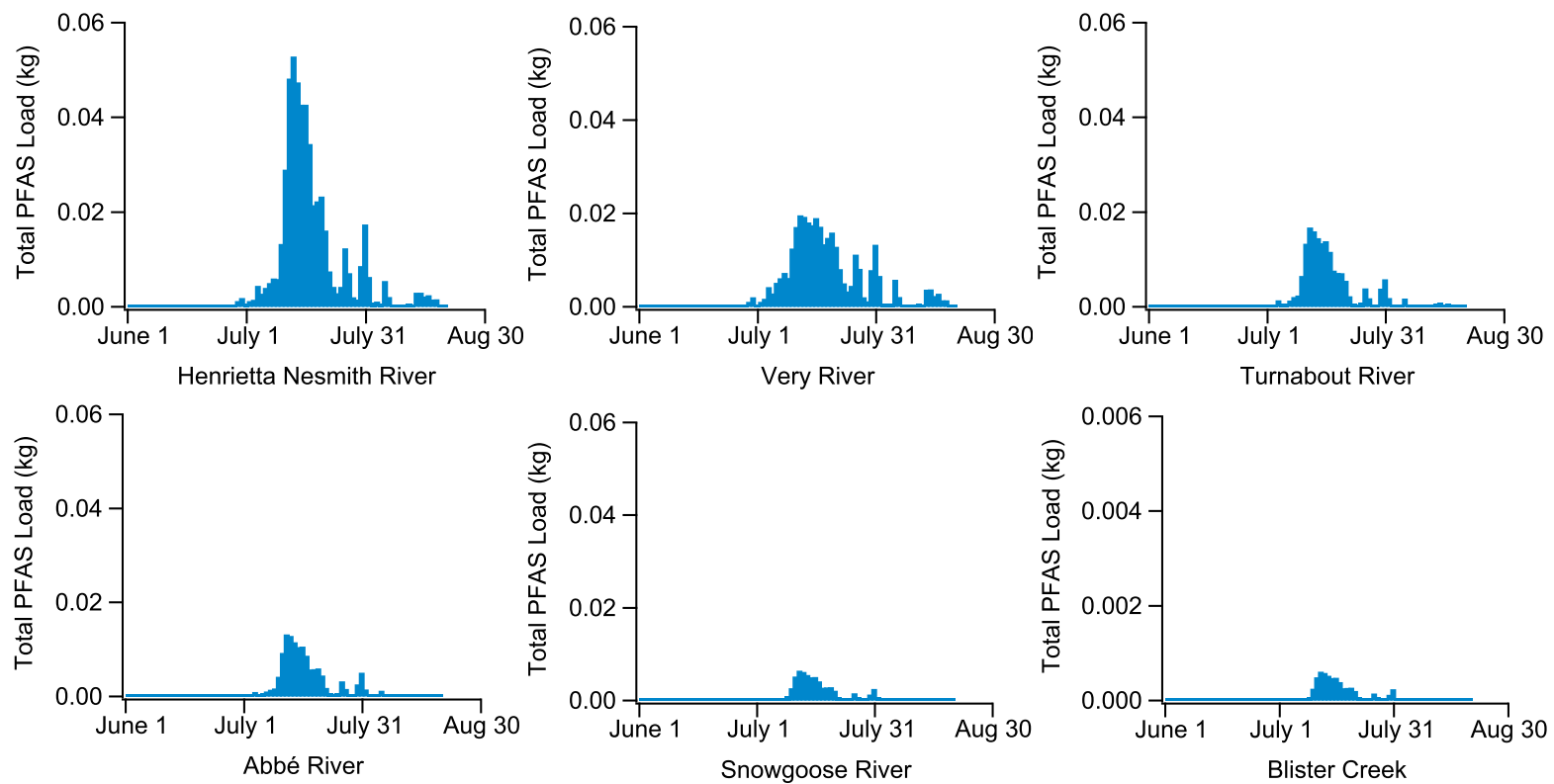


Figure D3 Glacial riverine fluxes of total PFAS in the Lake Hazen watershed from 1 June to 19 August 2015. Glacial riverine fluxes are estimated using a LOADEST log-linear model.

Literature Cited

- (1) St. Pierre, K. A.; St. Louis, V. L.; Lehnherr, I.; Gardner, A. S.; Serbu, J. A.; Mortimer, C. A.; Muir, D. C. G.; Wiklund, J. A.; Lemire, D.; Szostek, L.; Talbot, C. Drivers of Mercury Cycling in the Rapidly Changing Glacierized Watershed of the High Arctic's Largest Lake by Volume (Lake Hazen, Nunavut, Canada). *Environ. Sci. Technol.* **2019**, *53* (3), 1175–1185.